

# **Pharmacokinetics and metabolism of CNS-targeted natural products**

## **Inauguraldissertation**

zur

Erlangung der Würde eines Doktors der Philosophie

vorgelegt der

Philosophisch-Naturwissenschaftlichen Fakultät

der Universität Basel

von

**Volha Zabela**

aus Belarus

Basel, 2016

Original document stored on the publication server of the University of Basel  
**edoc.unibas.ch**



This work is licenced under the agreement  
„Attribution Non-Commercial No Derivatives – 3.0 Switzerland“ (CC BY-NC-ND 3.0 CH). The  
complete text may be reviewed here:

**[creativecommons.org/licenses/by-nc-nd/3.0/ch/deed.en](https://creativecommons.org/licenses/by-nc-nd/3.0/ch/deed.en)**

Genehmigt von der Philosophisch-Naturwissenschaftlichen Fakultät  
auf Antrag von

Prof. Dr. Matthias Hamburger

Prof. Dr. Laurent Decosterd

Basel, den 18.10.2016

Prof. Dr. Jörg Schibler  
Dekan



**Attribution-NonCommercial-NoDerivatives 3.0 Switzerland**  
(CC BY-NC-ND 3.0 CH)

**You are free: to Share** — to copy, distribute and transmit the work

**Under the following conditions:**



**Attribution** — You must attribute the work in the manner specified by the author or licensor (but not in any way that suggests that they endorse you or your use of the work).



**Noncommercial** — You may not use this work for commercial purposes.



**No Derivative Works** — You may not alter, transform, or build upon this work.

**With the understanding that:**

- **Waiver** — Any of the above conditions can be **waived** if you get permission from the copyright holder.
- **Public Domain** — Where the work or any of its elements is in the **public domain** under applicable law, that status is in no way affected by the license.
- **Other Rights** — In no way are any of the following rights affected by the license:
  - Your fair dealing or **fair use** rights, or other applicable copyright exceptions and limitations;
  - The author's **moral** rights;
  - Rights other persons may have either in the work itself or in how the work is used, such as **publicity** or privacy rights.
- **Notice** — For any reuse or distribution, you must make clear to others the license terms of this work. The best way to do this is with a link to this web page.



*To my Mom  
for sharing my dreams*



*First there is a mountain, then there is no mountain,  
then there is.*

-Zen proverb





## Table of contents

<b>List of abbreviations</b> .....	<b>11</b>
<b>Summary</b> .....	<b>13</b>
<b>Zusammenfassung</b> .....	<b>15</b>
<b>1 Aim of the work</b> .....	<b>17</b>
<b>2 Introduction</b> .....	<b>23</b>
<b>2.1 The current state of CNS drug discovery and development</b> .....	<b>25</b>
<b>2.2 Natural products as a source of CNS-active compounds</b> .....	<b>26</b>
<b>2.3 Drug metabolism and pharmacokinetics (DMPK)</b> .....	<b>32</b>
2.3.1 Drug metabolism .....	32
2.3.1.1 Phase I metabolism .....	32
2.3.1.2 Phase II metabolism .....	34
2.3.1.3 Factors affecting drug metabolism.....	36
2.3.2 Strategies to study drug metabolism.....	37
2.3.2.1 <i>In vitro</i> models .....	37
2.3.2.2 <i>In vivo</i> models .....	39
2.3.3 Pharmacokinetics.....	40
2.3.3.1 Pharmacokinetic parameters .....	40
2.3.3.2 Pharmacokinetic data analysis .....	43
2.3.4 Plasma protein binding .....	43
2.3.5 Techniques for measurement of plasma protein binding.....	43
2.3.6 Red blood cell binding.....	45
<b>2.4 Bioanalysis</b> .....	<b>47</b>
2.4.1 A brief history of bioanalysis .....	47
2.4.2 Operation principles of the QqQ and Q-TOF mass analyzers .....	48
2.4.3 Sample preparation.....	50

2.4.4 Method development.....	51
2.4.5 Method validation .....	52
2.4.6 Analysis of study samples .....	54
<b>2.5 Metabolite identification in early drug discovery.....</b>	<b>56</b>
<b>3 Results and discussion.....</b>	<b>59</b>
<b>3.1 Pharmacokinetics of dietary kaempferol and its metabolite 4-hydroxyphenylacetic acid in rats .....</b>	<b>61</b>
<b>3.2 Single dose pharmacokinetics of intravenous 3,4-dihydroxyphenylacetic acid and 3-hydroxyphenylacetic acid in rats .....</b>	<b>110</b>
<b>3.3 GABA<sub>A</sub> receptor activity modulating piperine analogs: <i>In vitro</i> metabolic stability, metabolite identification, CYP450 reaction phenotyping, and protein binding. ....</b>	<b>155</b>
<b>4 Conclusions and outlook .....</b>	<b>201</b>
<b>Acknowledgments .....</b>	<b>207</b>
<b>Curriculum vitae .....</b>	<b>209</b>

## List of abbreviations

AChE, acetylcholinesterase	HPLC, high pressure liquid chromatography
AChR, acetylcholine receptor	HR-MS, high resolution mass spectrometry
Acetyl-CoA, acetyl-coenzyme A	IS, internal standard
ADH, alcohol dehydrogenase	$k_e$ , elimination rate constant
ALDH, aldehyde dehydrogenase	LLE, liquid-liquid extraction
APCI, atmospheric pressure chemical ionization	LLOQ, lower limit of quantification
API, atmospheric pressure ionization	MAO, monoamine oxidase
AUC, area under the curve	MetID, metabolite identification
BBB, blood-brain barrier	MF, matrix factor
$C_0$ , initial drug concentration	mRNA, messenger ribonucleic acid
CAL, calibration standard	MS, mass spectrometry
CB <sub>1</sub> , cannabinoid receptor type 1	NADPH, nicotinamide adenine dinucleotide phosphate
cDNA, complementary deoxyribonucleic acid	PAPS, 3'-phosphoadenosine-5'-phosphosulfate
CID, collision induced dissociation	PK, pharmacokinetics
Cl, total clearance	PP, protein precipitation
CNS, central nervous system	QC, quality control
CV, coefficient of variation	QCH, quality control at a high level
CYP450, cytochrome P450	QCL, quality control at a low level
DMPK, drug metabolism and pharmacokinetics	QCM, quality control at a medium level
EMA, European Medicines Agency	QqQ, triple quadrupole
ESI, electrospray ionization	Q-TOF, quadrupole time-of-flight
FDA, Food and Drug Administration	RE, relative error
FMO, flavin-containing monooxygenase	RED, rapid equilibrium dialysis
F, bioavailability	SAM, S-adenosylmethionine
$f_u$ , unbound fraction	SLE, supported-liquid extraction
GABA <sub>A</sub> , $\gamma$ -aminobutyric acid receptor type A	SPE, solid phase extraction
GC, gas chromatography	SRM, selected reaction monitoring

SULT, sulfotransferase

$t_{1/2}$ , elimination half-life

TIC, total ion chromatogram

UDP, uridine diphosphate

UDPGA, uridine diphosphoglucuronic acid

UGT, UDP-glucuronosyltransferase

UHPLC, ultra-high performance liquid chromatography

ULOQ, upper limit of quantification

UV, ultraviolet

$V_d$ , apparent volume of distribution

WHO, World Health Organization

## Summary

Considerable progress has been made to increase the success rate of bringing new therapeutics to the market by implementation of drug metabolism and pharmacokinetics (DMPK) screening strategies in early drug discovery. DMPK screenings help to select leads with good oral bioavailability, low clearance, optimal half-life, and a desirable metabolic profile.

In previous studies with natural products, the flavonoids kaempferol and quercetin, and the alkaloid piperine have been characterized *in vivo* as central nervous system (CNS) acting compounds. To gain a better understanding of anxiolytic effects reported for the flavonoids, PK studies after oral and intravenous administrations in rats were conducted. UHPLC-MS/MS methods for quantification of the compounds of interest in rat plasma were developed and validated according to the principles of regulatory guidelines for industry to support PK studies. The validated methods were successfully applied to determine the concentration levels of the analytes in rat plasma, and PK parameters were calculated with the aid of the industry standard software WinNonlin. The findings suggest that poor oral bioavailability and extensive first-pass metabolism limit plasma exposure of kaempferol. After oral administration, the compound was found as phase II conjugates in plasma. Upon intravenous application, kaempferol was rapidly cleared (4-6 l/h/kg), demonstrating an extremely short half-life of around 4 min. Based on the results, it is more likely that the anxiolytic effect reported for this flavonoid is rather attributed to its metabolites. The major colonic metabolites of kaempferol and quercetin are 4-hydroxyphenylacetic acid (4-HPAA), 3-hydroxyphenylacetic acid (3-HPAA), and 3,4-dihydroxyphenylacetic acid (DOPAC). Moreover, anxiolytic activity has been reported for 4-HPAA and DOPAC. Thus, we aimed to obtain PK profiles of the metabolites upon intravenous application. It has been found that the metabolites were rapidly eliminated with a half-life of 20-30 min, so that effective concentrations in the brain do not appear to be reached. Taken together, it is not clear at this moment how the anxiolytic-like properties can be explained.

During a screening of natural products for  $\gamma$ -aminobutyric acid type A (GABA<sub>A</sub>) receptor activity, piperine was characterized as a positive allosteric modulator targeting a benzodiazepine-independent binding site. Due to pharmacological promiscuity of piperine, its

structure was systematically modified, and a library of piperine analogs was prepared. The most potent and efficacious analogs were identified from *in vitro* and *in vivo* studies. The information on metabolically labile sites of the selected analogs was needed to guide further lead optimization process. Thus, the objective of the second part of the PhD thesis was to investigate metabolism of the selected analogs. UHPLC-MS/MS methods for quantification of piperine and its analogs were initially developed to support *in vitro* metabolism studies. Microsomal stability assays revealed piperine as the metabolically most stable compound, whereas its analogs demonstrated high metabolic liability. To obtain metabolite profiles of the test compounds after incubation with human microsomes, UHPLC-Q-TOF-MS methods were developed. The high resolution accurate mass data were further processed with the aid of MetID software Mass-MetaSite. The principal routes of oxidative metabolism were found to be aliphatic hydroxylation, and N- and O-dealkylation. Additionally, CYP450 reaction phenotyping was performed to determine which CYP isozymes are involved in the metabolism of piperine and its analogs. It appeared that piperine was exclusively metabolized by CYP1A2, whereas CYP2C9 contributed significantly in the oxidative metabolism of all analogs. Moreover, extensive binding to blood constituents was observed for all compounds. Our findings showed that analogs were rapidly metabolized and demonstrated strong binding to blood constituents due to increased lipophilicity. The next cycle of medicinal chemistry optimizations should, therefore, be focused on reducing lipophilicity to lower metabolic liability and extensive binding of analogs.

## Zusammenfassung

Es wurden beträchtliche Fortschritte gemacht, um die Erfolgchancen bei der Einführung neuer Therapeutika auf den Markt zu erhöhen indem schon bei dem Screening von Leitstrukturen der Arzneimittel-Metabolismus und die Pharmakokinetik (DMPK) untersucht werden. DMPK Screenings sind geeignet, Leads, mit einer guten oralen Bioverfügbarkeit, niedrigerer Clearance, optimaler Halbwertszeit und einem wünschenswerten metabolischen Profil zu identifizieren.

In früheren Studien mit Naturstoffen wurden die Flavonoide Kaempferol und Quercetin, sowie das Alkaloid Piperin *in vivo* als auf das Zentralnervensystem (ZNS) wirkende Verbindungen charakterisiert. Um ein besseres Verständnis von anxiolytischen Effekten der Flavonoide gewinnen zu können, wurden pharmakokinetische (PK) Studien nach oraler und intravenöser Verabreichung bei Ratten durchgeführt. Die UHPLC-MS/MS-Verfahren zur Quantifizierung der Verbindungen in Rattenplasma wurden für PK Studien nach regulatorischen Vorgaben der Industrie entwickelt und validiert. Die validierten Verfahren wurden erfolgreich angewendet, um die Konzentrationen der Analyten in Rattenplasma zu bestimmen. Die PK Parameter wurden nachfolgend mit Hilfe der Industrie Standard Software WinNonlin berechnet. Die Ergebnisse weisen darauf hin, dass eine schlechte orale Bioverfügbarkeit zusammen mit einem ausgeprägten First-Pass Metabolismus die Plasmakonzentration von Kaempferol begrenzt. Nach oraler Verabreichung wurde die Verbindung als Phase-II Konjugat im Plasma nachgewiesen. Bei intravenöser Verabreichung wurde eine sehr hohe Clearance beobachtet (4-6 l/h/kg), was in einer extrem kurzen Halbwertszeit von etwa 4 min resultierte. Basierend auf den Ergebnissen ist es wahrscheinlicher, dass die anxiolytische Wirkung nicht durch das Flavonoid selbst, sondern durch seine Metaboliten bedingt ist. Die Flavonoide Kaempferol und Quercetin werden durch die Darmflora in 4-Hydroxyphenylelessigsäure (4-HPAA), 3-Hydroxyphenylelessigsäure (3-HPAA) und 3,4-Dihydroxyphenylelessigsäure (DOPAC) umgewandelt. Daneben, wurde die anxiolytische Aktivität für 4-HPAA und DOPAC berichtet. Dementsprechend, wurde es notwendig PK Profile von den Metaboliten nach intravenöser Verabreichung zu erhalten. Es wurde herausgefunden, dass die entsprechenden Metaboliten mit einer Halbwertszeit von 20-30 min eliminiert wurden, so dass pharmakologisch wirksame Konzentrationen im Gehirn

unwahrscheinlich sind. Es ist daher noch nicht klar, wie die beobachteten anxiolytischen Effekte der Flavonoide erklärt werden können.

In einem Screening von Naturstoffen mit  $\gamma$ -Aminobuttersäure Typ A (GABA<sub>A</sub>) Rezeptor-aktivierenden Eigenschaften wurde Piperin als positiver allosterischer Modulator charakterisiert, der mit einer Benzodiazepin-unabhängigen Bindungsstelle interagiert. Aufgrund der promiskuitiven Pharmakologie von Piperin wurde die Struktur systematisch verändert und eine Bibliothek von Piperin-Derivaten hergestellt. Die wirksamsten Analoga wurden durch verschiedene *in vitro* und *in vivo* Studien identifiziert. Weitere Informationen in Bezug auf metabolisch labile Stellen der ausgewählten Analoga wurden benötigt, um weitere Schritte in der Lead-Optimierung zu planen. Aus diesem Grund war das Ziel des zweiten Teils der Dissertation, den Metabolismus von ausgewählten Analoga zu untersuchen. Zunächst wurden UHPLC-MS/MS-Verfahren zur Quantifizierung von Piperin und seiner Analoga entwickelt, um *in vitro*-Metabolismus-Studien durchführen zu können. In mikrosomalen Stabilitätsassays erwies sich Piperin als metabolisch stabilste Verbindung, während seine Analoga hohe metabolische Anfälligkeit zeigten. Nach der Inkubation von Test-Verbindungen mit humanen Mikrosomen wurden ihre Metabolitprofile mittels UHPLC-Q-TOF-MS aufgenommen. Die somit erhaltenen Daten wurden mit Hilfe der MetID Software Mass-MetaSite verarbeitet. Im oxidativen Stoffwechsel wurden drei Hauptwege identifiziert: aliphatische Hydroxylierung, N- und O-Dealkylierung. Zusätzlich wurde eine Phänotypisierung der CYP450-Reaktion durchgeführt um festzustellen, welche CYP-Isoenzyme am Stoffwechsel von Piperin und der Piperin-Analoga beteiligt sind. Es zeigte sich, dass Piperin ausschließlich durch CYP1A2 metabolisiert wird, während CYP2C9 deutlich zum oxidativen Stoffwechsel aller Piperin-Analoga beiträgt. Darüber hinaus wurde für alle getesteten Verbindungen eine starke Bindung an Blutbestandteile beobachtet. Unsere Ergebnisse zeigten, dass Piperin-Analoga schnell metabolisiert wurden und aufgrund der höheren Lipophilie eine starke Bindung an Blutbestandteile aufweisen. Der nächste Schritt in der medizinisch-chemischen Strukturoptimierung sollte daher auf eine Verringerung der Lipophilie fokussieren, um die Metabolisierung und die Bindung an Blutbestandteile der Piperin-Analoga zu verringern.



## **1 Aim of the work**



In previous studies with natural products, the flavonoids kaempferol and quercetin, and the alkaloid piperine have been characterized *in vivo* as central nervous system (CNS) acting compounds. It has been shown that kaempferol and quercetin exert anxiolytic activity in mice upon oral administration, while no behavioral changes were observed upon intraperitoneal administration, or upon oral administration in gut sterilized animals (1). Thus, it appeared that these flavonoids have to undergo metabolic transformations to pharmacologically active metabolites. The major colonic metabolites of kaempferol and quercetin are 4-hydroxyphenylacetic acid (4-HPAA), 3-hydroxyphenylacetic acid (3-HPAA), and 3,4-dihydroxyphenylacetic acid (DOPAC) (2, 3). Anxiolytic activity upon intraperitoneal administration has been reported for 4-HPAA and DOPAC (1). Knowledge of pharmacokinetic (PK) profiles of all compounds was required for a better understanding of their pharmacological effects, and thus PK studies in rats were conducted with the aim to evaluate PK properties of the compounds after oral and intravenous administrations.

At first, we aimed to develop UHPLC-MS/MS methods for quantification of the compounds of interest in lithium heparinized Sprague-Dawley rat plasma. Thereafter, bioanalytical methods were validated following the principles of regulatory guidelines for industry to demonstrate reliability, reproducibility, and robustness for quantitative measurements in a given matrix (4, 5). The validated methods were later applied to determine the concentration levels of the analytes in rat plasma, and PK parameters were calculated for each compound with the industry standard software WinNonlin using non-compartmental and compartmental analyses.

Furthermore, during a screening of natural products for  $\gamma$ -aminobutyric acid type A (GABA<sub>A</sub>) receptor activity, piperine was identified as a positive allosteric modulator targeting a benzodiazepine-independent binding site (6). However, piperine is also an activator of TRPV1 receptors (transient receptor potential vanilloid type 1) involved in pain signaling and thermoregulation. Therefore, the structure of piperine was systematically modified to dissect GABA<sub>A</sub> and TRPV1 activating properties, and a library of piperine analogs was prepared (7, 8). The most potent and efficacious analogs were selected from *in vitro* and *in vivo* studies (8, 9). The information on metabolically labile sites of the selected analogs was needed to guide further lead optimization process. Thus, the objective of the second part of the PhD thesis was to investigate metabolism of the selected analogs.

In a first step, we aimed to develop specific and robust UHPLC-MS/MS methods for quantification of the compounds of interest in potassium phosphate buffer. These methods were later applied to support microsomal stability assays with the analogs, and the generated data were used for calculation of *in vitro* intrinsic clearances. In a second step, we developed UHPLC-Q-TOF-MS methods for qualitative analysis of metabolite profiles obtained after incubation of the analogs with human liver microsomes, and identified the metabolites with the aid of MetID software Mass-MetaSite.

## References

1. Vissienon, C., Nieber, K., Kelber, O., and Butterweck, V. (2012) Route of administration determines the anxiolytic activity of the flavonols kaempferol, quercetin and myricetin—are they prodrugs?, *J. Nutr. Biochem.* 23, 733-740.
2. Griffiths, L., and Smith, G. (1972) Metabolism of apigenin and related compounds in the rat. Metabolite formation *in vivo* and by the intestinal microflora *in vitro*, *Biochem. J.* 128, 901-911.
3. Winter, J., Popoff, M. R., Grimont, P., and Bokkenheuser, V. D. (1991) *Clostridium orbiscindens* sp. nov., a human intestinal bacterium capable of cleaving the flavonoid C-ring, *Int. J. Syst. Microbiol.* 41, 355-357.
4. FDA (Draft Guidance 2013) *Guidance for Industry: Bioanalytical Method Validation*, Center for Drug Evaluation and Research.
5. EMA (2011) *Guideline on bioanalytical method validation*, European Medicines Agency (EMA/CHMP/EWP/192217/2009).
6. Zaugg, J., Baburin, I., Strommer, B., Kim, H.-J., Hering, S., and Hamburger, M. (2010) HPLC-based activity profiling: discovery of piperine as a positive GABA<sub>A</sub> receptor modulator targeting a benzodiazepine-independent binding site, *J. Nat. Prod.* 73, 185-191.
7. Khom, S., Strommer, B., Schöffmann, A., Hintersteiner, J., Baburin, I., Erker, T., Schwarz, T., Schwarzer, C., Zaugg, J., and Hamburger, M. (2013) GABA<sub>A</sub> receptor modulation by piperine and a non-TRPV1 activating derivative, *Biochem. Pharmacol.* 85, 1827-1836.
8. Schöffmann, A., Wimmer, L., Goldmann, D., Khom, S., Hintersteiner, J., Baburin, I., Schwarz, T., Hintersteiner, M., Pakfeifer, P., Oufir, M., Hamburger, M., Erker, T., Ecker, G. F., Mihovilovic, M. D., and Hering, S. (2014) Efficient modulation of  $\gamma$ -aminobutyric acid type A receptors by piperine derivatives, *J. Med. Chem.* 57, 5602-5619.
9. Wimmer, L., Schönbauer, D., Pakfeifer, P., Schöffmann, A., Khom, S., Hering, S., and Mihovilovic, M. D. (2015) Developing piperine towards TRPV1 and GABA<sub>A</sub> receptor ligands—synthesis of piperine analogs via Heck-coupling of conjugated dienes, *Org. Biomol. Chem.* 13, 990-994.



## **2 Introduction**





## 2.1 The current state of CNS drug discovery and development

Disorders of the central nervous system (CNS) continue to be the most devastating illnesses afflicting humanity. According to the World Health Organization (WHO), neurological disorders affect up to one billion people worldwide (1). In Europe, the economic cost of neurological disorders was estimated at €798 billion in 2010 (2). The WHO estimates that over 18 million people in the world suffer from Alzheimer's disease, and projections are for 34 million cases by 2025 (3). Parkinson's disease affects about 5 million people (4), while 2.5 million have been diagnosed with multiple sclerosis (5), and 120 million suffer from depression (6). The extremely high impact of mental illnesses at the personal, social, and economic levels underscores the urgent need for development of new, and better CNS drugs.

CNS drug discovery and development is a long, complex and financially risky process. The low probability of success for CNS drugs is attributable to the complexity of the brain, and to the blood-brain barrier (BBB) with its active drug efflux transporters (e.g. P- glycoprotein). Only 2% of small molecules can cross the BBB and achieve effective therapeutic concentrations in the brain (7). The time to get a new CNS drug to the market takes 13-16 years, whereas for a non-CNS drug it takes 10-12 years (8). Development of CNS drugs costs more than for drugs in any other therapeutic area, yet it has the highest attrition rate. More than 90% of the CNS drug candidates are abandoned during phases I or II of clinical trials. Despite this, the CNS therapeutic area comprises approximately 15% of total pharmaceutical sales, representing about \$50 billion per annum globally (9). Current CNS medicines can relieve symptoms in people with various CNS disorders, but a large number of individuals either do not respond to existing therapies, or the level of improvement from medicinal treatment does not significantly enhance their quality of life. Therefore, new generations of CNS drugs providing higher benefits to patients are urgently needed.

## 2.2 Natural products as a source of CNS-active compounds

*„It is clear Nature will continue to be a major source of new structural leads (...)”*

-Gordon M. Cragg and David J. Newman, *BBA General Subjects*, p. 3670

Mankind has always relied on Nature to fulfill their basic needs, one of which is remedies for the treatment of a wide variety of illnesses (10). In particular, plants as remedies have been used over thousands of years and have formed the basis of sophisticated traditional medical systems (10). The first records on medicinal properties of plants, written on Assyrian clay tablets, are dated from about 2000 B.C. In Europe, the use of plants for medicinal purposes was described in the works of Hippocrates (5<sup>th</sup> century B.C.), Dioscorides (1<sup>st</sup> century A.D.) and Galen (2<sup>nd</sup> century A.D.) (11). Centuries later, Paracelsus (1493-1541) developed the first idea of active principles contained in a medicinal plant (the so-called *Arcanum*, which he considered as an immaterial principle), and the concept of dose dependency for drug action and toxicity (*sola dosis facit venenum*) (11, 12).

The use of natural products as psychoactive agents probably dates from the dawn of humankind, when shamans experimented with mind-altering plants (13). Therefore, it is notable that the psychoactive analgesic morphine was the first alkaloid to be purified from a plant (1805) (13). Modern societies have extensively produced and broadly consumed psychoactive drugs such as coffee, alcohol, and tobacco (14). Natural product screening programs have led to the discovery of a number of CNS active molecules. Most common examples of natural products acting in the brain are summarized in Table 1.

Table 1. Selected CNS-active natural products.

Compound	Source	Type	Mechanism of action	Psychoactivity type	Ref.
Arecoline	<i>Areca catechu</i>	P	M <sub>1</sub> - and M <sub>2</sub> -muscarinic receptor agonist	anti-Alzheimer's	(15)
Bicuculline	<i>Dicentra cucullaria</i>	P	GABA <sub>A</sub> antagonist	convulsant	(16)
Caffeine	<i>Coffea arabica</i>	P	adenosine receptor antagonist	stimulant	(17)
Cocaine	<i>Erythroxylum coca</i>	P	monoamine reuptake blocker	stimulant, analgesic	(17)
Cytisine	<i>Fabaceae</i> family	P	partial nicotinic AChR agonist	stimulant	(18)
Huperzine A	<i>Huperzia serrata</i>	P	AChE inhibitor	anti-Alzheimer's	(11)
Kaempferol	<i>Angiospermae</i> families	P	unknown	anxiolytic	(19)
Mescaline	<i>Lophophora williamsii</i>	P	partial serotonin receptor agonist	hallucinogen	(20)
Morphine	<i>Papaver somniferum</i>	P	μ-opioid receptor agonist	analgesic	(17)
Muscimol	<i>Amanita muscaria</i>	F	GABA <sub>A</sub> agonist	hallucinogen	(17)
Myristicin	<i>Myristica fragrans</i>	P	dopaminergic	hallucinogen	(17)
Nicotine	<i>Nicotiana tabacum</i>	P	nicotinic AChR agonist	stimulant	(17)
Piperine	<i>Piper nigrum</i>	P	GABA <sub>A</sub> agonist	anxiolytic, sedative	(21)
Psilocybin	<i>Psilocybe</i> genus	P	partial serotonin receptor agonist	hallucinogen	(22)
Quercetin	<i>Angiospermae</i> families	P	unknown	anxiolytic	(19)
Salvinorin A	<i>Salvia divinorum</i>	P	κ-opioid receptor agonist	analgesic, hallucinogen, dissociative	(23, 24)
Δ9-Tetrahydrocannabinol	<i>Cannabis sativa</i>	P	non-specific CB <sub>1</sub> receptor agonist	analgesic, hallucinogen	(11, 25)

P: plant; F: fungi; CB<sub>1</sub>: cannabinoid receptor type 1; AChR: acetylcholine receptor; AChE: acetylcholinesterase; GABA<sub>A</sub>: γ-aminobutyric acid receptor type A

There are a number of marketed CNS drugs originating from natural sources. Dihydroergotamine (Migranal<sup>®</sup> nasal spray) is a serotonin 5-HT (1D) receptor agonist introduced as a semi-synthetic product in 1946 for the treatment of migraine and cluster headache. Stoll and Hoffmann prepared it by hydrogenation of the alkaloid ergotamine isolated from fungi of the genus *Claviceps* (26, 27).

Galantamine (Reminyl<sup>®</sup>) is a competitive AChE inhibitor and nicotinic AChR agonist developed by Janssen Pharmaceuticals that was approved in 2001 for the treatment of Alzheimer's disease and various other memory impairments. Galantamine was first isolated from snowdrop (*Galanthus* species) (28, 29).

Another example of an anti-Alzheimer's drug of natural origin is rivastigmine (Exelon<sup>®</sup>). It was developed by Novartis and approved in 2006. The structure of rivastigmine is inspired from the alkaloid physostigmine isolated from *Physostigma venenosum* (27, 30).

Varenicline (Chantix<sup>®</sup> in the USA and Champix<sup>®</sup> in Canada and Europe) is a partial agonist of the  $\alpha_4\beta_2$  nicotinic AChR developed by Pfizer that was approved in 2006 for the treatment of nicotine addiction (31, 32). The structure of varenicline is based on the alkaloid cytosine which is found in various members of *Fabaceae* family (31).

Fingolimod (Gilenya<sup>®</sup>) is a sphingosine-1-phosphate receptor modulator developed by Novartis that was approved by the FDA in 2010 for reducing relapses and delaying disability progression in patients with multiple sclerosis. The design of fingolimod is based on the structure of the fungal metabolite myriocin from *Isaria sinclairii* (31).

Several natural compounds are undergoing clinical evaluation at present. ELND005 (scyllo-inositol) is a naturally occurring inositol stereoisomer found most abundantly in the coconut palm (*Cocos nucifera*). ELND005 is developed by Transition Therapeutics and has been evaluated for the treatment of agitation/aggression in patients with moderate Alzheimer's disease (completed phase II), and for the treatment of Down syndrome patients without dementia (completed phase II) (31, 33).

Epigallocatechin gallate is a green tea polyphenol that prevents aggregation of  $\beta$ -amyloid to toxic oligomers and thus has a positive influence on the course of Alzheimer's disease. It is being investigated in phase II clinical trials by the Charité Clinic (31, 34).

GTS-21 is a derivative of the alkaloid anabaseine produced by Pacific nemertine worm *Paranemertes peregrine*. It is being evaluated as a sustained release formulation by the University of Colorado in a phase II trial for the treatment of patients with schizophrenia who also smoke cigarettes (31, 35).

Natural products represent an invaluable source of bioactive compounds and structural diversity, with recognized potential in drug discovery. They complement synthetic molecules since about 40% of the chemical scaffolds present in natural products are absent in today's medicinal chemistry (36). Natural products demonstrate advanced binding properties compared to synthetics, most probably due to their sterically complex structures (36). However, screening of natural products extracts is a time-consuming process because the screening step has to be followed by isolation of the active compound from the hit extract and structure elucidation. Other challenges related to natural products are the resupply of raw material since it is not constantly available in sufficient amounts, and political objections due to protection of biological resources (36). Although natural products-based drug discovery is associated with some difficulties, a significant number of natural products and their derivatives as marketed drugs or in various stages of clinical development emphasize the importance of natural products as sources of new drug candidates.

## References

1. WHO (2007) *Neurological disorders: Public health challenges*, WHO.
2. Nutt, D. J., and Attridge, J. (2014) CNS drug development in Europe—past progress and future challenges, *Neurobiol. Dis.* 61, 6-20.
3. Kapoor, M. C. (2011) Alzheimer's disease, anesthesia and the cholinergic system, *J. Anaesthesiol. Clin. Pharmacol.* 27, 155.
4. Dorsey, E. R., Constantinescu, R., Thompson, J. P., Biglan, K. M., Holloway, R. G., Kieburtz, K., Marshall, F. J., Ravina, B. M., Schifitto, G., and Siderowf, A. (2007) Projected number of people with Parkinson disease in the most populous nations, 2005 through 2030, *Neurology.* 68, 384-386.
5. Haussleiter, I. S., Brüne, M., and Juckel, G. (2009) Review: Psychopathology in multiple sclerosis: diagnosis, prevalence and treatment, *Ther. Adv. Neurol. Disord.* 2, 13-29.
6. WHO (2001) *Mental health: new understanding, new hope*, WHO.
7. Pardridge, W. M. (2006) Molecular Trojan horses for blood–brain barrier drug delivery, *Curr. Opin. Pharmacol.* 6, 494-500.
8. Alavijeh, M. S., Chishty, M., Qaiser, M. Z., and Palmer, A. M. (2005) Drug metabolism and pharmacokinetics, the blood-brain barrier, and central nervous system drug discovery, *NeuroRx.* 2, 554-571.
9. Kelly, J. (2009) *Principles of CNS drug development: from test tube to clinic and beyond*, John Wiley & Sons, Singapore.
10. Cragg, G. M., and Newman, D. J. (2013) Natural products: a continuing source of novel drug leads, *Biochim. Biophys. Acta.* 1830, 3670-3695.
11. Potterat, O., and Hamburger, M. (2008) Drug discovery and development with plant-derived compounds, in *Natural Compounds as Drugs Volume I* (Petersen, F., and Amstutz, R., Eds.), pp 45-118, Birkhäuser Basel.
12. Ravina, E. (2011) *The evolution of drug discovery: from traditional medicines to modern drugs*, John Wiley & Sons, Weinheim.
13. Clement, J. A., Yoder, B. J., and Kingston, D. G. I. (2004) Natural products as a source of CNS-active agents, *Mini Rev. Org. Chem.* 1, 183-208.
14. Ujváry, I. (2014) Psychoactive natural products: overview of recent developments, *Ann. I. Super. Sanita.* 50, 12-27.
15. Asthana, S., Greig, N. H., Holloway, H. W., Raffaele, K. C., Berardi, A., Schapiro, M. B., Rapoport, S. I., and Soncrant, T. T. (1996) Clinical pharmacokinetics of arecoline in subjects with Alzheimer's disease, *Clin. Pharmacol. Ther.* 60, 276-282.
16. Johnston, G. A. R. (2013) Advantages of an antagonist: bicuculline and other GABA antagonists, *Br. J. Pharmacol.* 169, 328-336.
17. Spinella, M. (2001) *The psychopharmacology of herbal medicine: plant drugs that alter mind, brain, and behavior*, 1st ed., MIT Press, London.
18. Papke, R. L., and Heinemann, S. F. (1994) Partial agonist properties of cytisine on neuronal nicotinic receptors containing the beta 2 subunit, *Mol. Pharmacol.* 45, 142-149.
19. Vissienon, C., Nieber, K., Kelber, O., and Butterweck, V. (2012) Route of administration determines the anxiolytic activity of the flavonols kaempferol, quercetin and myricetin—are they prodrugs?, *J. Nutr. Biochem.* 23, 733-740.
20. Halberstadt, A. L. (2015) Recent advances in the neuropsychopharmacology of serotonergic hallucinogens, *Behav. Brain Res.* 277, 99-120.
21. Zaugg, J., Baburin, I., Strommer, B., Kim, H.-J., Hering, S., and Hamburger, M. (2010) HPLC-based activity profiling: discovery of piperine as a positive GABA<sub>A</sub> receptor modulator targeting a benzodiazepine-independent binding site, *J. Nat. Prod.* 73, 185-191.
22. Lee, H.-M., and Roth, B. L. (2012) Hallucinogen actions on human brain revealed, *Proc. Natl. Acad. Sci. USA* 109, 1820-1821.
23. Roth, B. L., Baner, K., Westkaemper, R., Siebert, D., Rice, K. C., Steinberg, S., Ernsberger, P., and Rothman, R. B. (2002) Salvinorin A: a potent naturally occurring nonnitrogenous  $\kappa$  opioid selective agonist, *Proc. Natl. Acad. Sci. USA.* 99, 11934-11939.

24. MacLean, K. A., Johnson, M. W., Reissig, C. J., Prisinzano, T. E., and Griffiths, R. R. (2013) Dose-related effects of salvinorin A in humans: dissociative, hallucinogenic, and memory effects, *Psychopharmacology*. 226, 381-392.
25. Gaoni, Y., and Mechoulam, R. (1964) Isolation, structure, and partial synthesis of an active constituent of hashish, *J. Am. Chem. Soc.* 86, 1646-1647.
26. Silberstein, S. D., and McCrory, D. C. (2003) Ergotamine and dihydroergotamine: history, pharmacology, and efficacy, *Headache*. 43, 144-166.
27. Sneader, W. (1996) *Drug Prototypes and their Exploitation*, John Wiley & Son, Bath.
28. Heinrich, M., and Teoh, H. L. (2004) Galanthamine from snowdrop—the development of a modern drug against Alzheimer's disease from local Caucasian knowledge, *J. Ethnopharmacol.* 92, 147-162.
29. Lilienfeld, S. (2002) Galantamine—a novel cholinergic drug with a unique dual mode of action for the treatment of patients with Alzheimer's disease, *CNS Drug Rev.* 8, 159-176.
30. Orhan, G., Orhan, I., Subutay-Oztekin, N., Ak, F., and Sener, B. (2009) Contemporary anticholinesterase pharmaceuticals of natural origin and their synthetic analogues for the treatment of Alzheimer's disease, *Recent Pat. CNS Drug Discov.* 4, 43-51.
31. Butler, M. S., Robertson, A. A. B., and Cooper, M. A. (2014) Natural product and natural product derived drugs in clinical trials, *Nat. Prod. Rep.* 31, 1612-1661.
32. Rollema, H., Chambers, L. K., Coe, J. W., Glowa, J., Hurst, R. S., Lebel, L. A., Lu, Y., Mansbach, R. S., Mather, R. J., and Rovetti, C. C. (2007) Pharmacological profile of the  $\alpha 4\beta 2$  nicotinic acetylcholine receptor partial agonist varenicline, an effective smoking cessation aid, *Neuropharmacol.* 52, 985-994.
33. Salloway, S., Sperling, R., Keren, R., Porsteinsson, A. P., Van Dyck, C. H., Tariot, P. N., Gilman, S., Arnold, D., Abushakra, S., and Hernandez, C. (2011) A phase 2 randomized trial of ELND005, scyllo-inositol, in mild to moderate Alzheimer disease, *Neurology*. 77, 1253-1262.
34. Dragicevic, N., Smith, A., Lin, X., Yuan, F., Copes, N., Delic, V., Tan, J., Cao, C., Shytle, R., and Bradshaw, P. C. (2011) Green tea epigallocatechin-3-gallate (EGCG) and other flavonoids reduce Alzheimer's amyloid-induced mitochondrial dysfunction, *J. Alzheimers Dis.* 26, 507-521.
35. Freedman, R., Olincy, A., Buchanan, R. W., Harris, J. G., Gold, J. M., Johnson, L., Allensworth, D., Alejandrina Guzman-Bonilla, B. A., Clement, B., and Ball, M. P. (2008) Initial phase 2 trial of a nicotinic agonist in schizophrenia, *Am. J. Psych.* 165, 1040-1047.
36. Müller-Kuhrt, L. (2003) Putting nature back into drug discovery, *Nat. Biotechnol.* 21, 602.

## 2.3 Drug metabolism and pharmacokinetics (DMPK)

„By far the most complex systems that we have are our own bodies”

-Stephen Hawking, “*The Universe in a Nutshell*”, p. 37

High attrition rate in drug development remains one of the key challenges for pharmaceutical industry (1). Over the past decades, considerable progress has been made to reduce the number of failures caused by a poor DMPK profile of drug substances. DMPK screenings incorporated in early drug discovery help to identify leads with favorable DMPK characteristics. Numerous *in vitro* and *in vivo* models, along with advanced instrumentation, are now available to make relatively reliable predictions from *in vitro* to *in vivo*, and from animals to humans (2). Thus, implementation of DMPK screening strategies in early drug discovery has increased the success rate due to the selection of better quality candidates moving through the pipeline.

### 2.3.1 Drug metabolism

Drug metabolism is the process where drugs are enzymatically altered, typically to more water soluble metabolites, to aid excretion from the body (3). Rapidly metabolized drugs may require multiple daily dosing or higher doses to maintain a sufficient level needed to produce a therapeutic effect. For prodrugs, which are administered as an inactive form and then converted into the active drugs in the body, rapid metabolism is beneficial (3). Very slowly metabolized drugs may remain in the body for long periods, causing accumulation and toxicity. Drug metabolism is generally divided into two groups, termed phase I and phase II metabolism.

#### 2.3.1.1 Phase I metabolism

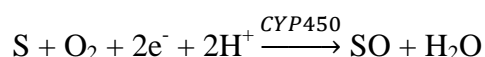
Phase I metabolism includes reactions such as oxidation, reduction and hydrolysis (Table 2). The major enzymes that catalyze phase I reactions are the cytochrome P450 (CYP450) superfamily, the flavin-containing monooxygenases (FMO), the monoamine oxidases (MAO), alcohol (ADH) or aldehyde (ALDH) dehydrogenases, reductases, esterases, amidases and epoxide hydrolases (3). CYP450 and FMO enzymes are bound to the membrane of the smooth endoplasmic reticulum, the fragments of which, after differential centrifugation, are associated with the microsomal fractions. Non-microsomal enzymes (e.g. MAO, ADH, ALDH) are mainly present in mitochondria and cytoplasm of hepatocytes.



Table 2: Phase I metabolic reactions. Modified from Davis, A., 2014 (4).

Reaction type	Pathway
Oxidation	Aromatic hydroxylation Aliphatic hydroxylation Epoxidation N-, O-, S-dealkylation Alcohol oxidation Aldehyde oxidation N-, S-oxidation Dehydrogenation
Reduction	Nitro-reduction to hydroxylamine, amines Carbonyl-, aldehyde-, aldose-reduction to alcohol
Hydrolysis	Ester hydrolysis to acid and alcohol Amide hydrolysis to acid and amine

Since most of the marketed drugs are cleared by hepatic CYP-mediated metabolism, CYP450 enzymes will be further discussed in this subchapter. CYP450 enzymes are a superfamily of heme-containing proteins that catalyze the oxidative metabolism of drugs. The CYP-mediated oxidation proceeds as follows:



The oxygen is bound to the heme of the CYP enzyme. Two protons, which are essential for a reductive splitting of the molecular oxygen into atoms, are provided by NAD(P)H cofactors. CYP450 inserts one oxygen atom to a substrate (S) and reduces the second oxygen to a water molecule. CYP450 utilizes two electrons that are provided by NAD(P)H via a reductase protein (5). In humans, nearly 60 CYPs have been identified thus far, however only some CYP isoforms are relevant to drug metabolism (Fig. 1).

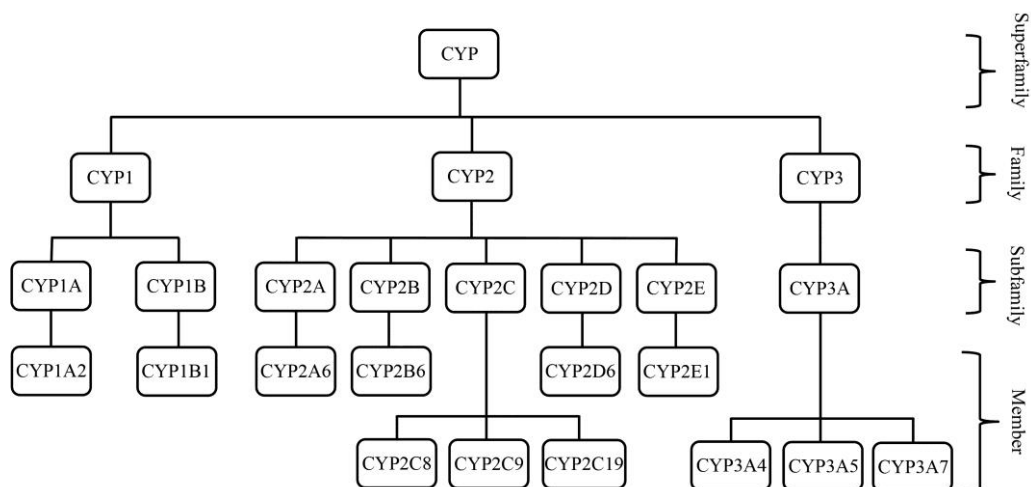


Figure 1: CYP450 nomenclature with the most relevant isoforms to drug metabolism. Modified from Nassar, A. F., 2009 (6).

Drugs, food constituents, and environmental chemicals can either induce or inhibit CYP enzymatic activity which may cause unanticipated clinical consequences. Enzyme induction can lead to a potential reduction in drug efficacy or an increased formation of reactive (toxic) metabolites. In the case of enzyme inhibition, decreased metabolism may result in elevated plasma levels of the drug and may cause toxicity. A selected list of CYP450 inducers and inhibitors appears in Table 3.

Table 3: Selected CYP450 inducers and inhibitors.

<b>CYP isoform</b>	<b>Inducers</b>	<b>Inhibitors</b>
CYP1A2	Broccoli, cigarette smoking, omeprazole	Furafylline, cimetidine, amiodarone
CYP1B1	Polycyclic aromatic hydrocarbons, $\beta$ -naphthoflavone	Coumarins, resveratrol, flutamide
CYP2A6	Phenobarbital, rifampin	Tranlycypromine, methoxsalen
CYP2B6	Phenobarbital, rifampin, phenytoin	Clopidogrel, ticlopidine, thiotepa
CYP2C8	Phenobarbital, rifampin	Quercetin, montelukast, gemfibrozil
CYP2C9	Secobarbital, rifampin	Sulfaphenazole, fluconazole, valproic acid
CYP2C19	Carbamazepine, rifampin, artemisinin	Fluoxetine, chloramphenicol, moclobemide
CYP2D6	Rifampin	Fluoxetine, quinidine, Cimetidine, paroxetine
CYP2E1	Ethanol, acetone, isoniazid	Diethyldithiocarbamate, clomethiazole, diallyl disulfide
CYP3A4/5	Phenobarbital, rifampin, carbamazepine	Ketoconazole, itraconazole, verapamil, grapefruit juice

The highest expression of CYP enzymes is found in the liver, while lower levels of CYPs are also found in extra-hepatic sites such as intestine, lungs, kidneys, brain, skin, nasal and tracheal mucosa, placenta, ovaries, testes, adrenal gland, and pancreas (7). Contribution of extra-hepatic CYPs to the overall metabolism of drugs and total body clearance is minor; however extra-hepatic CYPs may affect the absorption of drugs into systemic circulation and their local disposition, and may therefore modify pharmacological effects of drugs (7).

### **2.3.1.2 Phase II metabolism**

Phase II metabolism involves conjugation with an endogenous substance (e.g. glucuronic acid, sulfate, glutathione). Phase II reactions can be sequential to Phase I reactions or may occur directly if susceptible functional groups such as  $-\text{OH}$ ,  $-\text{COOH}$ ,  $-\text{NH}_2$ ,  $-\text{SH}$  are present on the molecule (3). Phase II metabolizing enzymes mainly belong to the class of transferases

(Table 4). Most of phase II enzymes are found in the cytosol of the hepatocytes, except uridine diphosphate (UDP)-glucuronosyltransferase which is a microsomal enzyme.

Table 4: Phase II metabolic reactions. Modified from Evans, G., 2004 (8).

<b>Reaction type</b>	<b>Enzyme</b>
Glucuronidation	UDP-glucuronosyltransferase
Sulfation	Sulfotransferase
Methylation	Methyltransferase
Acetylation	Acetyltransferase
Glutathione conjugation	Glutathione-S-transferase
Amino acid conjugation	Acyl-CoA synthetase and acyl-CoA: amino acid N-acyltransferase

Generally, the conjugative metabolism diminishes or abolishes biological activities. However, in some cases, like with morphine-6-glucuronide and 4-hydroxytramterene sulfate, the conjugated metabolites possess enhanced biological activity (9, 10). Glucuronidation is a significant pathway in the phase II metabolism of various exogenous and endogenous compounds. The conjugation of glucuronic acid to a substrate is catalyzed by a family of enzymes called UDP-glucuronosyltransferases or UGTs (8). The cofactor uridine diphosphoglucuronic acid (UDPGA) acts as a donor of glucuronic acid for UGTs. The glucuronide conjugates are recognized by the biliary and renal organic anion transporter proteins, which enable their excretion into urine and bile. Although the liver is recognized as the major site of glucuronidation, many other organs such as nasal mucosa, the gut, kidneys, skin, leukocytes, lungs, brain, breast, placenta, prostate, and uterus have also been reported to express a panel of UGT isoforms (11). In humans, two subfamilies of UGT1A and UGT2B are mainly involved in the metabolism of xenobiotics.

Another significant phase II detoxification pathway is sulfation. The reactions are catalyzed by the family of enzymes called sulfotransferases (SULTs). These enzymes catalyze the transfer of sulfonate group ( $\text{SO}_3^-$ ) from the cofactor 3'-phosphoadenosine-5'-phosphosulfate (PAPS) to a substrate. In humans four SULT families (SULT1, SULT2, SULT4 and SULT6) have been identified. Similar to the glucuronidation reactions, sulfation occurs in various tissues, but the main sites are the liver and small intestine (8).

Methylation is a common but minor metabolic route in the overall metabolism of xenobiotics which does not generally increase the aqueous solubility of substrates. It is primarily involved

in the metabolism of endogenous compounds (e.g. neurotransmitters). Methyltransferases catalyze the transfer of a methyl group from the co-factor S-adenosylmethionine (SAM) to a substrate.

Acetylation is an important biotransformation pathway for xenobiotics containing either aromatic amines or hydrazines, which are converted to aromatic amides and hydrazides (8). Acetyltransferases catalyze the transfer of an acetyl group from the cofactor acetyl-coenzyme A (acetyl-CoA) to a substrate.

Conjugation of glutathione with reactive metabolites plays an important role in the detoxification mechanism of many xenobiotics. Glutathione is a tripeptide ( $\gamma$ -glutamic acid-cysteine-glycine) which can be found in every cell of the human body with the highest concentration in hepatocytes. Glutathione conjugated metabolites are immediately excreted into bile or transported to the kidneys where they are subjected to further metabolism into mercapturic acids and excretion into urine (8).

Xenobiotics with a carboxyl group can undergo conjugation with amino acids, most commonly glycine, glutamine and taurine (8). The mechanism of biotransformation includes two enzymatic processes: first, formation of a reactive xenobiotic-CoA thioester intermediate catalyzed by acyl-CoA synthetase, and second, linkage of the activated acyl group via an acyl-CoA: amino acid N-acyltransferase to the amino group of the acceptor amino acid (12).

### **2.3.1.3 Factors affecting drug metabolism**

Factors affecting drug metabolism can be divided into three major categories: genetic, environmental, and physiological. Individual variability in drug efficacy and safety can be explained in some cases by genetic variations (genetic polymorphism) resulting in four different phenotypes: poor metabolizers, intermediate metabolizers, extensive metabolizers and ultrarapid metabolizers (3). Genetic differences in the expression of metabolizing enzymes are more commonly observed in specific ethnic groups. For instance, the CYP2D6 poor metabolizer phenotype is more frequent in the Caucasian population compared to Asians (3). Conversely, the CYP2C19 poor metabolizer phenotype is more frequent in the Asian population compared to the Caucasian population (3). Environmental factors include environmental chemicals (e.g. heavy metals, industrial pollutants, insecticides, herbicides) which may induce and/or inhibit the activity of metabolizing enzymes. Physiological factors include those related to age, disease state, and gender (including hormonal cycle) (6). Metabolism differs between the very young and the elderly. Newborns lack drug metabolizing enzymes except CYP3A7 and SULT (6). In the elderly a decrease in metabolic rate is often observed due to the reduced hepatic blood flow (6). Some pathological

conditions like impaired hepatic and renal function can significantly affect drug metabolism leading to the risk of adverse effects.

## **2.3.2 Strategies to study drug metabolism**

### **2.3.2.1 *In vitro* models**

Since the liver is the major metabolic organ, the *in vitro* models used to investigate drug metabolism often focus on hepatocytes or subcellular fractions of the liver where concentrations of metabolizing enzymes are high [3].

#### **Metabolic stability assessment**

##### *Liver microsomes*

Microsomes are subcellular fractions containing the endoplasmic reticulum-localized metabolizing enzymes. Microsomes are the most widely used *in vitro* system to investigate both CYP-mediated and UGT-mediated metabolism. Incubations with microsomes require an addition of the appropriate cofactor (NADPH or UDPGA). The advantages of using microsomes in metabolism studies are their relatively low cost, easy preparation and storage, and applicability to high throughput screening. However, for compounds which are mainly eliminated from the body via phase II metabolism, microsomal incubations tend to underpredict intrinsic clearance (3). In addition, metabolites formed by cytosolic enzymes will not be detected with this system.

##### *Liver S9*

Liver S9 is the post-mitochondrial supernatant fraction containing both microsomal and cytosolic enzymes (3). As with microsomes, incubations with S9 require an addition of the appropriate cofactor. Because of the lower enzymatic activity in the S9 fractions compared to microsomes, the S9 systems are often used for qualitative purposes to identify if cytosolic enzymes are responsible for the formation of a metabolite (3).

##### *Hepatocytes*

Hepatocytes are whole cells containing the full spectrum of phase I and phase II metabolizing enzymes, cofactors, and transporters. Cryopreservation techniques ensure cell viability and enable cells to be stored for long periods of time (3). The drawbacks of this system are associated with a complicated, time consuming, and costly hepatocyte isolation method, inter-lot variability in enzymatic activity, and short incubation time (due to limited viable period of hepatocytes) for the experiments.

## **Reaction phenotyping**

Reaction phenotyping is used to determine which enzymes are involved in the metabolism of a test substance (3). The data from these studies can be important for identification of the potential drug interactions with common co-medications used in the clinic, and also the possible differences in pharmacokinetics caused by genetic polymorphism in certain enzymes (3). Several *in vitro* approaches have been developed to study reaction phenotyping:

### *Correlation analysis*

Correlation analysis relies on statistical analysis to establish a correlation between the metabolic rates of a test compound and marker substrate for each individual CYP enzyme (13). Pools of human liver microsomes (donors  $\geq 10$ ) previously characterized for activity towards individual probe substrates are used to correlate with the activity towards the test compound (3).

### *Inhibition of metabolism*

Inhibition of specific enzymatic pathways using selective chemical inhibitors or antibodies is another approach for reaction phenotyping. A battery of incubations with various inhibitors and a test compound is performed to identify which inhibitor reduces the overall metabolism to the greatest extent, and thus uncover the enzymatic pathway that contributes to the clearance of a test compound (14).

### *Recombinant enzymes*

Recombinant enzymes are manufactured by transfecting a human cDNA of a specific enzyme into a vector, with its further transfer into a rapidly growing and easily cultured host (e.g. *Escherichia coli*) (6). A panel of recombinant human CYP and UGT enzymes is available to investigate the metabolic pathways of a test compound by substrate-depletion method.

### *Silensomes™*

Recently, novel systems called Silensomes™ have been developed for CYP reaction phenotyping. Silensomes™ are human pooled liver microsomes in which one specific CYP has been chemically and irreversibly inactivated using mechanism based inhibitors. Incubations with Silensomes™ are accompanied by control incubations in which enzymatic activity of all CYPs is preserved. Contribution of each CYP isoform can be determined by comparing the substrate disappearance in Silensomes™ and the controls.

## **CYP450 induction/inhibition assessment**

CYP450 induction assays help to identify a potential of the test compound to increase the activity of CYP isoenzymes. Induction of CYP isoenzymes may lead to therapeutic failure of the drug caused by a decreased systemic exposure or to toxicity as a result of increased

formation of toxic metabolites. Incubations of a test substance and isoform specific probe substrates are conducted with human hepatocytes from at least three donors and compared to controls. Increased mRNA levels due to increased transcription of CYP genes, as well as increased formation of the isoform specific metabolites in the presence of the test compound indicate induction of CYP isoenzymes.

CYP450 inhibition assays help to identify a potential of the test compound to inhibit a specific CYP450 enzyme. Inhibition of a drug's metabolism may lead to increased plasma levels resulting in toxicity. Isoform-specific probe substrates are incubated individually with the test compound in the presence of human liver microsomes or recombinant enzymes, and a cofactor (3). Ideally, probe substrates should be predominantly metabolized by a single isoenzyme with no sequential metabolism (3). Formation of metabolites is monitored in the test incubations and compared to the controls.

#### **2.3.2.2 *In vivo* models**

Multi-species animal metabolism studies are initially conducted with non-radiolabeled compounds to understand the main elimination pathways and systemic metabolite exposure, and to find relevant species for preclinical development. Thereafter, mass balance studies with <sup>14</sup>C- or <sup>3</sup>H-radiolabeled compounds are performed to obtain additional information, including (i) mass recovery, (ii) metabolic profile, (iii) abundance of metabolites in excreta and circulation, (iv) exposure of parent compound and its metabolites in different organs and tissues at different time intervals, and (v) pharmacokinetic properties of parent compound and its metabolites (12). The preclinical *in vivo* data are used to predict human outcomes, and select candidates for progression towards phase I clinical studies. Human metabolites can differ from those identified in the animal species or be present at disproportionately higher levels, and thus can raise safety concerns (15). Radiolabeled human metabolism studies to address safety related issues of drug metabolites are mandatory early in clinical development before large numbers of patients get enrolled in clinical trials.

### 2.3.3 Pharmacokinetics

Pharmacokinetics (PK) is a quantitative study of the time course of drug and metabolite concentrations in the body (16). The term PK originates from the ancient Greek words pharmakon and kinetikos meaning "drug" and "moving", respectively. PK data are used to optimize the dose, dosage regime, and dosage form. Five key PK parameters that are used in drug discovery and development will be discussed in more detail below, namely elimination half-life, area under the curve, total clearance, apparent volume of distribution, and bioavailability.

#### 2.3.3.1 Pharmacokinetic parameters

##### *Elimination half-life*

Elimination half-life ( $t_{1/2}$ ) is the time required to reduce the drug concentration by half (17). The unit for  $t_{1/2}$  is typically expressed in min or h. The  $t_{1/2}$  can be calculated as follows:

$$t_{1/2} = \frac{0.693}{k_e}$$

The  $k_e$  is the elimination rate constant which can be determined from the slope of the line (so called linear regression analysis) fitted to the terminal portion of ln (Fig. 2A) or log (Fig. 2B) drug concentrations versus time profile.

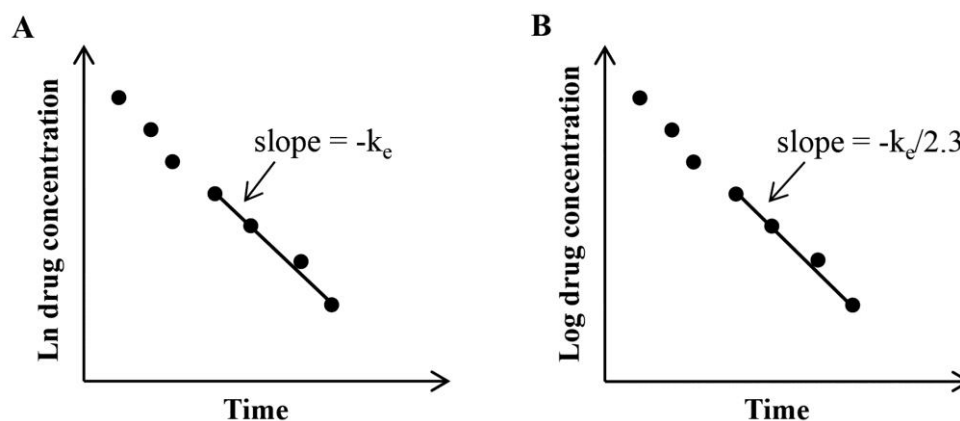


Figure 2: Determination of the elimination rate constant ( $k_e$ ) by linear regression analysis for ln (A) and log (B) drug concentrations versus time profiles.

The  $t_{1/2}$  depends on volume of distribution ( $V_d$ ) and clearance (Cl), and thus can be calculated using the following equation:

$$t_{1/2} = 0.693 \times \frac{V_d}{Cl}$$

The  $t_{1/2}$  is used to determine the dosing interval. Drugs with a shorter half-life (higher elimination rate) should be generally given more frequently, than drug with a longer half-life



(lower elimination rate) (17). With each subsequent dose, maximum (peak) and minimum (trough) concentrations increase until equilibrium is reached (17). When equilibrium occurs, peak and trough concentrations remain constant with each subsequent dose (17). The condition at which the amount of drug administered over a dosing interval equals the amount of drug being eliminated over that same period is called steady state (17). The time of four to five half-lives is needed to reach the steady state.

#### *Area under the curve*

Area under the curve (AUC) is a measure of the total drug exposure over time (18). The AUC is expressed as h\*mg/l. The most common method for the calculation of AUC is the linear trapezoidal rule, where the drug concentrations versus time plot is considered as a sequence of trapezoids (Fig. 3). The trapezoidal area between two data points (for example,  $C_1, t_1$  and  $C_2, t_2$ ) can be calculated as follows:

$$AUC_{t_1 \rightarrow t_2} = 0.5 \times (C_1 + C_2) \times (t_2 - t_1)$$

The total area of all the trapezoids reflects the AUC. Comparison of AUCs from drug leads helps to select the lead with the highest exposure level. Also, the AUC is used to calculate other PK parameters, such as clearance and bioavailability.

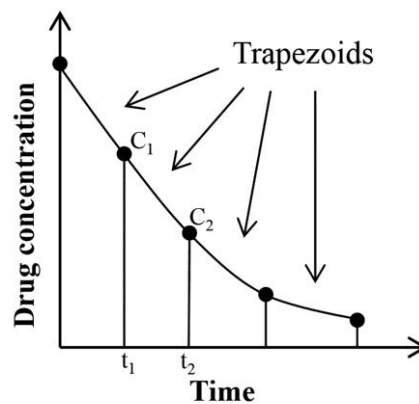


Figure 3: Area under the drug concentrations versus time curve viewed as a sequence of trapezoids.

#### *Total clearance*

Total clearance (Cl) is the volume of body fluid cleared from the drug per unit of time (17). Drugs, either in unchanged forms or as metabolites, are eliminated from the body by excretion and metabolism. Thus, the total Cl is the sum of all individual organ clearances. The unit for Cl is expressed in l/h. The total Cl can be calculated from the expression:

$$Cl = \frac{\text{Dose}}{\text{AUC}}$$

If there is no saturation of elimination mechanisms, the Cl is constant over the dose range, and the drug follows first-order kinetics. Highly cleared drugs require higher doses or frequent administration to maintain a certain level of exposure needed to achieve the therapeutic effect. This negatively impacts cost and treatment acceptability.

#### *Apparent volume of distribution*

Apparent volume of distribution ( $V_d$ ) indicates how widely the compound is distributed in the body (19). The unit for  $V_d$  is typically reported in l/kg or ml/kg of body weight. The  $V_d$  can be calculated using the following expression:

$$V_d = \frac{\text{Dose}}{C_0}$$

$C_0$  is the initial drug concentration in plasma after intravenous administration, before elimination has started.  $C_0$  can be determined on the semi-logarithmic graph of drug concentrations versus time by extrapolation back to time zero. The  $V_d$  is associated with Cl and  $k_e$  and thus can be calculated as follows:

$$V_d = \frac{\text{Cl}}{k_e}$$

$V_d$  is dependent on the properties of the drug. Hydrophilic drugs have small  $V_d$ , close to the volume of blood (approximately 0.07 l/kg) (19). Those drugs tend to be restricted to the bloodstream and do not enter the tissues in significant amounts (19). Moderately lipophilic drugs have  $V_d$  which is in the range of the volume of body water (approximately 0.7 l/kg) (19). Highly lipophilic drugs tend to bind extensively to tissues, and thus have a  $V_d$  which exceeds the volume of body water.

#### *Bioavailability*

Bioavailability (F) is a fraction of the administered dose that reaches the systemic circulation in the unchanged form (19). It is expressed in %. When a drug is administered intravenously, the F is equal to 100%. The F of orally administered (po) drugs can be determined from the equation:

$$F = 100 \times \frac{\text{AUC}_{\text{po}} \times \text{Dose}_{\text{iv}}}{\text{AUC}_{\text{iv}} \times \text{Dose}_{\text{po}}}$$

The F can be affected by several factors, such as incomplete intestinal absorption, first-pass metabolism, decomposition of the drug in the lumen, drug formulation, and presence/absence of food (food effect). Low bioavailability causes high patient-to-patient variability in plasma concentrations and thus may have a negative impact on the treatment outcome. Thereby, for orally administered drug candidates to be taken into clinical development, many pharmaceutical companies set the F limit of 20% (20).

### **2.3.3.2 Pharmacokinetic data analysis**

The main PK parameters can be calculated as described above using non-compartmental analysis in which a body is considered as a kinetically homogenous unit. Another approach in the PK data processing includes compartmental analysis which applies mathematical models to describe the changes in drug concentration over time. In compartmental analysis a body is considered as subdivided into one, two or multi compartments, each representing a group of similar tissues or fluids. Therefore, blood (plasma), heart, lungs, liver, and kidneys are combined into one compartment usually referred to as the central compartment (17). The adipose tissue, muscles, bones are grouped in the peripheral compartment. In compartmental analysis calculation of the PK parameters are based on fitting an appropriate compartmental model to the PK data. Specific computer programs (e.g. WinNonlin<sup>®</sup>) are usually used to do that. WinNonlin<sup>®</sup> includes a library of PK compartmental and pharmacodynamic models, non-compartmental analysis, and it also supports the creation of custom models.

### **2.3.4 Plasma protein binding**

Plasma protein binding is the reversible association of a drug with the plasma proteins (8). The interactions of drugs and plasma proteins are electrostatic and hydrophobic (19). Common human plasma proteins that drugs bind to are human serum albumin and  $\alpha$ 1-acid glycoprotein. The drug-plasma protein complex cannot diffuse across the cell membranes to reach the target tissue. Only free drug passes through membranes, and only free drug is available for liver metabolism and renal excretion (19). Drugs that are highly and tightly bound to plasma proteins may not be able to exert their therapeutic effect, but if the drug has a fast kinetic (high dissociation rate) protein binding may not impact distribution of the drug into tissues, its metabolism, excretion, and efficacy (19). Plasma protein binding can influence the PK properties of the drug ( $V_d$ , Cl,  $t_{1/2}$ ) and, therefore, the extent of protein binding should be determined during the lead optimization process.

### **2.3.5 Techniques for measurement of plasma protein binding**

#### *Equilibrium dialysis*

Equilibrium dialysis is the gold standard for measurement of plasma protein binding. As a typical example of equilibrium dialysis, the mixture of a drug with plasma proteins is separated from a buffer solution by a semi-permeable membrane with a known molecular mass cut-off (Da) (8). Diffusion of the drug across the membrane continues until the concentration of free drug is equal on both sides of the membrane (equilibrium has been reached) (8). After the incubation at the desired temperature, samples from both reservoirs

are taken and analyzed for drug concentrations. The unbound fraction ( $f_u$ ) can be calculated as follows:

$$f_u = 1 - \left( \frac{CP - CB}{CP} \right)$$

CP is the drug concentration in the plasma reservoir; CB is the drug concentration in the buffer reservoir. Even though equilibrium dialysis approach has been widely used, it suffers from several drawbacks that limit its application in the pharmaceutical industry. The method requires a big sample volume, pre-conditioning of the dialysis membrane, long time to reach equilibrium (up to 24 h). Such long incubation time may associate with volume shift, meaning an increase in plasma volume and decrease in buffer volume due to the difference in osmotic pressure between plasma and buffer (21). Also, long incubation time may result in drug degradation in plasma. As an alternative to classic dialysis, *rapid equilibrium dialysis* (RED) method has been developed. The RED device represents a 96-well plate with equilibrium dialysis membrane inserts. Each insert is comprised of two chambers for sample and buffer with a semi-permeable membrane in between. The RED does not require pre-conditioning of the dialysis membrane. The increased membrane surface-to-volume ratio allows achieving equilibrium in 4 h. The base plate of RED device is made from Teflon to minimize non-specific binding of test compound. The RED is a fast and reliable technique which suitable for high-throughput screening format.

#### *Ultrafiltration*

Ultrafiltration is based on the physical separation of free drug in plasma from the drug bound to proteins, by filtering plasma samples through a semipermeable membrane with a known molecular mass cut-off under a positive pressure generated by centrifugation (21). The unbound fraction can be calculated from the equation:

$$f_u = \frac{C_f}{C_p}$$

$C_f$  is the concentration of drug in the ultrafiltrate after centrifugation;  $C_p$  is the initial concentration of drug in plasma before centrifugation. The ultrafiltration technique has several advantages over equilibrium dialysis: small sample volume, fast (takes 15-30 min), no buffer needed, relative low cost (21). However, a major drawback is non-specific binding of a drug to the plastic surfaces or to the ultrafiltration membrane. Although non-specific binding can be overcome by pre-treatment of the ultrafiltration membrane with Tween-80, or by performing separate studies using water spiked with the drug (used for correction of non-specific binding), equilibrium dialysis is considered to be a more reliable method for protein binding measurements, if non-specific binding is more than 20% (21).

### *Ultracentrifugation*

In ultracentrifugation, the drug-protein complex is pelleted by using high speed centrifugation (e.g. 500000 g), leaving the free drug in the supernatant (8). After centrifugation, an aliquot of supernatant is taken to measure the free drug concentration (8). The unbound fraction can be calculated as follows:

$$f_u = \frac{C_s}{C_p}$$

$C_s$  is the concentration of drug in the supernatant;  $C_p$  is the initial concentration of drug in plasma before the experiment. Several factors like costly equipment, long centrifugation time, low sample throughput, physical phenomena (sedimentation, back diffusion) limit the application of this technique (8).

### **2.3.6 Red blood cell binding**

The PK parameters are usually determined by quantification of drug in plasma rather than whole blood. Therefore, drug molecules that bind to erythrocytes will not be measured in the sample (19). Extensive binding to erythrocytes limits the amount of free drug available for metabolizing enzymes and thus reduces the drug clearance. Binding of a drug to erythrocytes could be an explanation for low plasma concentrations or unexplained clearance, especially from iv dosing (19). Therefore, evaluation of red blood cell binding is important for the thorough interpretation of the drug's PK.

## References

1. Waring, M. J., Arrowsmith, J., Leach, A. R., Leeson, P. D., Mandrell, S., Owen, R. M., Pairedeau, G., Pennie, W. D., Pickett, S. D., and Wang, J. (2015) An analysis of the attrition of drug candidates from four major pharmaceutical companies, *Nat. Rev. Drug Discov.* *14*, 475-486.
2. Zhang, D., Luo, G., Ding, X., and Lu, C. (2012) Preclinical experimental models of drug metabolism and disposition in drug discovery and development, *Acta Pharm. Sin. B.* *2*, 549-561.
3. Cyprotex (2015) *Everything you need to know about ADME*, 2nd ed., Cyprotex PLC.
4. Davis, A., and Ward, S. E. (2014) *The Handbook of Medicinal Chemistry: Principles and Practice*, Royal Society of Chemistry, Cambridge.
5. Meunier, B., De Visser, S. P., and Shaik, S. (2004) Mechanism of oxidation reactions catalyzed by cytochrome P450 enzymes, *Chem. Rev.* *104*, 3947-3980.
6. Nassar, A. F. (2009) *Drug metabolism Handbook: Concepts and applications*, John Wiley & Sons, Hoboken.
7. Pavek, P., and Dvorak, Z. (2008) Xenobiotic-induced transcriptional regulation of xenobiotic metabolizing enzymes of the cytochrome P450 superfamily in human extrahepatic tissues, *Curr. Drug Metab.* *9*, 129-143.
8. Evans, G. (2004) *A handbook of bioanalysis and drug metabolism*, CRC press, Boca Raton.
9. Osborne, R., Thompson, P., Joel, S., Trew, D., Patel, N., and Slevin, M. (1992) The analgesic activity of morphine-6-glucuronide, *Br. J. Clin. Pharmacol.* *34*, 130-138.
10. Busch, A. E., Suessbrich, H., Kunzelmann, K., Hipper, A., Greger, R., Waldegger, S., Mutschler, E., Lindemann, B., and Lang, F. (1996) Blockade of epithelial Na<sup>+</sup> channels by triamterenes—Underlying mechanisms and molecular basis, *Pflügers Archiv.* *432*, 760-766.
11. Guillemette, C. (2003) Pharmacogenomics of human UDP-glucuronosyltransferase enzymes, *Pharmacogenomics J.* *3*, 136-158.
12. Lyubimov, A. (2012) *Encyclopedia of Drug Metabolism and Interactions*, John Wiley & Sons, Hoboken.
13. Lu, A. Y. H., Wang, R. W., and Lin, J. H. (2003) Cytochrome P450 in vitro reaction phenotyping: a re-evaluation of approaches used for P450 isoform identification, *Drug Metab. Dispos.* *31*, 345-350.
14. Harper, T. W., and Brassil, P. J. (2008) Reaction phenotyping: current industry efforts to identify enzymes responsible for metabolizing drug candidates, *AAPS J.* *10*, 200-207.
15. FDA (2008) *Guidance for Industry: Safety Testing of Drug Metabolites*, Center for Drug Evaluation and Research.
16. Smith, D. A., Allerton, C., Kalgutkar, A. S., Waterbeemd, H., and Walker, D. K. (2012) *Pharmacokinetics and metabolism in drug design*, 3rd ed., John Wiley & Sons, Weinheim.
17. DiPiro, J. T. (2010) *Concepts in clinical pharmacokinetics*, ASHP, Bethesda.
18. Tozer, T. N., and Rowland, M. (2006) *Introduction to pharmacokinetics and pharmacodynamics: the quantitative basis of drug therapy*, Lippincott Williams & Wilkins, Philadelphia.
19. Kerns, E. H., and Li, D. (2008) *Drug-like properties: concepts, structure design and methods from ADME to Toxicity Optimization*, 1st ed., Elsevier-Academic Press, San Diego.
20. Evens, R. (2007) *Drug and biological development: From Molecule to Product and Beyond*, Springer Science+Business Media, LLC, New York.
21. Kwon, Y. (2001) *Handbook of essential pharmacokinetics, pharmacodynamics and drug metabolism for industrial scientists*, Kluwer Academic/Plenum Publishers, New York.

## 2.4 Bioanalysis

*„In mass spectrometry there are no problems, only challenges!”*

-Professor Jan van der Greef

Bioanalysis is a sub-discipline of analytical chemistry focusing on the qualitative and quantitative determination of xenobiotics (drugs and their metabolites, environmental chemicals) and biotics (DNA, proteins) in a given biological matrix, such as blood, plasma, serum, or urine (1, 2). The quantitative bioanalysis applies to all stages of the drug discovery and development process: from *in vitro* testing to preclinical and clinical studies.

### 2.4.1 A brief history of bioanalysis

In the 1940s paper chromatography has been developed to separate drugs from its metabolites. Later, thin-layer chromatography was used to quantify drugs in biological fluids, although its main application was in the separation of radiolabeled metabolites (3). However, these techniques did not provide sufficient sensitivity to measure the new drugs of the 1950s, such as “tricyclics” that had levels of ng/ml (3). In the 1950s, gas chromatography (GC) coupled to nitrogen phosphorus detector was widely used in the pharmaceutical industry. Thereafter, a wide variety of detectors became commercially available, of which mass spectrometric (MS) detectors were the most preferred due to improved sensitivity (3). Since the separation for GC is carried out in the gas phase, the analyte of interest should be volatile and thermostable. Thus, the major drawback of GC was a time-consuming chemical derivatization of nonvolatile compounds prior to the analysis. In the late 1960s and early 1970s, high pressure liquid chromatography (HPLC) became the most powerful tool in analytical chemistry (3). HPLC coupled to ultraviolet (UV), electrochemical, and fluorescent detectors were primarily used in bioanalysis before HPLC-MS became the first-choice technique. In the 1980s, invention of the atmospheric pressure ionization (API) technique improved sensitivity of HPLC-MS systems (3). For quantitative purposes high specificity and selectivity were attained with the employment of triple quadrupole (QqQ) or ion trap mass analyzers capable of MS/MS fragmentation (4). In 2004, ultra-high performance liquid chromatography (UHPLC) was introduced to improve chromatographic separation efficiency. UHPLC allowed reduced solvent consumption, ultra-fast analysis, and increased throughput, while maintaining resolution. The combination of UHPLC-MS/MS offered benefits in

sensitivity, selectivity, specificity, and speed, and thus has obtained widespread application in the bioanalysis of small molecules and biologics. Nowadays, high resolution MS (HR-MS) based on quadrupole time-of-flight (Q-TOF) or Orbitrap mass analyzers is receiving more attention. HR-MS enables accurate mass measurements at high resolving power, and provides simultaneous qualitative and quantitative information in a single injection (5).

#### **2.4.2 Operation principles of the QqQ and Q-TOF mass analyzers**

Before entering a mass analyzer, the sample molecules are converted into ions in the ionization source. Among the most used ionization techniques are electrospray ionization (ESI) and atmospheric pressure chemical ionization (APCI). In the ESI source, liquid samples are pumped through a metal capillary maintained at 3 to 5 kV and nebulized at the tip of the capillary to form a fine spray of charged droplets:  $[M+H]^+$  or  $[M-H]^-$  (6). Charged droplets are further evaporated by the application of heat and nitrogen, and the residual electrical charge on the droplets is transferred to the analytes (6). In contrast to ESI, the APCI source operates at higher temperatures and includes a corona discharge pin which is responsible for ionizing the solvent molecules. These ions then react with the analytes and ionize them via charge transfer (6, 7). APCI generates singly charged ions, whereas ESI produces multiple charged ions. APCI is applied for thermostable and non-polar molecules, while ESI is used for labile and polar analytes (7). Both techniques are considered to be “soft”, meaning that little or no fragmentation of the analytes occurs during ionization (6).

Upon ionization, charged ions are transferred through an octopole ion guide into a mass analyzer, where they are separated based on their mass-to-charge ratio ( $m/z$ ). The QqQ mass analyzer consists of three quadrupoles aligned in series, where the first (Q1) and the third (Q3) quadrupoles act as selective mass filters, and the middle quadrupole (Q2) is a collision cell. Each mass filter contains four parallel metal rods controlled by direct current and radio frequency potentials and thus only ions with the certain  $m/z$  value can pass through (8). For quantitative analysis, the most common mode allowing increased sensitivity and selectivity is selected reaction monitoring (SRM) (6, 8). In SRM, Q1 selects ions with a specific  $m/z$  (precursor ions) and filters out ions with different  $m/z$ . In Q2, precursor ions strike collision gas molecules ( $N_2$  or Ar) generating product ions, so called collision induced dissociation (CID). Product ions with a specific  $m/z$  are selected in Q3 and are finally detected by an electron- or photo-multiplier detector (Fig. 4). Therefore, SRM mode is denoted as a double mass filter able to significantly reduce background noise.



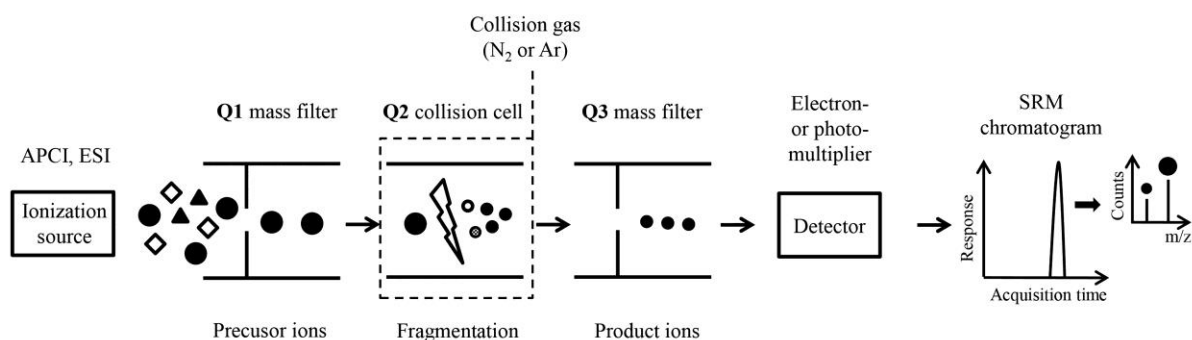


Figure 4: Schematic representation of a triple quadrupole (QqQ) mass analyzer operating in selected reaction monitoring (SRM) mode.

In the Q-TOF mass analyzer, the third quadrupole is replaced by a flight tube (Fig. 5). The beam of ions enters the ion pulser, where the ions are accelerated orthogonally by a high voltage pulse. The ion mirror reverses the direction of flying ions making them arrive at the detector. The flight time for each particular  $m/z$  is unique. Ions with small  $m/z$  have higher velocity and thus arrive at the detector earlier than ions with larger  $m/z$ . The time-of-flight analysis provides high mass accuracy (mass errors less than 5 ppm) and high resolution (up to 50000) (9, 10). The Q-TOF mass analyzer allows data acquisition at high speed of around 20 spectra/s without sacrificing sensitivity and resolution in the full scan and MS/MS modes (11).

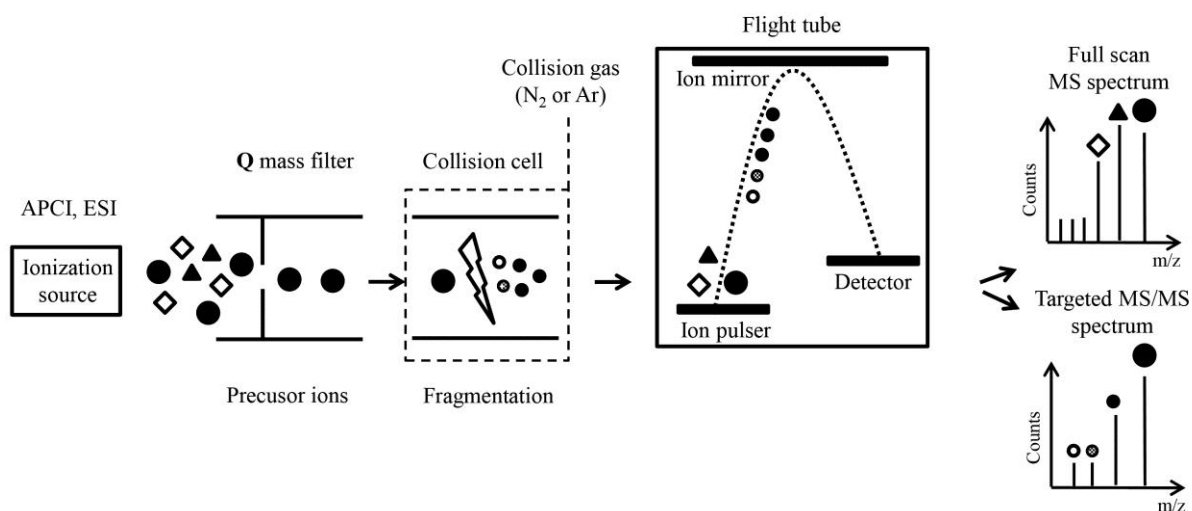


Figure 5: Schematic representation of a quadrupole time-of-flight (Q-TOF) mass analyzer operating simultaneously in the full scan MS and targeted MS/MS modes.

### 2.4.3 Sample preparation

The primary goal of sample preparation is to isolate the analyte of interest from a wide variety of matrix components (e.g. phospholipids, proteins, salts), which can affect (suppress or enhance) the ionization of the analyte (12-14). This phenomenon is termed matrix effect, and can lead to inaccurate quantification (14). Moreover, sample preparation is performed to enrich the sample with respect to the analyte, thus maximizing the sensitivity of LC-MS/MS system (13). Prior to analysis, biological samples are processed by using one of the following procedures: dilution, protein precipitation (PP), liquid-liquid extraction (LLE), supported-liquid extraction (SLE), and solid phase extraction (SPE).

#### *Dilution*

Dilution is a fast and simple technique of sample preparation, only requiring the dilution of the sample with water or mobile phase prior to LC-MS/MS analysis. The main disadvantage of this technique is that it does not remove any matrix interferences, and dilutes out the analyte of interest (12).

#### *Protein precipitation (PP)*

PP removes proteins present in the biological matrix through denaturation caused by external stress such as strong acid/base, heat or, most commonly, organic solvent (methanol, acetonitrile) (1). The organic solvent is added to the sample in a ratio of 3:1 (v/v) (15). The denatured proteins are then removed by centrifugation, but the desired analyte remains in the supernatant liquid (1). PP is an inexpensive, simple, and widely applicable procedure for sample preparation. However, it is time-consuming when handled manually for a large number of samples, and it does not always provide sufficient sample clean-up (1).

#### *Liquid-liquid extraction (LLE)*

LLE separates an analyte from matrix interferences based on their different solubility into two immiscible phases (polar aqueous and non-polar organic). Low molecular weight lipophilic drugs will preferentially reside in the organic phase, while polar matrix components remain in the aqueous phase (13). LLE yields cleaner samples than PP, but it has several drawbacks: low recovery of polar analytes, relatively large volume of costly solvents and biological samples required, labor intensive, and time-consuming (14).

#### *Supported-liquid extraction (SLE)*

SLE is an alternative to the conventional LLE extraction technique, which is suitable for 96-well format operation. The SLE cartridge is packed with inert diatomaceous earth sorbent material, which absorbs the aqueous sample with the analyte of interest. An immiscible solvent is then used to elute the desired analyte (16). SLE provides clean extracts with a high

recovery and reproducibility, but it has a limited sample aliquot volume (<400 µl) in order to maintain a 96-well plate format (16, 17).

#### *Solid phase extraction (SPE)*

SPE separates an analyte from matrix interferences based on the affinity of the analyte towards a stationary phase. The analyte is retained by the stationary phase through hydrophobic (reverse-phase SPE) or electrostatic (ion-exchange SPE) interactions, while matrix interferences are washed off (14). The retained analyte is then eluted with an appropriate solvent (mobile phase). Different stationary phases have been developed to provide the cleanest extract, thus minimizing matrix effect. The main disadvantage of this technique is the high cost per sample.

#### **2.4.4 Method development**

For a robust LC-MS/MS method development, it is important to follow several steps such as:

(i) *Assessment of physicochemical properties*: Physicochemical properties of the analyte of interest should be initially assessed to select appropriate solvents, and to take the necessary precautions during the method development process (e.g. protection from light for photosensitive compounds).

(ii) *Selection of internal standard (IS)*: IS must have the same or similar physicochemical properties as the analyte of interest, so that it can mimic closely the performance of the analyte in every stage of analysis: from the sample preparation to MS detection (17). For quantification, the use of signal ratio of the analyte to the IS (rather than the use of the analyte absolute signal) is preferable. The losses and variations of the analyte, which may occur during sample preparation or during LC-MS/MS analysis, can thus be corrected (17). The best IS is a stable isotopic (e.g.  $^2\text{H}$ ,  $^{13}\text{C}$ ,  $^{15}\text{N}$ )-labeled compound due to its very similar physicochemical properties as the analyte. However, the high cost for synthesis of isotopically labeled compounds limits their application. As a cheaper alternative, structural analogs can be used.

(iii) *Optimization of MS/MS parameters*: For successful MS detection and quantification, a number of parameters, such as ionization mode, SRM transitions, capillary voltage, cone voltage, source temperature, desolvation gas flow, and collision energy should be optimized for analyte and corresponding IS.

(iv) *Optimization of LC method*: For optimal separation conditions, the composition of mobile phase, gradient, flow rate, column type, and temperature (column oven temperature, autosampler temperature) should be optimized.

(v) *Selection of sample preparation procedure*: In general, PP extraction is considered to be the first choice if the required lower limit of quantification (LLOQ) is in the range of ng/ml (17). Because PP extraction does not remove matrix effect, it is recommended that the maximal sample aliquot volume should not be more than 100  $\mu$ l (17). If the target LLOQ is at pg/ml, more sophisticated procedures like LLE, SLE and SPE can be employed.

(vi) *Quantification range and carry-over assessment*: A quantification range should be chosen based on the concentrations expected in a particular study, and should be described by the simplest regression model possible (linear or quadratic) (2, 17).

Carry-over can be assessed by injecting a blank sample immediately after the upper limit of quantification (ULOQ). If carry-over is observed, it is critical to determine the source of carry-over (autosampler injector carry-over or LC column carry-over) in order to eliminate or minimize it. Selection of the appropriate needle wash solvent, addition of acid or base modifier to the mobile phase may increase the solubility of the analyte and thus may help to overcome autosampler injector carry-over (17). LC column carry-over can be minimized by changing the LC method to isocratic conditions or a flat gradient, or by switching to a less retentive LC column (17).

#### **2.4.5 Method validation**

Validation of bioanalytical methods is performed to demonstrate reliability and reproducibility of a particular method used for quantification of analytes in a given biological matrix (2). Validation should be conducted in compliance with guidelines defined by regulatory agencies: the US Food and Drug Administration (FDA) and/or the European Medicines Agency (EMA) (2, 18). The main characteristics that ensure performance acceptability of the bioanalytical method are: calibration curve and LLOQ, accuracy, precision, selectivity, specificity, carry-over, matrix effect, recovery, dilution integrity, and stability (2, 18).

##### *Calibration curve and LLOQ*

The calibration curve describes the relationship between instrument response and known concentrations of the analyte (2). A calibration curve comprises a double blank sample (matrix without analyte and IS), a calibrator zero sample (matrix without analyte but with IS), a minimum of six calibration standards (CALs), and quality controls (QCs) prepared in the same biological matrix as the samples (2). Concentrations of CALs should be chosen based on the concentration range expected in a particular study (2). The LLOQ is defined by two parameters: (i) an experimental concentration within  $\pm 20\%$  of the nominal value (2, 18), and (ii) a signal to noise (S/N) ratio, which should be  $\geq 10$ . QCs are prepared at three

concentration levels: low (QCL), medium (QCM), and high (QCH). QCL should be 3 times higher than LLOQ, while QCM and QCH should be 50% and 80% of the ULOQ, respectively (2, 18). Each analytical run is opened and closed by the set of CALs, while six QCs are placed randomly between two sets. The back calculated concentrations of CALs and QCs should be within  $\pm 15\%$  of the nominal value, except for the LLOQ for which it should be within  $\pm 20\%$  (2, 18). At least 75% of CALs and 67% of QCs should fulfill these criteria to obtain a valid run (2, 18).

#### *Accuracy and precision*

The accuracy describes the closeness of the measured concentrations to the nominal concentrations. The accuracy is usually measured in terms of inaccuracy expressed as the relative error (RE, %):

$$RE = \frac{\text{Measured conc.} - \text{Nominal conc.}}{\text{Nominal conc.}} \times 100$$

The precision describes the closeness of the repeated individual measures of the analyte, and is usually measured in terms of imprecision expressed as the coefficient of variation (CV, %):

$$CV = \frac{\text{Standard deviation}}{\text{Mean conc.}} \times 100$$

The accuracy and precision should be measured using a minimum of five replicates per concentration level at LLOQ, QCL, QCM, QCH, and ULOQ (2, 18). Precision and accuracy are further subdivided into within-run (accuracy and precision of a single analytical run) and between-run (accuracy and precision of at least three runs analyzed on at least two different days) (2, 18). According to the guidelines, RE should be  $\pm 15\%$  ( $\pm 20\%$  at the LLOQ), and CV should not exceed 15% (20% at the LLOQ) (2, 18).

#### *Selectivity and specificity*

Selectivity and specificity are defined as the ability of an analytical method to differentiate and quantify the analyte of interest in the presence of matrix interferences (2). The selectivity is tested by spiking at least six sources of the appropriate matrix with the analyte at LLOQ (2). The specificity of the method is evaluated by analyzing at least six sources of the blank matrix, and confirmed if no interferences are found at the retention time of the analyte (2).

#### *Carry-over*

Carry-over of the analyte and corresponding IS should be evaluated during the method development by injecting a blank sample immediately after ULOQ. According to the EMA guideline, carry-over should not be greater than 20% for the analyte and 5% for the IS (18).

### *Matrix effect*

The EMA guideline recommends evaluation of matrix effect with the aid of the matrix factor (MF). The MF is the ratio of the peak area in the presence of matrix to the peak area in absence of matrix (18). The MF of the analyte should be normalized by the MF of the IS. The MF = 1 indicates no matrix effect, MF <1 indicates ion suppression, MF >1 indicates ion enhancement (15). The CV of the IS-normalized MF calculated for at least 6 sources of matrix should not be greater than 15% (18).

### *Recovery*

Recovery (= extraction efficiency) of the analyte should be evaluated at three concentration levels (QCL, QCM, and QCH). It does not need to be 100%, but the extent of recovery over the different concentration levels should be consistent (2).

### *Dilution integrity*

Dilution of the study samples is required when the sample concentration is expected to be outside the quantification range. To demonstrate that the analyte of interest can be accurately measured by the bioanalytical method after dilution, QCs at the concentration above ULOQ should be prepared, and then diluted with blank matrix (18).

### *Stability*

Evaluation of the analyte stability in the studied matrix should be carried out to ensure that the analyte concentration is not affected during storage, sample preparation and analysis steps. Stability should be proven after short-term storage (benchtop stability at room temperature, autosampler stability) and long-term storage (frozen at the intended storage temperature), and after freeze and thaw cycles. Stability of the analyte and the corresponding IS in stock solution should also be assessed (2, 18).

## **2.4.6 Analysis of study samples**

The validated LC-MS/MS method is further applied for the analysis of study samples. As for the method validation, an analytical run should be opened and closed by the set of CALs, in-between study samples together with six QCs should be placed randomly. An analytical run can be considered valid if the back calculated concentrations of at least 75% CALs and 67% QCs are within  $\pm 15\%$  of the nominal value ( $\pm 20\%$  for LLOQ).

## References

1. Kole, P. L., Venkatesh, G., Kotecha, J., and Sheshala, R. (2011) Recent advances in sample preparation techniques for effective bioanalytical methods, *Biomed. Chrom.* 25, 199-217.
2. FDA (Draft Guidance 2013) *Guidance for Industry: Bioanalytical Method Validation*, Center for Drug Evaluation and Research.
3. Hill, H. (2009) Development of bioanalysis: a short history, *Bioanalysis*. 1, 3-7.
4. Niessen, W. M. A. (2003) Progress in liquid chromatography–mass spectrometry instrumentation and its impact on high-throughput screening, *J. Chromatogr. A.* 1000, 413-436.
5. Huang, M.-Q., Lin, Z., and Weng, N. (2013) Applications of high-resolution MS in bioanalysis, *Bioanalysis*. 5, 1269-1276.
6. Pitt, J. J. (2009) Principles and applications of liquid chromatography-mass spectrometry in clinical biochemistry, *Clin. Biochem. Rev.* 30, 19-34.
7. Ashcroft, A. E. (1997) *Ionization methods in organic mass spectrometry*, Royal Society of Chemistry, Cambridge.
8. Dass, C. (2007) *Fundamentals of contemporary mass spectrometry*, John Wiley & Sons, Hoboken.
9. Ferrer, I., and Thurman, E. M. (2009) *Liquid chromatography time-of-flight mass spectrometry*, John Wiley & Sons, Hoboken.
10. Sleno, L. (2013) *Applications of high-resolution mass spectrometry in drug discovery and development*, Future Medicine, London.
11. Xie, C., Zhong, D., Yu, K., and Chen, X. (2012) Recent advances in metabolite identification and quantitative bioanalysis by LC-Q-TOF MS, *Bioanalysis*. 4, 937-959.
12. Soltani, S., and Jouyban, A. (2014) Biological sample preparation: attempts on productivity increasing in bioanalysis, *Bioanalysis*. 6, 1691-1710.
13. Prabu, S. L., and Suriyaprakash, T. N. K. (2012) Extraction of drug from the biological matrix: a review, in *Applied Biological Engineering - Principles and Practice* (Naik, G. R., Ed.), INTECH.
14. Chiu, M. L., Lawi, W., Snyder, S. T., Wong, P. K., Liao, J. C., and Gau, V. (2010) Matrix effects—a challenge toward automation of molecular analysis, *J. Lab. Autom.* 15, 233-242.
15. Zhou, M. (2011) *Regulated Bioanalytical Laboratories: Technical and Regulatory Aspects from Global Perspectives*, John Wiley & Sons, Hoboken.
16. Pan, J., Jiang, X., and Chen, Y.-L. (2010) Automatic supported liquid extraction (SLE) coupled with HILIC-MS/MS: an application to method development and validation of erlotinib in human plasma, *Pharmaceutics*. 2, 105-118.
17. Xu, Q. A., and Madden, T. L. (2012) *LC-MS in Drug Bioanalysis*, Springer Science & Business Media, LLC, New York.
18. EMA (2011) *Guideline on bioanalytical method validation*, European Medicines Agency (EMA/CHMP/EWP/192217/2009).

## 2.5 Metabolite identification in early drug discovery

A critical step in early drug discovery is the detection and identification of metabolites of drug leads. It provides information on metabolically labile sites of the molecules suggesting structural modifications to reduce their clearance, and also allows an early safety assessment via the identification of reactive metabolites (1-4). Metabolite profiles for drug leads are typically determined using liver fractions (microsomes, S9) or hepatocytes (5, 6). For the detection and quantification of metabolites often present at trace levels in a complex matrix, MS instruments providing high resolution, high sensitivity, and accurate mass measurements (e.g. Q-TOF) are required (7-10). Afterwards, high resolution accurate mass data along with MS/MS fragmentation are processed with the aid of metabolite identification (MetID) software packages to generate elemental formulae for metabolites and to provide insight about metabolite structures (11). There are many MetID tools, such as Mass-MetaSite (Molecular Discovery), ACD/Labs MetID (ACD/Labs), MetabolitePilot (AB Sciex), MassHunter Metabolite ID (Agilent) available on the market. Data processing with these computer programs follow a similar workflow. For a better understanding, Mass-MetaSite program will be taken as an example to describe the algorithm used in data processing. The initial step imports HR-MS data and the structure of a parent compound into the computer program. The next step involves prediction of possible metabolites from the parent structure, and calculation of their exact masses. Mass-MetaSite provides an option for selecting the type of metabolites (phase I and/or phase II) to be generated. For example, if the metabolic stability assay was performed with microsomes, there would be no need to generate phase II metabolites, and thus the time for data analysis could be shortened. After mass calculations, the program searches for matches in the experimental total ion chromatogram (TIC). Metabolite structures are proposed based on the fragmentation pattern, and presented using a Markush notation. Hypothetical fragments for each metabolite are produced by breaking each bond, excluding aromatic, double, triple bonds, and bonds to hydrogen atoms (12). Fragments for a parent compound are generated by breaking a maximum of four bonds (12). Then the fragmentation pattern of a metabolite is compared with the parent one, and a score is assigned based on the number of matches/mismatches (12). Mass shifts and mass defects also assist in structural characterization (13). The predicted metabolites are classified as to whether they are related to first-, second- or higher-generation metabolites (12). Generally, three different acquisition files are needed for data processing: (i) a blank file for monitoring the background



noise which will be subtracted from other files; (ii) a substrate (parent compound) file ( $t_0$ ) for analysis of the fragmentation pattern; and (iii) an incubation file ( $t_x$ ) that contains all the products after incubation (remaining parent compound and metabolites) (12). Following data processing, the biotransformation map will be automatically created.

A combination of HR-MS and MetID software significantly accelerates the data acquisition and interpretation process allowing high-throughput metabolite identification early in the drug discovery. The data generated from MetID studies is useful as a guide for medicinal chemists during lead optimization, thus transforming metabolic information into rational drug design.

## References

1. Kirkpatrick, P. (2009) Drug metabolism: seeking the soft spots, *Nat. Rev. Drug Discov.* 8, 196.
2. Stepan, A. F., Mascitti, V., Beaumont, K., and Kalgutkar, A. S. (2013) Metabolism-guided drug design, *Med. Chem. Commun.* 4, 631-652.
3. Shu, Y.-Z., Johnson, B. M., and Yang, T. J. (2008) Role of biotransformation studies in minimizing metabolism-related liabilities in drug discovery, *AAPS J.* 10, 178-192.
4. Han, C., Davis, C. B., and Wang, B. (2010) *Evaluation of drug candidates for preclinical development: pharmacokinetics, metabolism, pharmaceuticals, and toxicology*, John Wiley & Sons, Hoboken.
5. Zhang, D., Luo, G., Ding, X., and Lu, C. (2012) Preclinical experimental models of drug metabolism and disposition in drug discovery and development, *Acta Pharm. Sin. B.* 2, 549-561.
6. Jia, L., and Liu, X. (2007) The conduct of drug metabolism studies considered good practice (II): *in vitro* experiments, *Curr. Drug Metab.* 8, 822-829.
7. Sleno, L. (2013) *Applications of high-resolution mass spectrometry in drug discovery and development*, Future Medicine, London.
8. Zhu, M., Zhang, H., and Humphreys, W. G. (2011) Drug metabolite profiling and identification by high-resolution mass spectrometry, *J. Biol. Chem.* 286, 25419-25425.
9. Meyer, M. R., and Maurer, H. H. (2012) Current applications of high-resolution mass spectrometry in drug metabolism studies, *Anal. Bioanal. Chem.* 403, 1221-1231.
10. Xie, C., Zhong, D., Yu, K., and Chen, X. (2012) Recent advances in metabolite identification and quantitative bioanalysis by LC-Q-TOF MS, *Bioanalysis.* 4, 937-959.
11. Kirchmair, J., Göller, A. H., Lang, D., Kunze, J., Testa, B., Wilson, I. D., Glen, R. C., and Schneider, G. (2015) Predicting drug metabolism: experiment and/or computation?, *Nat. Rev. Drug Discov.* 14, 387-404.
12. Zamora, I., Fontaine, F., Serra, B., and Plasencia, G. (2013) High-throughput, computer assisted, specific MetID. A revolution for drug discovery, *Drug Discov. Today Technol.* 10, e199-e205.
13. Shaha, P. V., Shahc, J. V., Saroja, S. D., Jairaja, V., and Rathodb, R. (2015) Metabolite identification by mass spectrometry, *Int. J. Pharm. Res. Allied Sci.* 4, 9-17.

## **3 Results and discussion**



### **3.1 Pharmacokinetics of dietary kaempferol and its metabolite 4-hydroxyphenylacetic acid in rats**

**Volha Zabela**, Chethan Sampath, Mouhssin Oufir, Fahimeh Moradi-Afrapoli, Veronika Butterweck, and Matthias Hamburger

*Fitoterapia* (in press)

DOI information: 10.1016/j.fitote.2016.10.008

Previous studies have shown that kaempferol and its major intestinal metabolite 4-hydroxyphenylacetic acid (4-HPAA) exert anxiolytic activity in mice. To gain a better understanding of their pharmacological effects, pharmacokinetic (PK) studies were conducted with the aim to evaluate PK properties of the compounds after oral and intravenous administrations. At first, UHPLC-MS/MS methods were developed and validated according to the principles of current regulatory guidelines for industry. The validated methods were later applied for quantification of kaempferol and 4-HPAA in rat plasma. PK parameters were calculated with the industry standard software WinNonlin using non-compartmental and compartmental analyses. PK studies revealed that kaempferol and its metabolite 4-HPAA are highly cleared compounds so that effective concentrations at the site of action do not appear to be reached. At present, it is not clear how the anxiolytic-like effects reported for the compounds can be explained.

*My contributions to this publication: development and validation of UHPLC-MS/MS quantification methods according to the principles of current regulatory guidelines for industry, plasma sample preparation and analysis, non-compartmental and compartmental pharmacokinetic data analysis, writing the manuscript draft, and preparation of figures and tables.*

*Volha Zabela*

## **MANUSCRIPT**

### **Pharmacokinetics of dietary kaempferol and its metabolite 4-hydroxyphenylacetic acid in rats**

Volha Zabela<sup>a</sup>, Chethan Sampath<sup>b</sup>, Mouhssin Oufir<sup>a</sup>, Fahimeh Moradi-Afrapoli<sup>a</sup>, Veronika Butterweck<sup>b,1</sup> and Matthias Hamburger<sup>a\*</sup>

<sup>a</sup>Pharmaceutical Biology Laboratory, Department of Pharmaceutical Sciences, University of Basel, Klingelbergstrasse 50, CH-4056 Basel, Switzerland

<sup>b</sup>Department of Pharmaceutics, College of Pharmacy, University of Florida, 1345 Center Drive, Gainesville, FL, USA

#### **Author's present address:**

<sup>1</sup>Institute for Pharma Technology, School of Life Sciences, University of Applied Sciences Northwestern Switzerland, Gründenstrasse 40, CH-4132 Muttenz, Switzerland

#### **Author's e-mails:**

volha.zabela@unibas.ch (Zabela); chethan@ufl.edu (Sampath); mouhssin.oufir@unibas.ch (Oufir); veronika.butterweck@fhnw.ch (Butterweck); matthias.hamburger@unibas.ch (Hamburger)

#### **\*Corresponding author:**

Professor Matthias Hamburger

**E-mail:** matthias.hamburger@unibas.ch

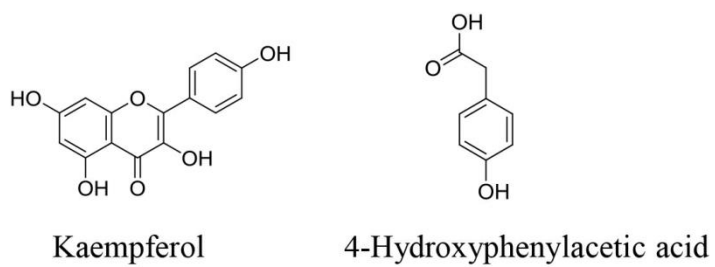
**Fax:** +41 61 267 14 74

**Address:** Pharmaceutical Biology Laboratory, Department of Pharmaceutical Sciences, University of Basel, Klingelbergstrasse 50, CH-4056, Basel, Switzerland

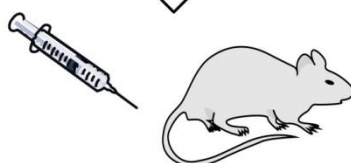
## Abbreviations

AA, acetic acid	NCA, non-compartmental analysis
AIC, Akaike's information criterion	p.o., per os
AUC, area under the curve	PEG, polyethylene glycol
AUMC, area under the first moment curve	PK, pharmacokinetics
BBB, blood-brain barrier	QCs, quality controls
b.w., body weight	QCL, quality control at a low level
C <sub>0</sub> , concentration at time 0	QCM, quality control at a medium level
CA, compartmental analysis	QCH, quality control at a high level
Cals, calibrators	RE, relative error
CL, clearance	RT, room temperature
C <sub>max</sub> , maximal concentration	SD, Sprague Dawley
CV, coefficient of variation	SBC, Schwarz's Bayesian criterion
FA, formic acid	SS, stock solution
4-HPAA, 4-hydroxyphenylacetic acid	t <sub>1/2</sub> , half-life
i.p., intraperitoneally	UV, ultraviolet
IS, internal standard	V <sub>d</sub> , volume of distribution during the terminal phase
i.v., intravenously	WS1, working solution 1
k <sub>e</sub> , elimination rate constant	WS2, working solution 2
LLOQ, lower limit of quantification	WSSR, weighted sum of squared residuals
MRM, multiple reaction monitoring	
MRT, mean residence time	

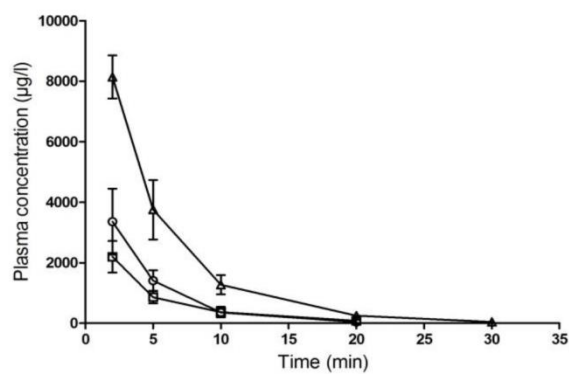
## Graphical abstract



PK studies in rats



Quantification by UHPLC-MS/MS





## **Abstract**

Kaempferol is a major flavonoid in the human diet and in medicinal plants. The compound exerts anxiolytic activity when administered orally in mice, while no behavioural changes were observed upon intraperitoneal administration, or upon oral administration in gut sterilized animals. 4-hydroxyphenylacetic acid (4-HPAA), which possesses anxiolytic effects when administered intraperitoneally, is a major intestinal metabolite of kaempferol. Pharmacokinetic properties of the compounds are currently not clear.

UHPLC-MS/MS methods were validated to support pharmacokinetic studies of kaempferol and 4-HPAA in rats. Non-compartmental and compartmental analyses were performed. After intravenous administration, kaempferol followed a one-compartment model, with a rapid clearance (4.40-6.44 l/h/kg) and an extremely short half-life of 2.93-3.79 min. After oral gavage it was not possible to obtain full plasma concentration-time profiles of kaempferol. Pharmacokinetics of 4-HPAA was characterized by a two-compartment model, consisting of a quick distribution phase (half-life 3.04-6.20 min) followed by a fast elimination phase (half-life 19.3-21.1 min).

Plasma exposure of kaempferol is limited by poor oral bioavailability and extensive metabolism. Both compounds are rapidly eliminated, so that effective concentrations at the site of action do not appear to be reached. At present, it is not clear how the anxiolytic-like effects reported for the compounds can be explained.

**Keywords:** 4-HPAA, kaempferol, pharmacokinetics, UHPLC-MS/MS.

## 1 Introduction

Kaempferol occurs in numerous vegetables, fruits and medicinal plants, and is thus a commonly ingested flavonoid. The compound reportedly possesses a wide range of biological and pharmacological activities [1, 2]. However, flavonoids are extensively metabolized by the colonic microflora [3, 4] and activities reported for kaempferol may not necessarily be due to the compound itself but possibly to metabolites. Recent *in vitro* study on the intestinal permeability of kaempferol showed that the compound undergoes significant biotransformation, with only a small fraction of the unchanged kaempferol able to cross the intestinal barrier [5]. A major intestinal metabolite of kaempferol is 4-hydroxyphenylacetic acid (4-HPAA) [6, 7]. Anxiolytic activity of kaempferol was shown in behavioural paradigms in mice. However, the anxiolytic properties were only seen after oral administration, while no behavioural changes were observed upon intraperitoneal (i.p.) administration. In contrast, 4-HPAA showed anxiolytic effect after i.p. application [8]. In addition, the anxiolytic effect of orally administered kaempferol was absent in gut sterilized mice, supporting the hypothesis that kaempferol requires metabolic transformation into a pharmacologically active compound. In a comparison of kaempferol, quercetin and myricetin, the number of hydroxyl groups on the B-ring of flavonols appeared to affect the anxiolytic-like properties of flavonoids, as decreasing activity was seen with an increasing number of hydroxyl groups [8].

4-HPAA is not only an intestinal metabolite of kaempferol, but also an endogenous metabolite of the neurotransmitter dopamine. 4-HPAA has been described as a possible biological marker for depression, since decreased 4-HPAA concentration has been linked to depression and anxiety [9, 10]. To gain a better understanding of the antidepressant effect of kaempferol and 4-HPAA we here investigated the pharmacokinetic (PK) properties of kaempferol and 4-HPAA after intravenous and oral administration in rats. Several PK and metabolism studies with kaempferol have been published, whereby HPLC coupled with ultraviolet (UV) [11, 12], electrochemical [13], chemiluminescence [14] and MS [15] detection was used for the quantification in rat or human plasma. However, these methods do not meet current requirements for bioanalytical methods, and the above mentioned MS assays, in our hands, did not meet validation criteria of the FDA and EMA guidelines for industry [16, 17]. We here report on the development and validation of UHPLC-MS/MS methods for determination of kaempferol and 4-HPAA in Sprague Dawley rat plasma, and on the evaluation of the PK properties of the compounds.

## 2 Materials and methods

### 2.1 Chemicals and reagents

Kaempferol (Figure 1A) (purity 97.7%) was purchased from Tokyo Chemical Industry Co. (Tokyo, Japan). 4-HPAA (Figure 1C) (purity 98%), solution of glucuronidase/sulfatase from *Helix pomatia* ( $\geq 100000$  and  $\geq 2000$  units/ml, respectively), bovine serum albumin (BSA), Cremophor, Tween-80, PEG were from Sigma-Aldrich (St. Louis, MO, USA). Kaempferol-3-O-glucuronide (Figure 1B) (purity 99.6%) was purchased from Extrasynthese (Genay, France).  $^{13}\text{C}_{15}$ -kaempferol was obtained from IsoLife Company (Wageningen, The Netherlands), and  $^2\text{H}_2$ -labeled 4-HPAA was from Diverchim (Roissy-en-France, France). Methanol (HPLC grade), ammonium formate, formic (FA) and acetic acid (AA) (purity 98-100%) were from Biosolve BV (Valkenswaard, the Netherlands). ACN, isopropanol (HPLC grade) and DMSO were supplied by Scharlau S.L. (Barcelona, Spain). Deionized water was obtained from an EASY pure II (Barnstead; Dubuque, IA, USA) water purification system. Blank male Sprague-Dawley (SD) lithium heparin rat plasma was purchased from Seralab (Haywards Heath, UK).

### 2.2 Standards and stock solutions

Stock solutions (SS) of kaempferol, kaempferol-3-O-glucuronide and 4-HPAA were prepared in DMSO by weighing the compounds on a micro balance (Sartorius, Göttingen, Germany). Working solutions 1 (WS1)

at a concentration of 100  $\mu\text{g}/\text{ml}$  of the analytes were prepared in methanol. The WS1 of  $^{13}\text{C}_{15}$ -labeled kaempferol was prepared in methanol by diluting the SS at a concentration of 500  $\mu\text{g}/\text{ml}$ . For  $^{13}\text{C}_{15}$ -labeled kaempferol, a second working solution 2 (WS2), at a concentration of 200 ng/ml, was prepared daily from WS1. The WS1 of  $^2\text{H}_2$ -labeled 4-HPAA was prepared in methanol at a concentration of 50  $\mu\text{g}/\text{ml}$ . A WS2 (500 ng/ml) was prepared every day from WS1. All the SSs and WSs were stored below  $-65^\circ\text{C}$  until analysis.

### 2.3 Preparation of calibration standards and samples for quality control

Two sets of calibrators (Cals) over the range of 20.0-2000 ng/ml, and quality controls (QCs) at low, medium and high levels (QCL = 60 ng/ml, QCM = 1000 ng/ml, QCH = 1600 ng/ml) were prepared in rat plasma (for kaempferol) and in BSA (for 4-HPAA), by serial dilution of the WS (100  $\mu\text{g}/\text{ml}$ ). For kaempferol-3-O-glucuronide, two sets of CALs over the range of 5-500 ng/ml and QCs (QCL = 15 ng/ml, QCM = 250 ng/ml, QCH = 400 ng/ml) were prepared in rat plasma. All samples were aliquoted into polypropylene tubes, and stored below  $-65^\circ\text{C}$  until analysis.

### 2.4 Sample processing

#### 2.4.1 *Kaempferol extraction from rat plasma*

A volume of 75 µl of plasma was loaded onto a 96-well Ostro plate (Waters Corp., Milford, MA, USA). 225 µl of WS2 of the internal standard (IS) (200 ng/ml) were added to achieve a 3:1 solvent/plasma ratio. Samples were eluted into a 96-deepwell plate under a positive pressure of 40 psi for 7 min (Pressure + 96, Biotage, Sweden), and dried under a heated nitrogen flow (EVX-96, Apricots, Covina, CA, USA). Dried residues were reconstituted with 200 µL of solvent consisting of 50% A (10 mM ammonium formate + 0.05% FA) and 50% B (ACN + 0.05% FA). The plate was shaken (Mixmate, Eppendorf, Hamburg, Germany) for 30 min at 2000 rpm before injection (5 µl).

#### 2.4.2 *4-HPAA extraction from BSA*

An aliquot of 75 µl of BSA was mixed with 150 µl of WS2 of the corresponding IS (500 ng/ml) and 300 µl ACN in 1.5 ml tubes. The mixture was briefly vortexed, and centrifuged at 10°C for 15 min at 13200 rpm (Centrifuge 5415R, Eppendorf, Schönenbuch, Switzerland). Afterwards, 400 µl of supernatant were collected into a 96-deepwell plate. Samples were dried under a heated nitrogen flow and reconstituted with 200 µl of 50% A (5 mM aqueous AA) and 50% B (ACN + 5 mM AA). The plate was shaken for 30 min at 2000 rpm prior to injection (10 µl).

#### 2.4.3 *Extraction of total kaempferol after treatment with glucuronidase/sulfatase*

Buffer was prepared with water, ascorbic acid (0.5%, w/v), and acetic acid (10%, v/v) at a 1:1:1 ratio. An aliquot (15 µl) of buffer was mixed with 38 µl of plasma samples, and 4 µl of enzyme solution were added. The mixture was incubated at 37°C for 1 h. Aliquots (57 µl) of the reaction mixture were loaded into a 96-well Ostro plate, and 171 µl of IS (<sup>13</sup>C<sub>15</sub>-kaempferol) solution (200 ng/ml) were added for extraction as described in 2.4.1.

#### 2.4.4 *Extraction of kaempferol-3-O-glucuronide from rat plasma*

Aliquots (38 µl) of plasma, and 114 µl of WS2 of the IS (1000 ng/ml) were loaded onto a 96-well Ostro plate for extraction as described in 2.4.1.

#### 2.5 *LC-MS/MS instrumentation and chromatographic conditions*

An Agilent UHPLC 1290 system consisting of a binary pump, autosampler, column oven, and needle wash unit was coupled to an Agilent 6430 triple quadrupole mass spectrometer (Agilent Technologies, USA). The instrument was controlled by MassHunter software (version 6.0; Agilent Technologies, USA). Nitrogen generated by a nitrogen generator N2-Mistral (Schmidlin AG, Neuheim, Switzerland) was used for desolvation and nebulization. Nitrogen was also used as collision gas. The MS parameters for each compound are summarized in Table 1.

Chromatography of kaempferol and IS was performed on an Acquity BEH C18 column (1.7  $\mu\text{m}$ , 2.1  $\times$  50 mm) (Waters Corp., Milford, MA, USA). Column temperature was set at 80°C, and the autosampler temperature at 10°C. The mobile phase consisting of eluent A (0.1 % aqueous FA) and eluent B (ACN with 0.1 % FA) was delivered at a flow rate of 0.6 ml/min. Separation was achieved with the following gradient: 0-1 min, 15% B, 1-3 min, 15-60% B, 3-3.1 min, 60-100% B, 3.1-4 min, 100% B, 4-4.1, 100-15% B, 4.1-5.0 min, 15% B. The total run time was 5 min. The needle wash solvent consisted of water and methanol (50:50, v/v). Chromatography of 4-HPAA and IS was performed on an Acquity HSS T3 column (1.8  $\mu\text{m}$ , 2.1  $\times$  100 mm) (Waters Corp., Milford, MA, USA). Column temperature was set at 45°C, and the autosampler temperature at 10°C. The mobile phase consisting of eluent A (5 mM aqueous AA) and eluent B (ACN with 5 mM AA) was delivered at a flow rate of 0.5 ml/min. Separation was achieved with the following gradient: 0-1 min, 5% B, 1-3 min, 5-100% B, 3-4 min, 100% B, 4-4.1 min, 100-5% B, 4.1-5, 5% B. The total run time was 5 min. The needle wash solvent consisted of water/methanol/isopropanol/ACN (1:1:1:1, v/v/v/v). The separation of kaempferol-3-O-glucuronide and IS was performed on a Kinetex XB column (1.7  $\mu\text{m}$ , 2.1 $\times$ 100 mm) (Phenomenex, Torrance, CA, USA). Column temperature was set at 55°C, and the autosampler temperature at 10°C. The mobile phase consisting of eluent A (0.1% FA) and eluent B (ACN with 0.1% FA) was delivered at a flow rate 0.5 ml/min. The separation was achieved with the following gradient: 0-1 min, 2% B, 1-6 min, 2-50% B, 6.0-6.01 min, 50-100% B, 6.01-7 min, 100% B, 7-7.01 min, 100-2% B, 7.01-8 min, 2% B. The total run time was 8 min. The needle wash solvent consisted of water/methanol/isopropanol/ACN (1:1:1:1, v/v/v/v).

## 2.6 Method validation

The regression curves obtained for kaempferol and 4-HPAA from two sets of seven calibrators over the range 20.0-2000 ng/ml were validated by six QCs. Carryover was assessed by two extracted blank matrices injected immediately after the ULOQ. Selectivity of the method was confirmed by six QC samples at the LLOQ, prepared in three different batches of rat plasma (for kaempferol), or in three different lots of BSA (for 4-HPAA). Due to the endogenous presence of 4-HPAA in blank plasma samples, a BSA solution (60 g/l) was used as a surrogate matrix. Specificity of the methods was checked with six blank samples (three different batches of rat plasma or BSA in replicates). To fulfill acceptance criteria, the peak area measured in the blank samples had to be within 20% of the analyte peak area at LLOQ. The intra-day imprecision (CV) and inaccuracy (RE) were estimated by performing six replicates of LLOQ, QCL, QCM, QCH and ULOQ. The inter-run CV and RE were

assessed by the same QCs on three different days. Extraction yields of analytes and the corresponding IS were evaluated at three levels before extraction, and spiked with the IS after extraction, in comparison to six blank samples spiked after extraction. The dilution QC samples (10 000 ng/ml) were prepared and diluted at 10- and 100-fold. Short-term (three overnight freeze-thaw cycles, 4 h benchtop stability at RT, 48 h autosampler stability at 10°C) and long-term stability tests were performed. Stability of the SS of kaempferol after 180 days of storage below -65°C and stability of the SS of 4-HPAA after 35 days of storage below -65°C were confirmed by comparison with freshly prepared SSs.

## 2.7 PK studies

### 2.7.1 Animals

Male SD rats (body weight 320-350 g) were purchased from Charles River (Wilmington, MA, USA) The animals were individually housed in plastic cages and maintained under a 12 h/12 h light/dark cycle. The rats received water *ad libitum* and a standard chow. Before being used in experiments, the animals were allowed to acclimate to their environment for one week. All animal experiments were performed according to the policies and guidelines of the Institutional Animal Care and Use Committee (IACUC) of the University of Florida, Gainesville, USA, study protocol # 200903448.

### 2.7.2 Design of PK studies in rats

Rats (n = 8 per group) were randomly divided into six groups and used for oral (p.o) and intravenous (i.v.) studies. Kaempferol was given by i.v. bolus injection in the doses of 1, 2 and 4 mg/kg body weight (b.w.). After a one week washout period the same rats received kaempferol at 5, 10, 20 mg/kg b.w. p.o. 4-HPAA was administered i.v. at 1, 2 and 4 mg/kg b.w. Both compounds were dissolved in a vehicle consisting of Cremophor/Tween-80/PEG/ethanol/water (2:1:1:1:5, v/v/v/v/v) for p.o. and i.v. administrations. Blood samples (500 µl) were collected from the sublingual vein into heparinized tubes at 0 (prior to dosing), 2, 5, 10, 20, 30 min, 1, 2, 4, 6, 8 and 12 h. The loss of blood volume was replaced with 1 ml normal saline. Plasma samples were obtained by centrifugation at 4000 rpm for 15 min at 4°C, then transferred into 1.5 ml tubes and stored at below -65°C until analysis.

## 2.8 PK data analysis

Mean plasma concentrations of kaempferol and 4-HPAA versus time were plotted in Graphpad Prism (version 5.01; San Diego, CA, USA). PK parameters were determined by non-compartmental (NCA) and compartmental (CA) analyses using WinNonlin<sup>®</sup> software (version 5.2.1; Pharsight Corporation, St. Louis, MO, USA).

### 2.8.1 Non-compartmental analysis

The PK parameters included the extrapolated concentration at time 0 ( $C_0$ ), terminal elimination rate constant ( $k_e$ ), terminal half-life ( $t_{1/2}$ ), area under the concentration-time curve (AUC), area under the first moment curve (AUMC), mean residence time (MRT), volume of distribution at terminal phase ( $V_d$ ), and the plasma clearance (CL). The slope of the terminal phase was estimated by log-linear regression using the “best fit” method and uniform weighting. The  $k_e$  was derived from the slope. The  $t_{1/2}$  was calculated as  $0.693/k_e$ . The linear trapezoidal rule was applied for determination of the area under the curve from time 0 to the last measurable concentration ( $AUC_{0-last}$ ) and extrapolated to infinity ( $AUC_{0-\infty}$ ). The CL following the i.v. dosing was calculated as  $Dose/AUC_{0-\infty}$ . The  $V_d$  was calculated as  $CL/k_e$ .

### 2.8.2 Compartmental analysis

A one-compartment body model with different weighting factors was fitted to the kaempferol data, and a two-compartment body model with different weighting factors was fitted to the 4-HPAA data. The goodness of fit was estimated by Akaike's information criterion (AIC), Schwarz's Bayesian criterion (SBC), and weighted sum of squared residuals (WSSR). The equation for the i.v. bolus one-compartment model was as follows:  $C_{p(t)}=C_0 \times \exp^{-k_e t}$ , where  $C_{p(t)}$  is a concentration of a drug in plasma at time  $t$ ;  $C_0$  is the extrapolated concentration at time 0;  $k_e$  is an elimination rate constant; and  $t$  is the time after drug administration. The equation for the i.v. bolus two-compartment model was as follows:  $C_{p(t)}=A \times \exp^{-\alpha t} + B \times \exp^{-\beta t}$ , where  $A$  and  $B$  were mathematical coefficients,  $\alpha$  the distribution rate constant and  $\beta$  the elimination rate constant.

### 2.9 Statistics

The analytical data were calculated in Excel and presented as mean  $\pm$  SD with CV and RE.

## 3 Results

### 3.1 Validation of the bioanalytical methods for kaempferol and 4-HPAA

Detection and quantification of kaempferol and 4-HPAA were performed by UHPLC-MS/MS. Figure 2 shows extracted multiple reaction monitoring (MRM) chromatograms of kaempferol in rat plasma and 4-HPAA in BSA, and their corresponding ISs. Two UHPLC-MS/MS methods were fully validated according to industry guidelines for bioanalytical methods [16, 17]. CV was within 15%, and RE did not exceed  $\pm 15\%$  of the nominal value, except at the LLOQ (20%). Calibration curves were quadratic in the range of 20.0-2000 ng/ml, with a  $1/X$  weighting factor, and a mean  $r^2$  of 0.9993 for kaempferol, and 0.9995 for 4-

HPAA (Supporting information Tables 1 and 2). No carryover was detected (Supporting information Tables 3 and 4). Both methods were shown to be selective, with CV and RE <20% (Supporting information tables 5 and 6). In the blank samples, no peaks were observed at the retention time of analytes, confirming specificity of the methods (Data not shown). Results from the intra- and inter-day imprecision and inaccuracy for both compounds are summarized in Table 2. The mean extraction recovery of kaempferol from plasma was 61.7% (QCL), 60.2% (QCM), and 73.2% (QCH), and recovery of  $^{13}\text{C}_{15}$ -labeled kaempferol was 69.2% (Supporting information Table 7). The extraction yield of 4-HPAA from BSA was 80.2% (QCL), 91.0% (QCM), and 92.3% (QCH), and recovery of  $^2\text{H}_2$ -4-HPAA was 112% (Supporting information Table 8). To demonstrate that there was no impact of dilution on the results, blank samples spiked with the analyte at 10000 ng/ml were prepared and then diluted 10- and 100-fold. For both dilution factors, the CV was below 2.22%, and RE was between -1.48% and 7.63% (Supporting information Tables 9 and 10).

Kaempferol and 4-HPAA were stable in biological samples during sample collection and handling, after three freeze and thaw cycles, after 4 h storage at RT, and after 48 h storage in the autosampler at 10°C (Supporting information Tables 11 and 12). Kaempferol in plasma and 4-HPAA in BSA were shown to be stable during a year of storage below -65°C (Supporting information Figures 1 and 2). The SS of kaempferol stored below -65°C for 180 days and kept for 6 h at RT before analysis was shown to be stable. Degradation expressed as a percentage of the difference was 3.23% (Supporting information Table 13). Degradation of the SS of 4-HPAA (stored below -65°C for 35 days and kept for 6 h at RT) was -0.737% (Supporting information Table 14). Hence, the bioanalytical methods were shown to be reliable and reproducible for the quantification of kaempferol and 4-HPAA.

### 3.2 Pharmacokinetics of kaempferol

Linear and semi-logarithmic plots of mean plasma concentration-time profiles in rats after i.v. administration are presented in Figure 3, and main PK parameters of kaempferol after a single i.v. dose of 1, 2 and 4 mg/kg were calculated by NCA using WinNonlin<sup>®</sup> (Table 3). For the doses of 1 and 2 mg/kg, the plasma concentration of kaempferol dropped below the LLOQ 20 min after injection (Fig. 3). Kaempferol plasma concentrations at time 0, and  $\text{AUC}_{0-\infty}$  increased in a dose-proportional manner over the dose range tested (Fig. 4). The  $k_e$  was high (10.4-13.9  $\text{h}^{-1}$ ), resulting in an extremely short terminal  $t_{1/2}$  of 3.01-4.05 min (Table



3). PK studies of kaempferol in rats showed very high plasma CL (4.00-5.77 l/h/kg) and  $V_d$  of 0.344-0.414 l/kg.

A one-compartment i.v. bolus model with first-order elimination and  $1/\hat{Y}^2$  as weighting factor was chosen as the best fit model, and goodness of fit was confirmed by the AIC, SBC, and WSSR (Supporting information Table 15). The goodness of fit was also shown in a comparison of simulated and observed concentrations vs. time profiles using the one-compartment body model (Fig. 5). PK parameters obtained from a compartmental modeling are summarized in Table 4. The values of AUC, MRT,  $V_d$  and CL of the compartmental analysis were close to those obtained by NCA analysis.

Individual plasma concentrations vs. time profiles after a single oral dose of 5, 10 and 20 mg/kg are shown in Figure 6. After oral administration it was not possible to obtain full concentration-time profiles needed for an estimation of the AUC, and for calculation of the absolute bioavailability (Fig. 6). Plasma samples were then treated with  $\beta$ -glucuronidase/sulfatase to indirectly detect phase II metabolites of kaempferol, and to quantify total kaempferol in plasma (Fig. 7). The data showed that kaempferol was present almost exclusively as conjugates, and that phase II metabolites increased very rapidly after oral administration of kaempferol to reach maximum concentration at 8 h ( $7308 \pm 2213 \mu\text{g/l}$ ). With the aid of a reference compound, one metabolite was identified as kaempferol-3-O-glucuronide. The second metabolite was either the 7- or 4-O-glucuronide, but the exact position of glucuronidation could not be established in this case due to non-availability of reference compounds. While plasma concentrations of glucuronides reached a maximum 30 to 60 min after oral administration and gradually decreased over the sampling period of 12 h, the concentration of total sulfate/glucuronide conjugates reached its maximum at 8 h, before starting to decline slowly. A strong plasma protein binding of sulfate conjugates is probably the most reasonable explanation for this behavior. However, this should be further substantiated in future investigations.

### 3.3 Pharmacokinetics of 4-HPAA

We first determined plasma concentrations of 4-HPAA in the pre-dose samples, and concentrations in the range of 31-127  $\mu\text{g/l}$  were found. For each rat the pre-dose values were subtracted from all post-dose concentrations prior to PK analysis. Concentration-time profiles (linear and semi-logarithmic plots) after a single i.v. administration of 1, 2 and 4 mg/kg of 4-HPAA are shown in Fig. 8. At the dose of 4 mg/kg the compound was detected for up to 8 h (Fig. 8B). For the doses of 1 and 2 mg/kg, in contrast, the plasma concentration of 4-HPAA

dropped below the LLOQ after 2 h. The  $C_0$  and  $AUC_{0-\infty}$  showed a linear increase over the range of administered doses, and thus confirmed dose proportionality (Fig. 9). The PK parameters obtained from the NCA are given in Table 5. The  $k_e$  of 4-HPAA ranged from 1.88-2.45  $h^{-1}$ , resulting in a short terminal  $t_{1/2}$  of 18.6-28.3 min. The compound showed high plasma CL (0.876-1.13 l/h/kg) and  $V_d$  of 0.391-0.666 l/kg.

A two-compartment i.v. bolus model with first-order elimination and  $1/\hat{Y}^2$  as weighting factor fitted the 4-HPAA data well for the groups of 2 and 4 mg/kg b.w. The goodness of fit was confirmed by the AIC, SBC, WSSR (Supporting information Table 16). A comparison of simulated and observed concentrations vs. time profiles with the two-compartment body model also confirmed goodness of fit (Fig. 10). PK parameters of the two-compartment body model are summarized in Table 6. 4-HPAA was quickly distributed from central compartment to peripheral tissues ( $t_{1/2\alpha} = 3.04$ -6.20 min). The distribution phase characterized by rapid decline in 4-HPAA concentrations ( $\alpha = 10.0$ -15.4  $h^{-1}$ ) followed by slower elimination phase ( $\beta = 1.47$ -2.34  $h^{-1}$ ) with elimination half-life ( $t_{1/2\beta}$ ) of 19.3-21.1 min. The values of AUC ( $h \times \mu g/l$ ), AUMC ( $h \times h \times \mu g/l$ ), and MRT (min) were 1884-3914, 554-1666, 22.7-23.1, respectively, and confirmed results obtained from the NCA. In contrast, the two-compartment body model with first-order elimination and  $1/\hat{Y}^2$  as weighting factor did not provide the best fit for the data of the 1 mg/kg dosing group.

In addition, we determined plasma concentrations of 4-HPAA after oral administration of kaempferol (20 mg/kg). The increase of plasma concentration was statistically insignificant in comparison to the endogenous level of the compound (Data not shown).

#### 4 Discussion

After i.v. application, PK of kaempferol followed a one-compartment model. PK study revealed that kaempferol had a high clearance, resulting in an extremely short half-life. Upon oral administration, kaempferol showed low bioavailability due to extensive pre-systemic metabolism. In plasma the compound was present as phase II conjugates. Our findings are supported by the results from *in vitro* intestinal permeability study which demonstrated extensive metabolism of kaempferol in Caco-2 cell model [5]. Further, Barrington et al. identified biotransformation of kaempferol into glucuronides and sulfates inside the Caco-2 cells [18]. Several PK studies with kaempferol have been reported in the literature [11, 14, 15]. From a current perspective, however, they suffered from methodological limitations, such as non-specific detection, and/or from inappropriately high dosing of kaempferol in the

animals. Barve *et al.* [11] evaluated the PK parameters after i.v. application of kaempferol at doses of 10 and 25 mg/kg, and after oral doses of 100 and 250 mg/kg. For the quantification of kaempferol they used UV-detection, which is insensitive and not sufficiently selective for application to PK studies and explains why these extraordinary doses were necessary. In another study [14] kaempferol was administered orally at doses of 1250 and 2500 mg/kg. Such high doses can result in damage to tight junctions causing an increase in intestinal permeability. These examples show the importance of sensitive and validated bioanalytical methods, and appropriate dosing in PK studies with natural products.

For kaempferol a wide range of biological activities have been reported with *in vitro* assays [1, 2], in which the compound was typically tested at micromolar concentrations. Given that we found plasma concentrations of free kaempferol that were one to two orders of magnitude lower than concentrations used in these *in vitro* pharmacological studies, the relevance of reported activities has to be seriously questioned. Future pharmacological studies with kaempferol should, therefore, focus on the properties of the metabolites rather than the parent compound. Examples of pharmacologically active phase II drug metabolites include morphine-6-glucuronide [19] and 4-hydroxytriamterene sulfate [20].

To the best of our knowledge, we determined the first concentration-time profile of 4-HPAA, a major intestinal metabolite of kaempferol. PK of 4-HPAA was characterized by a two-compartment model, with a quick distribution into peripheral tissues as well as a rapid elimination from the body. The plasma levels of 4-HPAA did not increase after oral administration of kaempferol in rats. This can be explained by inability of 4-HPAA to permeate through the intestinal barrier [5].

CNS active molecules need to cross the blood-brain barrier (BBB) in order to exert a pharmacological effect. BBB permeability of kaempferol and 4-HPAA has been previously evaluated in BBB models with rat and human derived cell lines, whereby high permeability of kaempferol and no permeability of 4-HPAA was found [5]. Lacking BBB permeation of 4-HPAA could be due to the negative membrane potential of the BBB, on the one hand, and the negatively charged 4-HPAA ( $\text{clogD}_{7.4} = -1.86$ ) [5, 21], on the other.

#### **4.1 Conclusions**

UHPLC-MS/MS methods for the quantification of kaempferol and 4-HPAA in rat plasma were developed and validated in compliance to international regulatory guidelines for bioanalytical method validation [16, 17]. Poor oral bioavailability and extensive metabolism are the factors limiting the plasma exposure of kaempferol, and the low plasma

concentrations found in our study cast a serious doubt on the relevance of numerous *in vitro* pharmacological data with this flavonoid. Kaempferol was mostly present as phase II metabolites. Among these, one glucuronide could be identified, and high and persistent levels of sulfates were indirectly deduced from the enzymatic treatment of plasma samples. Thus, it is not clear whether *in vivo* pharmacological effects of kaempferol reported in the literature are to be attributed to the parent compound or to its phase II metabolites. PK studies revealed that kaempferol and its metabolite 4-HPAA are highly cleared compounds so that effective concentrations at the site of action do not appear to be reached. Therewith, plasma levels of 4-HPAA were not significantly increased after oral administration of kaempferol. Hence, it is unclear how CNS-related pharmacological effects reported for kaempferol and 4-HPAA are to be explained.

### **Acknowledgements**

Volha Zabela was a recipient of a scholarship from the Swiss Federal Commission. Financial support from the Swiss National Science Foundation (project 105320\_126888) is gratefully acknowledged. Authors thank Orlando Fertig for technical assistance.

### **Conflict of interest**

The authors declare no conflicts of interest.

## 5 References

- [1] J.M. Calderon-Montano, E. Burgos-Moron, C. Pérez-Guerrero, M. López-Lázaro, A review on the dietary flavonoid kaempferol, *Mini Rev. Med. Chem.* 11 (2011) 298-344.
- [2] A.Y. Chen, Y.C. Chen, A review of the dietary flavonoid, kaempferol on human health and cancer chemoprevention, *Food Chem.* 138 (2013) 2099-2107.
- [3] P.C.H. Hollman, Absorption, bioavailability, and metabolism of flavonoids, *Pharm. Biol.* 42 (2004) 74-83.
- [4] J. Van Duynhoven, E.E. Vaughan, D.M. Jacobs, R.A. Kemperman, E.J.J. Van Velzen, G. Gross, L.C. Roger, S. Possemiers, A.K. Smilde, J. Doré, J.A. Westerhuis, T. Van de Wiele, Metabolic fate of polyphenols in the human superorganism, *Proc. Natl. Acad. Sci. USA.* 108 (2011) 4531-4538.
- [5] F. Moradi-Afrapoli, M. Oufir, F.R. Walter, M.A. Deli, M. Smiesko, V. Zabela, V. Butterweck, M. Hamburger, Validation of UHPLC-MS/MS methods for the determination of kaempferol and its metabolite 4-hydroxyphenyl acetic acid, and application to *in vitro* blood-brain barrier and intestinal drug permeability studies, *J. Pharm. Biomed. Anal.* 128 (2016) 264-274.
- [6] L. Griffiths, G. Smith, Metabolism of apigenin and related compounds in the rat. Metabolite formation *in vivo* and by the intestinal microflora *in vitro*, *Biochem. J.* 128 (1972) 901-911.
- [7] J. Winter, M.R. Popoff, P. Grimont, V.D. Bokkenheuser, *Clostridium orbiscindens* sp. nov., a human intestinal bacterium capable of cleaving the flavonoid C-ring, *Int. J. Syst. Microbiol.* 41 (1991) 355-357.
- [8] C. Vissienon, K. Nieber, O. Kelber, V. Butterweck, Route of administration determines the anxiolytic activity of the flavonols kaempferol, quercetin and myricetin—are they prodrugs?, *J. Nutr. Biochem.* 23 (2012) 733-740.
- [9] H. Sabelli, J. Kawcett, E. Gusovsky, J. Edwards, H. Jeffriess, J. Javid, Phenylacetic acid as an indicator in bipolar affective disorders, *J. Clin. Psychopharmacol.* 3 (1983) 268-270.
- [10] B. Davis, D. Durden, R. O'reilly, The effect of age, sex, weight and height on the plasma concentrations in healthy subjects of the acidic metabolites of some biogenic monoamines involved in psychiatric neurological disorders, *Prog. Neuropsychopharmacol. Biol. Psychiatry* 15 (1991) 503-512.
- [11] A. Barve, C. Chen, V. Hebbar, J. Desiderio, C. Saw, A. Kong, Metabolism, oral bioavailability and pharmacokinetics of chemopreventive kaempferol in rats, *Biopharm. Drug Dispos.* 30 (2009) 356-365.
- [12] S. Yodogawa, T. Arakawa, N. Sugihara, K. Furuno, Glucurono- and sulfo-conjugation of kaempferol in rat liver subcellular preparations and cultured hepatocytes, *Biol. Pharm. Bull.* 26 (2003) 1120-1124.
- [13] A. Bolarinwa, J. Linseisen, Validated application of a new high-performance liquid chromatographic method for the determination of selected flavonoids and phenolic acids in human plasma using electrochemical detection, *J. Chromatogr. B.* 823 (2) (2005) 143-151.
- [14] Q. Zhang, Y. Zhang, Z. Zhang, Z. Lu, Sensitive determination of kaempferol in rat plasma by high-performance liquid chromatography with chemiluminescence detection and application to a pharmacokinetic study, *J. Chromatogr. B.* 877 (2009) 3595-3600.
- [15] W.-D. Zhang, X.-J. Wang, S.-Y. Zhou, Y. Gu, R. Wang, T.-L. Zhang, H.Q. Gan, Determination of free and glucuronidated kaempferol in rat plasma by LC-MS/MS: Application to pharmacokinetic study, *J. Chromatogr. B.* 878 (23) (2010) 2137-2140.
- [16] FDA, Guidance for Industry: Bioanalytical Method Validation, Center for Drug Evaluation and Research, Draft Guidance 2013. Available at <http://www.fda.gov/downloads/drugs/guidancecomplianceregulatoryinformation/guidances/ucm368107.pdf>. Accessed February 15, 2016.
- [17] EMA, Guideline on bioanalytical method validation, European Medicines Agency (EMA/CHMP/EWP/192217/2009), 2011. Available at [http://www.ema.europa.eu/docs/en\\_GB/document\\_library/Scientific\\_guideline/2011/08/WC500109686.pdf](http://www.ema.europa.eu/docs/en_GB/document_library/Scientific_guideline/2011/08/WC500109686.pdf). Accessed February 15, 2016.
- [18] R. Barrington, G. Williamson, R.N. Bennett, B.D. Davis, J.S. Brodbelt, P.A. Kroon, Absorption, conjugation and efflux of the flavonoids, kaempferol and galangin, using the intestinal CaCo-2/TC7 cell model, *J. Funct. Foods.* 1 (2009) 74-87.

- [19] R. Osborne, P. Thompson, S. Joel, D. Trew, N. Patel, M. Slevin, The analgesic activity of morphine-6-glucuronide, *Br. J. Clin. Pharmacol.* 34 (1992) 130-138.
- [20] A.E. Busch, H. Suessbrich, K. Kunzelmann, A. Hipper, R. Greger, S. Waldegger, E. Mutschler, B. Lindemann, F. Lang, Blockade of epithelial Na<sup>+</sup> channels by triamterenes—Underlying mechanisms and molecular basis, *Pflügers Archiv.* 432 (1996) 760-766.
- [21] L. Di, E.H. Kerns, *Drug-like properties: concepts, structure design and methods from ADME to toxicity optimization*, 2nd ed., Academic Press, New York, 2015.

## Legends for Figures

Figure 1. Chemical structures of kaempferol (A), kaempferol-3-O-glucuronide (B) and 4-HPAA (C).

Figure 2. Typical MRM chromatograms of kaempferol quantifier (A), kaempferol qualifier (B),  $^{13}\text{C}_{15}$ -labeled kaempferol (C) in rat plasma, and 4-HPAA quantifier (D), 4-HPAA qualifier (E), and  $^2\text{H}_2$ -labeled 4-HPAA (F) in BSA. Both analytes presented at LLOQ (20 ng/ml).

Figure 3. Plasma concentrations of kaempferol (mean  $\pm$  S.D.) after a single intravenous administration of 1, 2 and 4 mg/kg b.w., shown as linear (A) and semi-logarithmic (B) plots.

Figure 4.  $C_0$  and  $\text{AUC}_{0-\text{inf}}$  (mean  $\pm$  S.D.) of kaempferol vs. dosing group (solid line) and fitted simple linear regression (dashed line, for visual comparison).

Figure 5. Observed (mean  $\pm$  S.D.) and simulated concentration vs. time profiles of kaempferol in rats after a single intravenous dose of 1 (A), 2 (B), and 4 (C) mg/kg b.w.

Figure 6. Plasma concentration vs. time profiles of kaempferol after a single oral dose of 5 (A), 10 (B), and 20 (C) mg/kg b.w. Data for individual rats are shown.

Figure 7. Plasma concentration of free kaempferol and its glucuronide conjugates (oral dosage = 20 mg/kg) determined after enzymatic treatment ( $n = 7$ ). Data are shown as mean  $\pm$  SD.

Figure 8. Plasma concentrations of 4-HPAA (mean  $\pm$  S.D.) after a single intravenous administration of 1, 2 and 4 mg/kg b.w., shown as linear (A) and semi-logarithmic (B) plots.

Figure 9.  $C_0$  and  $\text{AUC}_{0-\text{inf}}$  (mean  $\pm$  S.D.) of 4-HPAA vs. dosing group (solid lines), and fitted simple linear regression (dashed line, for visual comparison).

Figure 10. Observed (mean  $\pm$  S.D.) and simulated concentration vs. time profiles of 4-HPAA in rats after a single intravenous dose of 2 (A) and 4 (B) mg/kg b.w.

## **TABLES**

Table 1: MS/MS parameters of the analytes and the internal standards.

Compound	Precursor ion ( <i>m/z</i> )	Product ion ( <i>m/z</i> )	Fragmentor (V)	Collision energy (V)	ESI polarity
Kaempferol quantifier	287.06	69.0	155	54	positive
Kaempferol qualifier	287.06	152.9	155	34	positive
Kaempferol-3-O-glucuronide quantifier	463.09	287	113	10	positive
Kaempferol-3-O-glucuronide qualifier	463.09	153	113	62	positive
<sup>13</sup> C <sub>15</sub> -kaempferol	302.0	160.1	167	38	positive
4-HPAA quantifier	151.0	107.0	102	10	negative
4-HPAA qualifier	151.0	106.6	102	6	negative
<sup>2</sup> H <sub>2</sub> -4-HPAA	153.1	109.0	102	10	negative



Table 2: Within (n = 6)- and between (n = 18)-run imprecision (expressed as CV%) and inaccuracy (expressed as RE%) of kaempferol QC samples in rat plasma and 4-HPAA QC samples in BSA solution, based on 3 series at 5 different levels.

Nominal level (ng/ml)	Kaempferol					4-HPAA				
	20.0	60.0	1000	1600	2000	20.0	60.0	1000	1600	2000
Intra-run mean	19.4	60.8	1029	1652	2009	20.4	63.3	1026	1613	1980
Intra-run S.D.	1.32	2.15	23.3	69.5	39.7	1.83	1.94	13.4	14.0	8.83
Intra-run CV %	6.82	3.54	2.26	4.21	1.97	9.00	3.06	1.31	0.865	0.446
Intra-run RE %	-3.15	1.39	2.89	3.24	0.448	1.82	5.48	2.55	0.829	-1.01
Inter-run mean	19.8	62.5	1030	1637	1994	21.0	63.4	1038	1649	2049
Inter-run S.D.	1.06	1.97	18.9	41.6	36.2	1.21	1.84	14.3	42.1	29.2
Inter-run CV%	5.35	3.16	1.84	2.53	1.81	5.84	2.93	1.38	2.55	1.43
Inter-run RE %	-1.25	4.11	2.97	2.28	-0.291	4.97	5.70	3.75	3.05	2.44

Table 3: PK parameters of kaempferol after a single intravenous administration of 1, 2 and 4 mg/kg b.w., calculated by non-compartmental analysis (mean  $\pm$  S.D.).

Dosing group (mg/kg)	1	2	4
n	6	6	6
C <sub>0</sub> ( $\mu\text{g/l}$ )	3880 $\pm$ 1019	5780 $\pm$ 2358	13270 $\pm$ 2242
k <sub>e</sub> (1/h)	11.8 $\pm$ 1.13	13.9 $\pm$ 1.34	10.4 $\pm$ 0.992
t <sub>1/2</sub> (min)	3.56 $\pm$ 0.344	3.01 $\pm$ 0.280	4.05 $\pm$ 0.404
AUC <sub>0-last</sub> (h $\times$ $\mu\text{g/l}$ )	262 $\pm$ 77.0	368 $\pm$ 107	992 $\pm$ 107
AUC <sub>0-<math>\infty</math></sub> (h $\times$ $\mu\text{g/l}$ )	266 $\pm$ 76.9	372 $\pm$ 108	996 $\pm$ 108
AUMC <sub>0-last</sub> (h $\times$ h $\times$ $\mu\text{g/l}$ )	18.7 $\pm$ 3.94	20.7 $\pm$ 5.19	73.3 $\pm$ 16.6
AUMC <sub>0-<math>\infty</math></sub> (h $\times$ h $\times$ $\mu\text{g/l}$ )	20.0 $\pm$ 9.43	22.1 $\pm$ 5.75	75.9 $\pm$ 17.2
CL (l/h/kg)	4.00 $\pm$ 0.975	5.77 $\pm$ 1.60	4.06 $\pm$ 0.432
V <sub>d</sub> (l/kg)	0.341 $\pm$ 0.0837	0.414 $\pm$ 0.109	0.396 $\pm$ 0.0624
MRT (min)	4.39 $\pm$ 0.876	3.61 $\pm$ 0.437	4.54 $\pm$ 0.615

Table 4: PK parameters of kaempferol after a single intravenous dose of 1, 2 and 4 mg/kg b.w., calculated by compartmental analysis<sup>a</sup> (mean  $\pm$  S.D.).

Dosing group (mg/kg)	1	2	4
n	6	6	6
C <sub>max</sub> ( $\mu\text{g/l}$ )	2928 $\pm$ 804	4663 $\pm$ 1146	9744 $\pm$ 1397
k <sub>e</sub> (1/h)	12.1 $\pm$ 1.57	14.3 $\pm$ 1.23	11.0 $\pm$ 0.777
t <sub>1/2</sub> (min)	3.51 $\pm$ 0.550	2.93 $\pm$ 0.255	3.79 $\pm$ 0.266
AUC (h $\times$ $\mu\text{g/l}$ )	250 $\pm$ 94.5	328 $\pm$ 86.1	887 $\pm$ 130
AUMC (h $\times$ h $\times$ $\mu\text{g/l}$ )	21.9 $\pm$ 12.1	23.3 $\pm$ 6.71	81.1 $\pm$ 14.8
CL (l/h/kg)	4.40 $\pm$ 1.30	6.44 $\pm$ 1.63	4.58 $\pm$ 0.621
V <sub>d</sub> (l/kg)	0.361 $\pm$ 0.0855	0.451 $\pm$ 0.109	0.417 $\pm$ 0.0556
MRT (min)	5.06 $\pm$ 0.794	4.23 $\pm$ 0.368	5.47 $\pm$ 0.384

a) A one-compartment model with  $1/\bar{Y}^2$  as weighting factor was fitted to the data.

Table 5: PK parameters of 4-HPAA after a single intravenous administration of 1, 2 and 4 mg/kg b.w., calculated by non-compartmental analysis (mean  $\pm$  S.D.).

Dosing group (mg/kg)	1	2	4
n	5	7	6
C <sub>0</sub> ( $\mu$ g/l)	3651 $\pm$ 1333	8763 $\pm$ 2415	19788 $\pm$ 1643
k <sub>e</sub> (1/h)	2.45 $\pm$ 1.42	2.42 $\pm$ 0.577	1.88 $\pm$ 0.860
t <sub>1/2</sub> (min)	20.8 $\pm$ 8.84	18.6 $\pm$ 6.88	28.3 $\pm$ 17.5
AUC <sub>0-last</sub> (h $\times$ $\mu$ g/l)	1352 $\pm$ 691	1882 $\pm$ 739	4095 $\pm$ 914
AUC <sub>0-<math>\infty</math></sub> (h $\times$ $\mu$ g/l)	1405 $\pm$ 699	1974 $\pm$ 759	4134 $\pm$ 909
AUMC <sub>0-last</sub> (h $\times$ h $\times$ $\mu$ g/l)	661 $\pm$ 494	600 $\pm$ 475	1682 $\pm$ 861
AUMC <sub>0-<math>\infty</math></sub> (h $\times$ h $\times$ $\mu$ g/l)	784 $\pm$ 556	774 $\pm$ 639	1978 $\pm$ 1000
CL (l/h/kg)	0.876 $\pm$ 0.427	1.13 $\pm$ 0.379	1.00 $\pm$ 0.179
V <sub>d</sub> (l/kg)	0.391 $\pm$ 0.163	0.472 $\pm$ 0.114	0.666 $\pm$ 0.447
MRT (min)	29.9 $\pm$ 13.6	21.4 $\pm$ 8.90	28.1 $\pm$ 11.9

Table 6: PK parameters of 4-HPAA after a single intravenous dose of 2 and 4 mg/kg b.w., calculated by compartmental analysis<sup>a</sup> (mean  $\pm$  S.D.).

Dosing group (mg/kg)	2	4
n	7	6
C <sub>max</sub> ( $\mu\text{g/l}$ )	9212 $\pm$ 2928	17987 $\pm$ 4202
A ( $\mu\text{g/l}$ )	5953 $\pm$ 2175	13266 $\pm$ 906
B ( $\mu\text{g/l}$ )	3259 $\pm$ 1177	4721 $\pm$ 3412
$\alpha$ (1/h)	15.4 $\pm$ 5.77	10.0 $\pm$ 6.46
$\beta$ (1/h)	2.34 $\pm$ 0.595	1.47 $\pm$ 1.13
t <sub>1/2<math>\alpha</math></sub> (min)	3.04 $\pm$ 1.15	6.20 $\pm$ 4.30
t <sub>1/2<math>\beta</math></sub> (min)	19.3 $\pm$ 7.21	21.1 $\pm$ 7.59
k <sub>10</sub> (1/h)	5.08 $\pm$ 1.30	4.41 $\pm$ 1.30
k <sub>12</sub> (1/h)	5.71 $\pm$ 3.57	4.62 $\pm$ 2.44
k <sub>21</sub> (1/h)	6.92 $\pm$ 2.18	5.68 $\pm$ 3.02
AUC <sub>0-<math>\infty</math></sub> (h $\times\mu\text{g/l}$ )	1884 $\pm$ 710	3914 $\pm$ 848
AUMC (h $\times$ h $\times\mu\text{g/l}$ )	554 $\pm$ 232	1666 $\pm$ 1196
CL (l/h/kg)	1.18 $\pm$ 0.390	1.06 $\pm$ 0.191
V <sub>c</sub> (l/kg)	0.238 $\pm$ 0.0766	0.253 $\pm$ 0.0740
V <sub>p</sub> (l/kg)	0.176 $\pm$ 0.0676	0.169 $\pm$ 0.0516
MRT (min)	22.7 $\pm$ 9.44	23.1 $\pm$ 9.63

a) A two-compartment model with  $1/Y^2$  as weighting factor was fitted to the data.

## **FIGURES**

Figure 1: Chemical structures of kaempferol (A), kaempferol-3-O-glucuronide (B) and 4-HPAA (C).

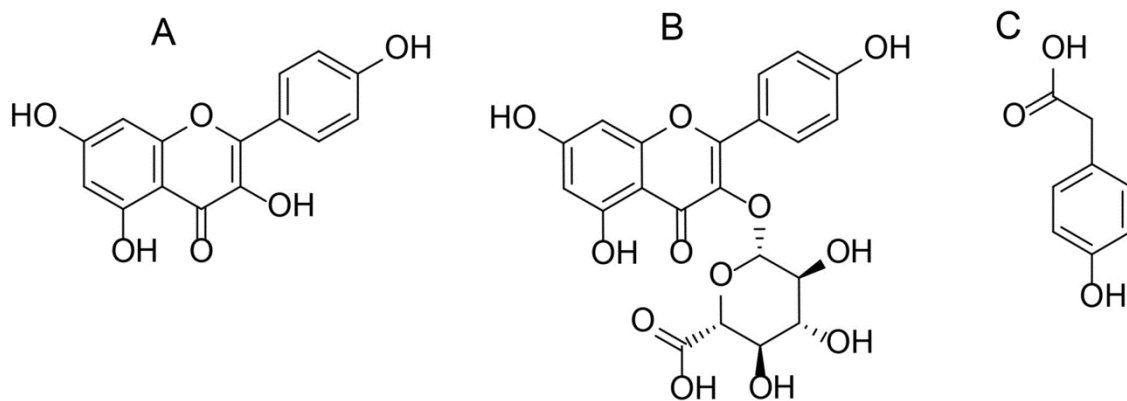


Figure 2: Typical MRM chromatograms of kaempferol quantifier (A), kaempferol qualifier (B),  $^{13}\text{C}_{15}$ -labeled kaempferol (C) in rat plasma, and 4-HPAA quantifier (D), 4-HPAA qualifier (E), and  $^2\text{H}_2$ -labeled 4-HPAA (F) in BSA. Both analytes presented at LLOQ (20 ng/ml).

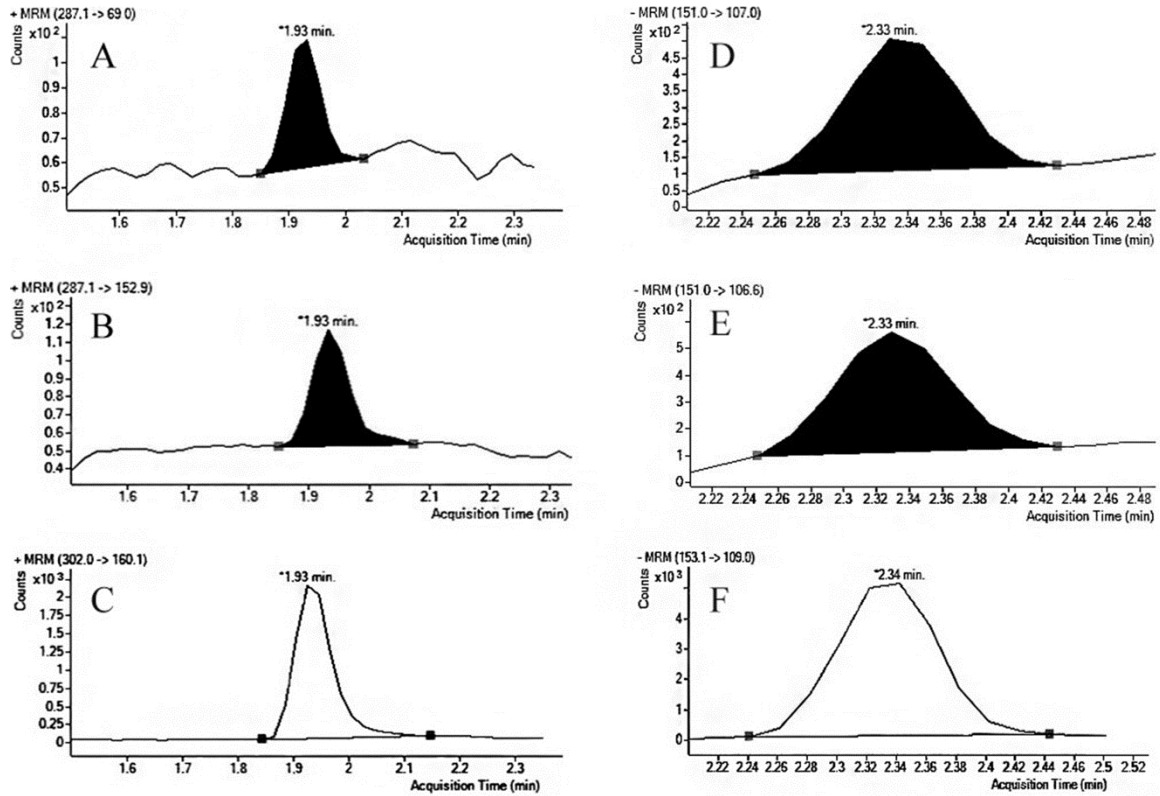


Figure 3: Plasma concentrations of kaempferol (mean  $\pm$  S.D.) after a single intravenous administration of 1, 2 and 4 mg/kg b.w., shown as linear (A) and semi-logarithmic (B) plots.

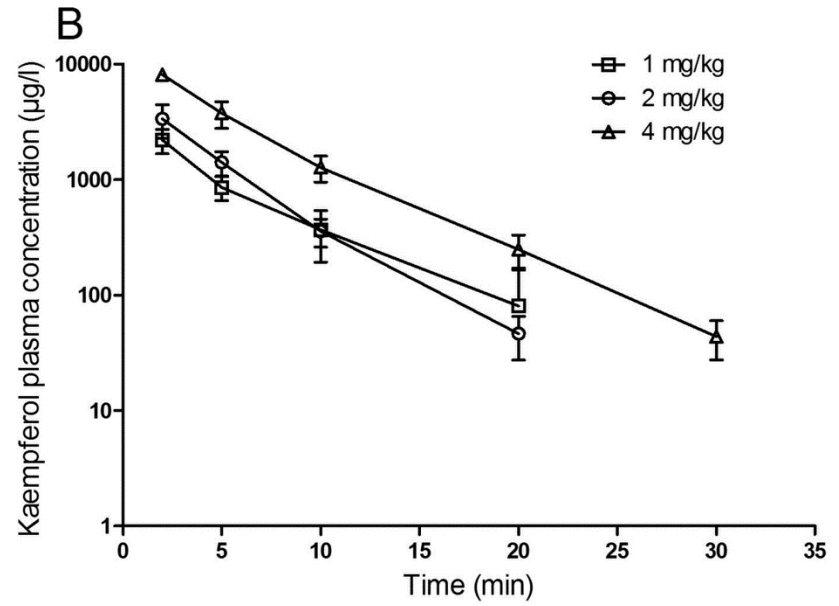
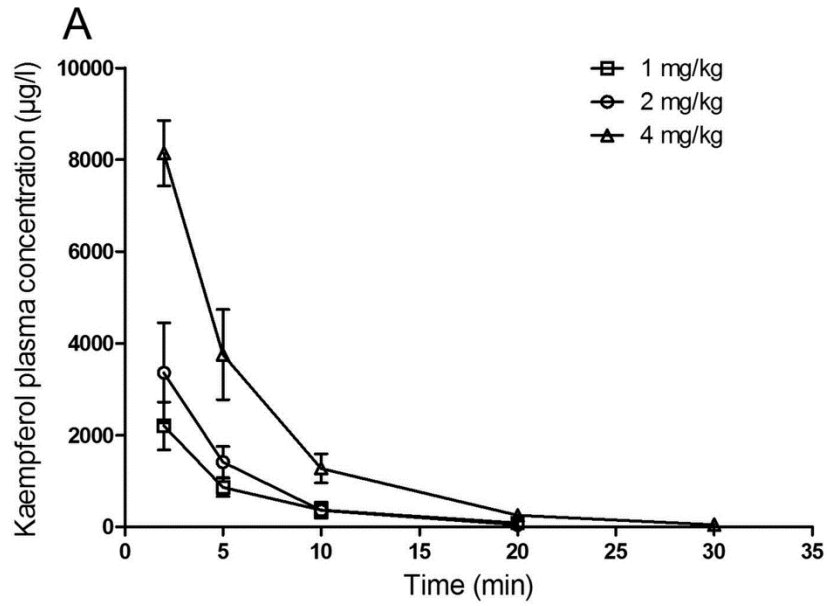




Figure 4:  $C_0$  and  $AUC_{0-inf}$  (mean  $\pm$  S.D.) of kaempferol vs. dosing group (solid line) and fitted simple linear regression (dashed line, for visual comparison).

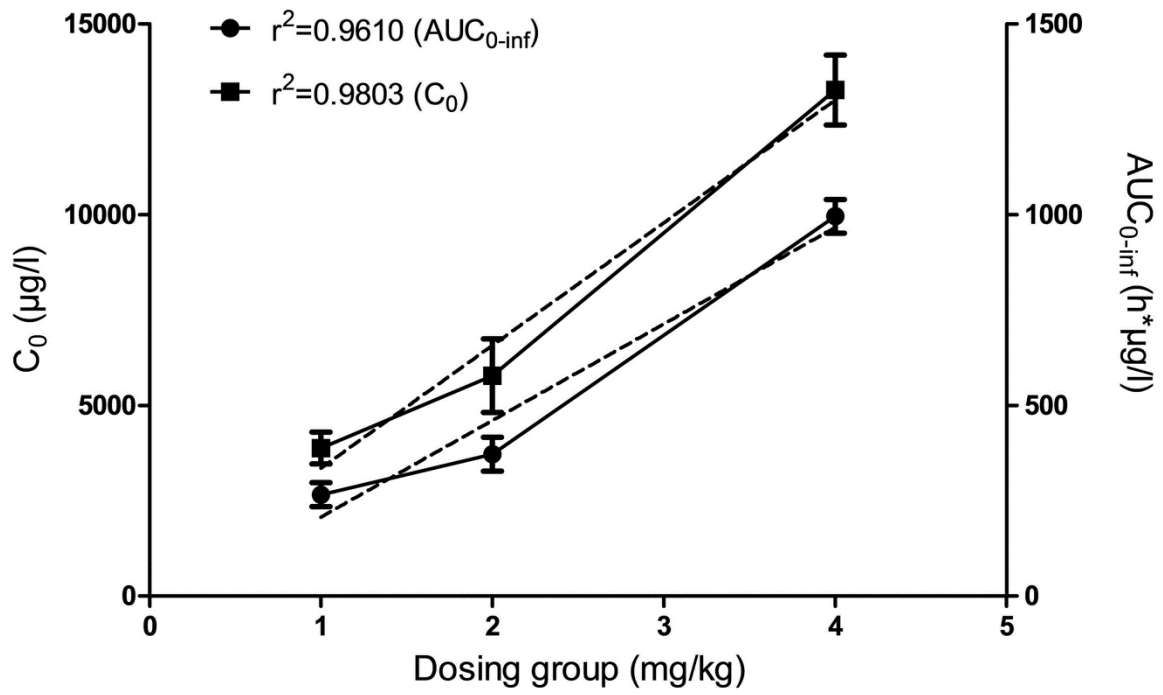


Figure 5: Observed (mean  $\pm$  S.D.) and simulated concentration vs. time profiles of kaempferol in rats after a single intravenous dose of 1 (A), 2 (B), and 4 (C) mg/kg b.w.

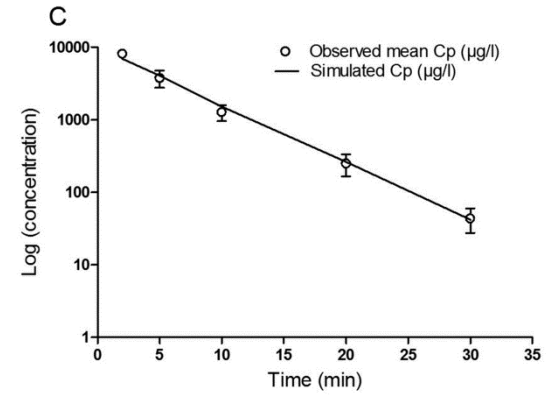
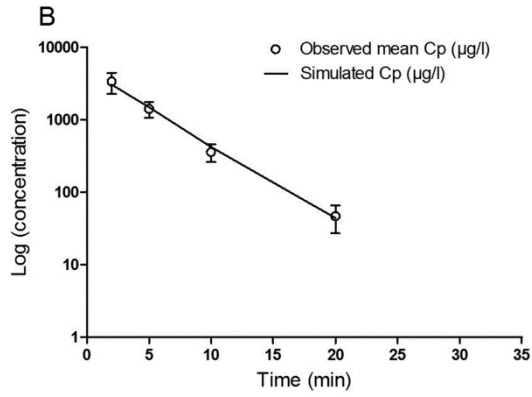
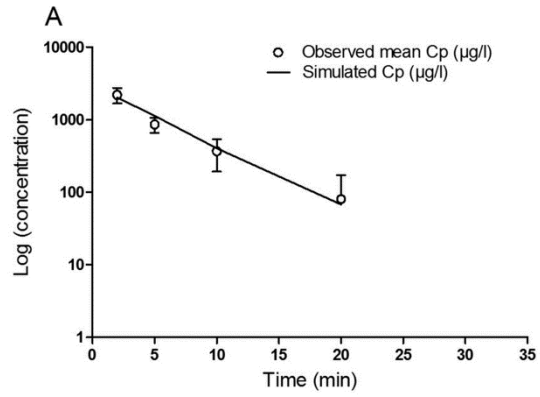


Figure 6: Plasma concentration vs. time profiles of kaempferol after a single oral dose of 5 (A), 10 (B), and 20 (C) mg/kg b.w. Data for individual rats are shown.

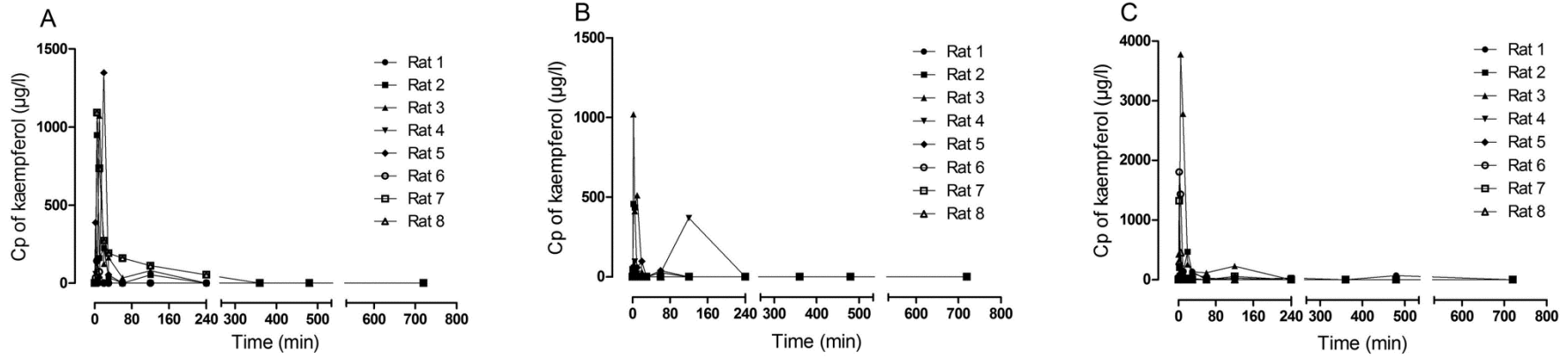


Figure 7: Plasma concentration of free kaempferol and its glucuronide conjugates (oral dosage = 20 mg/kg) determined after enzymatic treatment (n = 7). Data are shown as mean  $\pm$  S.D.

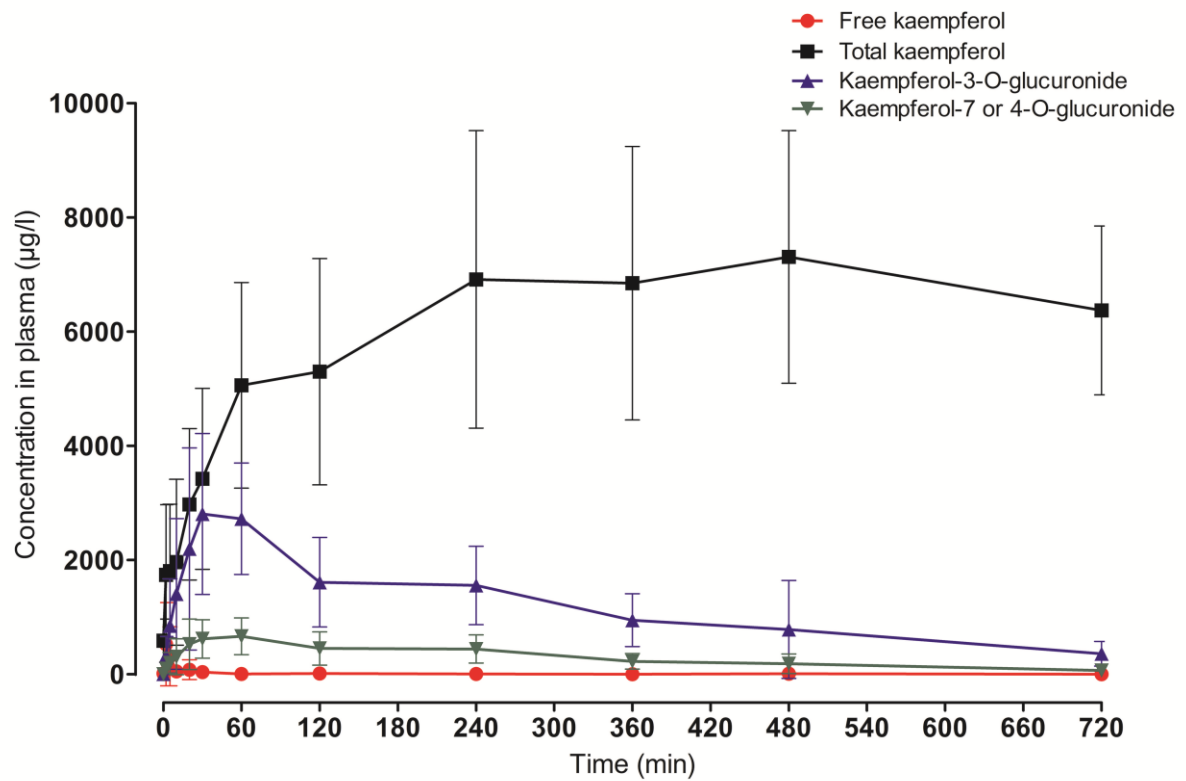


Figure 8: Plasma concentrations of 4-HPAA (mean  $\pm$  S.D.) after a single intravenous administration of 1, 2 and 4 mg/kg b.w., shown as linear (A) and semi-logarithmic (B) plots.

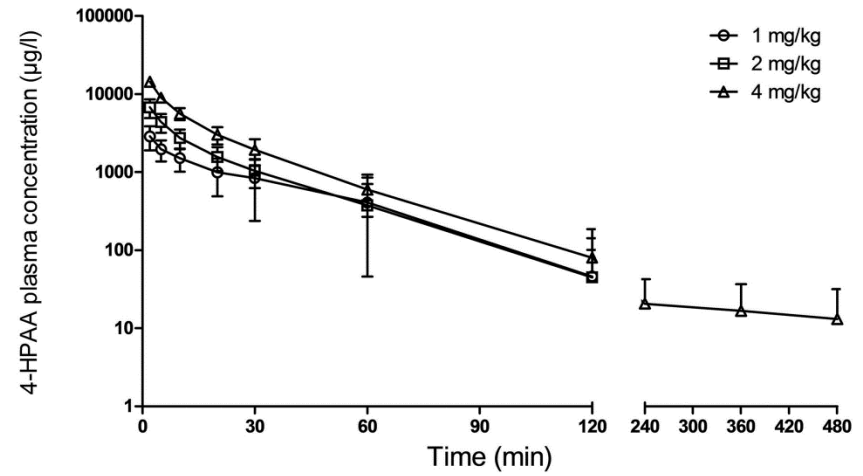
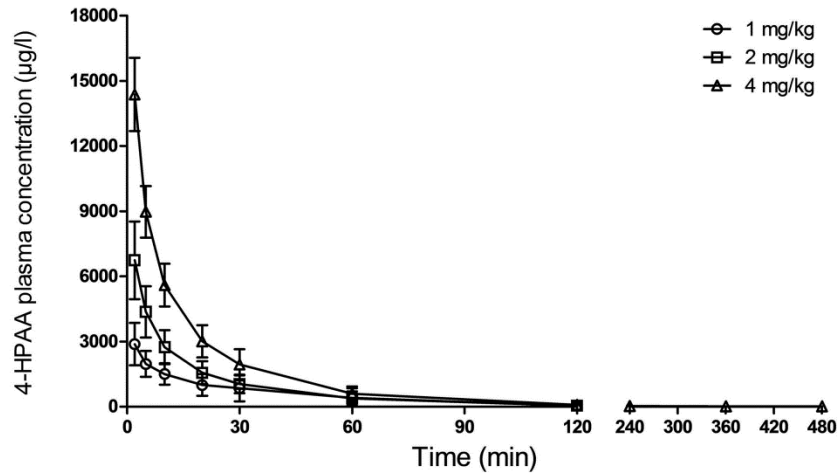


Figure 9:  $C_0$  and  $AUC_{0-inf}$  (mean  $\pm$  S.D.) of 4-HPAA vs. dosing group (solid lines), and fitted simple linear regression (dashed line, for visual comparison).

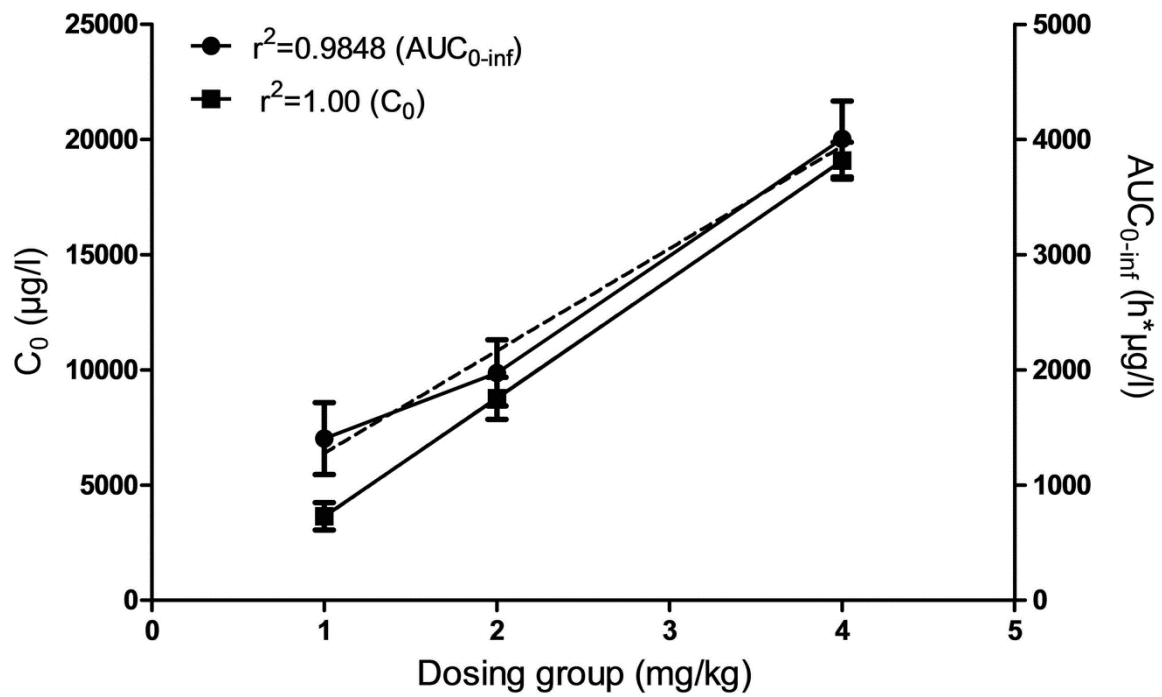
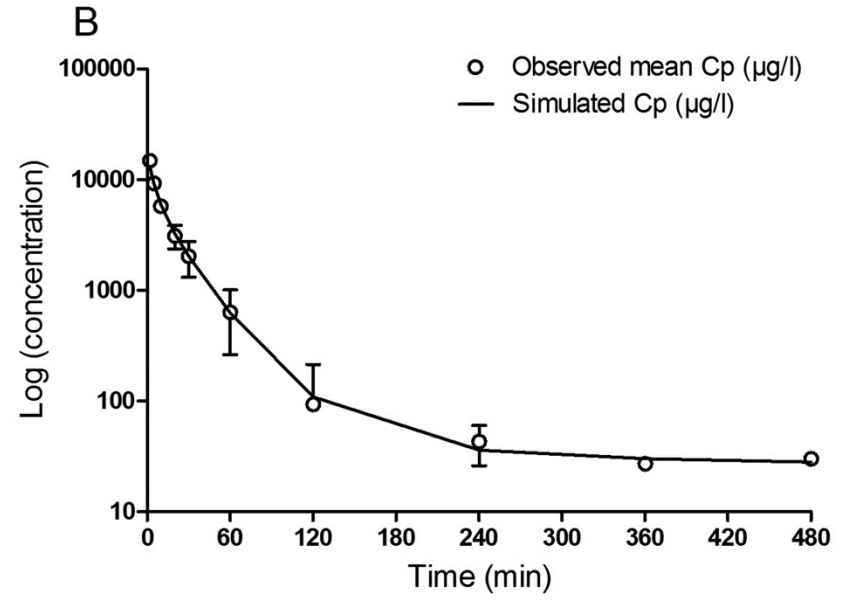
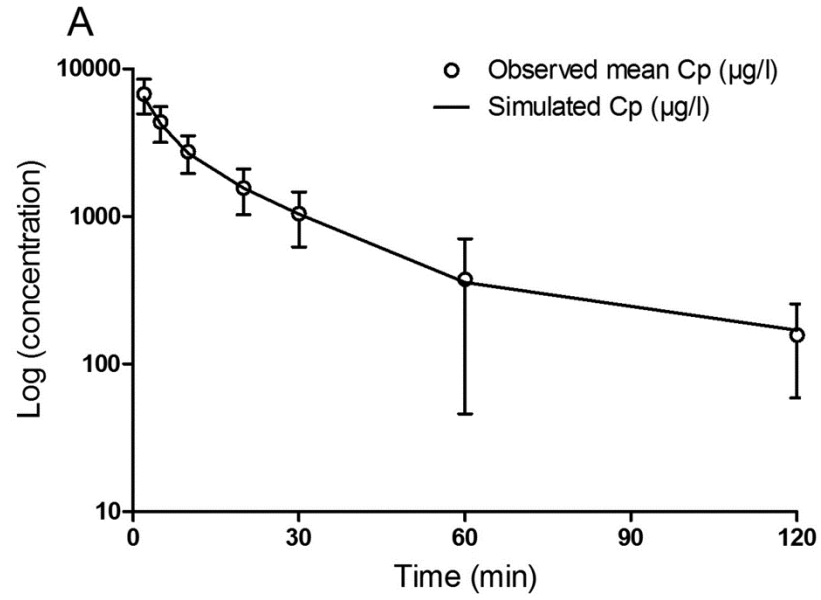


Figure 10: Observed (mean  $\pm$  S.D.) and simulated concentration vs. time profiles of 4-HPAA in rats after a single intravenous dose of 2 (A) and 4 (B) mg/kg b.w.



## **SUPPORTING INFORMATION**

### **Pharmacokinetics of dietary kaempferol and its metabolite 4-hydroxyphenylacetic acid in rats**

Volha Zabela<sup>a</sup>, Chethan Sampath<sup>b</sup>, Mouhssin Oufir<sup>a</sup>, Fahimeh Moradi-Afrapoli<sup>a</sup>, Veronika Butterweck<sup>b,1</sup> and Matthias Hamburger<sup>a\*</sup>

<sup>a</sup>Pharmaceutical Biology Laboratory, Department of Pharmaceutical Sciences, University of Basel, Klingelbergstrasse 50, CH-4056 Basel, Switzerland

<sup>b</sup>Department of Pharmaceutics, College of Pharmacy, University of Florida, 1345 Center Drive, Gainesville, FL, USA

#### **Author's present address:**

<sup>1</sup>Institute for Pharma Technology, School of Life Sciences, University of Applied Sciences Northwestern Switzerland, Gründenstrasse 40, CH-4132 Muttenz, Switzerland

#### **Author's e-mails:**

volha.zabela@unibas.ch (Zabela); chethan@ufl.edu (Sampath); mouhssin.oufir@unibas.ch (Oufir); veronika.butterweck@fhnw.ch (Butterweck); matthias.hamburger@unibas.ch (Hamburger)

#### **\*Corresponding author:**

Professor Matthias Hamburger

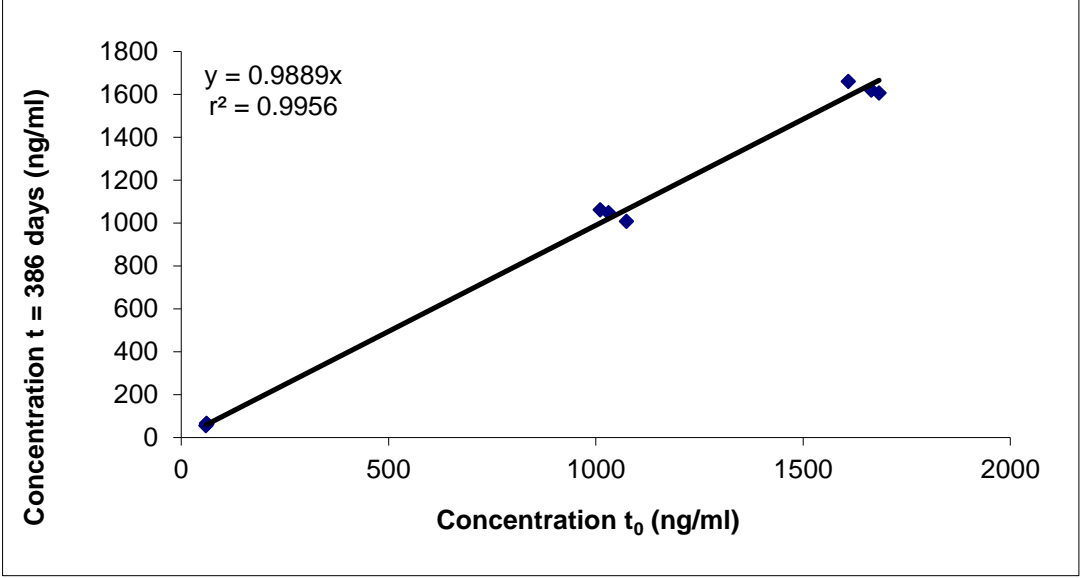
**E-mail:** matthias.hamburger@unibas.ch

**Fax:** +41 61 267 14 74

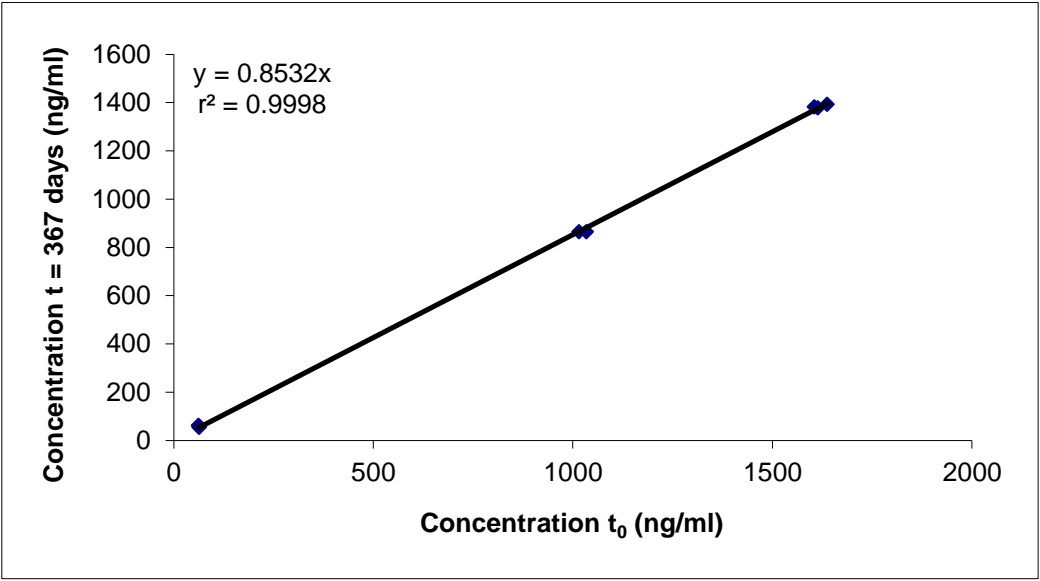
**Address:** Pharmaceutical Biology Laboratory, Department of Pharmaceutical Sciences, University of Basel, Klingelbergstrasse 50, CH-4056, Basel, Switzerland



Supporting information Figure 1: Long-term stability of kaempferol in rat plasma stored for 386 days below -65°C (n=3).



Supporting information Figure 2: Long-term stability of 4-HPAA in BSA stored for 367 days below -65°C (n=3).



Supporting information Table 1: Calibrators and calibration curve parameters of kaempferol (n=8).

Response:  $A \times \text{Conc.}^2 + B \times \text{Conc.} + C$ , Quadratic regression, 1/X weighting.

Run No.	Nominal level (ng/ml)							Regression parameters			
	20.0	50.0	100	250	500	1000	2000	A	B	C	R <sup>2</sup>
<b>1</b>	19.8	51.9	109	255	474	1052	2053	0.000000209	0.00413	0.0211	0.9984
	18.7	48.2	99.3	256	479	985	1938				
<b>2</b>	20.6	51.5	101	250	507	1005	1987	0.0000000810	0.00426	0.0133	0.9998
	19.4	48.8	99.1	243	509	981	2017				
<b>3</b>	20.2	49.6	106	243	505	983	1997	0.0000000812	0.00455	0.0204	0.9998
	18.8	50.8	100	252	502	1005	2007				
<b>4</b>	18.4	47.4	101	250	494	974	1950	0.0000000886	0.00409	0.0190	0.9992
	21.3	52.1	100	252	522	1000	2058				
<b>Mean</b>	19.7	50.0	102	250	499	998	2001	0.000000115	0.00426	0.0185	0.9993
<b>S.D.</b>	1.00	1.78	3.63	4.93	16.0	24.6	43.1	0.0000000626	0.000209		
<b>CV%</b>	5.11	3.55	3.56	1.97	3.22	2.46	2.15				
<b>RE%</b>	-1.74	0.0493	1.93	0.0880	-0.193	-0.197	0.0513				

Supporting information Table 2: Calibrators and calibration curve parameters of 4-HPAA (n=8).

Response:  $A \times \text{Conc.}^2 + B \times \text{Conc.} + C$ , Quadratic regression, 1/X weighting.

Run No.	Nominal level (ng/ml)							Regression parameters			
	20.0	50.0	100	250	500	1000	2000	A	B	C	R <sup>2</sup>
<b>1</b>	19.5	55.4	111	266	507	987	2003	0.0000000396	0.00235	0.0591	0.9988
	17.1	44.4	103	245	513	944	2024				
<b>2</b>	21.3	51.2	*2719	0.00	506	1004	2013	0.0000000365	0.00228	0.0513	0.9998
	19.1	49.1	100	239	499	1007	1982				
<b>3</b>	22.3	49.3	100	252	494	985	1996	0.00000000420	0.00225	0.0573	0.9997
	18.7	49.9	96.8	246	507	1023	0.00				
<b>4</b>	19.7	52.5	98.6	257	501	1009	2050	0.0000000104	0.00231	0.0675	0.9995
	20.8	48.2	96.5	241	507	989	1950				
<b>Mean</b>	19.8	50.0	101	249	504	993	2002	0.0000000227	0.00230	0.0588	0.9995
<b>S.D.</b>	1.65	3.22	5.12	9.51	5.92	23.7	31.5	0.0000000180	0.0000414		
<b>CV%</b>	8.31	6.44	5.08	3.81	1.17	2.39	1.57				
<b>RE%</b>	-0.948	0.0215	0.928	-0.205	0.837	-0.654	0.124				

\* > 15% outside acceptance criteria

Supporting information Table 3: Carry-over assessment of the analyte kaempferol and the internal standard (IS) <sup>13</sup>C<sub>15</sub>-labeled kaempferol (n=8).

Run No.	Replicate	Peak response (counts)				Carry-over (%)		Mean Carry-over (%)	
		Blank sample		LLOQ		Analyte	IS	Analyte	IS
<b>1</b>	1	0.00	0.00	332	3223	0.00	0.00	0.00	0.00
	2	0.00	0.00	385	3904	0.00	0.00		
<b>2</b>	1	0.00	0.00	399	3953	0.00	0.00	0.00	0.00
	2	0.00	0.00	394	4103	0.00	0.00		
<b>3</b>	1	0.00	0.00	467	4157	0.00	0.00	0.00	0.00
	2	0.00	0.00	487	4604	0.00	0.00		
<b>4</b>	1	0.00	0.00	469	4972	0.00	0.00	0.00	0.00
	2	0.00	0.00	452	4262	0.00	0.00		
<b>Mean</b>						0.00	0.00		

Supporting information Table 4: Carry-over assessment of the analyte 4-HPAA and the internal standard (IS) <sup>2</sup>H<sub>2</sub>-labeled 4-HPAA (n=8).

Run No.	Replicate	Peak response (counts)				Carry-over (%)		Mean Carry-over (%)	
		Blank sample		LLOQ		Analyte	IS	Analyte	IS
<b>1</b>	1	0.00	0.00	1892	18022	0.00	0.00	0.00	0.00
	2	0.00	0.00	1449	14601	0.00	0.00		
<b>2</b>	1	0.00	0.00	2420	24206	0.00	0.00	0.00	0.00
	2	0.00	0.00	2815	29673	0.00	0.00		
<b>3</b>	1	0.00	0.00	2459	22877	0.00	0.00	0.00	0.00
	2	0.00	0.00	2944	29612	0.00	0.00		
<b>4</b>	1	0.00	0.00	2610	23094	0.00	0.00	0.00	0.00
	2	0.00	0.00	3110	26920	0.00	0.00		
<b>Mean</b>						0.00	0.00		

Supporting information Table 5: Selectivity test of kaempferol, based on three different plasma lots spiked at LLOQ (n=6).

<b>Nominal level (ng/ml)</b>	<b>20.0</b>
Mean	21.2
S.D.	1.21
CV%	5.70
RE%	1.94

Supporting information Table 6: Selectivity test of 4-HPAA, based on three different BSA lots spiked at LLOQ (n=6).

<b>Nominal level (ng/ml)</b>	<b>20.0</b>
Mean	21.5
S.D.	2.95
CV%	13.7
RE%	-1.93

Supporting information Table 7: Absolute recovery of kaempferol and the IS <sup>13</sup>C<sub>15</sub>-labeled kaempferol from rat plasma (n=6).

<b>Kaempferol nominal level (ng/ml)</b>	<b>60.0</b>	<b>1000</b>	<b>1600</b>
Absolute recovery (%)	61.7	60.2	73.2
CV%	8.62	12.9	2.87
SD	5.32	7.78	2.10

<b>IS nominal level (ng/ml)</b>	<b>225</b>
Absolute recovery (%)	69.2
CV%	9.58
SD	6.63

Supporting information Table 8: Absolute recovery of 4-HPAA and the IS <sup>2</sup>H<sub>2</sub>-labeled 4-HPAA from BSA (n=6).

<b>4-HPAA nominal level (ng/ml)</b>	<b>60.0</b>	<b>1000</b>	<b>1600</b>
Absolute recovery (%)	80.2	91.0	92.3
CV%	6.62	2.17	3.11
SD	5.31	1.98	2.87

<b>IS nominal level (ng/ml)</b>	<b>286</b>
Absolute recovery (%)	112
CV%	9.75
SD	10.9



Supporting information Table 9: Dilution test of kaempferol in rat plasma at nominal concentration of 10000 ng/ml (n=6).

<b>Nominal level (ng/ml)</b>	<b>10000</b>	
<b>Dilution factor</b>	<b>10X</b>	<b>100X</b>
Mean	9852	10639
S.D.	163	186
CV%	1.66	1.75
RE%	-1.48	6.39

Supporting information Table 10: Dilution test of 4-HPAA in BSA solution at nominal concentration of 10000 ng/ml (n=6).

<b>Nominal level (ng/ml)</b>	<b>10000</b>	
<b>Dilution factor</b>	<b>10X</b>	<b>100X</b>
Mean	10744	10763
S.D.	135	239
CV%	1.26	2.22
RE%	7.44	7.63

Supporting information Table 11: Short-term stabilities of kaempferol, expressed as RE% (n=6).

<b>Nominal level (ng/ml)</b>	<b>60.0</b>	<b>1600</b>
Three successive freeze/thaw cycles below -65°C	2.74	-0.483
Benchtop at RT for 4 h	2.60	0.164
Autosampler at 10°C for 48 h	12.1	6.93

Supporting information Table 12: Short-term stabilities of 4-HPAA, expressed as RE% (n=6).

<b>Nominal level (ng/ml)</b>	<b>60.0</b>	<b>1600</b>
Three successive freeze/thaw cycles below -65°C	-1.81	5.52
Benchtop at RT for 4 h	-8.38	2.04
Autosampler at 10°C for 48 h	-13.2	4.01

Supporting information Table 13: Stock solution (SS) stability of kaempferol in DMSO, stored below -65°C for 180 days (n=6).

	<b>Kaempferol SS stored below -65°C for 180 days with freshly prepared IS SS</b>	<b>Freshly prepared kaempferol SS with freshly prepared IS SS</b>
Mean peak area ratio	2.70	2.61
S.D.	0.0122	0.0118
CV%	0.454	0.453
<b>Difference%</b>		3.23

Supporting information Table 14: Stock solution (SS) stability of 4-HPAA in DMSO, stored below -65°C for 35 days (n=6).

	<b>4-HPAA SS stored below -65°C for 35 days with freshly prepared IS SS</b>	<b>Freshly prepared 4-HPAA SS with freshly prepared IS SS</b>
Mean peak area ratio	628	632
S.D.	15.3	30.1
CV%	2.43	4.76
<b>Difference%</b>		-0.737

Supporting information Table 15: Diagnostic table for a one-compartment model with  $1/\hat{Y}^2$  as weighting factor fitted to the kaempferol data.

<b>Dosing group (mg/kg)</b>	<b>Goodness of fit</b>		
	<b>AIC</b>	<b>SBC</b>	<b>WSSR</b>
1	-6.79	-7.87	0.229
2	-6.77	-8.00	0.247
4	-7.73	-8.51	0.122

Supporting information Table 16: Diagnostic table for a two-compartment model with  $1/\hat{Y}^2$  as weighting factor fitted to the 4-HPAA data.

<b>Dosing group (mg/kg)</b>	<b>Goodness of fit</b>		
	<b>AIC</b>	<b>SBC</b>	<b>WSSR</b>
2	-22.2	-22.8	0.0133
4	-10.7	-10.4	0.214



### **3.2 Single dose pharmacokinetics of intravenous 3,4-dihydroxyphenylacetic acid and 3-hydroxyphenylacetic acid in rats**

**Volha Zabela**, Chethan Sampath, Mouhssin Oufir, Veronika Butterweck, and Matthias Hamburger

Submitted to: *European Journal of Pharmaceutical Sciences*

3,4-Dihydroxyphenylacetic acid (DOPAC) and 3-hydroxyphenylacetic acid (3-HPAA) are intestinal metabolites of the dietary flavonoid quercetin. DOPAC reportedly showed anxiolytic activity after intraperitoneal administration in rats. In this study, we aimed to evaluate PK properties of the compounds after intravenous administration. At first, UHPLC-MS/MS methods were developed and validated according to the principles of current regulatory guidelines for industry. The validated methods were later applied for quantification of DOPAC and 3-HPAA in rat plasma. PK parameters were calculated with the industry standard software WinNonlin using non-compartmental and compartmental analyses. PK studies revealed that DOPAC and 3-HPAA are quickly distributed into peripheral tissues, as well as rapidly cleared from the body.

*My contributions to this publication: development and validation of UHPLC-MS/MS quantification methods according to the principles of current regulatory guidelines for industry, plasma sample preparation and analysis, non-compartmental and compartmental pharmacokinetic data analysis, writing the manuscript draft, and preparation of figures and tables.*

*Volha Zabela*

## **MANUSCRIPT**

### **Single dose pharmacokinetics of intravenous 3,4-dihydroxyphenylacetic acid and 3-hydroxyphenylacetic acid in rats**

Volha Zabela<sup>a</sup>, Chethan Sampath<sup>b</sup>, Mouhssin Oufir<sup>a</sup>, Veronika Butterweck<sup>b,1</sup>, and Matthias Hamburger<sup>a,\*</sup>

<sup>a</sup>Pharmaceutical Biology Laboratory, Department of Pharmaceutical Sciences, University of Basel, Klingelbergstrasse 50, CH-4056 Basel, Switzerland

<sup>b</sup>Department of Pharmaceutics, College of Pharmacy, University of Florida, 1345 Center Drive, Gainesville, FL, USA

#### **Author's present address:**

<sup>1</sup>Institute for Pharma Technology, School of Life Sciences, University of Applied Sciences Northwestern Switzerland, Gründenstrasse 40, CH-4132 Muttenz, Switzerland

**Author's e-mails:** volha.zabela@unibas.ch (Zabela); chethan@ufl.edu (Sampath); mouhssin.oufir@unibas.ch (Oufir); veronika.butterweck@fhnw.ch (Butterweck); matthias.hamburger@unibas.ch (Hamburger).

#### **\*Corresponding author:**

Professor Matthias Hamburger

**E-mail:** matthias.hamburger@unibas.ch

**Fax:** +41 61 267 14 74

**Address:** Pharmaceutical Biology, Department of Pharmaceutical Sciences, University of Basel, Klingelbergstrasse 50, CH-4056 Basel, Switzerland

## Abbreviations

AIC, Akaike's information criterion

AUC, area under the curve

AUMC, area under the first moment curve

BBB, blood-brain barrier

BSA, bovine serum albumin

b.w., body weight

C<sub>0</sub>, concentration at time 0

CA, compartmental analysis

Cals, calibrators

CL, clearance

C<sub>max</sub>, maximal concentration

CV, coefficient of variation

DMSO, dimethyl sulfoxide

DOPAC, 3, 4-dihydroxyphenylacetic acid

3-HPAA, 3-hydroxyphenylacetic acid

IS, internal standard

k<sub>e</sub>, elimination rate constant

LLOQ, lower limit of quantification

MRM, multiple reaction monitoring

MRT, mean residence time

NCA, non-compartmental analysis

PEG, polyethylene glycol

PK, pharmacokinetic

QCH, quality control at a high level

QCL, quality control at a low level

QCM, quality control at a medium level

QCs, quality controls

RE, relative error

RT, room temperature

SBC, Schwarz's Bayesian criterion

SS, stock solution

t<sub>1/2</sub>, half-life

V<sub>d</sub>, volume of distribution during the terminal phase

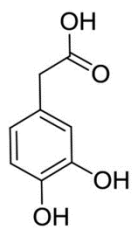
WS1, working solution 1

WS2, working solution 2

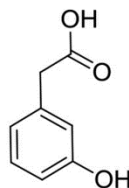
WSSR, weighted sum of squared residuals



## Graphical abstract

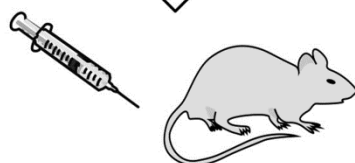


3,4-Dihydroxyphenylacetic acid

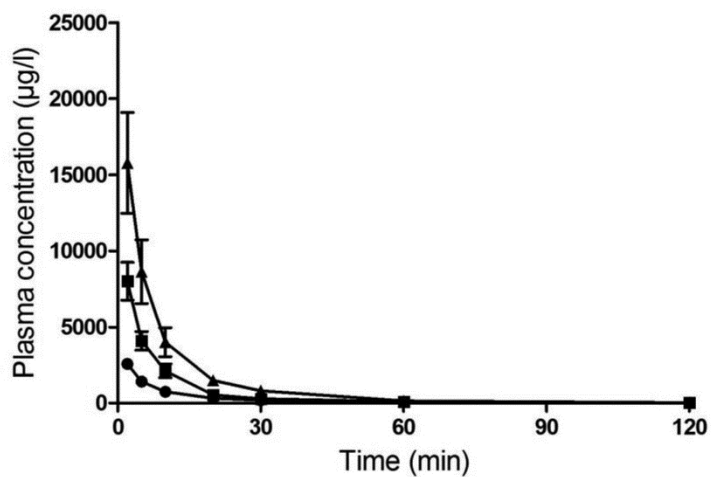


3-Hydroxyphenylacetic acid

PK studies in rats



Quantification by UHPLC-MS/MS



**Abstract**

3,4-Dihydroxyphenylacetic acid (DOPAC) and 3-hydroxyphenylacetic acid (3-HPAA) are intestinal metabolites of the dietary flavonoid quercetin. DOPAC reportedly showed anxiolytic activity after i.p. administration in rats. The fate of these metabolites after consumption, and the pharmacological properties of 3-HPAA in the body are largely unknown. The aim of the current study was to characterize pharmacokinetic properties of DOPAC and 3-HPAA after intravenous bolus application in rats. UHPLC-MS/MS methods for quantification of DOPAC and 3-HPAA levels in lithium heparin Sprague Dawley rat plasma were developed and validated according to international regulatory guidelines. Non-compartmental and compartmental analyses were performed. Pharmacokinetic profiles of DOPAC and 3-HPAA followed a two-compartment body model, with a fast distribution into peripheral tissues (half-lives of 3.27-5.26 min) and rapid elimination from the body (half-lives of 18.4-33.3 min).

**Keywords:** DOPAC, 3-HPAA, pharmacokinetics, UHPLC-MS/MS, validation.

## 1. Introduction

3,4-Dihydroxyphenylacetic acid (DOPAC) and 3-hydroxyphenylacetic acid (3-HPAA) are small phenolic acids which are formed by the intestinal microflora as metabolites of the flavonoid quercetin (Booth et al., 1956; Aura et al., 2002; Blaut et al., 2003). Quercetin has been shown to possess anxiolytic-like activity in mice, but only after oral administration. No anxiolytic properties were observed when the compound was given intraperitoneally (i.p.), or orally administered to gut sterilized mice. However, the metabolite DOPAC showed anxiolytic-like activity after i.p. administration (Vissiennon et al., 2012). These data suggested that quercetin requires metabolic transformation into pharmacologically active compounds.

Oral bioavailability of quercetin is poor, and low plasma concentrations of free quercetin have been reported in rats and humans after oral administration (Manach et al., 1997; Cai et al., 2013). In plasma, quercetin predominantly occurs in conjugated forms (glucuronides, sulfates, and as O-methyl derivatives) (Manach et al., 1998; Morand et al., 1998; Mullen et al., 2006), which are subsequently eliminated via renal and biliary excretion (Ueno et al., 1983; Crespy et al., 1999; Mullen et al., 2006). When excreted in the bile, conjugates of quercetin are released into the small intestine, where they can be converted by intestinal  $\beta$ -glucuronidases and sulfatases back to aglycones which are then transformed by the gut microbiota into phenolic acids. DOPAC and 3-HPAA are recovered in urine of rats and humans after oral consumption of quercetin (Booth et al., 1956; Hong and Mitchell, 2006; Gasperotti et al., 2015). DOPAC is not only an intestinal metabolite of quercetin, but also an endogenous metabolite of the neurotransmitter dopamine. Studies showed that reduced striatal levels of dopamine and DOPAC are associated with CNS disorders such as Parkinson's disease and schizophrenia (Cohrs et al., 2004; Ravenstijn et al., 2012).

Anxiolytic-like effects in rodents were also observed with oral administration of kaempferol, another commonly ingested flavonoid (Vissiennon et al., 2012). However, a pharmacokinetic (PK) study in rats showed low bioavailability of kaempferol, and extensive pre-systemic metabolism (Zabela et al., 2016). We here report on the PK properties of the major intestinal metabolites of quercetin, DOPAC and 3-HPAA.

## 2. Materials and methods

### 2.1. Chemicals and reagents

DOPAC (Fig. 1-1) (purity 99.8%) was purchased from Sigma-Aldrich (Buchs, Switzerland), and [ $^2\text{H}$ ]<sub>5</sub>-DOPAC with isotopic enrichment of 98% (Fig. 1-2) as internal standard (IS) was

from Cambridge Isotope Laboratories, Inc. (Andover, MA, USA). 3-HPAA (Fig. 1-3) (purity 99.2%), bovine serum albumin (BSA) as a surrogate matrix, Cremophor, Tween-80, and polyethylene glycol (PEG) were from Sigma-Aldrich (Steinheim, Germany). [ $^2\text{H}$ ]<sub>2</sub>-3-HPAA with isotopic enrichment of 96% (Fig. 1-4) was purchased from Diverchim (Roissy-en-France, France). Methanol (HPLC grade), and acetic acid (purity 98-100%) were from Biosolve BV (Valkenswaard, the Netherlands). Acetonitrile, isopropanol (HPLC grade), and dimethyl sulfoxide (DMSO) were supplied by Scharlau (Barcelona, Spain). Tween-20 was from Fluka (Buchs, Switzerland). HPLC grade water was obtained by a Milli-Q integral water purification system (Millipore Merck, Darmstadt, Germany).

## 2.2. Standards and stock solutions

Stock solutions (SS) of DOPAC, [ $^2\text{H}$ ]<sub>5</sub>-DOPAC, 3-HPAA and [ $^2\text{H}$ ]<sub>2</sub>-3-HPAA were prepared in DMSO by weighing compounds on a Sartorius micro balance (Göttingen, Germany). Appropriate dilution in methanol were prepared to obtain working solutions 1 (WS<sub>1</sub>) of DOPAC (200 µg/ml) and 3-HPAA (100 µg/ml). WS<sub>1</sub> of [ $^2\text{H}$ ]<sub>5</sub>-DOPAC and [ $^2\text{H}$ ]<sub>2</sub>-3-HPAA were prepared in methanol at a concentration of 50 µg/ml. A daily WS<sub>2</sub> was prepared from WS<sub>1</sub> to obtain a concentration of 250 ng/ml. All the SSs and WSs were stored below -65°C until use.

## 2.3. Preparation of calibration standards and quality control samples

To prevent adsorption of DOPAC to the container surfaces, polypropylene tubes were pre-treated with 0.2% Tween-20 before preparation of calibrators (Cals) and quality controls (QCs). Two sets of Cals over the range of 30-3000 ng/ml and QCs at low, medium and high levels (QCL = 90 ng/ml, QCM = 1500 ng/ml, QCH = 2400 ng/ml) were prepared in BSA solution (60 g/l) by serial dilution of the WS<sub>1</sub> (200 µg/ml). For 3-HPAA, two sets of Cals over the range of 20-2000 ng/ml and QCs (QCL = 60 ng/ml, QCM = 1000 ng/ml, QCH = 1600 ng/ml) were prepared in BSA solution by serial dilution of the WS<sub>1</sub> (100 µg/ml). All samples were stored below -65°C until analysis.

## 2.4. Sample processing

### 2.4.1. Extraction of DOPAC and 3-HPAA from BSA solution

An aliquot of 75 µl of sample was mixed in 1.5 ml tubes with 150 µl of WS<sub>2</sub> of the corresponding IS (250 ng/ml) and 300 µl of acetonitrile. Samples were mixed for 10 min at 1400 rpm on a Mixmate (Eppendorf, Schönenbuch, Switzerland), and then centrifuged for 15 min at 13200 rpm at 10°C (Centrifuge 5415R, Eppendorf, Schönenbuch, Switzerland). Clear supernatant (400 µl) was transferred into a 96-deepwell plate. The samples were dried by a nitrogen evaporator (Evaporex EVX-96, Apricots Designs Inc, USA) with upper temperature

of 30°C and lower temperature of 50°C, and reconstituted with 50% solvent A (5 mM acetic acid) and 50% solvent B (acetonitrile + 5 mM acetic acid) (V = 100 µl for DOPAC and V = 200 µl for 3-HPAA). The plate was shaken on a Mixmate for 30 min at 2000 rpm before UHPLC-MS/MS analysis.

## 2.5. LC-MS/MS instrument and chromatographic conditions

### 2.5.1. Mass spectrometry conditions

UHPLC-MS/MS analysis was performed with an UHPLC 1290 system consisting of a binary pump G4220A and autosampler G4226A set at 10°C, coupled with an 6460 triple quadrupole mass spectrometer (all Agilent Technologies, Waldbronn, Germany). An Agilent Jet Stream ionization source was used for DOPAC, and an electrospray ionization source for 3-HPAA. The instrument was controlled by MassHunter software (Version 7.0; Agilent Technologies, Waldbronn, Germany). Nitrogen, generated by a nitrogen generator N<sub>2</sub>-Mistral (Schmidlin AG, Neuheim, Switzerland), was used for both desolvation and nebulization, and as collision gas. MS parameters for each compound and their corresponding ISs are summarized in Table 1.

The following instrument parameters were used for quantification of DOPAC: nitrogen drying gas temperature of 150°C at a flow rate of 13 l/min, nebulizer pressure of 60 psi, sheath gas temperature of 400°C at a flow rate of 12 l/min, capillary voltage of 2000 V, nozzle voltage of 0 V, delta EMV(-) 200 V.

The following instrument parameters were applied for quantification of 3-HPAA: nitrogen drying gas temperature of 325°C at a flow rate of 13 l/min, nebulizer pressure of 60 psi, capillary voltage of 4000 V, delta EMV (-) 300 V.

### 2.5.2. Chromatographic conditions

Analysis of DOPAC and IS was performed on an Acquity HSS T3 column (1.8 µm, 2.1 × 100 mm; Waters Corp., Milford, MA, USA) heated at 45°C. The mobile phase consisted of eluent A (5 mM acetic acid) and eluent B (acetonitrile with 5 mM acetic acid), and the following gradient was used: 0-1 min, 2% B, 1-3 min, 2-100% B, 3-4 min, 100% B, 4-4.01, 100-2% B, 4.01-5 min, 2% B. The flow rate was 0.4 ml/min, and the injection volume was 5 µl. The needle wash solvent consisted of water and methanol (50:50, v/v).

Analysis of 3-HPAA and IS was performed on a Kinetex XB column (1.7 µm, 2.1×100 mm; Phenomenex, Torrance, CA, USA) heated at 55°C. The following gradient was used: 0-1 min, 5% B, 1-4 min, 5-100% B, 4-5 min, 100% B, 5-5.1, 100-5% B, 5.1-6 min, 5% B. The flow rate was 0.6 ml/min, and the injection volume was 5 µl. The needle wash solvent consisted of water/methanol/isopropanol/acetonitrile (1:1:1:1, v/v/v/v).

## 2.6. Method validation

Following EMA/FDA validation guidelines for industry, imprecision in analytical runs was calculated by the coefficient of variation (CV%), and had to be < 15% (< 20% at the LLOQ) of the nominal values at all concentration levels. Inaccuracy was represented by the relative error (RE%), and had to be within  $\pm 15\%$  (within  $\pm 20\%$  at the LLOQ) of the nominal values at all concentration levels (U.S. Food and Drug Administration, 2013; European Medicines Agency, 2011).

### 2.6.1. Chromatographic performance

A seven-point calibration curve was generated over the range 30-3000 ng/ml for DOPAC, and 20-2000 ng/ml for 3-HPAA.

### 2.6.2. Carryover

Carryover for both analytes was assessed by two extracted blank BSA solutions injected immediately after the two ULOQ levels.

### 2.6.3. Selectivity

Six QC samples of DOPAC and 3-HPAA at the LLOQ level were prepared in three different lots of BSA.

### 2.6.4. Specificity

Six BSA blanks were analyzed, and a peak area measured in the blank samples were less than 20% of the analyte peak area at LLOQ.

### 2.6.5. Intra-run repeatability and Inter-run reproducibility

The intra-day imprecision and inaccuracy were estimated by injecting six replicates of QC samples at five different levels (LLOQ, QCL, QCM, QCH and ULOQ), and expressed as CV% and RE%, respectively. The inter-run CV% and RE% were assessed by the same QCs on three different days.

### 2.6.6. Extraction yield

Extraction yields of analytes and ISs were evaluated at three levels (QCL, QCM and QCH) before extraction, and spiked with the IS after extraction, in comparison to six blank samples spiked after extraction (representing 100% of recovery).

### 2.6.7. Dilution test

The dilution QC samples (15000 ng/ml for DOPAC and 10000 ng/ml for 3-HPAA) were prepared and diluted with the BSA solution in a ratio of 1:10 and 1:100.

### 2.6.8. Short-term stabilities of DOPAC and 3-HPAA in BSA

One to three overnight freeze-thaw cycles below  $-65^{\circ}\text{C}$  were performed on six replicates of each analyte at low and high concentrations. Sample stability at room temperature was

assessed with six replicates of each analyte at low and high concentrations, kept on the bench at RT for 2 to 4 h. For assessment of processed sample stability in the autosampler at 10°C, six replicates of each analyte at low and high concentrations were analyzed and then stored for 24 h and 48 h in the autosampler at 10°C. Afterwards, these QCs were re-analyzed together with freshly prepared Cals and QCs.

#### *2.6.9. Long-term stability of DOPAC in lithium heparin rat plasma, and of 3-HPAA in BSA below -65°C*

Lithium heparin Sprague Dawley rat plasma was supplemented with 1% of ascorbic acid to prevent oxidation of DOPAC. Three replicates of QCL, QCM and QCH were prepared in stabilized rat plasma for DOPAC, or in BSA for 3-HPAA, and analyzed the next day after preparation ( $t_0$ ). Additional triplicates of QCs at the same concentrations were stored below -65°C (up to 3 months for DOPAC and up to 12 months for 3-HPAA). After each storage interval, the long-term stability samples were compared to freshly prepared Cals and QCs. Linear regression analysis was used to assess long-term stability data. Stability of the samples was verified by the slope deviation within  $1 \pm 0.15$ .

#### *2.6.10. Stock solution stability test*

Stock solutions of analytes and corresponding ISs, stored below -65°C over time, were compared with freshly prepared stock solutions. The eventual degradation should not exceed 5% for all compounds.

### *2.7. PK studies*

#### *2.7.1. Animals*

Male Sprague Dawley rats (body weight 320-350 g) were purchased from Charles River (Wilmington, MA, USA). The animals were individually housed in plastic cages and maintained under a 12 h/12 h light/dark cycle. The rats received water *ad libitum* and a standard chow. Before being used in experiments, animals were allowed to acclimate to their environment for one week. The rats were maintained on a 12 h/12 h light/dark cycle. All animal experiments were performed according to the policies and guidelines of the Institutional Animal Care and Use Committee (IACUC) of the University of Florida, Gainesville, USA, study protocol #200903448.

#### *2.7.2. Design of PK studies in rats*

The rats ( $n = 8$  per group) were randomly divided into six groups. DOPAC was given by the intravenous bolus injection in the doses of 1, 2 and 4 mg/kg body weight (b.w.). A pilot study on the PK of 3-HPAA was performed with doses of 2 and 4 mg/kg b.w. Both compounds were dissolved in a vehicle composition consisting of Cremophor/Tween-

80/PEG/ethanol/water (2:1:1:1:5, v/v/v/v/v). Blood samples (500  $\mu$ l) were collected from the sublingual vein into heparinized tubes at 0 (prior to dosing), 2, 5, 10, 20, 30 min, 1, 2, 4, 6, 8 and 12 h. The loss of blood volume was replaced with 1 ml normal saline. Plasma samples were obtained by centrifugation at 4000 rpm for 15 min at 4°C, then transferred into 1.5 ml tubes and stored at below -65°C until analysis.

## 2.8. PK data analysis

Mean plasma concentrations of DOPAC and 3-HPAA versus time were generated in Graphpad Prism (version 5.01; San Diego, CA, USA). PK parameters were determined by non-compartmental and compartmental analyses using WinNonlin software (version 5.2.1; Pharsight Corporation, St. Louis, MO, USA).

### 2.8.1. Non-compartmental analysis (NCA)

The PK parameters included the extrapolated concentration at time 0 ( $C_0$ ), terminal elimination rate constant ( $k_e$ ), terminal half-life ( $t_{1/2}$ ), area under the concentration-time curve (AUC), area under the first moment curve (AUMC), mean residence time (MRT), apparent volume of distribution ( $V_d$ ), and plasma clearance (CL). The slope of the terminal phase was estimated by log-linear regression using the “best fit” method and uniform weighting. The  $k_e$  was derived from the slope. The  $t_{1/2}$  was calculated as  $0.693/k_e$ . The linear trapezoidal rule was applied for determination of the area under the curve from time 0 to the last measurable concentration ( $AUC_{0-last}$ ) and then extrapolated to infinity ( $AUC_{0-\infty}$ ). The CL following the intravenous dosing was calculated as  $Dose/AUC_{0-\infty}$ . The  $V_d$  was calculated as  $CL/k_e$ .

### 2.8.2. Compartmental analysis (CA)

A two-compartment body model with different weighting factors was fitted to the DOPAC and 3-HPAA data. The goodness of fit was estimated by Akaike's information criterion (AIC), Schwarz's Bayesian criterion (SBC), and weighted sum of squared residuals (WSSR). The equation for the intravenous bolus two-compartment model was as follows:  $C_{p(t)}=A \times \exp^{-\alpha t} + B \times \exp^{-\beta t}$ , where  $C_{p(t)}$  is a concentration of a drug in plasma at time t; A and B are the Y-axis intercepts;  $\alpha$  and  $\beta$  are the initial and terminal slopes.

## 2.9. Statistics

Analytical values were calculated in Excel and presented as mean  $\pm$  SD with CV% and RE%.

## 3. Results

### 3.1. Validation of the bioanalytical methods for DOPAC and 3-HPAA



Quantification of DOPAC and 3-HPAA were performed by UHPLC-MS/MS. Figures 2 and 3 show extracted multiple reaction monitoring (MRM) chromatograms of the analytes and their corresponding ISs in BSA solution. Since DOPAC and 3-HPAA are also endogenous metabolites of neurotransmitters, BSA solution as an analyte-free (surrogate) matrix was chosen for the preparation of CALs and QCs (Jones et al., 2012). The developed UHPLC-MS/MS methods were fully validated in terms of accuracy, precision, selectivity, recovery, reproducibility and stability according to international regulatory guidelines (U.S. Food and Drug Administration, 2013; European Medicines Agency, 2011). The calibration curves were quadratic in the range of 30-3000 ng/ml for DOPAC, and 20-2000 ng/ml for 3-HPAA, with a 1/X weighting factor. Mean coefficients of determination for DOPAC and 3-HPAA were 0.9994 and 0.9991, respectively (Supporting information Tables 1 and 2). Carryover for DOPAC (12%) was within the acceptance criteria (Fig. 2, and Supporting information Table 3). No carryover was detected for 3-HPAA (Fig. 3, and Supporting information Table 4). Both methods were shown to be selective, with CV% and RE% < 20% (Supporting information Tables 5 and 6). In the blank BSA samples, no peaks were observed at the retention time of the analytes, confirming that both methods were specific for DOPAC and 3-HPAA (data not shown). Results from the intra- and inter-day imprecision and inaccuracy for both compounds are summarized in Table 2. The mean extraction recovery of DOPAC from BSA solution ranged from 57.2% to 77.4%, and recovery of the IS was 82.4% (Supporting information Table 7). The mean extraction recovery of 3-HPAA was from 106% to 114%, and recovery of the IS was 104% (Supporting information Table 8). No impact of dilution (10- and 100-fold) on the results was observed (Supporting information Tables 9 and 10). DOPAC was stable after one freeze and thaw cycle (after two and three cycles the stability of DOPAC could not be confirmed; data not shown), after 2 h storage at RT, and after 48 h storage in the autosampler at 10°C (Supporting information Table 11). 3-HPAA was stable after three freeze and thaw cycles, after 4 h storage at RT, and after 24 h storage in the autosampler at 10°C (Supporting information Table 12). DOPAC in plasma spiked with 1% ascorbic acid was stable for 89 days (Supporting information Figure 1). 3-HPAA in BSA solution was stable for 378 days of storage below -65°C (Supporting information Figure 2). Since degradation was less than 5%, SSs of DOPAC and 3-HPAA were stable below -65°C for 204 and 431 days, respectively (Supporting information Tables 13 and 14). The degradation of SSs of the IS [<sup>2</sup>H]<sub>5</sub>-DOPAC and [<sup>2</sup>H]<sub>2</sub>-3-HPAA was -1.45% and -0.39%, respectively (Supporting information Table 15 and 16). In conclusion, both bioanalytical

methods were precise, accurate, and reliable for the quantification of DOPAC and 3-HPAA in rat plasma.

### 3.2. Pharmacokinetics of DOPAC

PK profiles were characterized by a biphasic decline in plasma concentrations (Figure 4). DOPAC plasma concentrations fell below the LLOQ 2 h after injection for the doses of 2 and 4 mg/kg, whereas for the dose of 1 mg/kg the concentration of DOPAC in plasma was below the LLOQ already 1 h after administration (Fig. 4B). Dose proportionality for DOPAC was evaluated by a linear regression approach. A statistical linear relationship between dose-dependent PK parameters ( $C_0$  and  $AUC_{0-\infty}$ ) and doses was demonstrated (Fig. 5). The main PK parameters of DOPAC calculated by NCA are summarized in Table 3. The compound showed fast elimination ( $k_e = 1.32\text{-}2.96\text{ h}^{-1}$ ), with a short terminal  $t_{1/2}$  of 16.8-31.7 min. DOPAC had a moderate  $V_d$  (0.64-1.14 l/kg), and a high CL of 1.5-1.98 l/h/kg.

A two-compartment intravenous bolus model with first-order elimination and  $1/\hat{Y}^2$  as a weighting factor was fitted to the DOPAC data. The goodness of fit was confirmed by the AIC, SBC, WSSR (Supporting information Table 17). The goodness of fit was also assessed by a comparison of simulated and observed concentrations vs. time profiles with a two-compartment body model (Figure 6). PK parameters calculated for the compartmental model are summarized in Table 4. After administration of DOPAC, a rapid distribution to peripheral tissues ( $t_{1/2\alpha} = 3.27\text{-}5.26\text{ min}$ ) was observed, followed by a slower elimination phase ( $t_{1/2\beta} = 18.4\text{-}33.3\text{ min}$ ). The values of AUC, MRT,  $V_d$  and CL of the compartmental analysis were close to those obtained by NCA analysis.

### 3.3. Pharmacokinetics of 3-HPAA

A PK pilot study of intravenous 3-HPAA was performed in rats at the doses of 2 and 4 mg/kg. Plasma concentrations versus time profiles (linear and semi-log plots) are shown in Figure 7. At the dose of 4 mg/kg, 3-HPAA was detected for up to 4 h after administration (Fig. 7B). In contrast, the plasma concentration of 3-HPAA at the dose of 2 mg/kg dropped below the LLOQ after 2 h. The PK parameters obtained by NCA are given in Table 5. 3-HPAA showed a rapid rate of elimination ( $k_e = 2.1\text{-}2.39\text{ h}^{-1}$ ), resulting in a short terminal  $t_{1/2}$  of 19.9-26.2 min. 3-HPAA had a moderate  $V_d$  of 0.73-0.94 l/kg, and a high CL of 1.46-1.57 l/h/kg.

A two-compartment intravenous bolus model with first-order elimination and  $1/\hat{Y}^2$  as a weighting factor was fitted to the 3-HPAA data. The goodness of fit was confirmed by the AIC, SBC, WSSR (Supporting information Table 18). A comparison of simulated and observed concentrations vs. time profiles with a two-compartment body model also confirmed goodness of fit (Fig. 8). PK parameters of the two-compartment body model are summarized in Table 6. After administration of 3-HPAA, a rapid distribution to peripheral tissues ( $t_{1/2\alpha} = 4.3\text{-}4.66$  min) was observed, followed by a slower elimination phase ( $t_{1/2\beta} = 22\text{-}31.2$  min). The values of AUC, MRT,  $V_d$  and CL of the compartmental analysis were close to those obtained by NCA analysis.

#### 4. Discussion

PK of DOPAC and 3-HPAA after intravenous injection can be best described by a two-compartment model with first-order elimination. The plasma levels of DOPAC and 3-HPAA were low 60 min after the injection, demonstrating a rapid disappearance of the compounds from the circulation. Our findings are in agreement with a recent study that found high concentrations of DOPAC and 3-HPAA in urine and kidneys after intravenous administration in rats (Gasperotti et al., 2015).

To exert a direct anxiolytic the compounds have to cross the blood-brain barrier (BBB). However, results from a screening with an *in vitro* ECV304/C6 co-culture BBB model suggest that DOPAC and 3-HPAA may not cross the BBB (Youdim et al., 2003). In contrast, a recent study in rats reported that after intravenous injection of DOPAC an approx. 2-fold increased concentration was found in the brain as compared to basal concentrations in the control group (Gasperotti et al., 2015). However, the above studies suffered from some methodological limitations, such as non-specific and non-selective detection by HPLC-UV (Youdim et al., 2003), or from possible interactions due to a simultaneous injection of 23 different metabolites (Gasperotti et al., 2015). Acidic compounds like DOPAC and 3-HPAA tend to bind to a large extent to albumin, and thus may have a limited brain penetration. Also, metabolism in the brain needs to be taken into account, considering that CYP and UGT enzymatic activities in the brain have been reported (King et al., 1999; Gervasini et al., 2004). Taken together, pharmacologically relevant concentrations of these metabolites in the brain are unlikely to be achieved. Thus, it is not clear at this moment how the anxiolytic-like properties reported for DOPAC can be explained. Further investigations are needed to

identify pharmacologically active metabolites of flavonoids that are BBB penetrant and thus could exert anxiolytic-like effects.

## **5. Conclusions**

UHPLC-MS/MS methods for quantification of DOPAC and 3-HPAA in lithium heparin Sprague Dawley rat plasma were developed and validated according to international regulatory guidelines. After intravenous bolus injection in rats PK profiles of DOPAC and 3-HPAA followed a two-compartment model, with fast distribution to peripheral tissues, and rapid elimination from the body. At present, the anxiolytic-like properties reported for DOPAC cannot be explained.

## **Acknowledgements**

This study was financially supported by the Swiss National Science Foundation (project 105320\_126888). Volha Zabela acknowledges the Swiss Federal Commission for her PhD scholarship. The authors thank Orlando Fertig for technical assistance.

## **Conflict of interest**

The authors declare no conflict of interest.

## References

- Aura, A.-M., O'leary, K.A., Williamson, G., Ojala, M., Bailey, M., Puupponen-Pimiä, R., Nuutila, A.M., Oksman-Caldentey, K.-M., Poutanen, K., 2002. Quercetin derivatives are deconjugated and converted to hydroxyphenylacetic acids but not methylated by human fecal flora *in vitro*. *J. Agric. Food Chem.* 50, 1725-1730.
- Blaut, M., Schoefer, L., Braune, A., 2003. Transformation of flavonoids by intestinal microorganisms. *Int. J. Vitam. Nutr. Res.* 73, 79-87.
- Booth, A.N., Murray, C.W., Jones, F.T., DeEds, F., 1956. The metabolic fate of rutin and quercetin in the animal body. *J. Biol. Chem.* 223, 251-257.
- Cai, X., Fang, Z., Dou, J., Yu, A., Zhai, G., 2013. Bioavailability of quercetin: problems and promises. *Curr. Med. Chem.* 20, 2572-2582.
- Cohrs, S., Guan, Z., Pohlmann, K., Jordan, W., Pilz, J., Rütther, E., Rodenbeck, A., 2004. Nocturnal urinary dopamine excretion is reduced in otherwise healthy subjects with periodic leg movements in sleep. *Neurosci. Lett.* 360, 161-164.
- Crespy, V., Morand, C., Manach, C., Besson, C., Demigné, C., Remesy, C., 1999. Part of quercetin absorbed in the small intestine is conjugated and further secreted in the intestinal lumen. *Am. J. Physiol.* 277, G120-126.
- European Medicines Agency, 2011. Guideline on bioanalytical method validation.
- Gasperotti, M., Passamonti, S., Tramer, F., Masuero, D., Guella, G., Mattivi, F., Vrhovsek, U., 2015. Fate of microbial metabolites of dietary polyphenols in rats: is the brain their target destination? *ACS Chem. Neurosci.* 6, 1341-1352.
- Gervasini, G., Carrillo, J.A., Benitez, J., 2004. Potential role of cerebral cytochrome P450 in clinical pharmacokinetics. *Clin. Pharmacokinet.* 43, 693-706.
- Hong, Y.-J., Mitchell, A.E., 2006. Identification of glutathione-related quercetin metabolites in humans. *Chem. Res. Toxicol.* 19, 1525-1532.
- Jones, B.R., Schultz, G.A., Eckstein, J.A., Ackermann, B.L., 2012. Surrogate matrix and surrogate analyte approaches for definitive quantitation of endogenous biomolecules. *Bioanalysis.* 4, 2343-2356.
- King, C.D., Rios, G.R., Assouline, J.A., Tephly, T.R., 1999. Expression of UDP-glucuronosyltransferases (UGTs) 2B7 and 1A6 in the human brain and identification of 5-hydroxytryptamine as a substrate. *Arch. Biochem. Biophys.* 365, 156-162.
- Manach, C., Morand, C., Demigné, C., Texier, O., Régéat, F., Rémésy, C., 1997. Bioavailability of rutin and quercetin in rats. *FEBS Letters.* 409, 12-16.
- Manach, C., Morand, C., Crespy, V., Demigné, C., Texier, O., Régéat, F., Rémésy, C., 1998. Quercetin is recovered in human plasma as conjugated derivatives which retain antioxidant properties. *FEBS Letters.* 426, 331-336.
- Morand, C., Crespy, V., Manach, C., Besson, C., Demigné, C., Rémésy, C., 1998. Plasma metabolites of quercetin and their antioxidant properties. *Am. J. Physiol.* 275, R212-219.
- Mullen, W., Edwards, C.A., Crozier, A., 2006. Absorption, excretion and metabolite profiling of methyl-, glucuronyl-, glucosyl- and sulpho-conjugates of quercetin in human plasma and urine after ingestion of onions. *Br. J. Nutr.* 96, 107-116.
- Ravenstijn, P.G., Drenth, H.-J., O'Neill, M.J., Danhof, M., De Lange, E.C., 2012. Evaluation of blood-brain barrier transport and CNS drug metabolism in diseased and control brain after intravenous L-DOPA in a unilateral rat model of Parkinson's disease. *Fluids Barriers CNS*, 9.
- U.S. Food and Drug Administration, 2013. Guidance for Industry: Bioanalytical Method Validation.
- Ueno, I., Nakano, N., Hirono, I., 1983. Metabolic fate of [<sup>14</sup>C] quercetin in the ACI rat. *Jpn. J. Exp. Med.* 53, 41-50.
- Vissienon, C., Nieber, K., Kelber, O., Butterweck, V., 2012. Route of administration determines the anxiolytic activity of the flavonols kaempferol, quercetin and myricetin—are they prodrugs? *J. Nutr. Biochem.* 23, 733-740.
- Youdim, K.A., Dobbie, M.S., Kuhnle, G., Proteggente, A.R., Abbott, N.J., Rice-Evans, C., 2003. Interaction between flavonoids and the blood-brain barrier: *in vitro* studies. *J. Neurochem.* 85, 180-192.

Zabela, V., Sampath, C., Oufir, M., Moradi-Afrapoli, F., Butterweck, V., Hamburger, M., 'in press'.  
Pharmacokinetics of dietary kaempferol and its metabolite 4-hydroxyphenylacetic acid in rats.  
Fitoterapia. DOI information: 10.1016/j.fitote.2016.10.008.

## Legends for Figures

Figure 1. Chemical structures of DOPAC (1), [<sup>2</sup>H]<sub>5</sub>-DOPAC (2), 3-HPAA (3), and (4) [<sup>2</sup>H]<sub>2</sub>-3-HPAA.

Figure 2. Typical MRM chromatograms of the BSA blank spiked with DOPAC at 3000 ng/ml (ULOQ) and IS at 250 ng/ml (A), the BSA blank (B), the BSA blank spiked with DOPAC at 30 ng/ml (LLOQ) and IS at 250 ng/ml (C).

Figure 3. Typical MRM chromatograms of the BSA blank spiked with 3-HPAA (quantifier only) at 2000 ng/ml (ULOQ) and IS at 250 ng/ml (A), the BSA blank (B), the BSA blank spiked with 3-HPAA (quantifier only) at 20 ng/ml (LLOQ) and IS at 250 ng/ml (C).

Figure 4. Plasma concentrations of DOPAC (mean ± S.D.) after a single intravenous administration of 1, 2 and 4 mg/kg b.w., shown as linear (A) and semi-logarithmic (B) plots.

Figure 5. C<sub>0</sub> and AUC<sub>0-inf</sub> (mean ± S.D.) of DOPAC vs. dosing group (solid line) and fitted simple linear regression (dashed line, for visual comparison).

Figure 6. Observed (mean ± S.D.) and simulated concentrations vs. time profiles of DOPAC in rats after a single intravenous dose of 1 (A), 2 (B), and 4 (C) mg/kg b.w.

Figure 7. Plasma concentrations of 3-HPAA (mean ± S.D.) after a single intravenous administration of 2 and 4 mg/kg b.w., shown as linear (A) and semi-logarithmic (B) plots.

Figure 8. Observed (mean ± S.D.) and simulated concentrations vs. time profiles of 3-HPAA in rats after a single intravenous dose of 2 (A) and 4 (B) mg/kg b.w.

## **TABLES**

Table 1: MS/MS parameters of analytes and corresponding internal standards. An Agilent Jet Stream ionization source (AJS) was used for analysis of DOPAC, and an electrospray ionization source (ESI) was used for 3-HPAA.

Compound	Precursor ion ( <i>m/z</i> )	Product ion ( <i>m/z</i> )	Fragmentor (V)	Dwell time (ms)	Collision energy (V)	AJS/ESI polarity
DOPAC	167.03	123	52	400	6	negative
[ <sup>2</sup> H] <sub>5</sub> -DOPAC	172.1	128.1	67	400	6	negative
3-HPAA quantifier	151.04	107	55	250	6	negative
3-HPAA qualifier	151.04	65.1	55	250	26	negative
[ <sup>2</sup> H <sub>2</sub> ]-3-HPAA	153.05	109.0	65	250	6	negative



Table 2: Intra- (n = 6) and inter- (n = 18) run imprecision (expressed as CV %) and inaccuracy (expressed as RE %) of DOPAC QC samples in BSA, and 3-HPAA QC samples in BSA solution, based on 3 series at 5 different levels.

Nominal level (ng/ml)	DOPAC					3-HPAA				
	30	90	1500	2400	3000	20	60	1000	1600	2000
Intra-run mean	32.8	100	1657	2485	2926	21.2	64.4	1011	1613	1942
Intra-run S.D.	0.47	1.04	24.4	14.2	21.9	1.94	2.68	14.8	28.0	33.8
Intra-run CV %	1.42	1.04	1.48	0.57	0.75	9.16	4.16	1.46	1.73	1.74
Intra-run RE %	9.2	11.1	10.4	3.54	-2.47	5.94	7.35	1.12	0.8	-2.92
Inter-run mean	32.3	100	1653	2496	2969	21.0	60.8	969	1547	1914
Inter-run S.D.	0.38	0.8	18.8	20.4	17.5	1.8	3.24	19.6	33.3	75.4
Inter-run CV%	1.18	0.8	1.14	0.82	0.59	8.55	5.31	2.03	2.16	4.04
Inter-run RE %	7.6	11.3	10.2	4	-1.05	5.2	1.32	-3.11	-3.33	-4.28

Table 3: PK parameters of DOPAC after a single intravenous administration of 1, 2 and 4 mg/kg b.w., calculated by non-compartmental analysis (mean  $\pm$  S.D.).

Dosing group (mg/kg)	1	2	4
n	4	7	6
C <sub>0</sub> (μg/l)	3698 $\pm$ 392	12023 $\pm$ 2111	22748 $\pm$ 4938
k <sub>e</sub> (1/h)	2.52 $\pm$ 0.4	2.96 $\pm$ 1.8	1.32 $\pm$ 0.14
t <sub>1/2</sub> (min)	16.8 $\pm$ 2.9	18.1 $\pm$ 8.9	31.7 $\pm$ 3.2
AUC <sub>0-last</sub> (h $\times$ μg/l)	485 $\pm$ 49.3	1288 $\pm$ 236	2741 $\pm$ 585
AUC <sub>0-∞</sub> (h $\times$ μg/l)	511 $\pm$ 63.9	1322 $\pm$ 243	2776 $\pm$ 591
AUMC <sub>0-last</sub> (h $\times$ h $\times$ μg/l)	91.8 $\pm$ 20.4	197 $\pm$ 75.1	534 $\pm$ 107
AUMC <sub>0-∞</sub> (h $\times$ h $\times$ μg/l)	129 $\pm$ 44.8	251 $\pm$ 104	629 $\pm$ 126
CL (l/h/kg)	1.98 $\pm$ 0.24	1.57 $\pm$ 0.34	1.50 $\pm$ 0.34
V <sub>d</sub> (l/kg)	0.790 $\pm$ 0.06	0.639 $\pm$ 0.26	1.14 $\pm$ 0.24
MRT (min)	14.8 $\pm$ 3.2	11.0 $\pm$ 3.1	13.7 $\pm$ 0.64

Table 4: PK parameters of DOPAC after a single intravenous dose of 1, 2 and 4 mg/kg b.w., calculated by compartmental analysis (mean  $\pm$  S.D.). A two-compartment model with  $1/\hat{Y}^2$  as a weighting factor was fitted to the data.

Dosing group (mg/kg)	1	2	4
n	4	7	6
$C_{\max}$ ( $\mu\text{g/l}$ )	3500 $\pm$ 532	10445 $\pm$ 1885	16896 $\pm$ 3020
A ( $\mu\text{g/l}$ )	2892 $\pm$ 567	9803 $\pm$ 1521	16196 $\pm$ 3035
B ( $\mu\text{g/l}$ )	608 $\pm$ 140	642 $\pm$ 451	700 $\pm$ 352
$\alpha$ (1/h)	13.2 $\pm$ 2.5	11.1 $\pm$ 1.7	8.14 $\pm$ 1.6
$\beta$ (1/h)	2.36 $\pm$ 0.51	1.73 $\pm$ 0.97	1.35 $\pm$ 0.28
$t_{1/2\alpha}$ (min)	3.27 $\pm$ 0.67	3.82 $\pm$ 0.6	5.26 $\pm$ 0.88
$t_{1/2\beta}$ (min)	18.4 $\pm$ 4.9	33.3 $\pm$ 23.2	31.9 $\pm$ 6.2
k 10 (1/h)	7.35 $\pm$ 1.6	8.37 $\pm$ 1.4	6.67 $\pm$ 0.75
k 12 (1/h)	3.89 $\pm$ 0.75	2.19 $\pm$ 0.54	1.16 $\pm$ 0.68
k 21 (1/h)	4.27 $\pm$ 1.1	2.28 $\pm$ 1.3	1.66 $\pm$ 0.5
$AUC_{0-\infty}$ ( $\text{h}\times\mu\text{g/l}$ )	485 $\pm$ 68.0	1254 $\pm$ 171	2559 $\pm$ 551
AUMC ( $\text{h}\times\text{h}\times\mu\text{g/l}$ )	136 $\pm$ 55.1	371 $\pm$ 208	635 $\pm$ 132
CL (l/h/kg)	2.09 $\pm$ 0.28	1.62 $\pm$ 0.21	1.63 $\pm$ 0.36
$V_c$ (l/kg)	0.291 $\pm$ 0.04	0.197 $\pm$ 0.04	0.244 $\pm$ 0.05
$V_p$ (l/kg)	0.268 $\pm$ 0.04	0.299 $\pm$ 0.33	0.163 $\pm$ 0.06
MRT (min)	16.4 $\pm$ 4.2	18.1 $\pm$ 11.4	14.9 $\pm$ 0.53

Table 5: PK parameters of 3-HPAA after a single intravenous administration of 1, 2 and 4 mg/kg b.w., calculated by non-compartmental analysis (mean  $\pm$  S.D.).

Dosing group (mg/kg)	2	4
n	8	6
C <sub>0</sub> (μg/l)	6739 $\pm$ 1277	17522 $\pm$ 1989
k <sub>e</sub> (1/h)	2.39 $\pm$ 0.72	2.10 $\pm$ 0.9
t <sub>1/2</sub> (min)	19.9 $\pm$ 10.2	26.2 $\pm$ 17.5
AUC <sub>0-last</sub> (h $\times$ μg/l)	1243 $\pm$ 171	2735 $\pm$ 514
AUC <sub>0-∞</sub> (h $\times$ μg/l)	1300 $\pm$ 191	2804 $\pm$ 479
AUMC <sub>0-last</sub> (h $\times$ h $\times$ μg/l)	322 $\pm$ 110	778 $\pm$ 375
AUMC <sub>0-∞</sub> (h $\times$ h $\times$ μg/l)	436 $\pm$ 240	909 $\pm$ 340
CL (l/h/kg)	1.57 $\pm$ 0.21	1.46 $\pm$ 0.24
V <sub>d</sub> (l/kg)	0.732 $\pm$ 0.31	0.941 $\pm$ 0.8
MRT (min)	19.7 $\pm$ 8	19.2 $\pm$ 4.8

Table 6: PK parameters of 3-HPAA after a single intravenous dose of 2 and 4 mg/kg b.w., calculated by compartmental analysis (mean  $\pm$  S.D.). A two-compartment model with  $1/\hat{Y}^2$  as a weighting factor was fitted to the data.

Dosing group (mg/kg)	2	4
n	8	6
$C_{\max}$ ( $\mu\text{g/l}$ )	6442 $\pm$ 1360	16106 $\pm$ 5942
A ( $\mu\text{g/l}$ )	4671 $\pm$ 855	12798 $\pm$ 3852
B ( $\mu\text{g/l}$ )	1770 $\pm$ 843	3308 $\pm$ 2337
$\alpha$ (1/h)	10.9 $\pm$ 4	14.4 $\pm$ 10.6
$\beta$ (1/h)	2.26 $\pm$ 0.77	1.99 $\pm$ 1
$t_{1/2\alpha}$ (min)	4.30 $\pm$ 1.6	4.66 $\pm$ 3.5
$t_{1/2\beta}$ (min)	22.0 $\pm$ 13.1	31.2 $\pm$ 26
k 10 (1/h)	5.29 $\pm$ 1.2	6.21 $\pm$ 2.4
k 12 (1/h)	3.26 $\pm$ 2	3.25 $\pm$ 2.4
k 21 (1/h)	4.65 $\pm$ 2	4.76 $\pm$ 3.5
$\text{AUC}_{0-\infty}$ ( $\text{h}\times\mu\text{g/l}$ )	1232 $\pm$ 182	2642 $\pm$ 439
AUMC ( $\text{h}\times\text{h}\times\mu\text{g/l}$ )	453 $\pm$ 285	923 $\pm$ 348
CL (l/h/kg)	1.65 $\pm$ 0.23	1.55 $\pm$ 0.25
$V_c$ (l/kg)	0.322 $\pm$ 0.07	0.277 $\pm$ 0.1
$V_p$ (l/kg)	0.253 $\pm$ 0.2	0.255 $\pm$ 0.1
MRT (min)	21.5 $\pm$ 10.9	20.8 $\pm$ 5.8

## FIGURES

Figure 1: Chemical structures of DOPAC (A), [ $^2\text{H}$ ]<sub>5</sub>-DOPAC (B), 3-HPAA (C), and (D) [ $^2\text{H}$ ]<sub>2</sub>-3-HPAA.

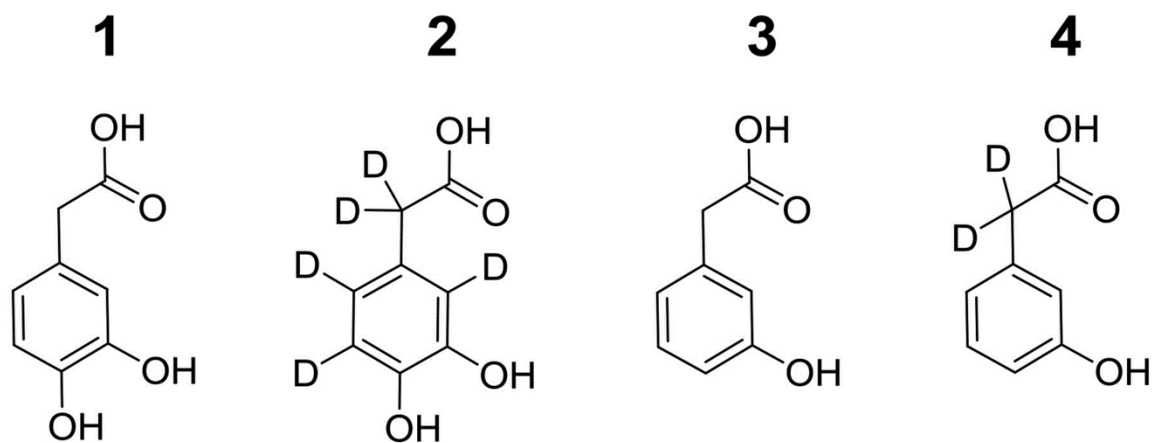


Figure 2: Typical MRM chromatograms of the BSA blank spiked with DOPAC at 3000 ng/ml (ULOQ) and IS at 250 ng/ml (A), the BSA blank (B), the BSA blank spiked with DOPAC at 30 ng/ml (LLOQ) and IS at 250 ng/ml (C).

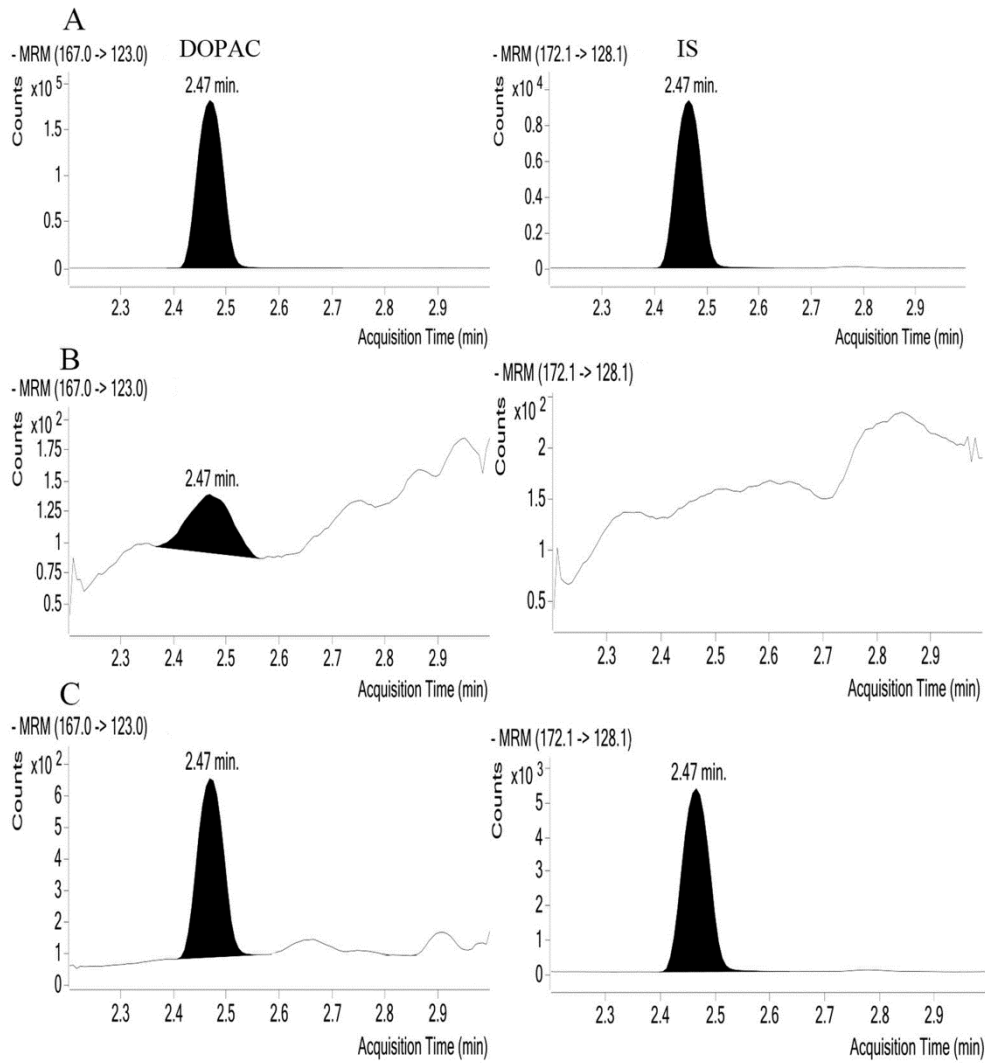


Figure 3: Typical MRM chromatograms of the BSA blank spiked with 3-HPAA (quantifier only) at 2000 ng/ml (ULOQ) and IS at 250 ng/ml (A), the BSA blank (B), the BSA blank spiked with 3-HPAA (quantifier only) at 20 ng/ml (LLOQ) and IS at 250 ng/ml (C).

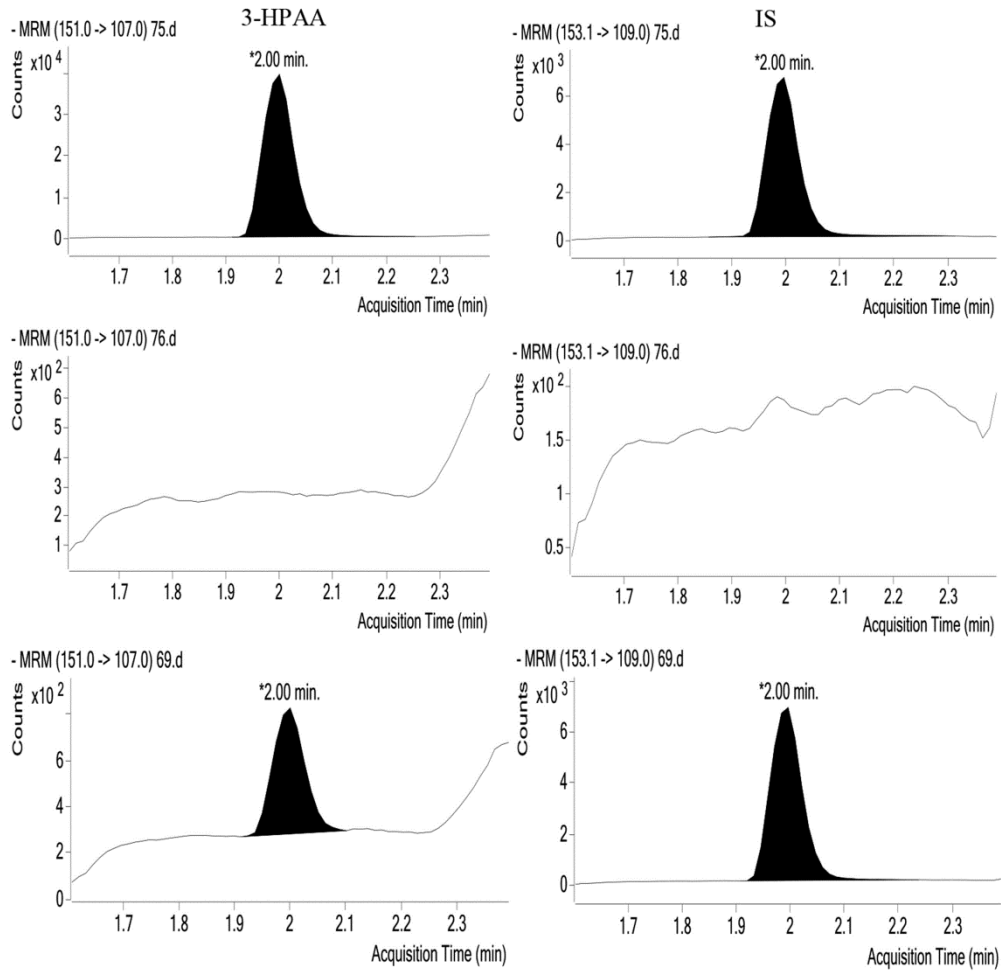




Figure 4: Plasma concentrations of DOPAC (mean  $\pm$  S.D.) after a single intravenous administration of 1, 2 and 4 mg/kg b.w., shown as linear (A) and semi-logarithmic (B) plots.

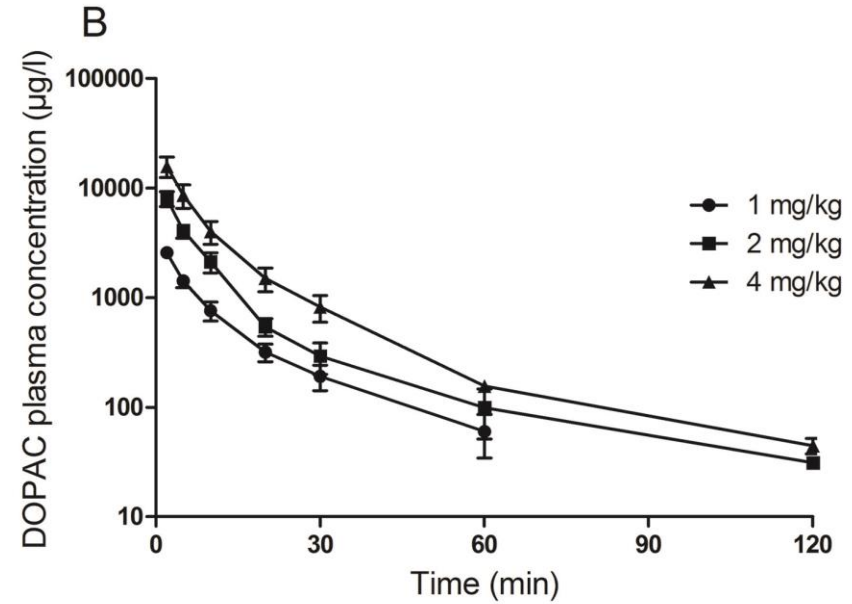
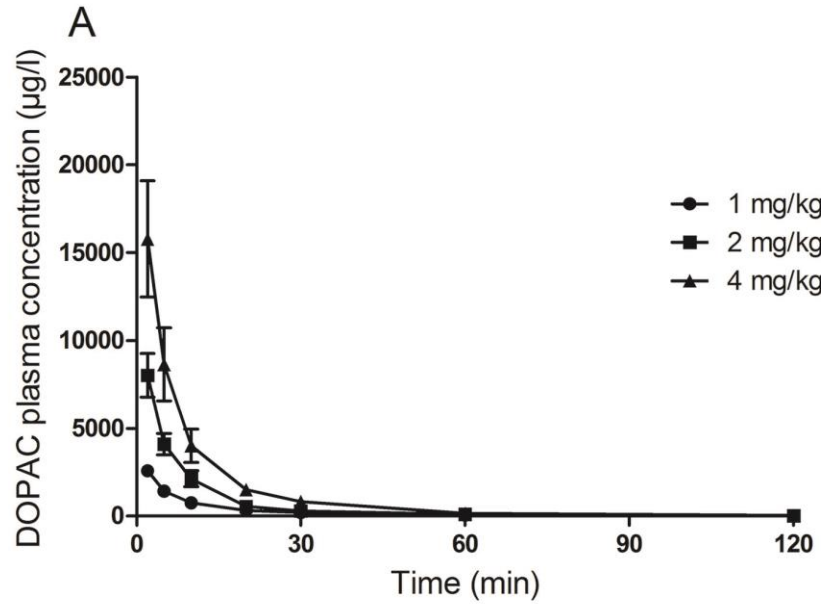


Figure 5:  $C_0$  and  $AUC_{0-inf}$  (mean  $\pm$  S.D.) of DOPAC vs. dosing group (solid line) and fitted simple linear regression (dashed line, for visual comparison).

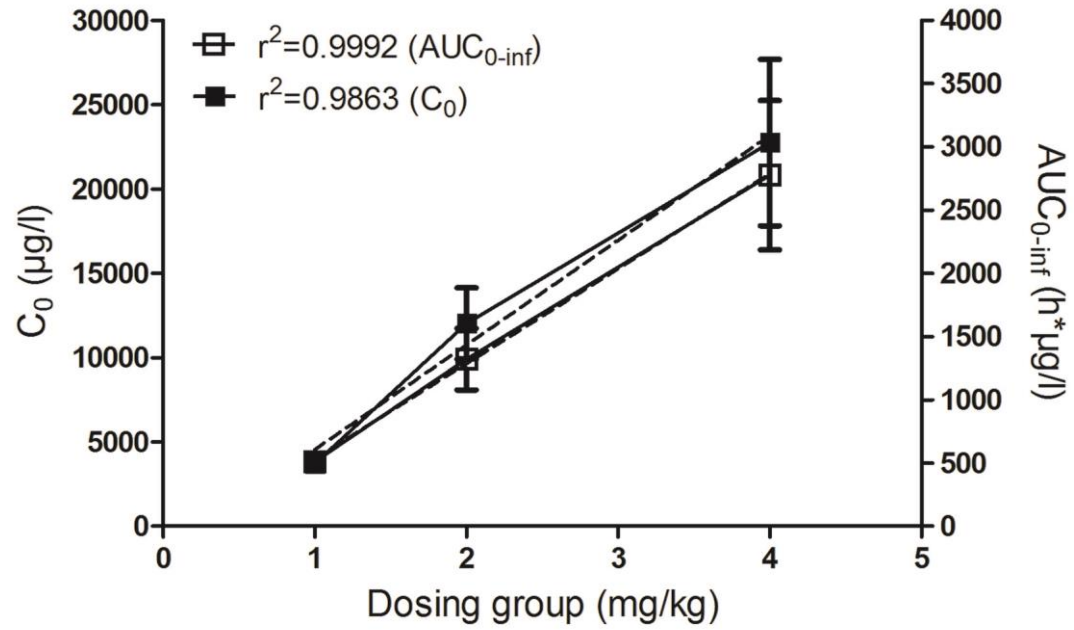


Figure 6: Observed (mean  $\pm$  S.D.) and simulated concentrations vs. time profiles of DOPAC in rats after a single intravenous dose of 1 (A), 2 (B), and 4 (C) mg/kg b.w.

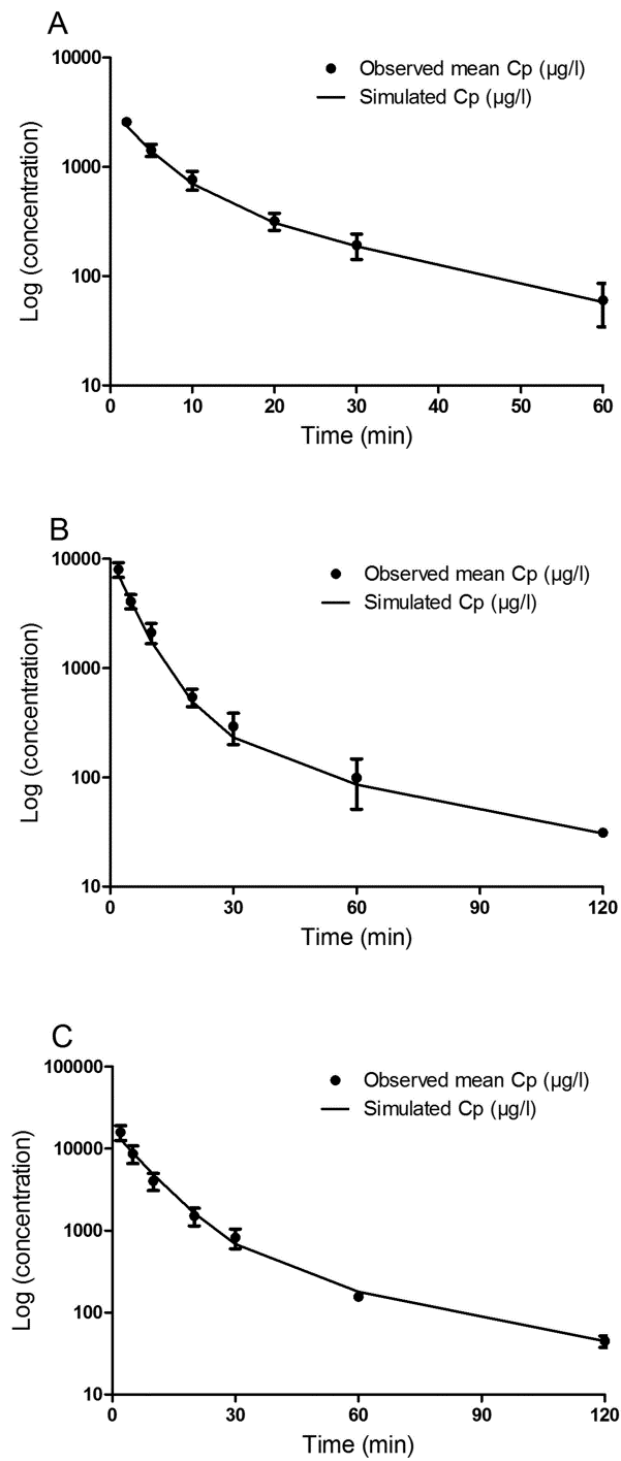


Figure 7: Plasma concentrations of 3-HPAA (mean  $\pm$  S.D.) after a single intravenous administration of 2 and 4 mg/kg b.w., shown as linear (A) and semi-logarithmic (B) plots.

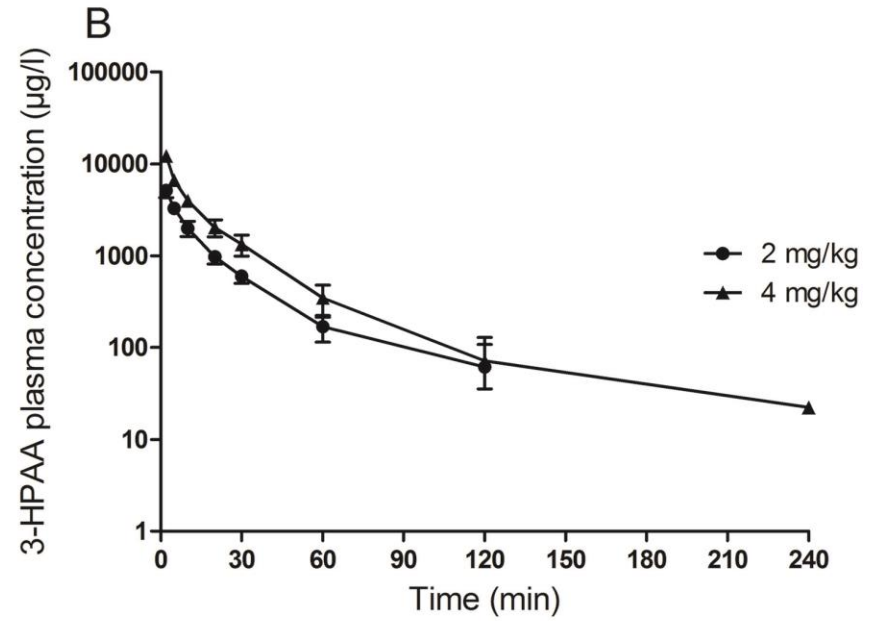
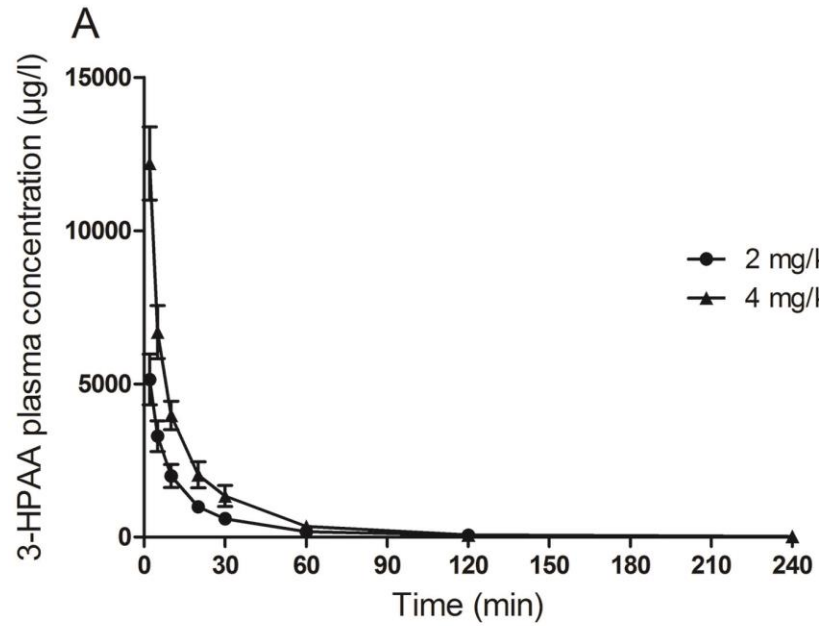
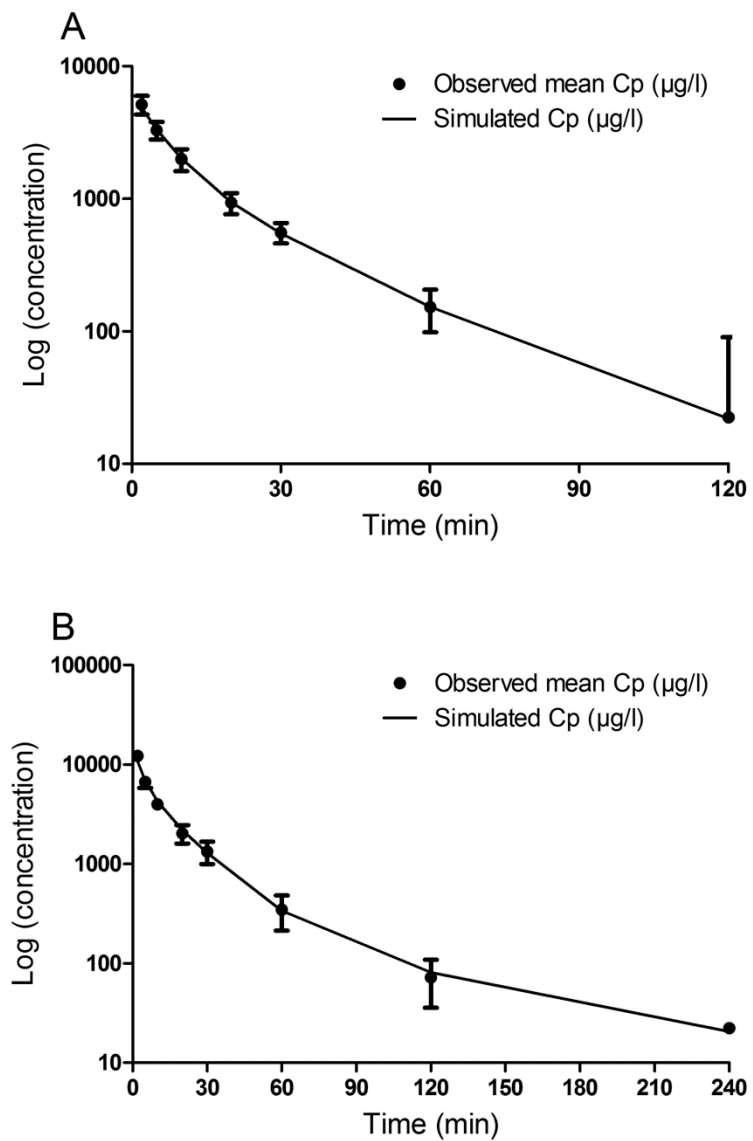


Figure 8: Observed (mean  $\pm$  S.D.) and simulated concentrations vs. time profiles of 3-HPAA in rats after a single intravenous dose of 2 (A) and 4 (B) mg/kg b.w.



## **SUPPORTING INFORMATION**

### **Single dose pharmacokinetics of intravenous 3,4-dihydroxyphenylacetic acid and 3-hydroxyphenylacetic acid in rats**

Volha Zabela<sup>a</sup>, Chethan Sampath<sup>b</sup>, Mouhssin Oufir<sup>a</sup>, Veronika Butterweck<sup>b,1</sup>, and Matthias Hamburger<sup>a,\*</sup>

<sup>a</sup>Pharmaceutical Biology Laboratory, Department of Pharmaceutical Sciences, University of Basel, Klingelbergstrasse 50, CH-4056 Basel, Switzerland

<sup>b</sup>Department of Pharmaceutics, College of Pharmacy, University of Florida, 1345 Center Drive, Gainesville, FL, USA

#### **Author's present address:**

<sup>1</sup>Institute for Pharma Technology, School of Life Sciences, University of Applied Sciences Northwestern Switzerland, Gründenstrasse 40, CH-4132 Muttenz, Switzerland

**Author's e-mails:** volha.zabela@unibas.ch (Zabela); chethan@ufl.edu (Sampath); mouhssin.oufir@unibas.ch (Oufir); veronika.butterweck@fhnw.ch (Butterweck); matthias.hamburger@unibas.ch (Hamburger).

#### **\*Corresponding author:**

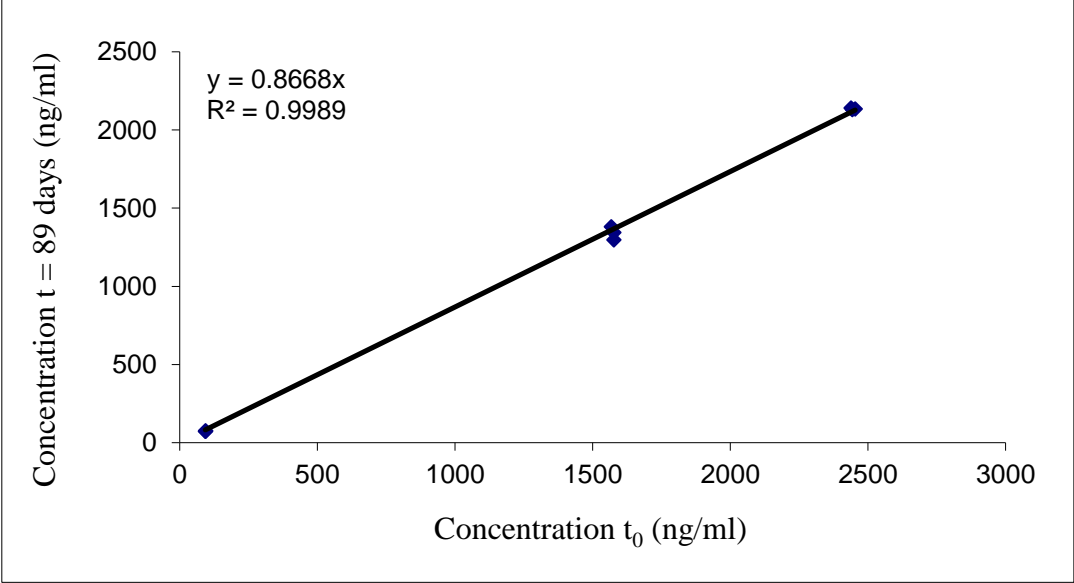
Professor Matthias Hamburger

**E-mail:** matthias.hamburger@unibas.ch

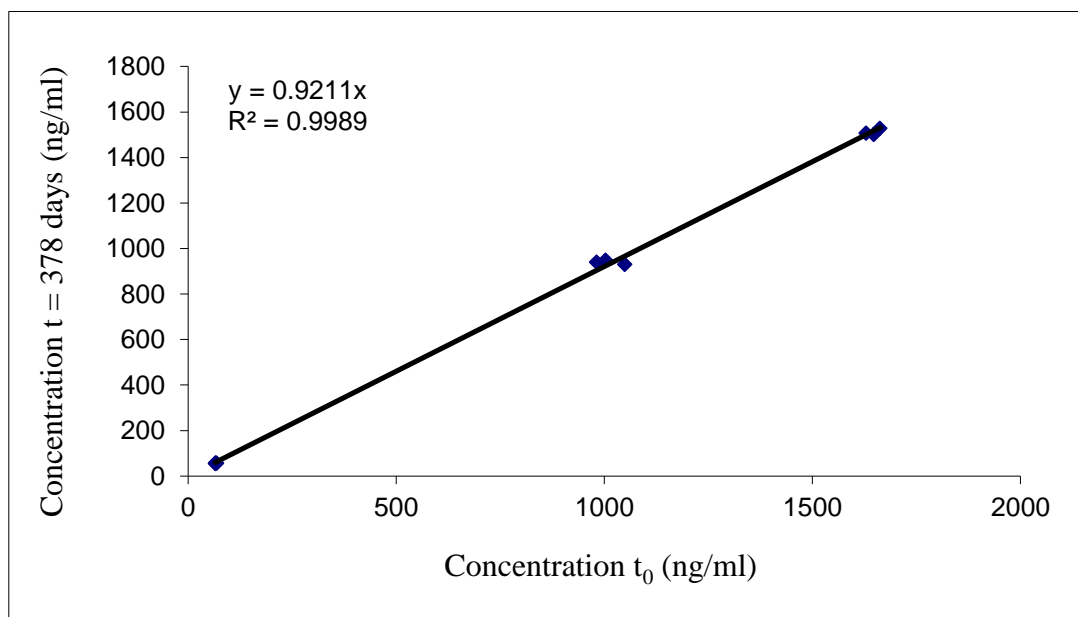
**Fax:** +41 61 267 14 74

**Address:** Pharmaceutical Biology, Department of Pharmaceutical Sciences, University of Basel, Klingelbergstrasse 50, CH-4056 Basel, Switzerland

Supporting information Figure 1: Long-term stability of DOPAC in rat plasma with 1% ascorbic acid, stored for 89 days below -65°C (n = 3).



Supporting information Figure 2: Long-term stability of 3-HPAA in BSA solution (60 g/l), stored for 378 days below -65°C (n = 3).





Supporting information Table 1: Calibrators and calibration curve parameters of DOPAC (n = 14).

Response:  $A \times \text{Conc.}^2 + B \times \text{Conc.} + C$ , Quadratic regression, 1/X weighting.

	Concentration (ng/ml)							Regression parameters			
	30	100	200	500	1000	2000	3000	A	B	C	r <sup>2</sup>
Mean	32.7	92.9	192	505	970	1990	2962	0.0067	0.59	0.1	0.9994
S.D.	1.1	3.06	5.63	12.3	132	27.8	154	0.01	0.73		
CV%	3.37	3.3	2.94	2.44	13.6	1.4	5.2				
RE%	9.09	-7.11	-4.1	0.92	-3.02	-0.48	-1.26				

Supporting information Table 2: Calibrators and calibration curve parameters of 3-HPAA (n = 14).

Response:  $A \times \text{Conc.}^2 + B \times \text{Conc.} + C$ , Quadratic regression, 1/X weighting.

	Concentration (ng/ml)							Regression parameters			
	20	50	100	250	500	1000	2000	A	B	C	r <sup>2</sup>
Mean	19.5	50.6	100	252	502	992	2003	-0.0000000029	0.0034	0.022	0.9991
S.D.	1.65	3.11	4.15	7.42	11	27.9	55.2	0.00000074	0.00021		
CV%	8.48	6.15	4.14	2.94	2.19	2.81	2.76				
RE%	-2.54	1.3	0.34	0.88	0.37	-0.76	0.16				

Supporting information Table 3: Carry-over assessment of the analyte DOPAC and [<sup>2</sup>H]<sub>5</sub>-DOPAC as IS (n = 14).

Run No.	Replicate	Peak response (counts)				Carry-over (%)		Mean Carry-over (%)	
		Blank sample		LLOQ		Analyte	IS	Analyte	IS
		Analyte	IS	Analyte	IS				
1	1	79.9	0.00	341	5760	23.4	0.00	24	0.00
	2	550	0.00	2232	41312	24.7	0.00		
2	1	131	0.00	1295	24438	10.1	0.00	12.2	0.00
	2	314	0.00	2192	43038	14.3	0.00		
3	1	353	0.00	4803	50564	7.35	0.00	7.35	0.00
	2	*38040	0.00	6613	81322	-	0.00		
4	1	470	0.00	10975	125820	4.28	0.00	5.96	0.00
	2	1421	0.00	18589	201847	7.65	0.00		
5	1	322	0.00	3608	40423	8.91	0.00	11.1	0.00
	2	714	0.00	5399	61315	13.2	0.00		
6	1	383	0.00	3991	40772	9.61	0.00	10.7	0.00
	2	887	0.00	7470	70479	11.9	0.00		
7	1	513	0.00	4998	37418	10.3	0.00	10.1	0.00
	2	963	0.00	9722	65313	9.9	0.00		
<b>Mean</b>						12	0.00		

\*: contamination

Supporting information Table 4: Carry-over assessment of the analyte 3-HPAA and [<sup>2</sup>H]<sub>2</sub>-3-HPAA as IS (n = 14).

Run No.	Replicate	Peak response (counts)				Carry-over (%)		Mean Carry-over (%)	
		Blank sample		LLOQ		Analyte	IS	Analyte	IS
		Analyte	IS	Analyte	IS				
1	1	0.00	0.00	272	3325	0.00	0.00	0.00	0.00
	2	0.00	0.00	504	6347	0.00	0.00		
2	1	0.00	0.00	448	5354	0.00	0.00	0.00	0.00
	2	0.00	0.00	656	7828	0.00	0.00		
3	1	0.00	0.00	334	2899	0.00	0.00	0.00	0.00
	2	0.00	0.00	*872	3962	-	-		
4	1	0.00	0.00	196	2408	0.00	0.00	0.00	0.00
	2	0.00	0.00	215	3057	0.00	0.00		
5	1	0.00	0.00	152	2431	0.00	0.00	0.00	0.00
	2	0.00	0.00	219	2831	0.00	0.00		
6	1	0.00	0.00	*179	2544	-	-	0.00	0.00
	2	0.00	0.00	265	2870	0.00	0.00		
7	1	0.00	0.00	317	2889	0.00	0.00	0.00	0.00
	2	0.00	0.00	309	3064	0.00	0.00		
<b>Mean</b>						0.00	0.00		

\*: LLOQ is outside the acceptance criteria ( $\pm 20\%$ ), carryover cannot be calculated.

Supporting information Table 5: Selectivity test of DOPAC, based on three different lots of BSA solution (60 g/l), spiked at LLOQ (n = 6).

<b>Nominal level (ng/ml)</b>	<b>30</b>
Mean	28.6
S.D.	3.65
CV%	12.7
RE%	10.7

Supporting information Table 6: Selectivity test of 3-HPAA, based on three different lots of BSA solution (60 g/l), spiked at LLOQ (n = 6).

<b>Nominal level (ng/ml)</b>	<b>20</b>
Mean	18.7
S.D.	1.94
CV%	10.4
RE%	-6.54

Supporting information Table 7: Absolute recovery of DOPAC and [<sup>2</sup>H]<sub>5</sub>-DOPAC (IS) from BSA solution (60 g/l) (n = 6).

<b>DOPAC nominal level (ng/ml)</b>	<b>90</b>	<b>1500</b>	<b>2400</b>
Absolute recovery (%)	57.2	75.4	77.4
CV%	2.21	1.23	1.22
SD	1.26	0.93	0.94

<b>IS nominal level (ng/ml)</b>	<b>286</b>
Absolute recovery (%)	82.4
CV%	1.87
SD	1.54

Supporting information Table 8: Absolute recovery of 3-HPAA and [<sup>2</sup>H]<sub>2</sub>-3-HPAA (IS) from BSA solution (60 g/l) (n = 6).

<b>3-HPAA nominal level (ng/ml)</b>	<b>60</b>	<b>1000</b>	<b>1600</b>
Absolute recovery (%)	113	114	106
CV%	8.94	3.88	8.04
SD	10.1	4.42	8.53

<b>IS nominal level (ng/ml)</b>	<b>143</b>
Absolute recovery (%)	104
CV%	4.12
SD	4.29

Supporting information Table 9: Dilution test of DOPAC in BSA solution (60 g/l) at nominal concentration of 15000 ng/ml (n = 6).

<b>Nominal level (ng/ml)</b>	<b>15000</b>	
<b>Dilution factor</b>	<b>10X</b>	<b>100X</b>
Mean	16675	17102
S.D.	198	201
CV%	1.19	1.18
RE%	11.2	14

Supporting information Table 10: Dilution test of 3-HPAA in BSA solution (60 g/l) at nominal concentration of 10000 ng/ml (n = 6).

<b>Nominal level (ng/ml)</b>	<b>10000</b>	
<b>Dilution factor</b>	<b>10X</b>	<b>100X</b>
Mean	10793	11332
S.D.	207	116
CV%	1.92	1.03
RE%	7.93	13.3

Supporting information Table 11: Short-term stabilities of DOPAC, expressed as RE% (n = 6).

<b>Nominal level (ng/ml)</b>	<b>90</b>	<b>2400</b>
One freeze/thaw cycles below -65°C	-0.89	-2.29
Benchtop at RT for 2 h	-8.2	-6.98
Autosampler at 10°C for 48 h	10.2	4.94

Supporting information Table 12: Short-term stabilities of 3-HPAA, expressed as RE% (n = 6).

<b>Nominal level (ng/ml)</b>	<b>60</b>	<b>1600</b>
Three freeze/thaw cycles below -65°C	5.15	7.41
Benchtop at RT for 4 h	-7.43	-3.48
Autosampler at 10°C for 24 h	-0.75	1.57

Supporting information Table 13: Stock solution (SS) stability of DOPAC in DMSO, stored below -65°C for 204 days and for 6 hours at RT (n = 6).

	<b>DOPAC SS stored below -65°C for 204 days with freshly prepared IS SS</b>	<b>DOPAC SS freshly prepared with freshly prepared IS SS</b>
Mean peak area ratio	4.73	4.78
S.D.	0.017	0.017
CV%	0.37	0.35
<b>Difference%</b>	-0.99	

Supporting information Table 14: Stock solution (SS) stability of 3-HPAA in DMSO, stored below -65°C for 431 days and for 4 hours at RT (n = 6).

	<b>3-HPAA SS stored below -65°C for 431 days with freshly prepared IS SS</b>	<b>3-HPAA SS freshly prepared with freshly prepared IS SS</b>
Mean peak area ratio	1.36	1.42
S.D.	0.01	0.0028
CV%	0.66	0.19
<b>Difference%</b>	-3.91	



Supporting information Table 15: Stock solution (SS) stability of [<sup>2</sup>H]<sub>5</sub>-DOPAC (IS) in DMSO, stored below -65°C for 168 days and for 4 hours at RT (n = 6).

	<b>[<sup>2</sup>H]<sub>5</sub>-DOPAC SS stored below -65°C for 168 days with freshly prepared DOPAC SS</b>	<b>Freshly prepared [<sup>2</sup>H]<sub>5</sub>-DOPAC SS with freshly prepared DOPAC SS</b>
Mean peak area ratio	0.21	0.21
S.D.	0.0013	0.00074
CV%	0.64	0.35
<b>Difference%</b>	-1.45	

Supporting information Table 16: Stock solution (SS) stability of [<sup>2</sup>H]<sub>2</sub>-3-HPAA (IS) in DMSO, stored below -65°C for 431 days and for 4 hours at RT (n = 6).

	<b>[<sup>2</sup>H]<sub>2</sub>-3-HPAA SS stored below -65°C for 431 days with freshly prepared 3-HPAA SS</b>	<b>Freshly prepared [<sup>2</sup>H]<sub>2</sub>-3-HPAA SS with freshly prepared 3-HPAA SS</b>
Mean peak area ratio	0.76	0.76
S.D.	0.0021	0.002
CV%	0.27	0.26
<b>Difference%</b>	-0.39	

Supporting information Table 17: Diagnostic table for a two-compartment model with  $1/\hat{Y}^2$  as a weighting factor fitted to the DOPAC data.

Dosing group (mg/kg)	Goodness of fit		
	AIC	SBC	WSSR
1	-15	-15.8	0.026
2	-12.8	-13.6	0.039
4	-6.54	-6.76	0.13

Supporting information Table 18: Diagnostic table for a two-compartment model with  $1/\hat{Y}^2$  as a weighting factor fitted to the 3-HPAA data.

Dosing group (mg/kg)	Goodness of fit		
	AIC	SBC	WSSR
2	-20.9	-21.6	0.018
4	-15.3	-15.6	0.078

### **3.3 GABA<sub>A</sub> receptor activity modulating piperine analogs: *In vitro* metabolic stability, metabolite identification, CYP450 reaction phenotyping, and protein binding**

**Volha Zabela**, Timm Hettich, Götz Schlotterbeck, Laurin Wimmer, Marko D. Mihovilovic, Fabrice Guillet, Belkacem Bouaita, Bénédicte Shevchenko, Matthias Hamburger, and Mouhssin Oufir

Submitted to: *European Journal of Pharmaceutical Sciences*

The alkaloid piperine and analogs (SCT-29, LAU 397, and LAU 399) have been previously identified as positive allosteric modulators of  $\gamma$ -aminobutyric acid type A (GABA<sub>A</sub>) receptors. We investigated metabolism of piperine and analogs to guide further cycles of lead optimization. Metabolic stability of compounds was tested in the presence of pooled human liver microsomes. Metabolites were analyzed by UHPLC-Q-TOF-MS, and with the aid of metabolite identification software Mass-MetaSite. Unbound fraction in whole blood was determined by rapid equilibrium dialysis. CYP450 reaction phenotyping studies were carried out with Silensomes<sup>™</sup>. Piperine was the metabolically most stable compound. Aliphatic hydroxylation, and N- and O-dealkylation were the major routes of oxidative metabolism. Piperine was exclusively metabolized by CYP1A2, whereas CYP2C9 contributed significantly in the oxidative metabolism of all analogs. Extensive binding to blood constituents was observed for all compounds.

*My contributions to this publication: development of UHPLC-MS/MS methods for quantification of piperine and analogs in potassium phosphate buffer, development of UHPLC-Q-TOF-MS methods for qualitative analysis of metabolites, design and performance of microsomal stability assays, CYP450 reaction phenotyping, unbound fraction determination in whole blood, and metabolite identification, writing the manuscript draft, and preparation of figures and tables.*

*Volha Zabela*

## **MANUSCRIPT**

### **GABA<sub>A</sub> receptor activity modulating piperine analogs: *In vitro* metabolic stability, metabolite identification, CYP450 reaction phenotyping, and protein binding**

Volha Zabela<sup>a</sup>, Timm Hettich<sup>b</sup>, Götz Schlotterbeck<sup>b</sup>, Laurin Wimmer<sup>c</sup>, Marko D. Mihovilovic<sup>c</sup>, Fabrice Guillet<sup>d</sup>, Belkacem Bouaita<sup>e</sup>, Bénédicte Shevchenko<sup>e</sup>, Matthias Hamburger<sup>a</sup>, and Mouhssin Oufir<sup>a\*</sup>

<sup>a</sup>Pharmaceutical Biology Laboratory, Department of Pharmaceutical Sciences, University of Basel, Klingelbergstrasse 50, CH-4056 Basel, Switzerland

<sup>b</sup>Institute for Chemistry and Bioanalytics, School of Life Sciences, University of Applied Sciences Northwestern Switzerland, Gründenstrasse 40, 4132 Muttenz, Switzerland

<sup>c</sup>Institute of Applied Synthetic Chemistry, Vienna University of Technology, Getreidemarkt 9, A-1060 Vienna, Austria

<sup>d</sup>Eurosafe, Parc d'Affaires La Bretèche, 35760 Saint Grégoire, France

<sup>e</sup>Biopredic International, Parc d'Affaires La Bretèche, 35760 Saint Grégoire, France

**Author's e-mails:** volha.zabela@unibas.ch (Zabela); timm.hettich@fhnw.ch (Hettich); goetz.schlotterbeck@fhnw.ch (Schlotterbeck); laurin.wimmer@tuwien.ac.at (Wimmer); marko.mihovilovic@tuwien.ac.at (Mihovilovic); fabrice.guillet@eurosafe.fr (Guillet); elkacem.bouaita@biopredic.com (Bouaita); benedicte.shevchenko@biopredic.com (Shevchenko); matthias.hamburger@unibas.ch (Hamburger); mouhssin.oufir@unibas.ch (Oufir)

#### **\*Corresponding author:**

Dr. Mouhssin Oufir

E-mail: mouhssin.oufir@unibas.ch

Tel: +41 61 207 15 44

Address: Pharmaceutical Biology, Department of Pharmaceutical Sciences, University of Basel, Klingelbergstrasse 50, CH-4056 Basel, Switzerland

## **Abbreviations**

au, arbitrary units

BBB, blood brain barrier

CYP450, cytochrome P450

DMSO, dimethyl sulfoxide

ESI, electrospray ionization

GABA<sub>A</sub>,  $\gamma$ -aminobutyric acid type A receptor

HPLC, high performance liquid chromatography

HR, high resolution

IS, internal standard

MetID, metabolite identification

MS, mass spectrometry

MRM, multiple reaction monitoring

PPB, potassium phosphate buffer

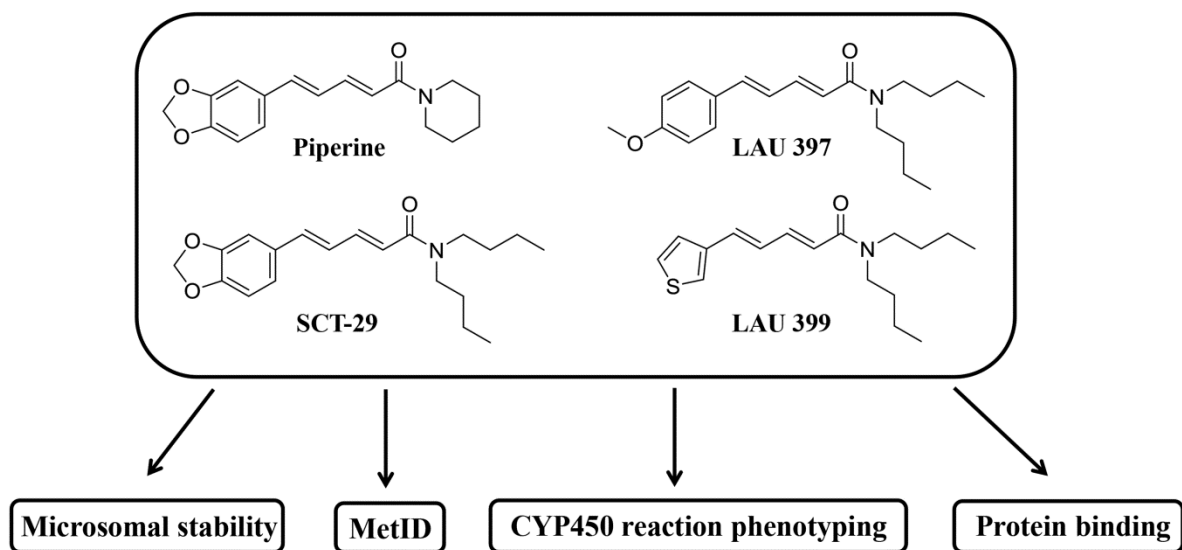
Q-TOF, quadrupole time-of-flight

RED, rapid equilibrium dialysis

TRPV1, transient receptor potential vanilloid type 1

UHPLC, ultra-high performance liquid chromatography

## Graphical abstract



## Abstract

In a screening of natural products for allosteric modulators of GABA<sub>A</sub> ( $\gamma$ -aminobutyric acid type A receptor), piperine was identified as a compound targeting a benzodiazepine-independent allosteric binding site. Given that piperine is also an activator of TRPV1 (transient receptor potential vanilloid type 1) receptors involved in pain signaling and thermoregulation, a series of piperine analogs were prepared in several cycles of structural optimization, with the aim of separating GABA<sub>A</sub> and TRPV1 activating properties. We here investigated the metabolism of piperine and selected analogs in view of further cycles of lead optimization.

Metabolic stability of the compounds was evaluated by incubation with pooled human liver microsomes, and metabolites were analyzed by UHPLC-Q-TOF-MS. CYP450 isoenzymes involved in metabolism of compounds were identified by reaction phenotyping with Silensomes<sup>™</sup>. Unbound fraction in whole blood was determined by rapid equilibrium dialysis.

Piperine was the metabolically most stable compound. Aliphatic hydroxylation, and N- and O-dealkylation were the major routes of oxidative metabolism. Piperine was exclusively metabolized by CYP1A2, whereas CYP2C9 contributed significantly in the oxidative metabolism of all analogs. Extensive binding to blood constituents was observed for all compounds.

**Keywords:** GABA<sub>A</sub>, *in vitro* metabolism, piperine analogs, UHPLC-Q-TOF-MS, Silensomes<sup>™</sup>.

## 1 Introduction

In a screening of natural products for GABA<sub>A</sub> ( $\gamma$ -aminobutyric acid type A receptor) modulatory properties, the alkaloid piperine was identified as a positive allosteric modulator targeting a benzodiazepine-independent binding site (Zaugg et al., 2010). Given that piperine is also an activator of TRPV1 (transient receptor potential vanilloid type 1) receptors involved in pain signaling and thermoregulation (McNamara et al., 2005), systematic structural modifications were carried out in several cycles of optimization, aiming at separating GABA<sub>A</sub> modulatory from TRPV1 activity. A first analog, SCT-66 (Fig. 1), did not activate TRPV1 receptors while maintaining GABA<sub>A</sub> receptor modulatory properties *in vitro* and *in vivo* (Khom et al., 2013). Subsequently, a library of 76 piperine analogs was prepared. Among these, SCT-64 and SCT-29 showed the highest potency and efficacy at GABA<sub>A</sub> receptors, and anxiolytic activity in mice (Schöffmann et al., 2014). Based on snapshot pharmacokinetic data, SCT-29 was selected for the next cycle of medicinal chemistry optimization (Schöffmann et al., 2014). All analogs synthesized up to this point contained a 1,3-benzodioxole moiety which is susceptible to metabolic degradation to an ortho-catechol that can be oxidized to a reactive ortho-quinone (Attia, 2010; Erve et al., 2013). Therefore, a library of 15 aryl-modified analogs was synthesized, of which LAU 397 and LAU 399 showed the highest efficacy and potency *in vitro* (Wimmer et al., 2015). Given that to this point no experimental drug metabolism data had been recorded, we here evaluated metabolic stability and metabolite formation in microsomal incubations of piperine and selected compounds from the three cycles of optimization (SCT-29, LAU 397 and LAU 399) to guide further cycles of structural modifications. In addition, reaction phenotyping was carried out to identify major CYP450 isoenzymes involved in oxidative metabolism of these compounds, and unbound fraction in blood was determined with the aid of rapid equilibrium dialysis.



## 2 Materials and Methods

### 2.1 Chemicals and reagents

Piperine analogs (2E,4E)-5-(benzo[*d*][1,3]dioxol-5-yl)-N,N-dibutylpenta-2,4-dienamide (SCT-29), (2E,4E)-N,N-dibutyl-5-(4-methoxyphenyl)penta-2,4-dienamide (LAU 397), (2E,4E)-N,N-dibutyl-5-(thiophen-3-yl)penta-2,4-dienamide (LAU 399) and (2E,4E)-5-(benzo[*d*][1,3]dioxol-5-yl)-N,N-dipropylpenta-2,4-dienamide (SCT-64), were synthesized at the Vienna University of Technology as described elsewhere (Schöffmann et al., 2014; Wimmer et al., 2015). Piperine ( $\geq 97.0\%$ ), Trizma<sup>®</sup> HCl ( $\geq 99.0\%$ ), NaOH ( $\geq 98.0\%$ ), MgCl<sub>2</sub> ( $\geq 98.0\%$ ), EDTA (99.9%), KH<sub>2</sub>PO<sub>4</sub> ( $\geq 98.0\%$ ), K<sub>2</sub>HPO<sub>4</sub> ( $\geq 99.0\%$ ), NaH<sub>2</sub>PO<sub>4</sub> ( $\geq 99.0\%$ ), Na<sub>2</sub>HPO<sub>4</sub> ( $\geq 99.0\%$ ), amodiaquine dihydrochloride ( $\geq 99.0\%$ ), N-desethylamodiaquine dihydrochloride solution (1 mg/ml), <sup>2</sup>H<sub>5</sub>-N-desethylamodiaquine dihydrochloride solution (100 µg/ml), diclofenac sodium salt ( $\geq 98.5\%$ ), 4'-hydroxy-diclofenac ( $\geq 98.0\%$ ), phenacetin ( $\geq 98.0\%$ ), paracetamol ( $\geq 99.0\%$ ), <sup>2</sup>H<sub>4</sub>-paracetamol ( $\geq 97.0\%$ ), dextromethorphan hydrobromide monohydrate ( $\geq 99.0\%$ ), dextroprphan ( $\geq 98\%$ ), <sup>2</sup>H<sub>3</sub>-dextroprphan solution (100 µg/ml), coumarin ( $\geq 99.0\%$ ), 7-hydroxycoumarin ( $\geq 99.0\%$ ), testosterone ( $\geq 98.0\%$ ), 6-β-hydroxytestosterone ( $\geq 97.0\%$ ), <sup>2</sup>H<sub>3</sub>-6-β-hydroxy-testosterone solution (100 µg/ml) were purchased from Sigma-Aldrich (Steinheim, Germany). Pooled human liver microsomes (50 donors) were purchased from BioreclamationIVT (Baltimore, USA). NADPH regenerating system containing solution A (26 mM NADP<sup>+</sup>, 66 mM glucose-6-phosphate, and 66 mM MgCl<sub>2</sub> in H<sub>2</sub>O) and solution B (40 U/ml glucose-6-phosphate dehydrogenase in 5mM sodium citrate) was supplied by Corning (Woburn, MA, USA). Silensomes<sup>™</sup> (>60 donors) and homologous controls were from Biopredic International (Rennes, France). Lithium heparin human blood (3 donors) was purchased from Blutspendezentrum SRK (Basel, Switzerland). Acetonitrile, methanol, formic acid, phosphoric acid, trifluoroacetic acid, and ammonium formate and acetate (all HPLC grade) were from BioSolve (Valkenswaard, the Netherlands). Dimethyl sulfoxide (DMSO) was from Scharlau (Barcelona, Spain). HPLC grade water was obtained by a Milli-Q integral water purification system (Millipore Merck, Darmstadt, Germany). A 100 mM potassium phosphate buffer (PPB) consisting of 0.1M KH<sub>2</sub>PO<sub>4</sub> and 0.1M K<sub>2</sub>HPO<sub>4</sub>, sample dilution buffer (PPB with 0.5M EDTA), and a 0.1M Tris/HCl buffer supplemented with MgCl<sub>2</sub> (5mM) were prepared in-house, adjusted to pH 7.4, filtered, and stored at 4°C.

## 2.2 Microsomal incubations

Due to non-specific adsorption of piperine and analogs to plastic containers, all incubations were conducted in glass vials. Daily working solutions of test compounds were prepared in sample dilution buffer from the stock solutions in DMSO, with a final DMSO concentration of 0.1-0.2% (v/v) in the incubation mixture. The incubation mixture, with a total volume of 500  $\mu$ l, contained PPB, a substrate (1  $\mu$ M), liver microsomes (0.5 mg proteins/ml), and a NADPH regenerating system which initiated the reaction. Reactions were quenched at 0, 15, 30, 60 min by adding 500  $\mu$ l of ice-cold acetonitrile with the corresponding internal standard (IS): LAU 399 for LAU 397 and SCT-64 for piperine, SCT-29, and LAU 399. Control incubations were performed without microsomes, without NADPH, and without both microsomes and NADPH to detect possible chemical instability or non-NADPH dependent enzymatic degradation. After incubation, samples were centrifuged (11688 g, 4°C) for 10 min, and 900  $\mu$ l of supernatant were collected and dried under nitrogen flow (Evaporex EVX-96, Apricots Designs Inc, USA). Dried residues were redissolved in 200  $\mu$ l of DMSO by shaking on a mixmate (1100 rpm) for 30 min prior to UHPLC-MS/MS analysis. All microsomal incubations were performed in triplicate, and the results were expressed as mean  $\pm$  S.D.

### 2.2.1 Calculations of *in vitro* half-life and apparent intrinsic clearance

Typical depletion profiles of the test compounds were obtained from microsomal incubations. The percentage of remaining substrates (on a log scale) was plotted against incubation time. A linear regression analysis was applied to estimate a slope. Elimination rate constant ( $k_e$ ,  $\text{min}^{-1}$ ) was calculated using equation 1:

$$k_e = -\text{slope} \times 2.3 \quad (\text{Eq.1})$$

*In vitro* half-life ( $t_{1/2}$ , min) was determined as follows:

$$t_{1/2} = \frac{0.693}{k_e} \quad (\text{Eq.2})$$

Apparent intrinsic clearance ( $CL_{in,a}$ ,  $\mu\text{l}/\text{min}/\text{mg}$  protein) was calculated according to:

$$CL_{in,a} = \frac{V_{incub} \times 0.693}{AP \times t_{1/2}} \quad (\text{Eq.3})$$

whereby  $V_{incub}$  was the volume of incubation mixture, and AP was the amount of protein in the incubation mixture.

### 2.3 Microsomal incubations for metabolite identification (MetID) studies

Microsomal incubations were performed as described above, with a substrate concentration of 5  $\mu$ M. Reactions were terminated after 120 min by adding 500  $\mu$ l of ice-cold methanol

without internal standard. The same extraction procedure as above was used, but residues were reconstituted in 100 µl of methanol.

#### 2.4 MetID data processing

MS and MS/MS data were analyzed with Mass-MetaSite version 5.1.1 (Molecular Discovery, Pinner, Middlesex, UK) and ACD/Labs MetID (ACD/Labs, Toronto, ON, Canada) metabolite identification software packages.

#### 2.5 Microsomal binding assay

The extent of non-specific binding of test compounds to human microsomes was determined by using rapid equilibrium dialysis (RED) plates with inserts (Thermo Scientific, Waltham, MA, USA). Each insert consisted of two chambers separated by a dialysis membrane with a 8 kDa cut-off. The mixture (500 µl) containing PPB, microsomes (0.5 mg/ml) and test compound (1 µM) was loaded into the sample chamber, and 750 µl of PPB were loaded into the buffer chamber. The RED plate was sealed with an aluminum foil, and incubated on an orbital shaker at 250 rpm, 37°C for 8 h (the time was defined experimentally). After incubation, 100 µl of both chambers were collected. Before extraction, 100 µl of PPB were added to the microsomal post-dialysis sample, and 100 µl of microsomes (0.5 mg/ml) were added to the buffer post-dialysis sample in order to obtain similar matrix effects in LC-MS/MS analysis. 600 µl of the corresponding IS in ice-cold acetonitrile were added to precipitate proteins. Samples were centrifuged (11688 g, 4°C) for 10 min, and 700 µl of supernatant were taken and dried under nitrogen flow. The residues were reconstituted in 200 µl of DMSO, and shaken on a mixmate (1100 rpm) for 30 min prior to UHPLC-MS/MS analysis. Microsomal fraction unbound ( $f_{u(mic)}$ ) was calculated by equation 4. The assay was performed in triplicate, and results were expressed as mean ± S.D.

$$f_{u(mic)} = 1 - \left( \frac{PAR_{mic} - PAR_{buf}}{PAR_{mic}} \right) \quad (\text{Eq.4})$$

$PAR_{mic}$  is the peak area ratio in microsomal post-dialysis sample,  $PAR_{buf}$  is the peak area ratio in buffer post-dialysis sample. PAR was calculated from the following equation:

$$PAR = \frac{\text{Peak area analyte}}{\text{Peak area IS}} \quad (\text{Eq.5})$$

The unbound intrinsic clearance ( $C_{in,u}$ , µl/min/mg protein) was calculated according to equation 6 (Giuliano et al., 2005).

$$Cl_{in,u} = \frac{Cl_{i,a}}{f_{u(mic)}} \quad (\text{Eq.6})$$

## 2.6 Whole blood binding assay

Pooled human blood (2 males and 1 female) was diluted with PPB (1:1, v/v) to avoid clogging of the dialysis membrane. Diluted blood was spiked with the test compound (1  $\mu$ M), and 500  $\mu$ l were loaded into the sample chamber of a RED plate. 750  $\mu$ l of PPB were loaded into the buffer chamber. The assay was carried out in the same way as described above. The unbound fraction was initially calculated in diluted (50%) blood (Eq.7), and then scaled to 100% using equation 8. The assay was done in triplicate, and the results were expressed as mean  $\pm$  S.D.

$$f_{u50\%} = 1 - \left( \frac{PAR_{blood} - PAR_{buf}}{PAR_{blood}} \right) \quad (\text{Eq.7})$$

$PAR_{blood}$  is the peak area ratio in blood post-dialysis sample;  $PAR_{buf}$  is the peak area ratio in buffer post-dialysis sample.

$$f_{u,blood\ 100\%} = \frac{f_{u50\%}}{2 - f_{u50\%}} \quad (\text{Eq.8})$$

## 2.7 Prediction of human hepatic clearance and extraction ratio from *in vitro* data

Physiological scaling factors were used to convert *in vitro*  $Cl_{in,u}$  into *in vivo*  $Cl_{in}$  (ml/min/kg) (Obach, 1999):

$$Cl_{in, in\ vivo} = Cl_{in,u} * \frac{45\ mg\ microsomes}{1\ gm\ liver} * \frac{20\ g\ liver}{1\ kg\ body\ weight} \quad (\text{Eq.9})$$

The well-stirred liver model was used to predict hepatic metabolic clearance ( $Cl_H$ , ml/min/kg) in humans (Gillette, 1971; Rowland et al., 1973; Wilkinson and Shand, 1975):

$$Cl_H = \frac{QH * f_{u,blood} * Cl_{in, in\ vivo}}{QH + f_{u,blood} * Cl_{in, in\ vivo}} \quad (\text{Eq.10})$$

$Q_H$  is the liver blood flow for a healthy adult, and equals 20 ml/min/kg,  $f_{u,blood}$  is the unbound fraction of the test compound in blood.

Hepatic extraction ratio was calculated from the following expression (Lau et al., 2002):

$$ER = \frac{Cl_H}{QH} \quad (\text{Eq.11})$$

## 2.8 *In silico* prediction of cytochrome P450 (CYP450)-mediated metabolism

Prediction of CYP450 isoforms involved in the oxidative metabolism of compounds was performed with Percepta software (ACD/Labs, Toronto, ON, Canada). The prediction outcome was then used to select CYP isoforms for reaction phenotyping (Fig S1).

## 2.9 CYP450 reaction phenotyping with Silensomes™

Silensomes™ are human pooled liver microsomes in which one given CYP450 isoenzyme has been irreversibly inactivated using mechanism based inhibitors (Parmentier et al., 2016). Each CYP-Silensome™ is associated with a homologous control that is produced under the same conditions but without the inhibitor. The following Silensomes™ were used: CYP3A4,

CYP2D6, CYP2C9, CYP1A2, CYP2A6, CYP2C8. Control experiments with homologous microsomes were performed at the same time as Silensome™ incubation. Incubations were performed in the same way as microsomal incubations, but Tris/HCl buffer supplemented with MgCl<sub>2</sub> was used. The metabolized fraction was calculated as follows:

$$f_m = 1 - \left( \frac{Clin\ Silensomes^{TM}}{Clin\ Control} \right) \quad (Eq.12)$$

The relative contribution of the CYP of interest was estimated as follows:

$$Contribution = \left( 1 - \left( \frac{Clin\ Silensomes^{TM}}{Clin\ Control} \right) \right) * 100\% \quad (Eq.13)$$

### 2.9.1 Incubation of CYP-specific substrates with Silensomes™

Silensomes™ and control microsomes (0.5 mg/ml) were incubated for 30 min at 37°C with 200 μM phenacetin (CYP1A2), 100 μM dextromethorphan (CYP2D6), 20 μM amodiaquine (CYP2C8), 75 μM testosterone (CYP3A4), 20 μM coumarin (CYP2A6) and 200 μM diclofenac (CYP2C9). Metabolisation was initiated by addition of 1 mM of NADPH, and the reaction was stopped by adding phosphoric acid (0.15M) (v/v). All samples were centrifuged at +4°C at 2500 g for 15min. Supernatants were diluted with corresponding ISs (1:1, v/v), and analyzed by HPLC-MS/MS to quantify the metabolites formed. The assay was done in triplicate, and the results were expressed as mean ± S.D.

### 2.10 HPLC-MS/MS analysis

A 1200SL HPLC system (Agilent, Santa Clara, CA, USA) coupled to an API3200 tandem mass spectrometer (AB Sciex, Framingham, MA, USA) was used for the analysis of CYP-specific substrate incubations with Silensomes™. Separation was performed on a Waters XSelect HSS T3 C18 column (2.5 μm, 4.6 × 75 mm; Waters Corp., Milford, MA, USA) heated at 50°C. Quantification was done with electrospray ionization (ESI) in negative or positive modes by multiple reaction monitoring (MRM). The ESI source was operated with the following settings: curtain gas 50 arbitrary units (au), source temperature 550°C, nebulizer gas 50 au, and auxiliary gas 30 au. Ion spray voltage, declustering potential, and collision energy were adapted for each analyte and corresponding ISs. The system was controlled by Analyst software (version 1.5.2; AB Sciex, ON, Canada). For the positive ion mode, the mobile phase consisted of 5mM ammonium acetate in water (A), and 0.3% formic acid in a mixture of methanol and acetonitrile (1:1, v/v) (B). For the negative ion mode, the mobile phase consisted of 0.01% formic acid in water (A), and acetonitrile (B). The flow rate was 1.5 ml/min, and the injection volumes ranged from 5 to 20 μl.

### 2.11 UHPLC-MS/MS analysis

An UHPLC 1290 system coupled to a 6460 tandem mass spectrometer (all Agilent Technologies, Waldbronn, Germany) was used to analyze the samples from microsomal stability, reaction phenotyping, and binding assays. Separation was achieved on a Kinetex PFP column (1.7  $\mu\text{m}$ , 2.1 x 50 mm; Phenomenex, Torrance, CA, USA) heated at 55°C. The flow rate was 0.5 ml/min, and the injection volume was 5  $\mu\text{l}$ . Quantification was done in MRM utilizing an Agilent Jet Stream electrospray ionization source in positive mode. The mobile phase consisted of 10 mM ammonium formate with 0.05% formic acid (A), and acetonitrile with 0.05% formic acid (B). The gradient started at 1 min with 40% of B and increased to 70% of B within 3.00 min, followed by a column washing step with 100% of B for 1 min. The source was operated with the following settings: nebulizer pressure 20 psi, nozzle voltage 0 V, sheath gas flow 11 l/min, sheath gas temperature 300°C, drying gas flow 10 l/min, drying gas temperature 320°C, capillary voltage 2500 V. Fragmentor voltage and collision energy for each analyte and corresponding IS were as described elsewhere (Eigenmann et al., 2016). The system was controlled by MassHunter software (version 7.0; Agilent Technologies, Santa Clara, CA, USA).

### 2.12 UHPLC-Q-TOF-MS analysis

An UHPLC 1290 system coupled to a 6540 quadrupole time-of-flight (Q-TOF) mass spectrometer (all Agilent Technologies, Santa Clara, CA, USA) was used for high-resolution accurate mass measurements. Separation of parent compounds and metabolites was performed on a Kinetex PFP column (1.7  $\mu\text{m}$ , 2.1 x 50 mm; Phenomenex, Torrance, CA, USA) heated at 55°C. The flow rate was 0.4 ml/min, and the injection volume was 5  $\mu\text{l}$ . Data acquisition was performed in MS scan and in targeted MS/MS modes: MS scan 100-1000  $m/z$  at 1 Hz, and MS/MS 50-350  $m/z$  also at 1 Hz. The mobile phase consisted of 10 mM ammonium formate with 0.05% formic acid (A), and acetonitrile with 0.05% formic acid (B). The gradient started at 1 min with 2% of B, from 1-8 min, 25% B, from 8-12 min, 35% B, from 12-16 min, 100% B, followed by a column washing step with 100% of B for 1 min, and re-equilibration for 3 min. The ESI source was operated in positive mode with the following settings: nebulizer pressure 30 psi, nozzle voltage 0 V, sheath gas flow 12 l/min, sheath gas temperature 400°C, drying gas flow 12 l/min, drying gas temperature 330°C, capillary voltage 2500 V, and fragmentor voltage 175 V. For the collision induced dissociation (CID) experiments the fragmentation was performed with two different collision energies of 20 and 40 V. The precursor isolation mass window of the quadrupole was set to 1.3  $m/z$  at full width half maximum. The acquired spectra were automatically recalibrated on-line by reference

ions with exact masses of 121.0509 and 922.0098  $m/z$ . The Q-TOF mass spectrometer was operated at 4 GHz analog-to-digital converter rate in dual channel mode at a resolving power of 19 000 (measured at  $m/z$  322). The system was controlled by MassHunter Acquisition and Qualitative Analysis (version 6.0; Agilent Technologies, Santa Clara, CA, USA).

### 3 Results

Metabolic stability of compounds was studied by incubation with pooled human liver microsomes. Piperine was the metabolically most stable compound, with a  $t_{1/2}$  of 141 min (Fig. 2, and Table 1). SCT-29 and LAU 397 showed  $t_{1/2}$  of approx. 45 min, whereas a  $t_{1/2}$  of only 24.9 min was found for LAU 399 (Fig. 2, and Table 1). Apparent intrinsic clearance was calculated (Table 1) and used to categorize compounds into low, medium, or high clearance (Nassar, 2009). Piperine was thus a low clearance compound, SCT-29 and LAU 397 were medium clearance, and LAU 399 was a high clearance compound. However, due to non-specific binding of substrates to microsomes, the unbound fractions were determined and employed to determine unbound intrinsic clearance of each molecule (Table 1). It appeared that all analogs had high unbound intrinsic clearance (267-411  $\mu\text{l}/\text{min}/\text{mg}$  protein). Human hepatic clearance and extraction ratio were predicted from *in vitro* microsomal stability data using the liver well-stirred model. *In vitro* unbound intrinsic clearance of each compound was converted into *in vivo* by applying physiological scaling factors (Table 2).

Binding of piperine and analogs in whole blood was determined since extensive binding negatively affects distribution of the compounds into deeper compartments and hence, concentrations at the target site. Unbound fractions of compounds in whole blood were determined, and used for the prediction of human hepatic clearance (Table 2). In addition, the hepatic extraction ratio was calculated (Table 2) to classify the compounds into low, medium, or high extraction categories (Lau et al., 2002). Based on these criteria, all compounds were low extraction ratio compounds.

Metabolite profiles of compounds after incubation with human microsomes were analyzed by high resolution (HR)-MS, and the acquired data were further processed by metabolite identification software. The presence of a diagnostic product ion from the parent compound in the MS spectra of metabolites supported metabolite identification. The fragmentation patterns of parent compounds are summarized in Figure S2. For piperine, extracted ion chromatograms of the blank,  $t_0$ , and  $t_{120}$  samples are shown for  $m/z$  201.0547 (diagnostic product ion) (Fig. S3). Extracted ion chromatograms of the  $t_{120}$  sample for  $m/z$  201.0547 (diagnostic product ion), and for  $m/z$  302.1387 and 304.1544 (metabolites) are given in

Figure 3. Microsomal incubation of piperine yielded four metabolites M1-M4 (Table 3). Metabolites M1-M3, all with  $m/z$  of 302.1387, were formed by hydroxylation of the piperidine ring (Fig. 4). M4 ( $m/z$  304.1544) was likely formed via opening of the piperidine ring by N-dealkylation, and reduction of the aldehyde (Fig. 4). MS spectra of piperine and metabolites are shown in Figure S4.

For SCT-29, extracted ion chromatograms of the blank,  $t_0$ , and  $t_{120}$  samples are shown for  $m/z$  201.0545 (diagnostic product ion) (Fig. S5). Extracted ion chromatograms of the  $t_{120}$  sample for  $m/z$  201.0545 (diagnostic product ion), and for  $m/z$  346.2013 (metabolites) are given in Figure 5. Microsomal incubation of SCT-29 yielded three metabolites M1-M3 (Table 3) with  $m/z$  of 346.2013 that was indicative of aliphatic hydroxylation (Fig. 4). MS spectra of SCT-29 and metabolites are provided in Figure S6.

For LAU 397, extracted ion chromatograms of the blank,  $t_0$ , and  $t_{120}$  samples for two diagnostic product ions at  $m/z$  187.0752 and 173.0602 are given in Figures S2, S7, and S8. Figure 6 shows extracted ion chromatograms of the  $t_{120}$  sample for  $m/z$  187.0752 (diagnostic product ion), and for  $m/z$  332.2220 (metabolites), and extracted ion chromatograms of the  $t_{120}$  sample for  $m/z$  173.0602 (diagnostic product ion), and  $m/z$  318.2061 and 302.2118 (metabolites) are given in Figure 7. Microsomal incubation of LAU 397 yielded seven metabolites M1-M7 (Table 3). Metabolites M1 and M2 with  $m/z$  of 318.2061 were formed through via O-dealkylation and aliphatic hydroxylation (Fig. 4). Metabolites M3-M5 with  $m/z$  of 332.2220 were formed by aliphatic hydroxylation, whereas metabolites M6 and M7 with  $m/z$  of 302.2118 were produced via O-dealkylation (Fig. 4). MS spectra of LAU 397 and metabolites are provided in Figures S9 and S10, respectively.

For LAU 399, extracted ion chromatograms of the blank,  $t_0$ , and  $t_{120}$  samples for the diagnostic product ion  $m/z$  163.0216 are provided in Figure S11, and extracted ion chromatograms of the  $t_{120}$  sample for  $m/z$  163.0216 (diagnostic product ion), and  $m/z$  308.1677 and 306.1522 (metabolites) are shown in Figure 8. Microsomal incubation of LAU 399 yielded three metabolites M1-M3 (Table 3). M1-2 with  $m/z$  of 308.1677 were formed by aliphatic hydroxylation, whereas M3 with  $m/z$  of 306.1522 was formed through aliphatic hydroxylation followed by oxidation of the alcohol (Fig. 4). MS spectra of LAU 399 and metabolites are provided in Figure S12.

CYP450 reaction phenotyping studies were performed with Silensomes<sup>™</sup>. The types of Silensomes<sup>™</sup> for the studies were selected based on the prediction from the CYP450 substrates module of ACD/labs Percepta 14.0 (Fig. S1), and further validated with CYP450-specific substrates (Fig. S13). Examples of typical CYP3A4 Silensomes<sup>™</sup> profiles



with/without enzyme contribution are provided in Figure S14, and results of the reaction phenotyping for piperine and analogs are summarized in Figure 9. Piperine and SCT-29 were metabolized exclusively by one CYP450 isoenzyme, CYP1A2 and CYP2C9, respectively. Metabolism of LAU 397 involved CYP3A4 and CYP2C9, and LAU 399 was metabolized by CYP2C9 and CYP1A2.

#### **4 Discussion**

*In vitro* metabolic stability is routinely assessed in early drug discovery to evaluate stability of leads, and to identify metabolically labile sites to guide lead optimization. We here investigated the metabolic stability of piperine and selected analogs in the presence of pooled human liver microsomes, and calculated *in vitro* unbound intrinsic clearance for each compound. Piperine was identified as the metabolically most stable compound, whereas the tested analogs were rapidly metabolized. Metabolites formed by microsomal incubation were analyzed. Interestingly, hydroxylation of piperine and analogs preferentially occurred on the aliphatic portion of the molecule. However, the exact position of hydroxylation could not be established due to a low abundance of metabolites.

CYP450 reaction phenotyping showed that piperine and SCT-29 are cleared by a single enzyme, CYP1A2 and CYP2C9, respectively, and thus are more sensitive to drug-drug interactions. CYP2C9 (Zhou et al., 2009) contributed significantly in the oxidative metabolism of all analogs. Genetic polymorphism of CYP2C9 may lead to individual variations in drug response (Tomalik-Scharte et al., 2008).

Piperine and all tested analogs exhibited extensive binding to blood constituents, which in turn resulted in a low hepatic extraction ratio calculated for all compounds. The strong protein binding can be explained by the lipophilicity of piperine (cLogP 3.27) and analogs (cLogP 4.70-5.21) (Eigenmann et al., 2016). Highly lipophilic compounds tend to bind strongly to plasma proteins, and high lipophilicity also leads to higher metabolic clearance (Tsaoun and Kates, 2011).

#### **5 Conclusions**

Piperine analogs (SCT-29, LAU 397, and LAU 399) were rapidly metabolized and showed strong binding to blood constituents due to increased lipophilicity. The next cycle of medicinal chemistry optimizations should, therefore, focus on reducing lipophilicity, in order to decrease metabolic liabilities and extensive protein binding.

## **Acknowledgements**

This study was supported by the Swiss National Science Foundation (project 205320\_126888, MH). Authors thank Orlando Fertig for technical assistance.

## **Conflict of interest**

Two co-authors, B. Bouaita and B. Shevchenko are employees of Biopredic International. F. Guillet is employee of Eurosafe.

## References

- Attia, S.M., 2010. Deleterious effects of reactive metabolites. *Oxid. Med. Cell Longev.* 3, 238-253.
- Eigenmann, D.E., Dürig, C., Jähne, E.A., Smieško, M., Culot, M., Gosselet, F., Cecchelli, R., Helms, H.C.C., Brodin, B., Wimmer, L., 2016. *In vitro* blood-brain barrier permeability predictions for GABA<sub>A</sub> receptor modulating piperine analogs. *Eur. J. Pharm. Biopharm* 103, 118–126.
- Erve, J.C.L., Gauby, S., Maynard Jr, J.W., Svensson, M.A., Tonn, G., Quinn, K.P., 2013. Bioactivation of sitaxentan in liver microsomes, hepatocytes, and expressed human P450s with characterization of the glutathione conjugate by liquid chromatography tandem mass spectrometry. *Chem. Res. Toxicol.* 26, 926-936.
- Gillette, J.R., 1971. Factors affecting drug metabolism. *Ann. N.Y. Acad. Sci.* 179, 43-66.
- Giuliano, C., Jairaj, M., Zafiu, C.M., Laufer, R., 2005. Direct determination of unbound intrinsic drug clearance in the microsomal stability assay. *Drug Metab. Dispos.* 33, 1319-1324.
- Khom, S., Strommer, B., Schöffmann, A., Hintersteiner, J., Baburin, I., Erker, T., Schwarz, T., Schwarzer, C., Zaugg, J., Hamburger, M., 2013. GABA<sub>A</sub> receptor modulation by piperine and a non-TRPV1 activating derivative. *Biochem. Pharmacol.* 85, 1827-1836.
- Lau, Y.Y., Krishna, G., Yumibe, N.P., Grotz, D.E., Sapidou, E., Norton, L., Chu, I., Chen, C., Soares, A., Lin, C.-C., 2002. The use of *in vitro* metabolic stability for rapid selection of compounds in early discovery based on their expected hepatic extraction ratios. *Pharm. Res.* 19, 1606-1610.
- McNamara, F., Randall, A., Gunthorpe, M., 2005. Effects of piperine, the pungent component of black pepper, at the human vanilloid receptor (TRPV1). *Br. J. Pharmacol.* 144, 781-790.
- Nassar, A.F., 2009. *Drug metabolism Handbook: Concepts and applications.* John Wiley & Sons, Hoboken.
- Obach, R.S., 1999. Prediction of human clearance of twenty-nine drugs from hepatic microsomal intrinsic clearance data: an examination of *in vitro* half-life approach and nonspecific binding to microsomes. *Drug Metab. Dispos.* 27, 1350-1359.
- Parmentier, Y., Pothier, C., Delmas, A., Caradec, F., Trancart, M.M, Guillet, F., Bouaita, B., Chesne, C., Houston, J.B., Walther, B., 2016. Direct and quantitative evaluation of the human CYP3A4 contribution (fm) to drug clearance using the *in vitro* SILENSOMES model, *Xenobiotica*, DOI: 10.1080/00498254.2016.1208854
- Rowland, M., Benet, L.Z., Graham, G.G., 1973. Clearance concepts in pharmacokinetics. *J. Pharmacokinet. Biopharm.* 1, 123-136.
- Schöffmann, A., Wimmer, L., Goldmann, D., Khom, S., Hintersteiner, J., Baburin, I., Schwarz, T., Hintersteiner, M., Pakfeifer, P., Oufir, M., Hamburger, M., Erker, T., Ecker, G.F., Mihovilovic, M.D., Hering, S., 2014. Efficient modulation of  $\gamma$ -aminobutyric acid type A receptors by piperine derivatives. *J. Med. Chem.* 57, 5602-5619.
- Tomalik-Scharte, D., Lazar, A., Fuhr, U., Kirchheiner, J., 2008. The clinical role of genetic polymorphisms in drug-metabolizing enzymes. *Pharmacogenomics J.* 8, 4-15.
- Tsaioun, K., Kates, S.A., 2011. *ADMET for medicinal chemists: a practical guide.* John Wiley & Sons, Hoboken.
- Wilkinson, G.R., Shand, D.G., 1975. A physiological approach to hepatic drug clearance. *Clin. Pharmacol. Ther.* 18, 377-390.
- Wimmer, L., Schönbauer, D., Pakfeifer, P., Schöffmann, A., Khom, S., Hering, S., Mihovilovic, M.D., 2015. Developing piperine towards TRPV1 and GABA<sub>A</sub> receptor ligands—synthesis of piperine analogs via Heck-coupling of conjugated dienes. *Org. Biomol. Chem.* 13, 990-994.
- Zaugg, J., Baburin, I., Strommer, B., Kim, H.-J., Hering, S., Hamburger, M., 2010. HPLC-based activity profiling: discovery of piperine as a positive GABA<sub>A</sub> receptor modulator targeting a benzodiazepine-independent binding site. *J. Nat. Prod.* 73, 185-191.
- Zhou, S.-F., Liu, J.-P., Chowbay, B., 2009. Polymorphism of human cytochrome P450 enzymes and its clinical impact. *Drug Metab. Rev.* 41, 89-295.

## Legends for Figures

Figure 1: Chemical structures of piperine and selected analogs from three cycles of optimization.

Figure 2: Metabolic stability of piperine and selected analogs SCT-29, LAU 397 and LAU 399 analogs in incubations with pooled human liver microsomes (n = 3).

Figure 3: Phase I metabolites of piperine produced by microsomal incubation. Extracted ion chromatograms of the  $t_{120}$  sample are shown for  $m/z$  201.0547 (diagnostic product ion), and for  $m/z$  302.1387 and 304.1544 (metabolites).

Figure 4: Phase I metabolites of piperine and analogs, as proposed by Mass-MetaSite.

Figure 5: Phase I metabolites of SCT-29 produced by microsomal incubation. Extracted ion chromatograms of the  $t_{120}$  sample are shown for  $m/z$  201.0545 (diagnostic product ion), and for  $m/z$  346.2013 (metabolites).

Figure 6: Phase I metabolites of LAU 397 produced by microsomal incubation. Extracted ion chromatograms of the  $t_{120}$  sample are shown for  $m/z$  187.0752 (diagnostic product ion), and for  $m/z$  332.2220 (metabolites).

Figure 7: Phase I metabolites of LAU 397 produced by microsomal incubation. Extracted ion chromatograms of the  $t_{120}$  sample are shown for  $m/z$  173.0602 (diagnostic product ion), and for  $m/z$  318.2061 and 302.2118 (metabolites).

Figure 8: Phase I metabolites of LAU 399 produced by microsomal incubation. Extracted ion chromatograms of the  $t_{120}$  sample are shown for  $m/z$  163.0216 (diagnostic product ion), and for  $m/z$  308.1677 and 306.1522 (metabolites).

Figure 9. CYP450 reaction phenotyping with Silensomes<sup>™</sup>. The graphs show the relative contribution of CYP450 isoenzymes to the oxidative metabolism of compounds.

## TABLES

Table 1: Metabolic stability of piperine and analogs in the presence of human liver microsomes (n = 3). Values are expressed as mean  $\pm$  S.D.

Compound	$t_{1/2}$ (min)	$Cl_{in,a}$ ( $\mu\text{l}/\text{min}/\text{mg}$ protein)	$f_u$ (mic)	$Cl_{in,u}$ ( $\mu\text{l}/\text{min}/\text{mg}$ protein)
Piperine	141 $\pm$ 33.2	10.3 $\pm$ 2.41	0.863 $\pm$ 0.213	12.0 $\pm$ 2.79
SCT-29	43.1 $\pm$ 5.31	32.6 $\pm$ 3.28	0.101 $\pm$ 0.0232	322 $\pm$ 35.6
LAU 397	45.7 $\pm$ 15.8	32.9 $\pm$ 9.00	0.0796 $\pm$ 0.0159	411 $\pm$ 113
LAU 399	24.9 $\pm$ 5.03	57.6 $\pm$ 10.2	0.216 $\pm$ 0.0252	267 $\pm$ 50.3

Table 2: Prediction of human hepatic clearance and extraction ratio from *in vitro* microsomal stability data. Values are expressed as mean  $\pm$  S.D.

Compound	$Cl_{in, in vivo}$ (ml/min/kg)	$f_{u, blood}$	$Cl_H$ (ml/min/kg)	ER
Piperine	10.8 $\pm$ 2.51	0.0303 $\pm$ 0.00239	0.317 $\pm$ 0.0729	0.0159 $\pm$ 0.00364
SCT-29	290 $\pm$ 32.1	0.000344 $\pm$ 0.0000598	0.0866 $\pm$ 0.00954	0.00433 $\pm$ 0.000477
LAU 397	370 $\pm$ 101	0.000245 $\pm$ 0.0000763	0.0737 $\pm$ 0.0201	0.00368 $\pm$ 0.00101
LAU 399	240 $\pm$ 45.3	0.00156 $\pm$ 0.000287	0.468 $\pm$ 0.0865	0.0234 $\pm$ 0.00432

Table 3: Observed phase I metabolites of piperine and analogs.

Compound	RT (min)	Mass shift	Chemical structure	Calculated $m/z$ [M+H] <sup>+</sup>	Observed $m/z$ [M+H] <sup>+</sup>	Mass error (ppm)	Diagnostic product ions
Piperine	13.22	-	C <sub>17</sub> H <sub>19</sub> NO <sub>3</sub>	286.1438	286.1440	-0.70	201.0547
M1	9.17	+15.9949	C <sub>17</sub> H <sub>19</sub> NO <sub>4</sub>	302.1387	302.1386	0.33	201.1029
M2	9.44	+15.9949	C <sub>17</sub> H <sub>19</sub> NO <sub>4</sub>	302.1387	302.1387	-0.12	201.0547
M3	9.54	+15.9949	C <sub>17</sub> H <sub>19</sub> NO <sub>4</sub>	302.1387	302.1387	-0.12	201.1026
M4	9.83	+18.0106	C <sub>17</sub> H <sub>21</sub> NO <sub>4</sub>	304.1543	304.1544	-0.33	201.0551
SCT-29	13.97	-	C <sub>20</sub> H <sub>27</sub> NO <sub>3</sub>	330.2064	330.2065	-0.30	201.0545
M1	13.30	+15.9949	C <sub>20</sub> H <sub>27</sub> NO <sub>4</sub>	346.2013	346.2014	-0.28	201.0544
M2	13.45	+15.9949	C <sub>20</sub> H <sub>27</sub> NO <sub>4</sub>	346.2013	346.2015	-0.52	201.0546
M3	13.57	+15.9949	C <sub>20</sub> H <sub>27</sub> NO <sub>4</sub>	346.2013	346.2017	-1.15	201.0547
LAU 397	14.00	-	C <sub>20</sub> H <sub>29</sub> NO <sub>2</sub>	316.2271	316.2272	-0.43	187.0752
M1	11.49	+1.9792	C <sub>19</sub> H <sub>27</sub> NO <sub>3</sub>	318.2064	318.2061	0.94	173.0602
M2	12.03	+1.9792	C <sub>19</sub> H <sub>27</sub> NO <sub>3</sub>	318.2064	318.2062	0.55	173.0601
M3	13.37	+15.9949	C <sub>20</sub> H <sub>29</sub> NO <sub>3</sub>	332.2220	332.2217	0.90	187.0752
M4	13.51	+15.9949	C <sub>20</sub> H <sub>29</sub> NO <sub>3</sub>	332.2220	332.2217	0.90	187.0752
M5	13.61	+15.9949	C <sub>20</sub> H <sub>29</sub> NO <sub>3</sub>	332.2220	332.2220	-0.74	187.0762
M6	13.63	-14.0157	C <sub>19</sub> H <sub>27</sub> NO <sub>2</sub>	302.2115	302.2118	-0.99	173.0602
M7	13.71	-14.0157	C <sub>19</sub> H <sub>27</sub> NO <sub>2</sub>	302.2115	302.2113	0.66	173.0596
LAU 399	13.96	-	C <sub>17</sub> H <sub>25</sub> NOS	292.1730	292.1736	-2.05	163.0216
M1	13.11	+15.9949	C <sub>17</sub> H <sub>25</sub> NO <sub>2</sub> S	308.1679	308.1677	0.65	163.0209
M2	13.34	+15.9949	C <sub>17</sub> H <sub>25</sub> NO <sub>2</sub> S	308.1679	308.1682	-0.97	163.0212 135.0337
M3	13.49	+13.9792	C <sub>17</sub> H <sub>23</sub> NO <sub>2</sub> S	306.1522	306.1522	0.02	163.0212

## **FIGURES**

Figure 1: Chemical structures of piperine and selected analogs from three cycles of optimization.

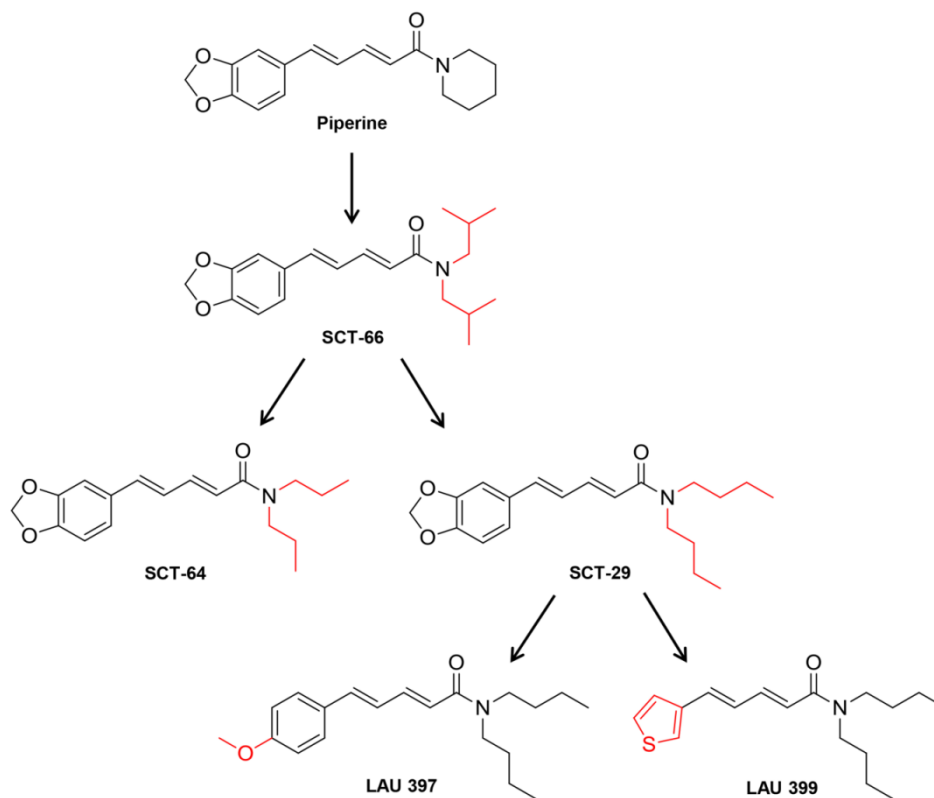




Figure 2: Metabolic stability of piperine and selected analogs SCT-29, LAU 397 and LAU 399 in incubations with pooled human liver microsomes (n = 3).

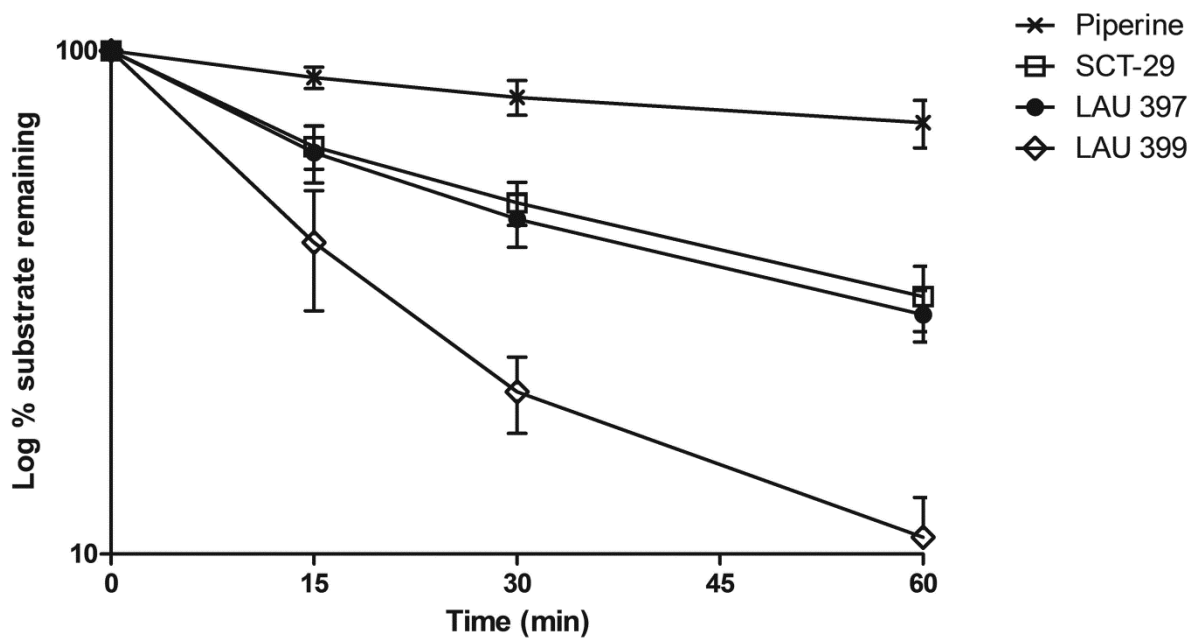


Figure 3: Phase I metabolites of piperine produced by microsomal incubation. Extracted ion chromatograms of the  $t_{120}$  sample are shown for  $m/z$  201.0547 (diagnostic product ion), and for  $m/z$  302.1387 and 304.1544 (metabolites).

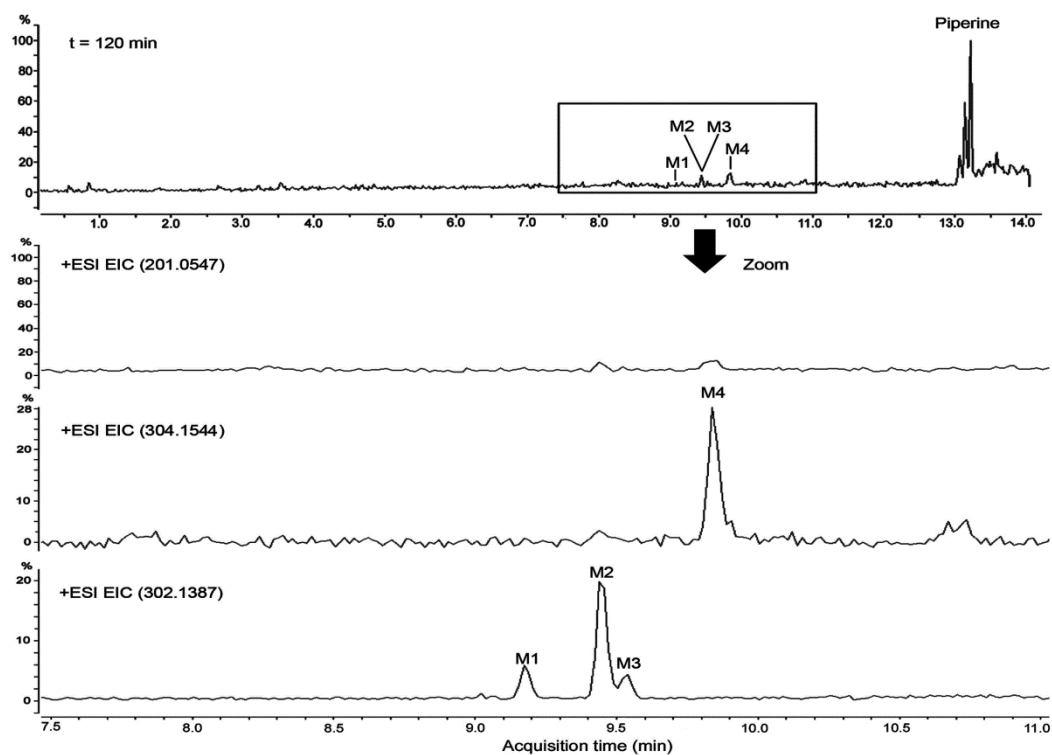


Figure 4: Phase I metabolites of piperine and analogs, as proposed by Mass-MetaSite.

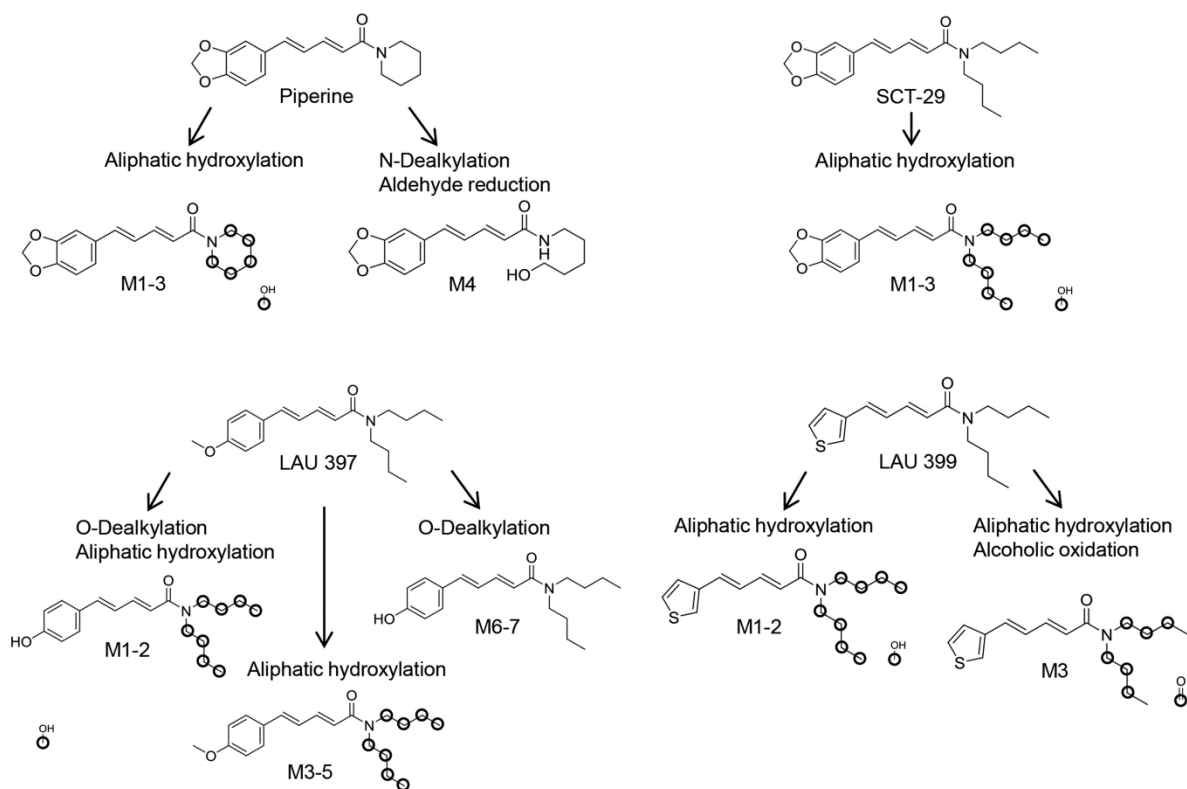


Figure 5: Phase I metabolites of SCT-29 produced by microsomal incubation. Extracted ion chromatograms of the  $t_{120}$  sample are shown for  $m/z$  201.0545 (diagnostic product ion), and for  $m/z$  346.2013 (metabolites).

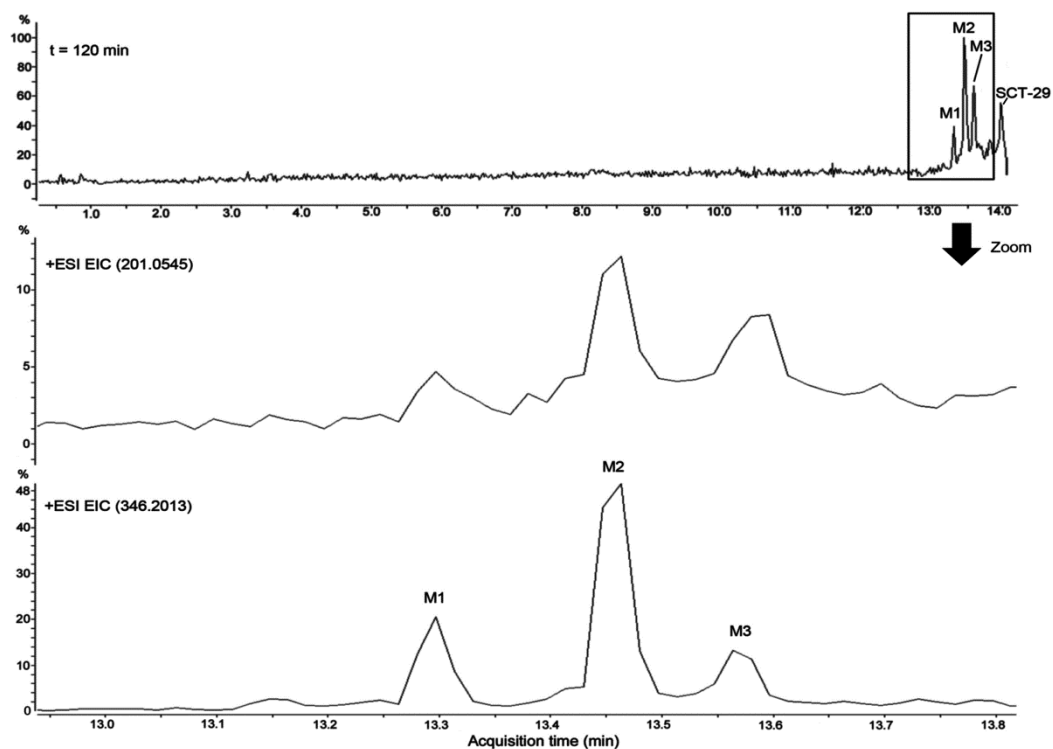


Figure 6: Phase I metabolites of LAU 397 produced by microsomal incubation. Extracted ion chromatograms of the  $t_{120}$  sample are shown for  $m/z$  187.0752 (diagnostic product ion), and for  $m/z$  332.2220 (metabolites).

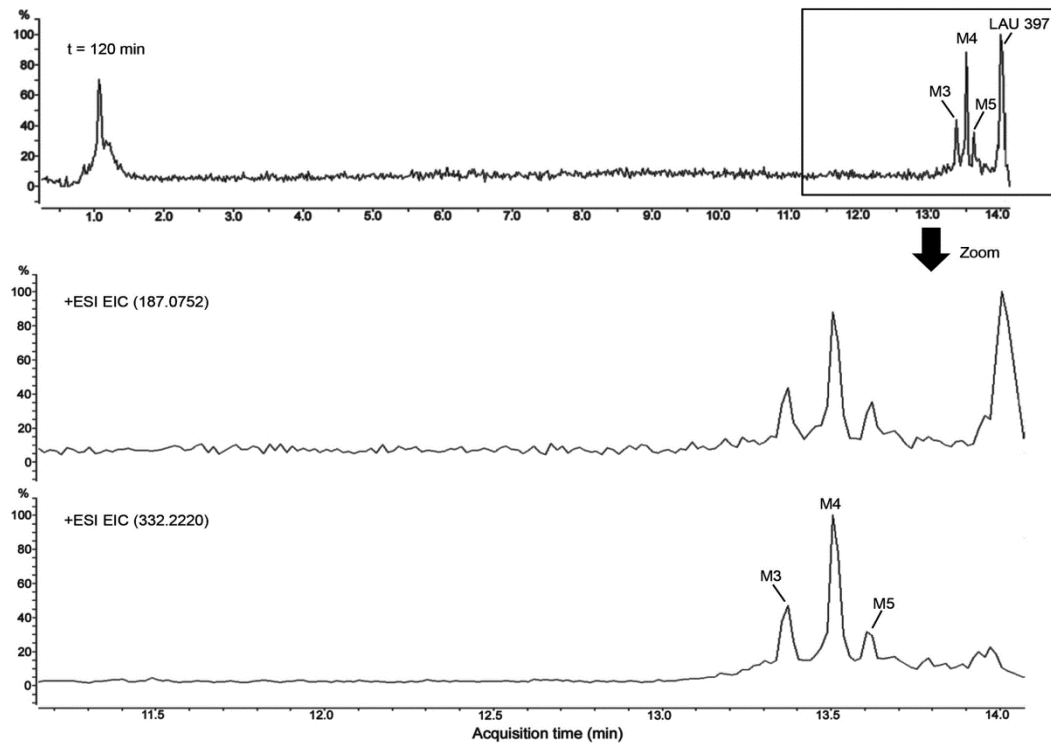


Figure 7: Phase I metabolites of LAU 397 produced by microsomal incubation. Extracted ion chromatograms of the  $t_{120}$  sample are shown for  $m/z$  173.0602 (diagnostic product ion), and for  $m/z$  318.2061 and 302.2118 (metabolites).

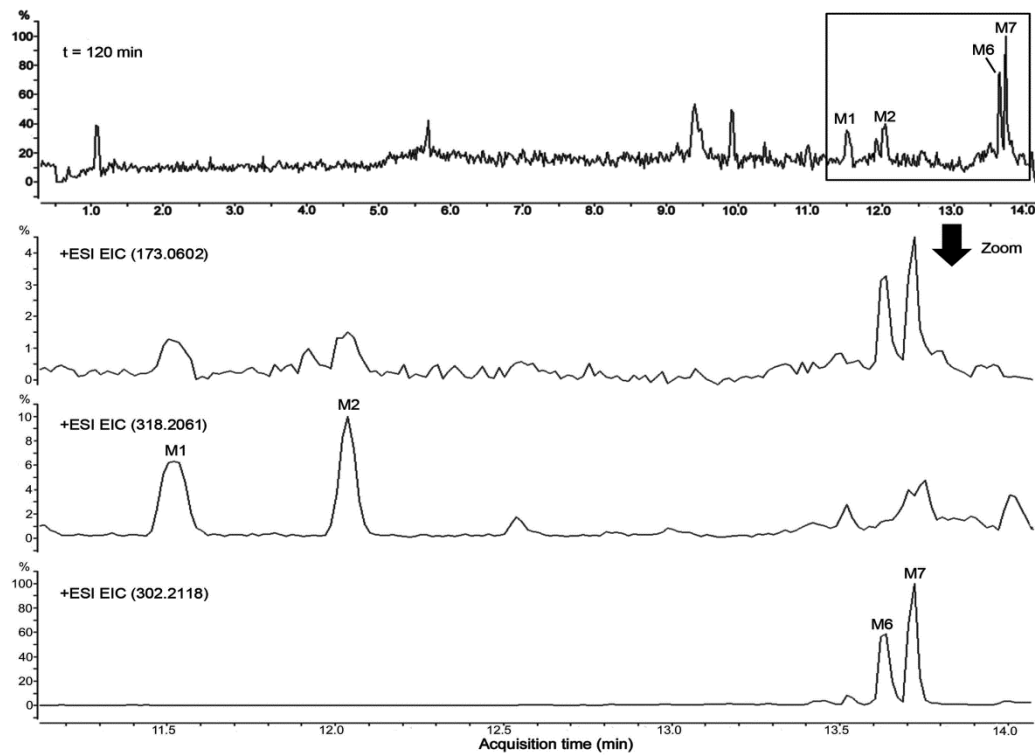


Figure 8: Phase I metabolites of LAU 399 produced by microsomal incubation. Extracted ion chromatograms of the  $t_{120}$  sample are shown for  $m/z$  163.0216 (diagnostic product ion), and for  $m/z$  308.1677 and 306.1522 (metabolites).

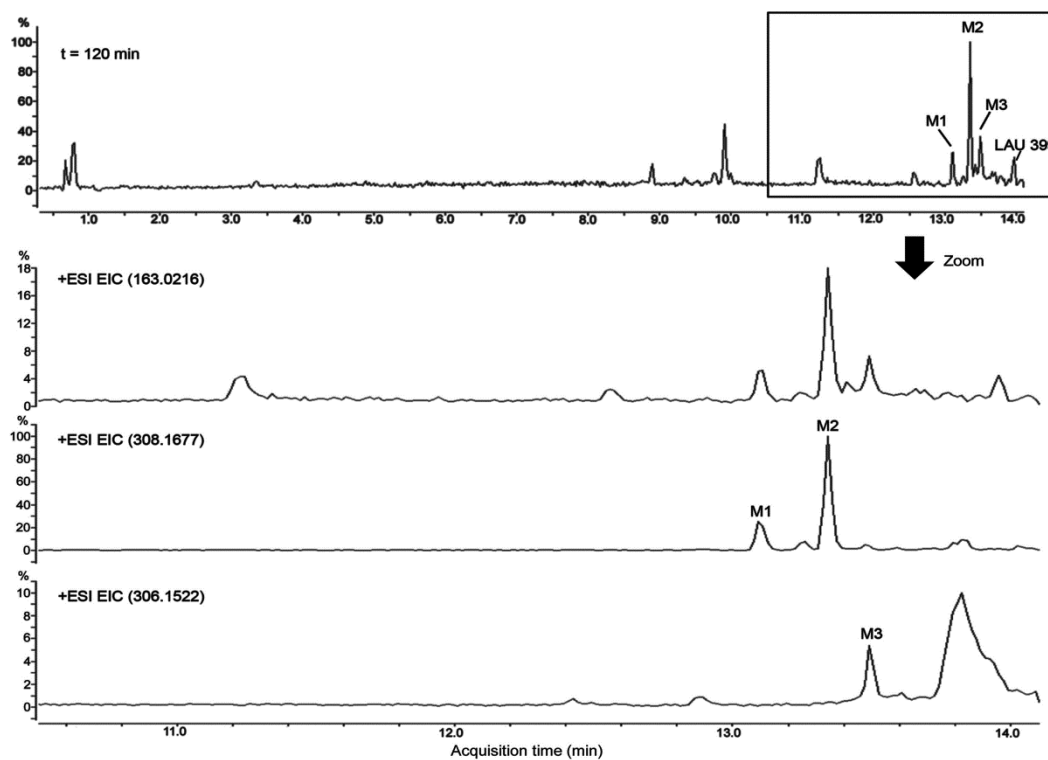
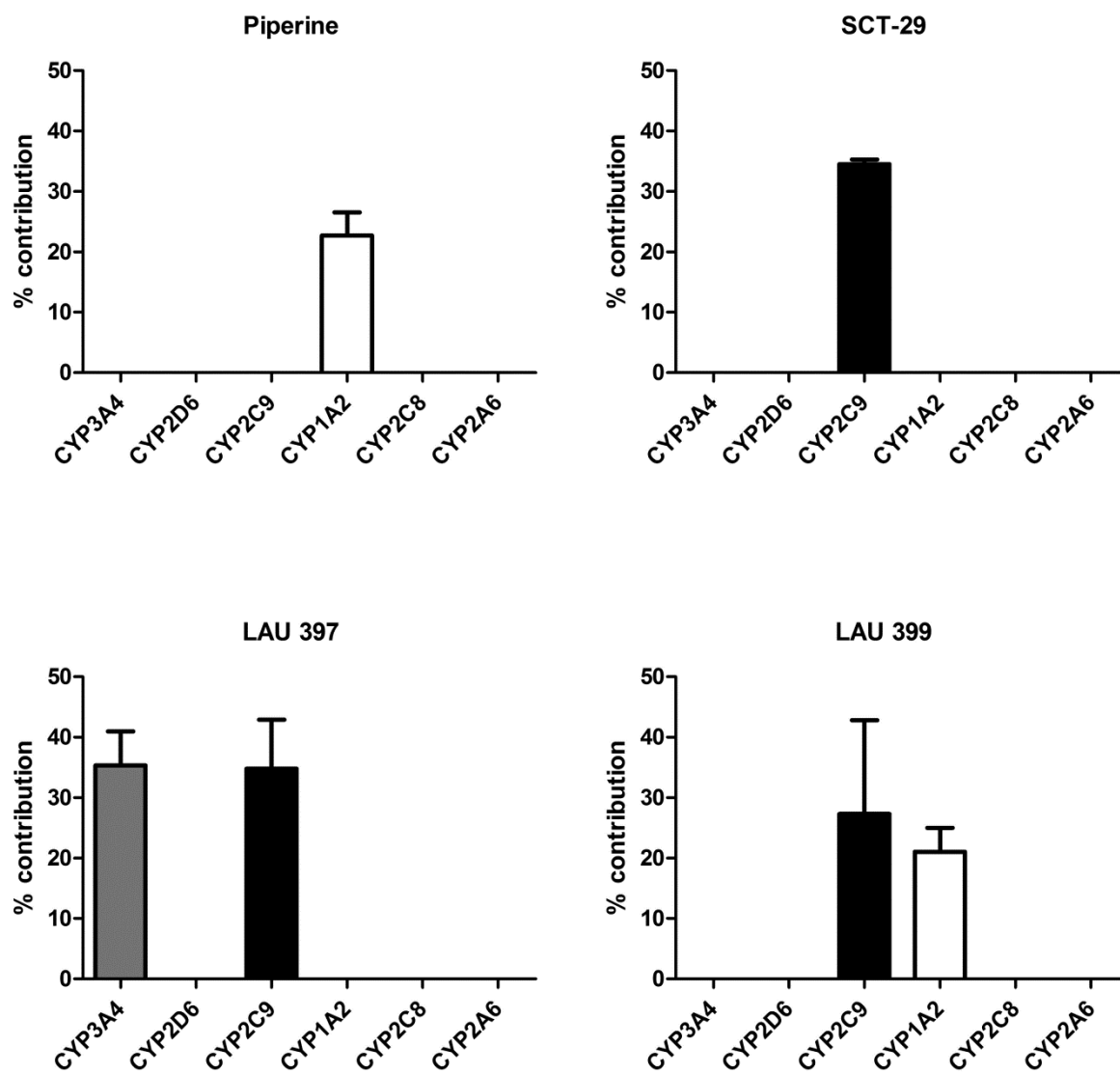


Figure 9: CYP450 reaction phenotyping with Silensomes™. The graphs show the relative contribution of individual CYP450 isoenzymes to the oxidative metabolism of compounds.





## **SUPPORTING INFORMATION**

### **GABA<sub>A</sub> receptor activity modulating piperine analogs: *In vitro* metabolic stability, metabolite identification, CYP450 reaction phenotyping, and protein binding**

Volha Zabela<sup>a</sup>, Timm Hettich<sup>b</sup>, Götz Schlotterbeck<sup>b</sup>, Laurin Wimmer<sup>c</sup>, Marko D. Mihovilovic<sup>c</sup>, Fabrice Guillet<sup>d</sup>, Belkacem Bouaita<sup>e</sup>, Bénédicte Shevchenko<sup>e</sup>, Matthias Hamburger<sup>a</sup>, and Mouhssin Oufir<sup>a\*</sup>

<sup>a</sup>Pharmaceutical Biology Laboratory, Department of Pharmaceutical Sciences, University of Basel, Klingelbergstrasse 50, CH-4056 Basel, Switzerland

<sup>b</sup>Institute for Chemistry and Bioanalytics, School of Life Sciences, University of Applied Sciences Northwestern Switzerland, Gründenstrasse 40, 4132 Muttenz, Switzerland

<sup>c</sup>Institute of Applied Synthetic Chemistry, Vienna University of Technology, Getreidemarkt 9, A-1060 Vienna, Austria

<sup>d</sup>Eurosafe, Parc d'Affaires La Bretèche, 35760 Saint Grégoire, France

<sup>e</sup>Biopredic International, Parc d'Affaires La Bretèche, 35760 Saint Grégoire, France

**Author's e-mails:** volha.zabela@unibas.ch (Zabela); timm.hettich@fhnw.ch (Hettich); goetz.schlotterbeck@fhnw.ch (Schlotterbeck); laurin.wimmer@tuwien.ac.at (Wimmer); marko.mihovilovic@tuwien.ac.at (Mihovilovic); fabrice.guillet@eurosafe.fr (Guillet); elkacem.bouaita@biopredic.com (Bouaita); benedicte.shevchenko@biopredic.com (Shevchenko); matthias.hamburger@unibas.ch (Hamburger); mouhssin.oufir@unibas.ch (Oufir)

#### **\*Corresponding author:**

Dr. Mouhssin Oufir

E-mail: mouhssin.oufir@unibas.ch

Tel: +41 61 207 15 44

Address: Pharmaceutical Biology, Department of Pharmaceutical Sciences, University of Basel, Klingelbergstrasse 50, CH-4056 Basel, Switzerland

Figure S1: Prediction of CYP450 isoenzymes involved in the oxidative metabolism of piperine and analogs by ACD/Labs Percepta. Green – confident non-substrate; gray – uncertain prediction.

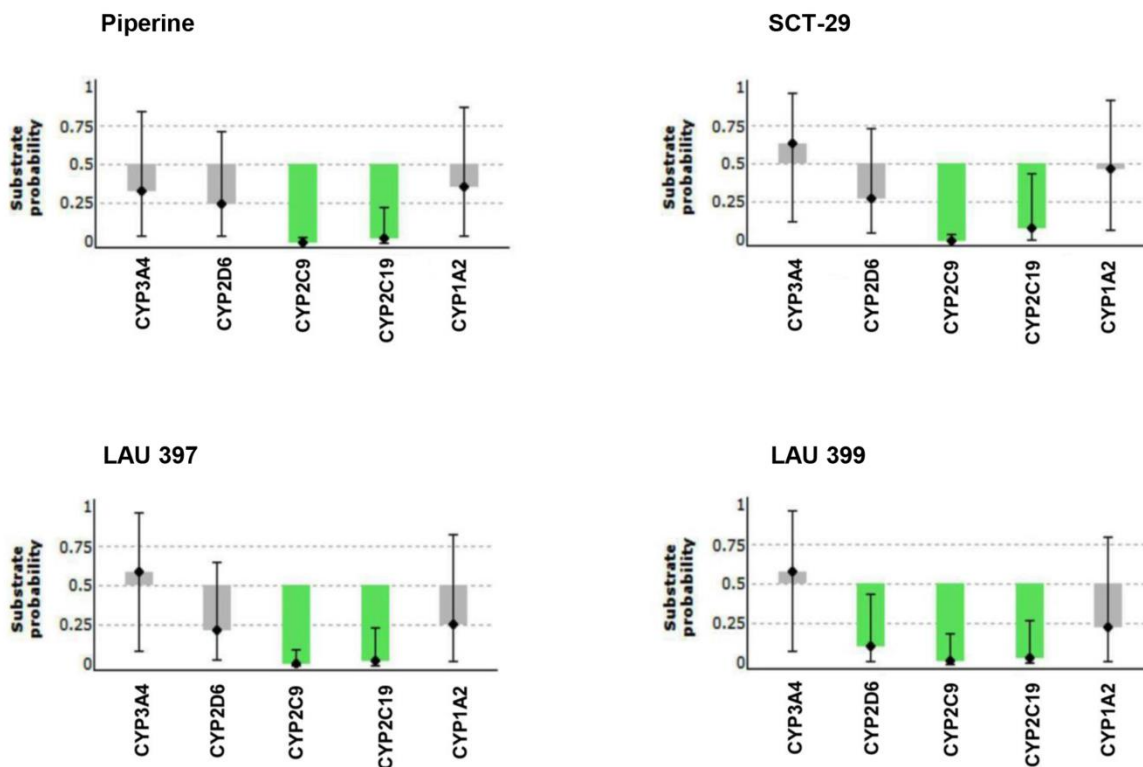


Figure S2: Fragmentation patterns of piperine and analogs.

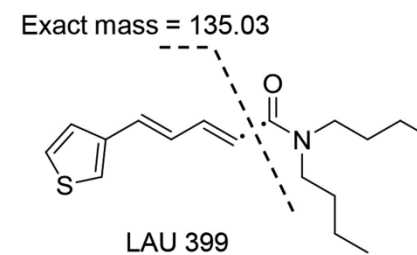
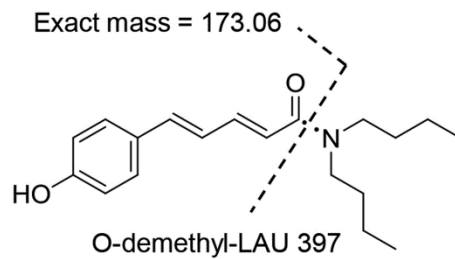
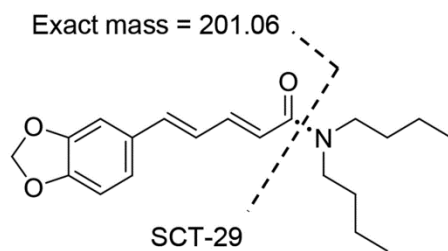
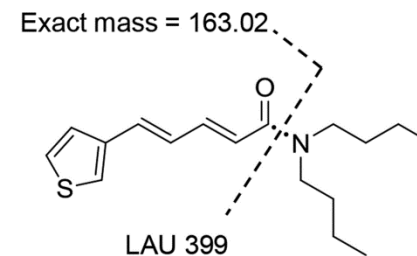
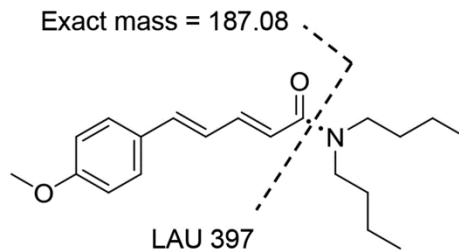
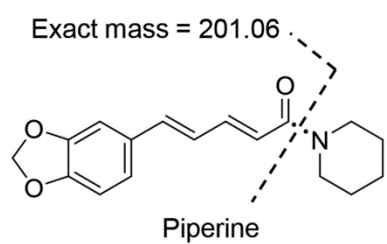


Figure S3: Phase I metabolites of piperine produced by microsomal incubation. Extracted ion chromatograms of the blank,  $t_0$ , and  $t_{120}$  samples are shown for diagnostic product ion  $m/z$  201.0547.

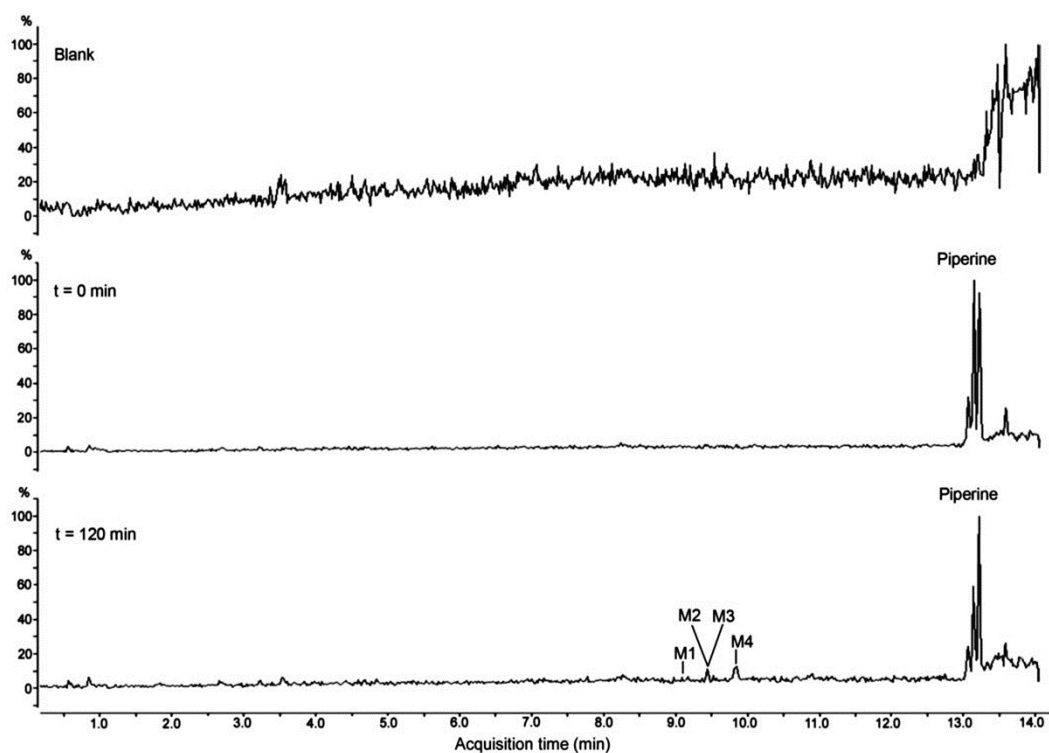


Figure S4: MS spectra of piperine and phase I metabolites M1-M4 processed with MassMetaSite.

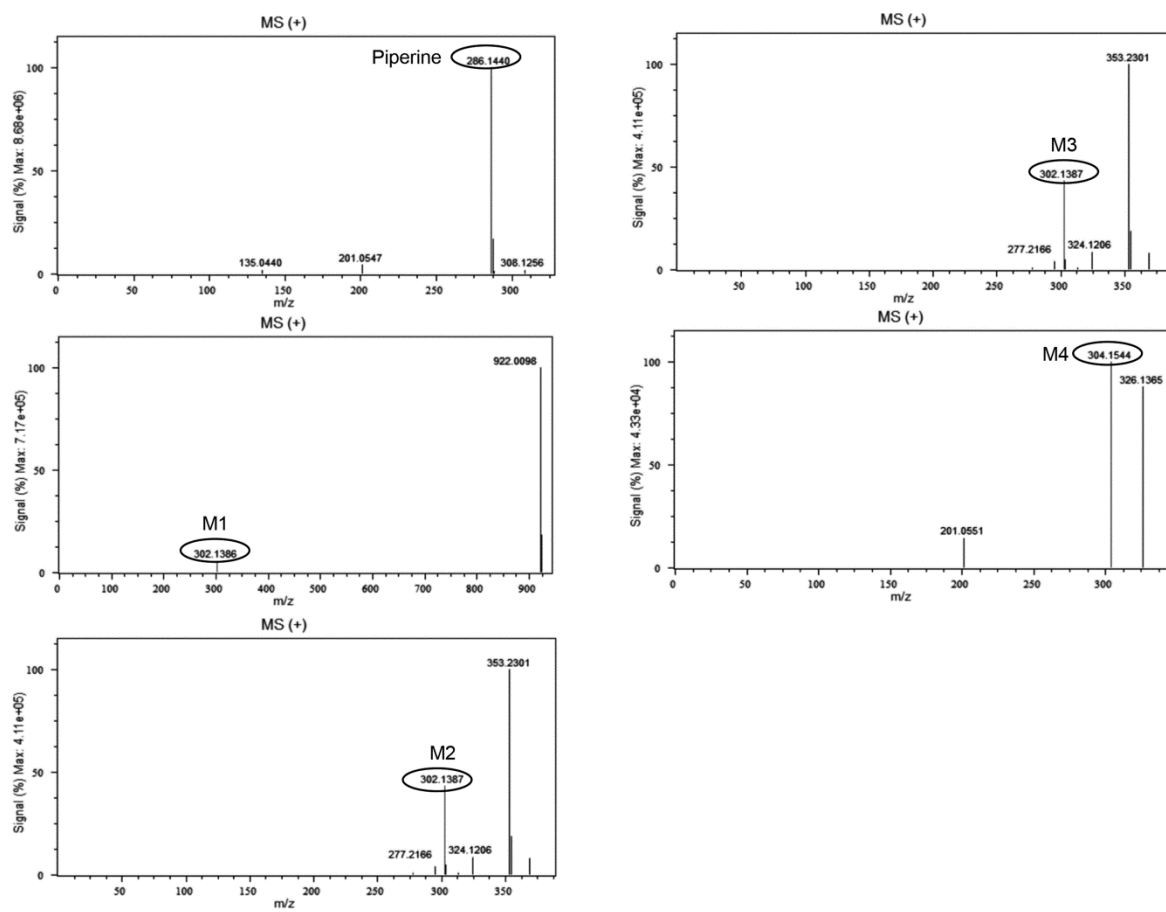


Figure S5: Phase I metabolites of SCT-29 produced by microsomal incubation. Extracted ion chromatograms of the blank,  $t_0$ , and  $t_{120}$  samples are shown for diagnostic product ion  $m/z$  201.0545.

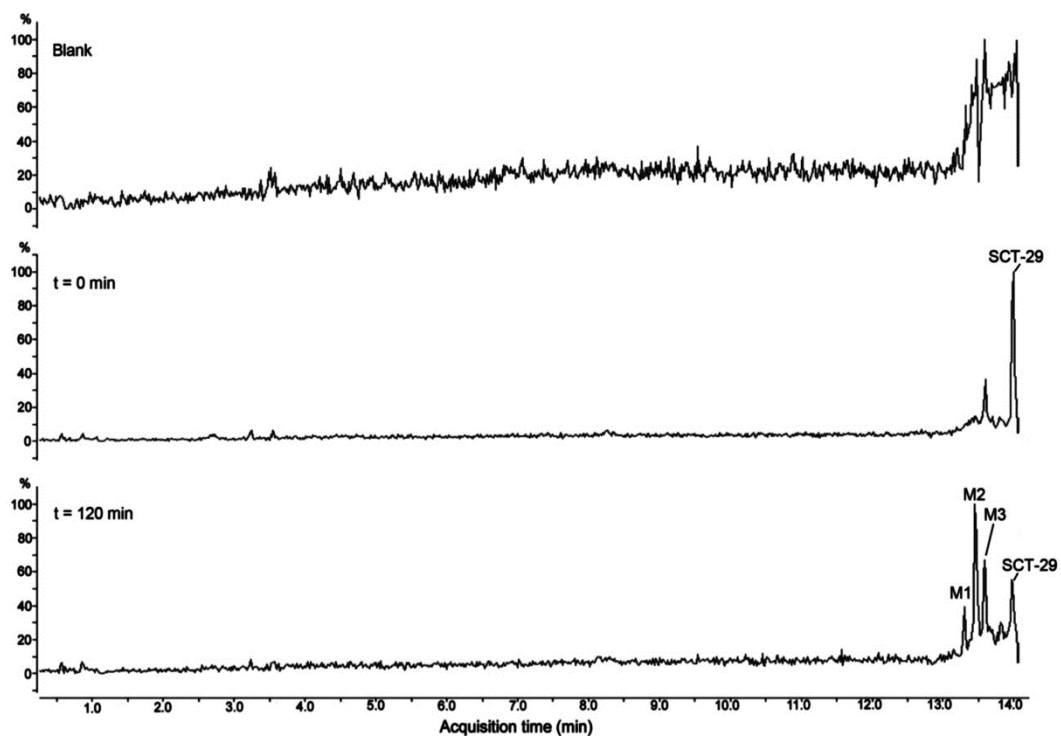


Figure S6: MS spectra of SCT-29 and phase I metabolites M1-M3 processed with MassMetaSite.

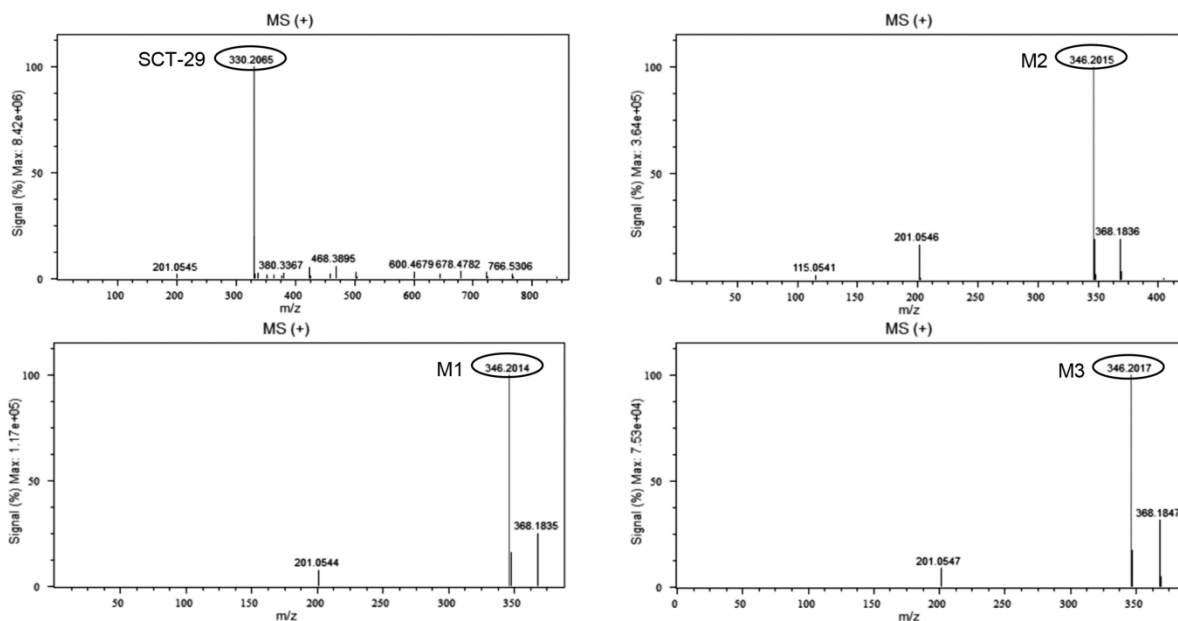


Figure S7: Phase I metabolites of LAU 397 produced by microsomal incubation. Extracted ion chromatograms of the blank,  $t_0$ , and  $t_{120}$  samples are shown for diagnostic product ion  $m/z$  187.0752.

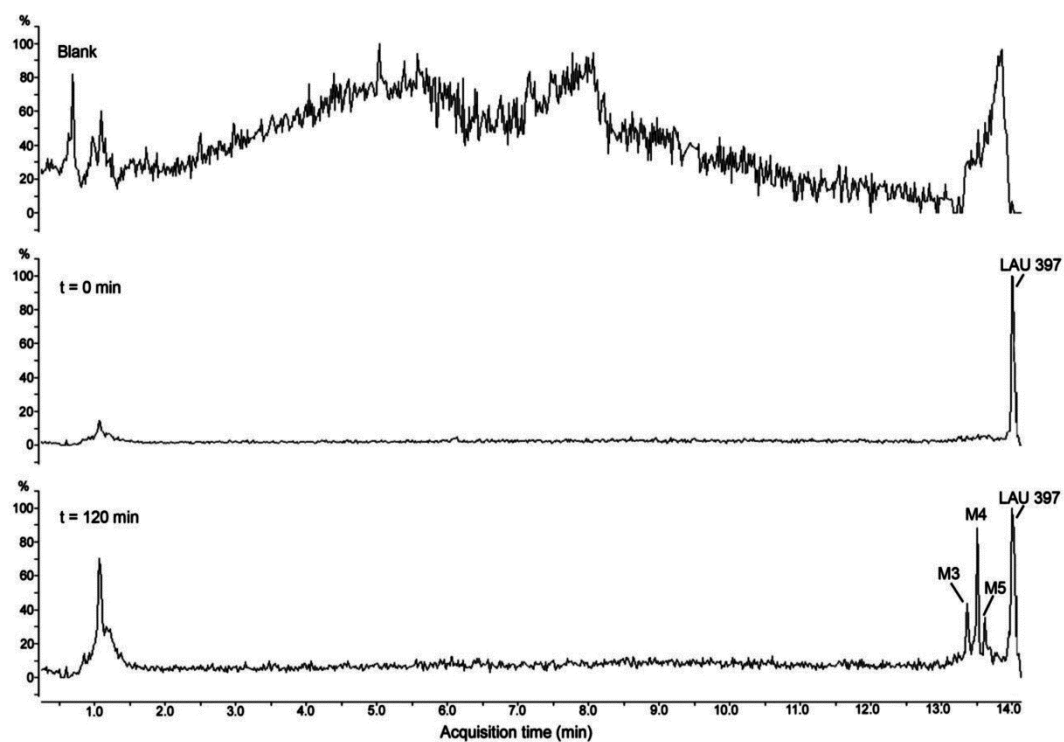




Figure S8: Phase I metabolites of LAU 397 produced by microsomal incubation. Extracted ion chromatograms of the blank,  $t_0$ , and  $t_{120}$  samples are shown for diagnostic product ion  $m/z$  173.0602.

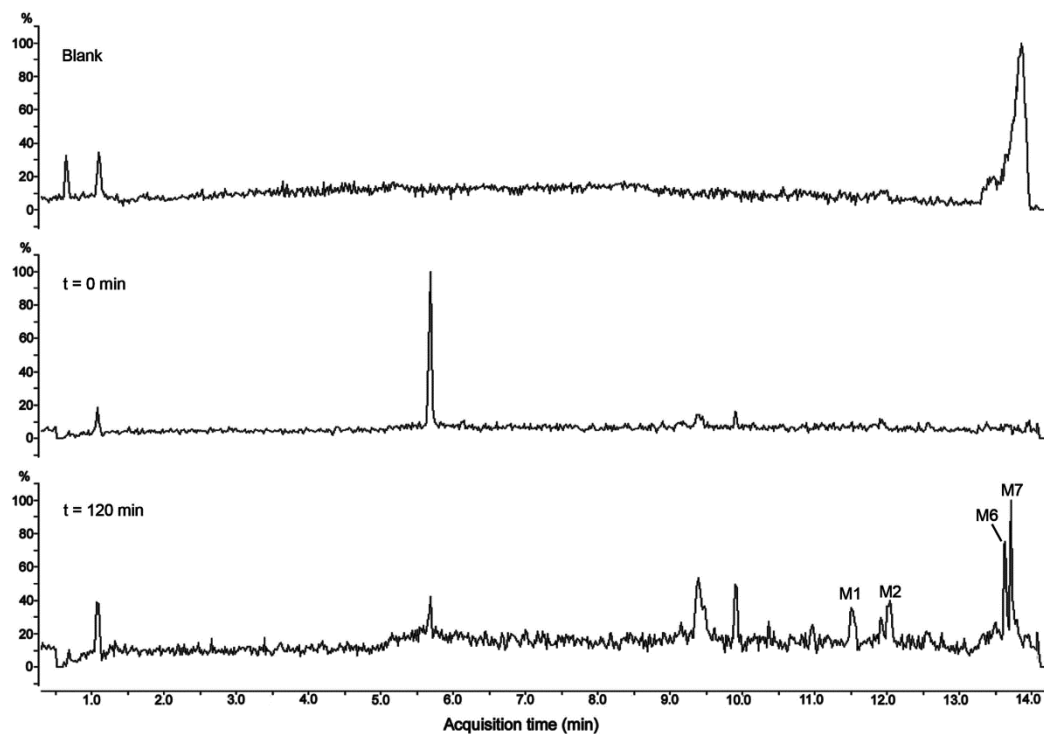


Figure S9: MS spectra of LAU 397 and phase I metabolites M3-M5 for diagnostic product ion  $m/z$  187.0752 processed with Mass-MetaSite.

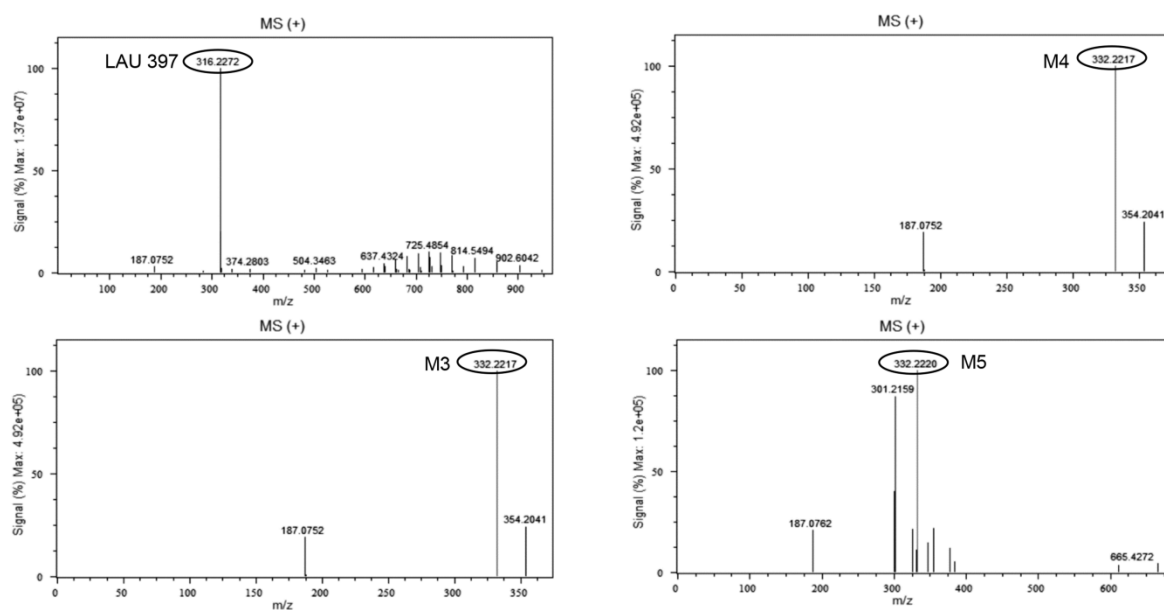


Figure S10: MS spectra of LAU 397 and phase I metabolites M1-M7 for diagnostic product ion  $m/z$  173.0602 processed with Mass-MetaSite.

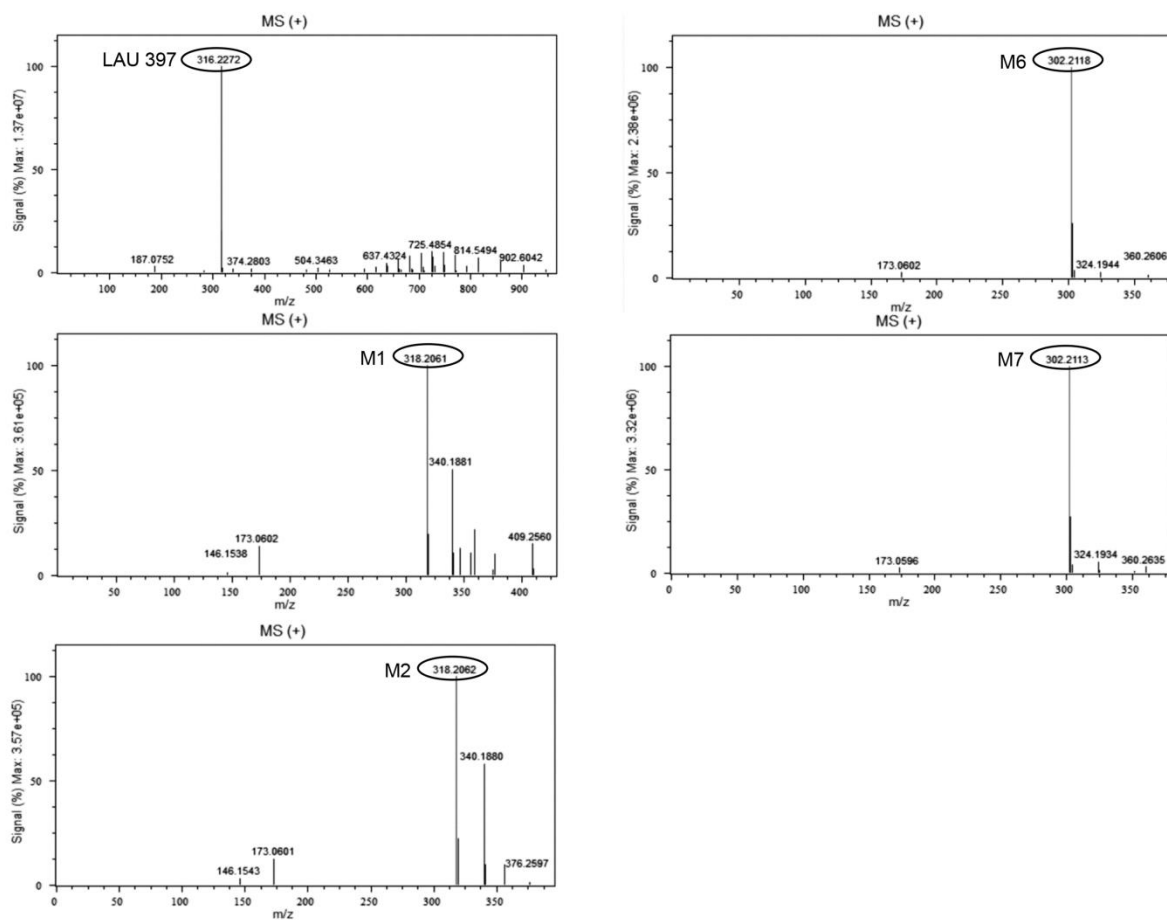


Figure S11: Phase I metabolites of LAU 399 produced by microsomal incubation. Extracted ion chromatograms of the blank,  $t_0$ , and  $t_{120}$  samples are shown for diagnostic product ion  $m/z$  163.0216.

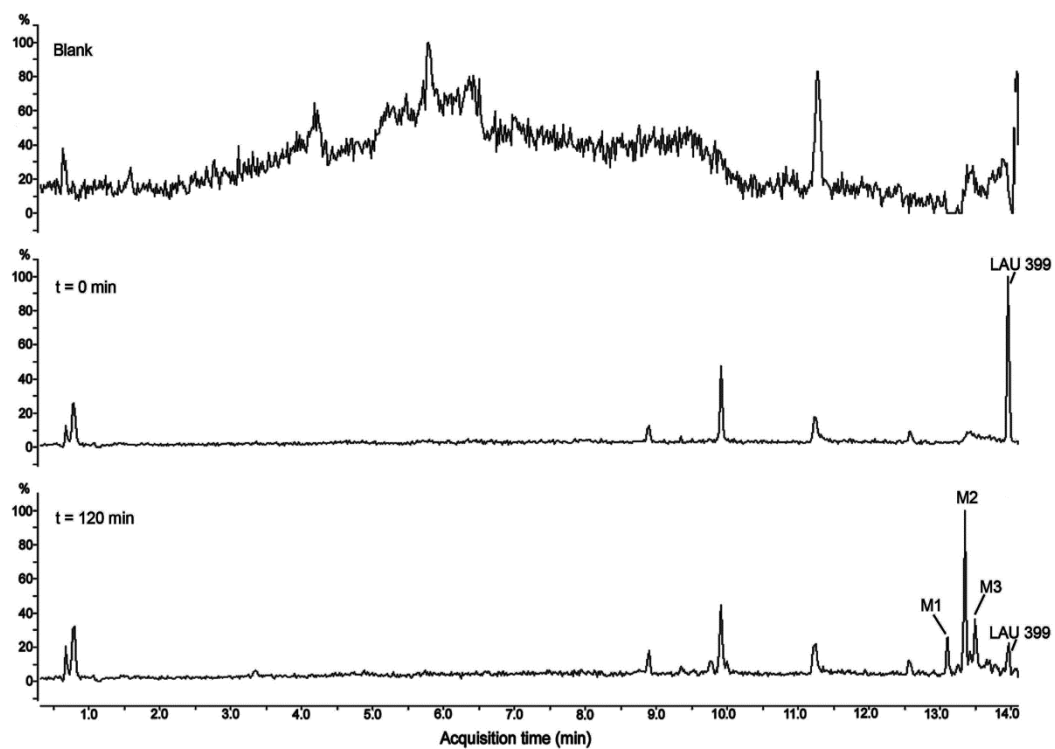


Figure S12: MS spectra of LAU 399 and phase I metabolites M1-M3 processed with MetaSite.

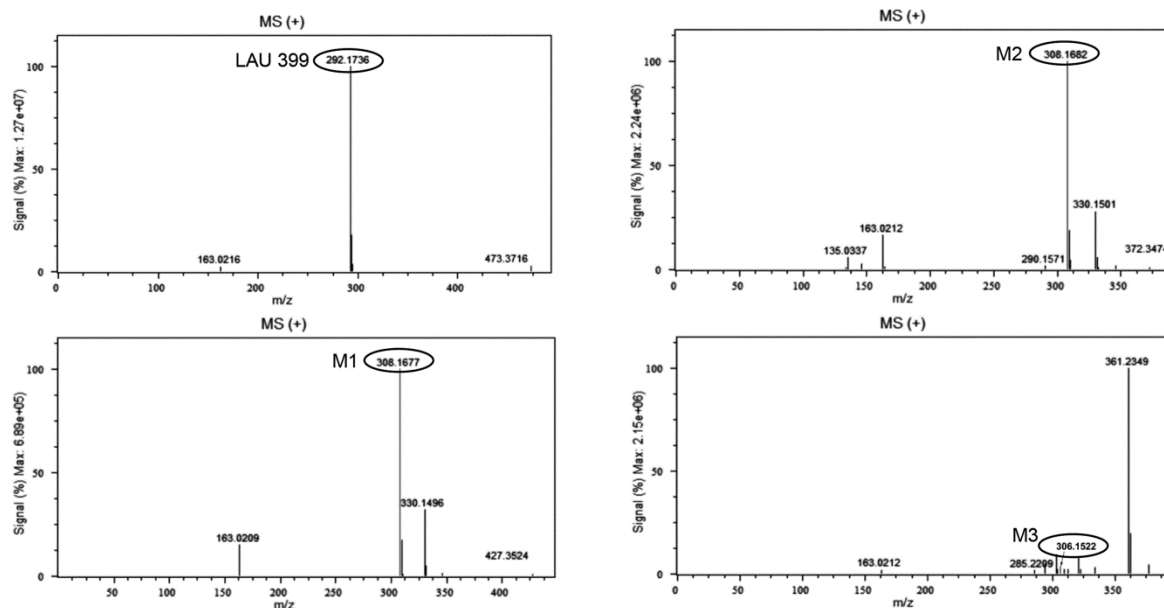


Figure S13: Validation of Silensomes™ with CYP450-specific substrates (n = 3): testosterone (CYP3A4), dextromethorphan (CYP2D6), diclofenac (CYP2C9), phenacetin (CYP1A2), amodiaquine (CYP2C8), coumarin (CYP2A6). The graph shows inhibition of metabolite formation in Silensomes™ compared to homologous controls.

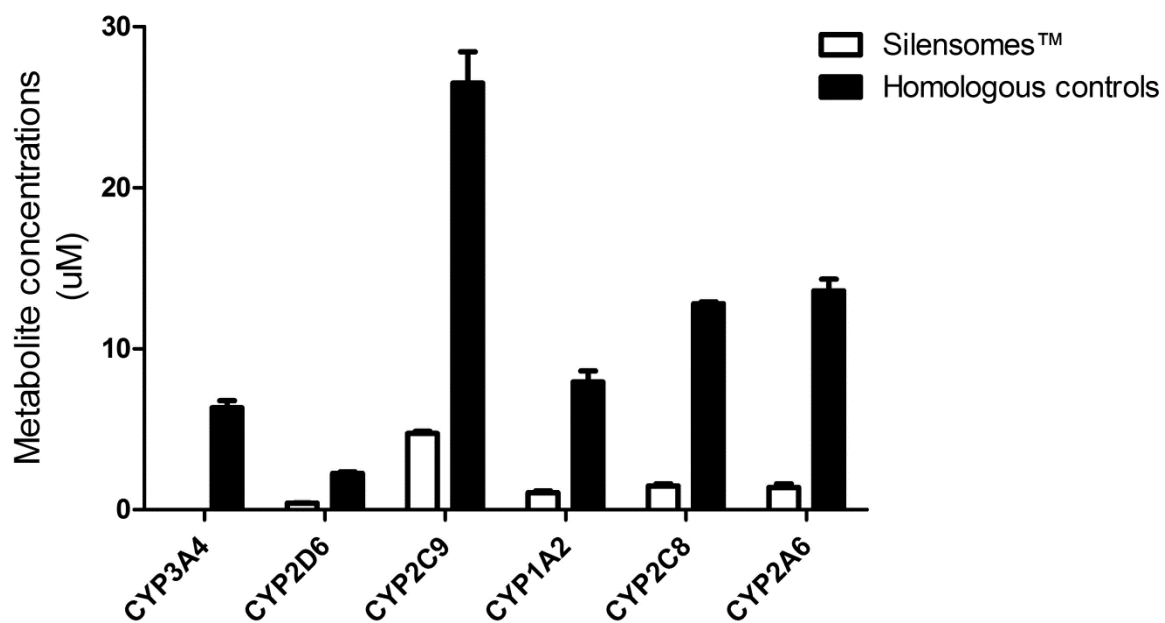
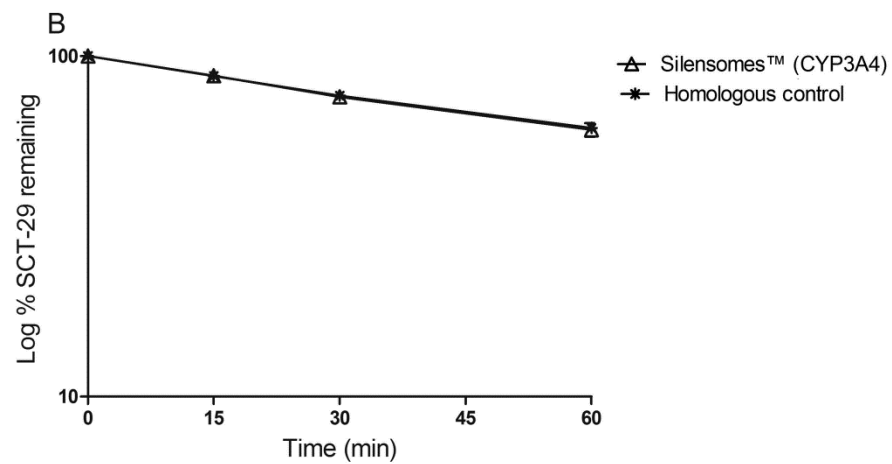
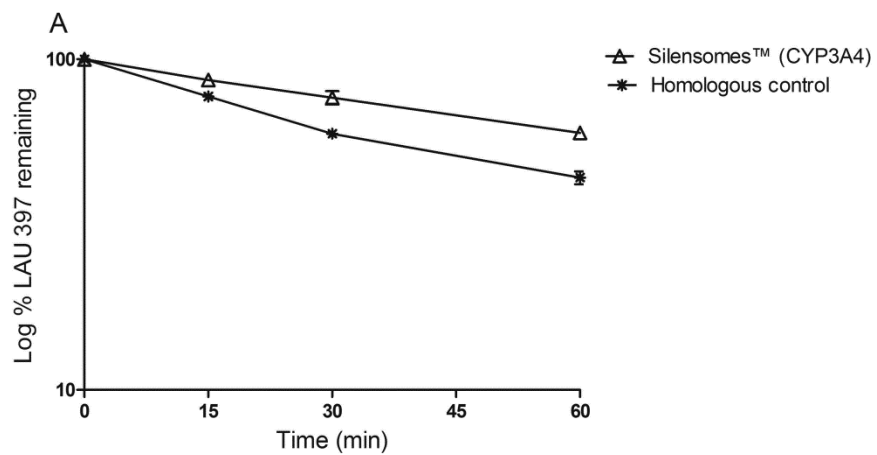


Figure S14: Example of typical CYP3A4 Silensome™ profiles for two piperine analogs, showing that LAU 397 (A) is a substrate, whereas SCT-29 (B) is not metabolized by this isoenzyme.







## **4 Conclusions and outlook**



Quantitative UHPLC-MS/MS methods were developed and validated in compliance to international regulatory guidelines for industry (1, 2) to support PK studies of kaempferol and the metabolites 4-HPAA, 3-HPAA, and DOPAC in rats. Several bioanalytical issues during UHPLC-MS/MS method development for DOPAC were encountered, and solved to reach acceptance criteria of the regulatory guidelines. Since DOPAC is an endogenous compound mainly originating from the neurotransmitter dopamine (3), the use of a surrogate matrix, which devoid of the target analyte (4), was mandatory. Bovine serum albumin solution at 60 g/l was used in this case (5). To prevent non-specific adsorption of DOPAC to plastic surfaces, pre-treatment of polypropylene tubes with 0.2% Tween-20 solution was done before the preparation of calibrators and quality controls (5). The example of DOPAC demonstrated the importance of bioanalytical method development and validation prior to a study sample analysis.

Upon intravenous application, PK of kaempferol followed a one-compartment model, with a rapid clearance (4-6 l/h/kg) and an extremely short  $t_{1/2}$  (3-4 min) (6). Upon oral dosing, low bioavailability for kaempferol was observed. In plasma the compound was present as phase II conjugates (6). Our findings were supported by the results from *in vitro* intestinal permeability assays which showed extensive metabolism of kaempferol in a Caco-2 cell model (7). Given that kaempferol undergoes extensive first-pass metabolism, it is more likely that the anxiolytic effect reported for this flavonoid is rather attributed to its metabolites.

PK profiles of the major colonic metabolites 4-HPAA, 3-HPAA, and DOPAC were obtained after intravenous application. PK of the metabolites followed two-compartment model, with a quick distribution ( $t_{1/2\alpha} = 3-6$  min) into peripheral tissues as well as a rapid elimination ( $t_{1/2\beta} = 18-33$  min) from the body (5, 6). With such a rapid elimination, pharmacologically relevant concentrations of these metabolites in the brain are unlikely to be achieved. Furthermore, acidic compounds like 4-HPAA, 3-HPAA, and DOPAC tend to bind, in a large extent, to albumin, and thus may have a limited brain penetration. Also, metabolism in the brain needs to be taken into account, considering that CYP and UGT enzymatic activities in the brain have been reported (8, 9). Taken together, it is not clear at this moment how the anxiolytic-like properties reported for the metabolites can be explained.

Further investigations are thus needed to identify pharmacologically active metabolites that are brain penetrant. Brain microdialysis experiments complemented with high resolution MS-

based untargeted metabolomics are planned for the future. Microdialysis technique will be employed for sampling the brain interstitial fluid to obtain metabolic profiles of control and test groups (10). High resolution MS-based untargeted metabolomics will be applied to compare metabolite levels in the brain between the groups (11). Afterwards, metabolomics data will be processed with the aid of the statistical software Agilent Mass Profiler Professional to uncover significant abundance differences of brain metabolites in control and test animals. The metabolites will be identified with the aid of MetID software Mass-MetaSite.

Specific and robust UHPLC-MS/MS methods for quantification of piperine and its analogs were developed to support *in vitro* metabolism studies of these compounds. Metabolic stability of piperine and its analogs was investigated in the presence of pooled human liver microsomes. Microsomal stability assays revealed piperine as the metabolically most stable compound with a  $t_{1/2}$  of 141 min (12). Analogs SCT-29 and LAU 397 demonstrated similar metabolic stability with a  $t_{1/2}$  of around 45 min, whereas analog LAU 399 was shown to be the metabolically most unstable compound with a  $t_{1/2}$  of 25 min (12). To obtain metabolite profiles of the test compounds after incubation with microsomes, UHPLC-Q-TOF-MS methods were developed. The high resolution accurate mass data were further processed with the aid of MetID software Mass-MetaSite. The principal routes of oxidative metabolism were found to be aliphatic hydroxylation, and N- and O-dealkylation (12). Additionally, CYP450 reaction phenotyping was performed to determine which CYP isozymes are involved in the metabolism of piperine and analogs. It appeared that piperine was exclusively metabolized by CYP1A2, whereas CYP2C9 contributed significantly in the oxidative metabolism of all analogs (12). Binding characteristics of piperine and analogs in whole blood were examined since extensive binding may impact their distribution into tissues. In fact, extensive binding to blood constituents was observed for all compounds (12). Summing up the results, it can be concluded that analogs were rapidly metabolized and showed strong binding to blood constituents due to increased lipophilicity. For analogs LogP values were in the range of 4.70-5.21 compared to piperine with a LogP 3.27 (13). The next cycle of medicinal chemistry optimizations should, therefore, be focused on reducing lipophilicity to lower metabolic liability and extensive binding of analogs. Adding polar groups such as hydroxyl, sulfhydryl or carbonyl in the molecule can be a solution to reduce lipophilicity (14).

## References

1. FDA (Draft Guidance 2013) *Guidance for Industry: Bioanalytical Method Validation*, Center for Drug Evaluation and Research.
2. EMA (2011) *Guideline on bioanalytical method validation*, European Medicines Agency (EMA/CHMP/EWP/192217/2009).
3. Munoz, P., Huenchuguala, S., Paris, I., and Segura-Aguilar, J. (2012) Dopamine oxidation and autophagy, *Parkinsons Dis.*, 1-13.
4. Jones, B. R., Schultz, G. A., Eckstein, J. A., and Ackermann, B. L. (2012) Surrogate matrix and surrogate analyte approaches for definitive quantitation of endogenous biomolecules, *Bioanalysis*. 4, 2343-2356.
5. Zabela, V., Sampath, C., Butterweck, V., Hamburger, M., Oufir, M. (submitted) Single dose pharmacokinetics of intravenous 3,4-dihydroxyphenylacetic acid and 3-hydroxyphenylacetic acid in rats, *Eur. J. Pharm. Sci.*
6. Zabela, V., Sampath, C., Oufir, M., Moradi-Afrapoli, F., Butterweck, V., and Hamburger, M. (in press) Pharmacokinetics of dietary kaempferol and its metabolite 4-hydroxyphenylacetic acid in rats, *Fitoterapia*. DOI: 10.1016/j.fitote.2016.10.008.
7. Moradi-Afrapoli, F., Oufir, M., Walter, F. R., Deli, M. A., Smiesko, M., Zabela, V., Butterweck, V., and Hamburger, M. (2016) Validation of UHPLC-MS/MS methods for the determination of kaempferol and its metabolite 4-hydroxyphenyl acetic acid, and application to *in vitro* blood-brain barrier and intestinal drug permeability studies, *J. Pharm. Biomed. Anal.* 128, 264–274.
8. Gervasini, G., Carrillo, J. A., and Benitez, J. (2004) Potential role of cerebral cytochrome P450 in clinical pharmacokinetics, *Clin. Pharmacokinet.* 43, 693-706.
9. Ouzzine, M., Gulberti, S., Ramalanjaona, N., Magdalou, J., and Fournel-Gigleux, S. (2014) The UDP-glucuronosyltransferases of the blood-brain barrier: their role in drug metabolism and detoxication, *Front. Cell. Neurosci.* 8, 1-9.
10. Ivanisevic, J., and Siuzdak, G. (2015) The role of metabolomics in brain metabolism research, *J. Neuroimmune Pharmacol.* 10, 391-395.
11. Vinayavekhin, N., and Saghatelian, A. (2010) Untargeted metabolomics, *Curr. Protoc. Mol. Biol.* 30, 1-24.
12. Zabela, V., Hettich, T., Schlotterbeck, G., Wimmer, L., Mihovilovic, M. D., Bouaita, B., Guillet, F., Shevchenko, B., Hamburger, M., and Oufir, M. (submitted) GABA<sub>A</sub> receptor activity modulating piperine analogs: *In vitro* metabolic stability, metabolite identification, CYP450 reaction phenotyping, and protein binding, *Eur. J. Pharm. Sci.*
13. Eigenmann, D. E., Dürig, C., Jähne, E. A., Smieško, M., Culot, M., Gosselet, F., Cecchelli, R., Helms, H. C. C., Brodin, B., and Wimmer, L. (2016) *In vitro* blood-brain barrier permeability predictions for GABA<sub>A</sub> receptor modulating piperine analogs, *Eur. J. Pharm. Biopharm.* 103, 118–126.
14. Kerns, E. H., and Li, D. (2008) *Drug-like properties: concepts, structure design and methods from ADME to Toxicity Optimization*, 1st ed., Elsevier-Academic Press, San Diego.



## Acknowledgement

First and foremost, I would like to express my sincere gratitude to Prof. Dr. Matthias Hamburger for providing me with the opportunity to do my PhD thesis within his group. I am very grateful for your enthusiasm, immense knowledge, active interest in my research, and useful advice. Your guidance helped me in all the time of my PhD study and writing of this thesis.

My heartfelt thanks go to Dr. Mouhssin Oufir, my direct supervisor. You are a guru of bioanalysis, and I owe my current knowledge to you. Thank you for pushing me to the limits, especially, in the beginning of my study, and for being always available to answer thousands of my questions. I am truly grateful for your precious support and the funny moments we shared together.

I acknowledge the Swiss Federal Commission for the Swiss Government Excellence Scholarship for Foreign Scholars which I was awarded with in 2012.

I thank Prof. Dr. Laurent A. Decosterd, who kindly accepted to review my dissertation, and to act as a co-referee of my examination committee. I acknowledge Prof. Dr. Veronika Butterweck for her scientific input and fruitful collaboration. Thanks to Prof. Dr. Hartmut Derendorf for the training on PK/PD modeling and simulation. I am thankful to Timm Hettich for his assistance in HR-MS measurements. Thanks to the current and former members of the Pharmaceutical Biology lab with its unique warm and friendly atmosphere. I am grateful for the friendships that have been formed during our time in the lab.

Lots of thanks go to my friends outside the lab: Konstantin, Viktor, Sinoy, Clitzia, Frederick, Valva, Tatiana, Roman, Michael, Olga, Ekaterina, Svetlana, and Natalia. I am so lucky to have you guys in my life.

Finally, my deepest gratitude goes to my family for your unconditional love and endless support. Words cannot express how grateful I am for all your help!

*Volha (Olga) Zabela*





# Curriculum vitae

## Personal information

---

Name: Volha Zabela  
Date of birth: 15.10.1987  
Nationality: Belarussian  
Mobile phone: +41 78 630 63 67  
E-mail: olgazabelo@gmail.com

## Education

---

**Nov. 2012-Oct. 2016**      **PhD in Pharmaceutical Sciences**  
Research topic “*Pharmacokinetics and metabolism of CNS-targeted natural products*”  
University of Basel, PharmaCenter, Basel, Switzerland

**2008-2010**      **Msc in Biology**  
Belarusian State University, Belarus, Minsk

**2005-2008**      **Bsc in Biology**  
Belarusian State University, Belarus, Minsk

## Professional experience

---

**Nov. 2012-Oct. 2016**      **PhD Candidate/Assistant** in Prof. Dr. Matthias Hamburger’s group  
EMA/FDA method development and validation for the analysis of small molecule natural products to support *in vitro* DMPK studies, metabolite identification (MetID), non-compartmental and compartmental PK data analysis  
University of Basel, PharmaCenter, Basel, **Switzerland**

**Jan.-May 2014**      **Visiting Scientist** in Prof. Dr. Hartmut Derendorf’s group  
Completed an advanced training in PK/PD modeling and simulation.  
University of Florida, College of Pharmacy, Gainesville, **USA**

**Apr. 2010-Sept. 2012**      **Research Assistant**  
Administration of substances to laboratory animals, blood sample collection, small animal surgeries, vessel reactivity examination, blood pressure monitoring  
National Academy of Sciences, Institute of Pharmacology and Biochemistry, Minsk, **Belarus**

## Honors and awards

---

**Nov. 2012-Oct. 2015**      Swiss Government Excellence Scholarship for Foreign Scholars

**2012**      Travel Grant from the Council for Basic Cardiovascular Science of the European Society of Cardiology

**2011**      Travel Grant from the Council for Basic Cardiovascular Science of the European Society of Cardiology

## Certificates

---

Sept. 2015	Patenting and Spin-off workshop
Oct. 2015	Learning how to lead and to build a successful work environment workshop

## Languages

---

Russian and Belarussian (native), English (fluent in written and spoken), German and French (ground courses at Sprachenzentrum)

## Publications

---

1. A. Zhiv, V. Shylau, V. Afonin, K. Bulanova, L. Lobanok, V. Alekseenko, **V. Zabela**, Development of the curcumin-based preservative solution for vascular surgery. *Science and Innovations*. 2015, 11, 68-72
2. **V. Zabela**, V. Shylau, Fixed-dose phytosynthetic combination of curcumin and valsartan with antihypertensive and antihypertrophic properties (in preparation)
3. **V. Zabela**, C. Sampath, M. Oufir, F. Moradi-Afrapoli, V. Butterweck, M. Hamburger, Pharmacokinetics of dietary kaempferol and its metabolite 4-hydroxyphenylacetic acid in rats. *Fitoterapia*. 2016 (in press). DOI: 10.1016/j.fitote.2016.10.008
4. **V. Zabela**, C. Sampath, M. Oufir, V. Butterweck, M. Hamburger, Single dose pharmacokinetics of intravenous DOPAC and 3-hydroxyphenylacetic acid in rats. *Eur. J. Pharm. Sci.* 2016 (submitted)
5. **V. Zabela**, T. Hettich, G. Schlotterbeck, L. Wimmer, M.D. Mihovilovic, F. Guillet, B. Bouaita, B. Shevchenko, M. Hamburger, M. Oufir, GABA<sub>A</sub> receptor activity modulating piperine analogs: *In vitro* metabolic stability, metabolite identification, CYP450 reaction phenotyping, and protein binding. *Eur. J. Pharm. Sci.* 2016 (submitted)
6. F. Moradi-Afrapoli, M. Oufir, F. R. Walter, M. A. Deli, M. Smiesko, **V. Zabela**, V. Butterweck, M. Hamburger, Validation of UHPLC-MS/MS methods for the determination of kaempferol and its metabolites 4-hydroxyphenylacetic acid, and application to *in vitro* blood-brain barrier and intestinal drug permeability studies. *J. Pharm. Biomed. Anal.* 2016, 128, 264-274
7. C. Guccione, M. Oufir, V. Piazzini, D.E. Eigenmann, E.A. Jähne, **V. Zabela**, M.T. Faleschini, M.C. Bergonzi, M. Smiesko, M. Hamburger, A.R. Bilia, Preparation and analysis of nanovectors for brain delivery of andrographolide as neuroprotective agent. *Colloids Surf., B* 2016 (submitted)

## **Selected list of posters presented at scientific meetings**

---

1. **V. Zabela**, T. Hettich, G. Schlotterbeck, L. Wimmer, M.D. Mihovilovic, F. Guillet, B. Bouaita, B. Shevchenko, M. Hamburger, M. Oufir “GABA<sub>A</sub> receptor modulating piperine analogs - *In vitro* metabolic stability, protein binding, CYP450 reaction phenotyping and metabolite identification” presented at the 9<sup>th</sup> Swiss Pharma Science Day, Bern, 2016
2. **V. Zabela**, C. Sampath, V. Butterweck, M. Hamburger, and M. Oufir “Bioanalytical validation issues of an UHPLC-MS/MS method for quantitation of DOPAC in Sprague Dawley rat plasma and application to pharmacokinetic studies” presented at the 42<sup>nd</sup> Symposium of HPLC, Geneva, 2015
3. **V. Zabela**, M. Oufir, C. Sampath, F. Moradi-Afrapoli, V. Butterweck and M. Hamburger “Pharmacokinetics of natural products with anxiolytic-like properties” presented at the annual meeting of the Group of Metabolism and Pharmacokinetics, Paris, 2015
4. **V. Zabela**, F. Moradi-Afrapoli, V. Butterweck, M. Hamburger and M. Oufir “Validation of UHPLC-MS/MS methods for quantification of kaempferol and 4-hydroxyphenylacetic acid in rat plasma, and application to pharmacokinetics studies” presented at the 20<sup>th</sup> International Mass Spectrometry Conference, Geneva, 2014
5. F. Moradi-Afrapoli, E. A. Jähne, D.E. Eigenmann, **V. Zabela**, F.R. Walter, M. A. Deli, V. Butterweck, G. Imanidis, M. Hamburger and M. Oufir “Validation of UHPLC-MS/MS methods for quantification of kaempferol and 4-hydroxyphenylacetic acid, and application to *in vitro* BBB and intestinal drug permeability assays” presented at the 20<sup>th</sup> International Mass Spectrometry Conference, Geneva, 2014
6. **V. Zabela**, V. Shylau, V. Afonin “Phytochemical drugs are the new progress in the genetically determined arterial hypertension treatment” presented at the European Society of Cardiology Congress, Munich, 2012. European Heart Journal (abstract supplement). 2012 (33):774
7. **V. Zabela**, V. Shylau, E. Fedulova, O. Kardash, N. Nadina, T. Krasnenkova, E. Shafranovskaya “Pharmacological instrument for the genetically determined arterial hypertension treatment” presented at the European Society of Cardiology Congress, Paris, 2011. European Heart Journal (abstract supplement). 2011 (32): 888-889